9-4-2014 12:00 AM

The Late Quaternary Paleolimnology of Lake Ontario

Ryan Hladyniuk, *The University of Western Ontario*

Supervisor: Dr. Fred J. Longstaffe, *The University of Western Ontario*

A thesis submitted in partial fulfillment of the requirements for the Doctor of Philosophy degree in Geology

THE LATE QUATERNARY PALEOLIMNOLOGY OF LAKE ONTARIO

(Thesis format: Integrated Article)

by

Ryan Hladyniuk

Graduate Program in Earth Sciences

A thesis submitted in partial fulfillment
of the requirements for the degree of
Doctor of Philosophy

The School of Graduate and Postdoctoral Studies
The University of Western Ontario
London, Ontario, Canada

Abstract

We examined the oxygen isotopic composition of biogenic carbonates, carbon and nitrogen abundances and isotopic compositions of bulk organic matter (OM), and the abundances and carbon isotopic compositions of individual *n*-alkanes (C_{17} to C_{35}) for samples from three, 18 m long sediment cores from Lake Ontario in order to: (i) assess how changing environmental parameters affected the hydrologic history of Lake Ontario, and (ii) evaluate changes in organic productivity and sources since the last deglaciation. Knowledge of the hydrologic and ecological behaviour of the Lake Ontario basin during past climate change provides insight into its future sensitivity. During the glacial period, the average lakewater oxygen-isotope composition was –17.5 ‰ (VSMOW), which indicates a significant glacial meltwater contribution. Higher abundances of mid-chain *n*-alkanes (C_{23} and C_{25}) with carbon-isotope compositions of –32.5 ‰ (VPDB) record allochthonous OM input, notwithstanding low bulk C/N ratios that normally indicate lacustrine productivity. These results suggest a degraded source, perhaps OM associated with clay minerals. Glacial retreat facilitated proliferation of terrestrial vegetation, as recorded in higher abundances of long-chain (terrestrial) *n*-alkanes (C_{27}, C_{29}, C_{31}). Cessation of glacial meltwater supply is marked by an increase in lakewater oxygen-isotope composition to ~ –12 ‰ by 13,000 cal BP. This increase was interrupted by a final inflow of low-^{18}O glacial meltwater that lasted ~500 years. Rerouting of the upper Great Lakes caused Lake Ontario to become hydrologically closed from 12,300 to 8,300 cal BP. The lakewater oxygen-isotope composition increased to –7 ‰ because of the end of glacial meltwater supply, and climate-related increases in evaporation and the oxygen-isotope composition of precipitation. A steady increase in terrestrial *n*-alkane abundances and their carbon-isotope compositions (–31 to –29 ‰) signified plant growth under water-stressed conditions until ~8,000 cal BP. Transition to a wetter climate (6,800 cal BP) and return of upper Great Lakes water supply (~5,300 cal BP) caused lake levels to rise. A decrease in carbon-isotope composition (~2 ‰) in all aquatic *n*-alkanes during this time signifies a change in the lacustrine carbon pool, whereas a decrease in the carbon-isotope composition of terrestrial *n*-alkanes signifies relief from more arid conditions.

Keywords

Great Lakes, Lake Ontario, paleolimnology, stable isotopes, ostracodes, clams, organic matter, *n*-alkanes, glacial meltwater, primary productivity, environmental change, Pleistocene, Holocene

Epigraph

Meltwaters did rush to the sea
They say – from Lake Agassiz
And that made it cold
We are constantly told
But the pathways aren't shown to me!

–FJL

Dedication

This thesis is dedicated to my parents, Zeferina and Peter Hladyniuk.

Acknowledgments

He who tops the list of acknowledgments is my supervisor Fred Longstaffe. Throughout the past 6 years, Fred has exemplified what it is to be a great supervisor. He offers creative academic ideas, encouragement towards research, virtually limitless patience and the ability to extend your mind in areas you never thought possible. Fred is also an excellent role model; his leadership has advanced my personal professional development skills while maintaining the highest ethical (academic and personal) integrity. Without Fred, I would not have been able to participate in the numerous conferences and field trips I attended. In addition, I would have not been a member of such a prestigious group of international and governmental collaborators. In my first meeting with Fred, Fred asked me; "*What do you know about lake sediment cores?*" I replied; "*All I know is that they are round.*" Getting your first question wrong (sediment cores are cylindrical) does not leave a particularly good first impression; however, Fred remained confident in my abilities then, as much as he does now. I can say with confidence, that without Fred I would not have progressed to be the scholar I am today. Fred, thank you for all that you have provided me (skills, life lessons and countless delicious 'feedings'). I am extremely honoured to have you as a supervisor –I am also grateful to call you my friend.

I also thank Allan Crowe (Canada Centre for Inland Waters, Environment Canada) for facilitating core sampling, and the captain and crew of the Canadian Coast Guard Ship *Limnos* for core collection –ultimately the foundation for my Ph.D. project. Also at Canada Centre for Inland Waters, I thank Christina Jaskot, Brian Trapp and Ian Droppo for allowing me to obtain grain-size measurements in their laboratory. I sincerely thank Francine McCarthy (Brock University) for welcoming me into her lab and teaching me the skills to extract pollen from lake sediments. In addition, I thank Francine for allowing me to attend her wonderful course on palynology. I am grateful to John King and staff (University of Rhode Island, Graduate School of Oceanography) for providing sediment core images and the University of Arizona (AMS laboratory) for radiocarbon dates.

Katrina Moser and Guy Plint (Ph.D. committee members) have also been a great help at various stages of project design and certainly advanced the project, thank you. I also thank the examination committee (Dan Shrubsole, Elizabeth Webb, Patricia Corcoran and Mike

Lewis) for their thoughtful revisions and skillful questions during my defense. All of you have greatly advanced this work.

Much of the analytical work would not be possible without the assistance of the staff of the Laboratory for Stable Isotope Science (The University of Western Ontario). I appreciate the time and patience offered by Kim Law, Grace Yau, and Li Huang. All of you have greatly advanced my technical skills in the field of stable isotope mass spectrometry and I thank you for that. I would also like to thank my laboratory and university colleagues that have provided helpful insight toward project design and assistance on experiments: Rebecca Macdonald, Ayumi Hyodo, Sam Russel, Duane Petts, Jessica Metcalfe, Beth Hundey, Natasha Bumstead, Nicolle Bellissimo, Christine Cizkowski, Nadine Wakabayashi, Paul Szpak, Scott Colborne, Farnoush Tahmasebi, Laura Sanchez and Nelson Cho.

A special 'thank you' is needed for; (i) Avner Ayalon (Geological Survey of Israel) for enhancing my critical thinking skills in the field of isotope science, (ii) Mike Lewis (Geological Survey of Canada), 'the godfather' of Great Lakes research, for the many delightful and constructive talks about limnology in general and (iii) Nadia Dildar for coaching me through the process of lipid extraction and *n*-alkane measurements.

The project would not be possible without funding. Operating funds were provided by a Natural Sciences and Engineering Research Council of Canada Discovery Grant (FJL) and an Ontario Graduate Scholarship (RH). Infrastructure support was provided by the Canada Foundation for Innovation and the Ontario Research Fund (FJL). The research was also made possible in part through additional research time provided through the Canada Research Chairs program. I also wish to express my gratitude toward the donors and organizations of the many scholarships I obtained; Robert and Ruth Lumsden Award, Graduate Thesis Research Award, Robert Hodder Travel Bursary, Kenneth N. Weaver Student Travel Award (Geological Society of America, North-eastern section), Geological Society of America Student Travel Award (North-central section), and the International Association for Great Lakes Research-Ontario Ministry of Natural Resources Student Travel Award.

I thank the many friends I have. All of you have contributed to my success in one way or another, thank you for keeping me level-headed. Furthermore, I appreciated all the fun we

have had together, especially the RRBD faithful (a short list of friends in no particular order): Carter Hutton, Billy Boquist, Mike and Kelly Sellan, Chris Unick, Adam Fron, Justin Everett, Troy Prezio, Brent Irwin, Steve Hosegood, Kevin Britton, Ryan Baird, Jeff Coull, Kory McEwan, Derrick Hosanna, Adam and Michelle Nemeth, Adam Fabiano, Brad and Nicole Yeo, Mark Davis, Peter Franchin, Kyle Lamb, Keyvan Hunt, Randy and Janelle Hanagan and the list goes on!

Thank you to the Andrews family for operating the Komoka Classics Senior 'AA' hockey club (formerly Lucan-Ilderton Jets) and allowing me to play for such a first class organization. I also thank my hockey teammates, coaches and trainers over the years (the list is long).

Last, but certainly not least, my family to whom I owe everything. Above all, I thank my parents Zeferina and Peter Hladyniuk for encouraging me to chase my dreams and make my university 'career' a reality. I had infinite support (both financial and emotional) from the best role models a son could ask for, thank you. I truly would not be the person I am today without Zef and Pete. In addition to thanking my parents, I would like to acknowledge my brother Nik Hladyniuk. He has always kept me 'in-line', as any big brother would, and has provided our family with countless hours of humour. Above all, he provides limitless enthusiasm towards my academic success and only thinks of the positive outcomes with respect to my goals. To my wife Melissa, I thank you for listening to my long-winded scientific problems and for constantly supporting my quest for knowledge. You are always there when I need you the most, thank you. I also appreciate Tatem and Hope for giving me the chance to live a well-rounded, family life. To my future son or daughter, thank you for the many kicks and the wave you gave me in the ultrasound; I cannot wait to meet you, hope this thesis makes you proud. I also have to mention my late Babcia and Dziadzia, they would have been proud to see this day and I miss them very much. Concluding, I have to thank the Kondakow's (Mickey, Louise, Megan and especially Mike for all the PYT concerts), the extended Hladyniuk family (Myron, Mary, Rose, Julie et al.) and my new, ever-growing family from Melissa.

Table of Contents

List of Tables

List of Figures

List of Appendices

Chapter 1

1 Introduction

1.1 Overview

The glacial history of the Laurentian Great Lakes (Fig. 1.1), and its relationship to global climatic and environmental changes, have been studied since the early 1900s. In particular, it has been suggested that meltwater from the ablating Laurentide Ice Sheet (LIS) was routed through the Great Lakes to the Atlantic Ocean, weakening thermohaline circulation (THC) in the Atlantic Meridional Overturning Circulation (AMOC) and triggering the Younger Dryas (YD) cooling event at ~12,900 cal [11,020 ^{14}C] BP (Teller, 1985; Broecker et al., 1989; Teller, 1990; Teller, 1995). This proposed history has been the subject of considerable debate over the past several decades (Fritz et al., 1975; Lewis et al., 1994; Rea et al., 1994; Fisher and Lowell, 2006; Cronin et al., 2008; Fisher et al., 2009; Murton et al., 2010; Teller, 2013). As such, there remains much to be investigated in the Great Lakes region to determine the specific timing and extent of meltwater contributions to each lake. The presence of glacial meltwater in the Great Lakes can be identified using proxies such as the oxygen isotopic composition of shelly fauna preserved in lake sediments. Lake Ontario – the focus of this thesis – is located at the end of the Great Lakes chain-of-lakes, and hence provides a unique opportunity to pinpoint meltwater passage from the lower Great Lakes to the Atlantic Ocean.

Lake Ontario sediments also contain organic matter (OM) proxies that offer an opportunity to investigate how post-glacial Lake Ontario responded to varying climate conditions since the end of the Pleistocene at 11,700 cal [10,100 ^{14}C] BP. Hydrologic closure of Lake Ontario began at 12,300 cal [10,400 ^{14}C] BP and was caused in large part by the routing of the upper Great Lakes through the North Bay outlet, bypassing Lake Erie and Lake Ontario (Anderson and Lewis, 2012). Hydrologic closure meaning the lake basin operated as a closed basin with no outlets as used by Anderson and Lewis (2012). During the ~4,000 years of hydrologic closure, southern Ontario's climate has been described as cold and dry (Edwards et al., 1996; Anderson and Lewis, 2012). Regional warming and increased precipitation, under still dry conditions, then caused

Figure 1.1. Satellite maps of the Laurentian Great Lakes (red circle). Figure modified from Google maps (http://www.google.com/maps).

Lake Ontario to return to overflow conditions at ~8,300 cal [7,500 ^{14}C] BP (Edwards et al., 1996; Anderson and Lewis, 2012). Continual warming and still wetter conditions developed by ~6,800 cal BP and with the return of upper Great Lakes drainage during the Nipissing rise at ~5,800 cal BP, Lake Ontario water levels rose abruptly by ~10 m, followed by a more gradual increase to near present levels by 3,000 cal [2,890 ^{14}C] BP (Edwards et al., 1996; Anderson and Lewis, 2012). Lake Ontario's ecological/environmental response to these shifting climatic conditions and water levels, as recorded in OM, has been examined in only a few previous studies (Silliman et al., 1996; McFadden et al., 2004; 2005). A more detailed historical baseline for Lake Ontario's response to changing climatic conditions should provide a useful frame of reference for anticipating the consequences of future climate change. In particular, OM in Lake Ontario sediments should contain a biochemical record of (i) its source (e.g., terrestrial or lacustrine), (ii) changes in primary production within the lake, and (iii) variations in allochthonous versus autochthonous OM contributions in response to shifting environmental conditions.

Previous studies on bulk chemical and isotopic analysis of OM by itself, however, is not always suitable for discrimination among the types of OM present, or its terrestrial versus lacustrine sources, especially in glacio-lacustrine deposits (Hyodo and Longstaffe, 2011). A multi-proxy approach, combining compound-specific measurements of lipid biomarkers such as *n*-alkanes with more traditional bulk OM analysis, allows for more accurate assessment of primary lacustrine productivity and terrestrial allochthonous inputs. A few previous studies of Lake Ontario have begun such work (Silliman et al., 1996; McFadden et al., 2004; 2005), and that approach is expanded upon here.

1.2 Research questions

This thesis investigates hydrologic, environmental and climatic changes recorded in Lake Ontario sediments since the late Pleistocene, in order to assess the impact of natural variability on the lacustrine–terrestrial system. A special effort is made to compare traditional lacustrine productivity proxies, such as bulk OM chemical and isotopic measurements, with compound-specific OM analysis. This approach is necessary in

order to identify changes in lacustrine productivity versus terrestrial OM inputs under varying environmental conditions – within the broader framework of regional and global climate change. One part of this thesis determines the timing and extent of glacial meltwater movement through Lake Ontario. As mentioned earlier, discharge to the Atlantic Ocean from glacial Lake Agassiz and other large proglacial lakes via the Great Lakes is posited to have disrupted THC (Fig. 1.2) and caused the YD (Broecker et al., 1989). More recent research, however, suggests that the meltwater entered the Arctic Ocean mostly through a northwestern outlet (Murton et al., 2010). Still other researchers suggest that Glacial Lake Agassiz evaporated rather than drained into either ocean (Fisher and Lowell, 2012; Lowell et al., 2013). Within this conceptual context, the timing and extent of glacial meltwater input into Lake Ontario, which sits at the end of the Great Lakes chain-of-lakes, has not yet been fully evaluated. Filling this knowledge gap provided my first research question:

(1) Does the timing of glacial meltwater input into Lake Ontario correlate with the onset of the YD and was the extent of meltwater input to Lake Ontario – if transported to the Atlantic Ocean – sufficient to cause changes to the THC?

To make this assessment, I used the oxygen-isotope compositions of ostracode valves and clam shells from three 18 meter Lake Ontario sediment cores as proxies for meltwater input to Lake Ontario and its precursors. Samples from the same cores were used for additional analyses, as summarized below.

The second facet of this thesis involves determining the sources of dissolved inorganic carbon (DIC) in ancestral Lake Ontario and the relative contributions of allochthonous and autochthonous OM to its sediments. This has been accomplished by addressing two research questions. The second research question was:

(2) How did the carbon isotopic composition of DIC and the bulk chemistry and isotopic composition of OM in Lake Ontario vary throughout its history and do these variations record changes in source inputs and in-lake productivity?

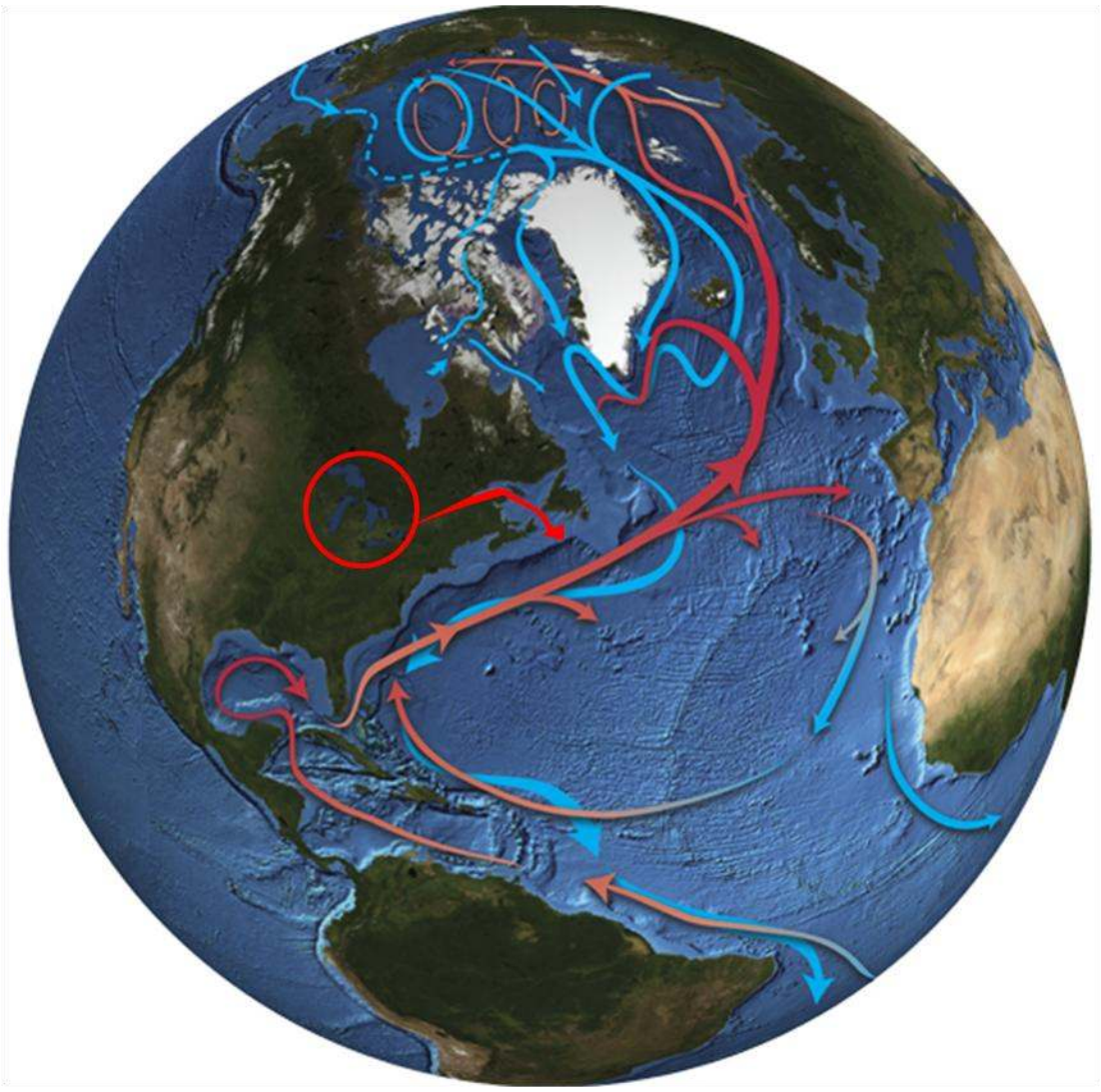

Figure 1.2. Thermohaline circulation (THC) in the Atlantic and Arctic Oceans. Warmer surface currents (red) and colder deep currents (blue) strongly influence Earth's climate. The Great Lakes (circled red) presently drain northeastward (red arrow) into the Atlantic Ocean at a critical location where the warm current transports heat (and salt) northward into the Nordic seas between Greenland and Norway and the Labrador Sea where convection processes (THC) occur. The northward-flowing warm surface current and returning deep cold current constitute the Atlantic Meridional Overturning Circulation (AMOC). Rapid outflows of freshwater from impoundments of meltwater during deglaciation of North America are thought to have diluted the warm salty surface current sufficiently to prevent sinkage (convection) during winter cooling in the north Atlantic and to have slowed THC and AMOC ~12,900-11,500 cal BP. The slowdown in convection is thought to have diverted the warm current eastward, thereby slowing northward transport of heat and inducing the YD cold event. Figure modified from Dickson and Dye (2007).

To assess changes in the DIC pool, I have used the carbon-isotope composition of ostracode valves and clam shells. To assess changes in OM sources and productivity, I have used traditional proxies, which include bulk OM carbon and nitrogen abundances and C/N ratios, and bulk OM carbon- and nitrogen-isotope compositions. The traditional proxies, however, returned results that did not allow increasing/decreasing primary productivity to be distinguished unambiguously from terrestrial input, particularly for the late Pleistocene glacial sediments. This provided my third research question:

(3) Can the abundances and compound-specific carbon-isotope compositions of *n*-alkanes be used to discriminate between various terrestrial OM sources and lacustrine productivity in Lake Ontario, and does this record reflect regional hydrologic, climatic and environmental changes in the region?

1.3 Research context

1.3.1 Quaternary history of the Great Lakes basin

Much of present-day eastern Canada and United States was covered by Wisconsinan Ice during the Last Glacial Maximum (Fig. 1.3), which peaked at 24,000 cal [20,000 ^{14}C] BP (Larson and Schaetzl, 2001). Numerous proglacial lakes formed along the edge of the LIS as ice retreated. The LIS controlled much of the volume and morphology of the proglacial lakes by impounding drainage outlets. At the time of deglaciation, there were six Laurentian Great Lakes (Lake Agassiz, Lake Superior, Lake Huron, Lake Michigan, Lake Erie and Lake Ontario). These lakes, from Lake Agassiz in the northwest to Lake Ontario in the southeast, linked together the drainage of more than half of North America (Teller, 1985; 1987).

Of most importance to this thesis is the Quaternary history of the Lake Ontario region. The Lake Ontario basin lies 200-300 km north of the maximum southern extent of the LIS (Hutchinson et al., 1993). Ancestral Lake Ontario was largely ice-free during the Mackinaw interstadial (16,000-15,300 cal [13,140-12,975 ^{14}C] BP) (Muller and Prest 1985; Barnett, 1992). The retreat of the ice also allowed Lake Ypsilanti (occupying the Lake Erie basin) to flow into ancestral Lake Ontario. Ancestral Lake Ontario's outlet

Figure 1.3. Maximum extent (~24,000 cal [20,000 ^{14}C] BP) of the Laurentide Ice Sheet (LIS) in North America. The Great Lakes are circled in red. Figure modified from the National Science Foundation website (http://www.nsf.gov).

was located in the southeastern portion of the lake, where upstream flow from Lake Ypsilanti continued eastward through the Lake Ontario Basin and drained through the Mohawk River Valley to the Atlantic Ocean. The connectivity between the Ontario and Erie basins was truncated when ice readvanced at 15,300 cal [12,975 ^{14}C] BP. For ~ 800 years, the Ontario lobe of the LIS completely covered the Lake Ontario basin and forced the newly formed Lake Whittlesey, which occupied the Erie basin, to flow westward toward present-day Lake Michigan.

The Lake Ontario basin became ice-free again at ~14,500 cal [12,400 ^{14}C] BP when the LIS retreated northward. The LIS impounded the St. Lawrence valley allowing water to rise in the Lake Ontario basin. The proglacial lake occupying the Lake Ontario basin at that time is called glacial Lake Iroquois. Glacial Lake Iroquois was the largest proglacial lake to occupy the Lake Ontario basin. At its maximum, water levels rose to ~35 (west) to 115 (east) m above present-day Lake Ontario (Coakley and Karrow, 1994; Anderson and Lewis, 2012). Drainage of glacial Lake Iroquois occurred at Rome, New York (Mohawk River valley), which connected to the Atlantic Ocean via the Hudson River valleys further east. From 14,500 to 13,260 cal [12,400-11,350 ^{14}C] BP glacial Lake Iroquois received water directly from the LIS and from upstream Glacial Lake Algonquin through the Fenelon Falls outlet to the north. Shortly thereafter, the LIS retreated further north, out of the St. Lawrence River valley, opening a new outlet for Lake Ontario. During this period, glacial Lake Iroquois lake levels fell through a series of lake phases: Frontenac, Sydney '?', Belleville-Sandy Creek and Trenton-Skinner Creek (Anderson and Lewis, 2012). The latter two lake phases in the Lake Ontario basin were confluent with the Fort-Ann phase of Lake Vermont, which occupied the Lake Champlain basin further east (Anderson and Lewis, 2012). The entire confluent water body flowed into the Atlantic Ocean via the Hudson River valley.

Continued retreat of the LIS at 12,900 cal [11,000 ^{14}C] BP caused Lake Trenton to drain to the early Lake Ontario level (Anderson and Lewis, 2012). At the same time, marine water invaded the St. Lawrence River valley to the east to form the Champlain Sea. Confluence between the Champlain Sea and early Lake Ontario was maintained as both

sea level rise and isostatic uplift of Lake Ontario occurred at nearly the same rate (Anderson and Lewis, 2012). Early Lake Ontario received meltwater from upstream sources (glacial Lake Algonquin) during this time period, which likely inhibited marine invasion by forcing water out of the basin. Closed basin conditions ensued shortly after 12,300 cal [10,400 ^{14}C] BP in Lake Ontario when upstream glacial Lake Algonquin switched its drainage pattern to new outlets at North Bay, which was produced by isostatic depression and ice retreat (Eschman and Karrow, 1985). This change, coupled with increased evaporation and decreased precipitation under cold and dry climatic conditions, caused Lake Ontario to fall below its outlet at the St. Lawrence River (Edwards et al., 1996; Anderson and Lewis, 2012). Hydrologic closure and associated low water levels lasted until 8,300 cal [7,500 ^{14}C] BP when increased precipitation once again allowed Lake Ontario to overflow its outlet. Connectivity with the upper Great Lakes was reestablished during the Nipissing rise when overflow was fully transferred from the North Bay outlet to the southern outlets at Port Huron-Sarnia (southern Lake Huron) and Chicago (southern Lake Michigan); the Nipissing rise peaked from 6,300 to 5,200 cal [5,500-4,500 ^{14}C] BP (Anderson and Lewis, 2012). Drainage was diverted entirely to the Port Huron-Sarnia outlet by ~4,200 [3,800^{14}C] cal BP (Larsen, 1985). Lake Ontario then continued to rise towards present-day levels under the re-established conditions of Upper Great Lake connectivity and increased precipitation in southern Ontario.

1.3.2 Limnology and stable isotope geochemistry

Changes in aquatic ecosystems are caused by changes in climatic and environmental conditions. Lakes function as natural traps for sediments and have the ability to preserve materials (proxies) whose physical, chemical and/or isotopic compositions can be used to deduce previous environmental conditions. Paleolimnology focuses on the interpretation of such sedimentary records and the processes that create and modify them (Wetzel, 2001). Paleolimnology follows the dictum that “the present is the key to past”. Changes in the proxy records that can be related to climatic or other environmental/ecological parameters can also provide a helpful basis for predictions of future behaviour.

Stable isotope limnology has become an essential part of climatic and environmental reconstructions over the last few decades, contributing significantly to our understanding of how lake-climate systems respond to environmental stressors. Advances in modern technology have allowed for cost-effective analysis of small samples of proxy materials using devices such as elemental analyzers and Multiprep autosamplers in which carbon-, nitrogen-, oxygen- and hydrogen-bearing gases characteristic of the sample are produced and then delivered to other instruments for chemical and isotopic measurements. This thesis uses this analytical approach to evaluate ancient climatic and environmental conditions, as reflected by proxy materials preserved in Lake Ontario sediments.

Biogenic carbonates (ostracodes and clams) are proxies that provide important information about environmental conditions through their oxygen isotopic compositions. The oxygen-isotope composition of a biogenic carbonate is a function of water temperature, the oxygen-isotope composition of the water at the time of shell formation and isotopic vital effects exerted by the species (see Chapter 2). Lakewater oxygen-isotope compositions depend on latitude, altitude, precipitation, temperature, relative humidity and regional watershed (see Chapter 2). Within this broader framework, the oxygen-isotope composition of biogenic carbonates can thus provide insight into changes in hydrological conditions within the Great Lakes region. This is of particular importance when assessing the timing and extent of glacial meltwater presence in Lake Ontario. The carbon-isotope composition of biogenic carbonates can be used to assess the DIC pool within the lake. Although the DIC system is complex in lacustrine environments (see Chapter 3), the carbon-isotope compositions of biogenic carbonates are a direct measure of the DIC pool, and thus can serve as a robust proxy for assessing changes in source inputs throughout the lakes history.

In the general case, OM in sediments can be used as a proxy for terrestrial versus lacustrine input to lakes through its C/N ratio. The carbon- and nitrogen-isotope compositions of OM are likewise useful for measuring changes in primary lacustrine productivity as well as the sources of OM delivered to the lake (see Chapter 3). However, glacial processes, complex mixing of varied OM sources, and degradation of OM can introduce ambiguity when interpreting data for bulk OM proxies (Hyodo and

Longstaffe, 2011). Compound-specific measurements of (plant) macromolecules offer one way to see through this complexity. In particular, the presence of certain *n*-alkanes has proven useful in distinguishing the origin (and type) of plant species entering a lake. For example, C_{17} and C_{19} *n*-alkanes are typical of algal OM whereas $\geq C_{27}$ *n*-alkanes are typical of higher terrestrial plants (see Chapter 4) (Eglinton and Hamilton, 1967; Rieley et al., 1991). In addition, the compound-specific carbon-isotope composition of individual *n*-alkanes can provide more detailed insight into the carbon sources, stresses and productivity of different plant categories (algal, aquatic, terrestrial) within a mixed OM assemblage (see Chapter 4). This approach can help to avoid some pitfalls (perplexing C/N ratios) associated with interpreting traditional OM chemical and isotopic proxy data, particularly in the glacio-lacustrine sediments of the Great Lakes.

1.3.3 Study area- Lake Ontario

Lake Ontario (Fig. 1.4) is the smallest in surface area (slightly less than 19,500 km^2) of the five existing Laurentian Great Lakes. It measures ~290 km long by ~85 km wide at its widest point and has a maximum water depth of 244 m deep (McFadden et al., 2005). Lake Ontario shares an international border between Canada (Ontario) and the United States of America (New York).

Lake Ontario's watershed is bounded by the Canadian Shield to the north, the Allegheny Plateau to the south, the Niagara Escarpment to the southwest and west, and the Adirondack Plateau to the east (Hutchinson et al., 1993). The Lake Ontario basin (bedrock) consists of Upper Ordovician shale and limestone, contained within a succession of Cambrian to Carboniferous sedimentary rocks that thickens southward into the Appalachian basin (Fig. 1.5) (Hutchinson et al., 1993). At the north and east end of the lake, these sedimentary rocks unconformably overlie the meta-igneous and meta-sedimentary rocks of the Grenville Province of the Canadian Shield (Fig. 1.5) (Hutchinson et al., 1993). Two bathymetric ridges (Whitby-Olcott (west) and Scotch Bonnet (east)) subdivide Lake Ontario into three main basins: Niagara (west), Mississauga (central) and Rochester (east). Major water inflow is dominated by the Niagara River in the southwest. It delivers (via Lake Erie) upper Great Lake water to Lake Ontario, which then exits eastward through the St. Lawrence River, presently Lake

Ontario's major outlet. The warm monomictic lake thermally stratifies once per year and has an average water residence time of ~8 years (McFadden et al., 2005).

The mean annual precipitation from 1996 to 2011, as recorded by the Burlington and Point Petre precipitation stations on the northern shore of Lake Ontario, averages 952 mm (Longstaffe et al., 2011). The average annual air temperature recorded by these stations is ~8 °C. From 1996 to 2011, Lake Ontario regional precipitation had an average oxygen- isotope composition of –8.5 ‰ (VSMOW) whereas the average lakewater had an oxygen-isotope composition of –6.6 ‰ (VSMOW) (Longstaffe et al., 2011).

1.3.4 Research Sample

In July 2008, three sediment cores were obtained from Lake Ontario by the Canadian Coast Guard Ship (CCGS) *Limnos* on cruise number 2008-00-004. On July 15, 2008, Core 1335 was obtained from the Mississauga basin (location, 43°33'10"N 78°09'04"W; water depth, 192.0 m; core length, 18.30 m). The next day, July 16, 2008, Core 1336 was obtained from the Rochester basin (location, 43°30'28"N 76°53'57"W; water depth, 221.5 m; core length, 18.41 m). Piston Core 1334 was obtained on July 17, 2008 from the Niagara basin (location, 43°24'21"N 79°00'08"W; water depth, 110.30 m; core length, 16.00 m) (Fig. 1.4). Associated benthos cores (~1 m in length), which captured the sediment-water interface, were also obtained from each site. All cores were cut into ~1 m sections on board the CCGS *Limnos* and stored vertically in a refrigerator at 4°C. These locations were chosen for coring because they are located in the deepest portions of Lake Ontario. These locations also allow for spatial comparisons across Lake Ontario from west to east. It was anticipated from preexisting geophysical studies that core from these locations would recover the complete Holocene history of sedimentation and perhaps also capture some sediments of Pleistocene age.

1.4 Structure of the dissertation

This thesis is divided into three main chapters, in addition to the introductory and concluding chapters (1 and 5, respectively). Chapter 2 investigates the timing and extent of glacial meltwater input into ancestral Lake Ontario. Meltwater contributions are

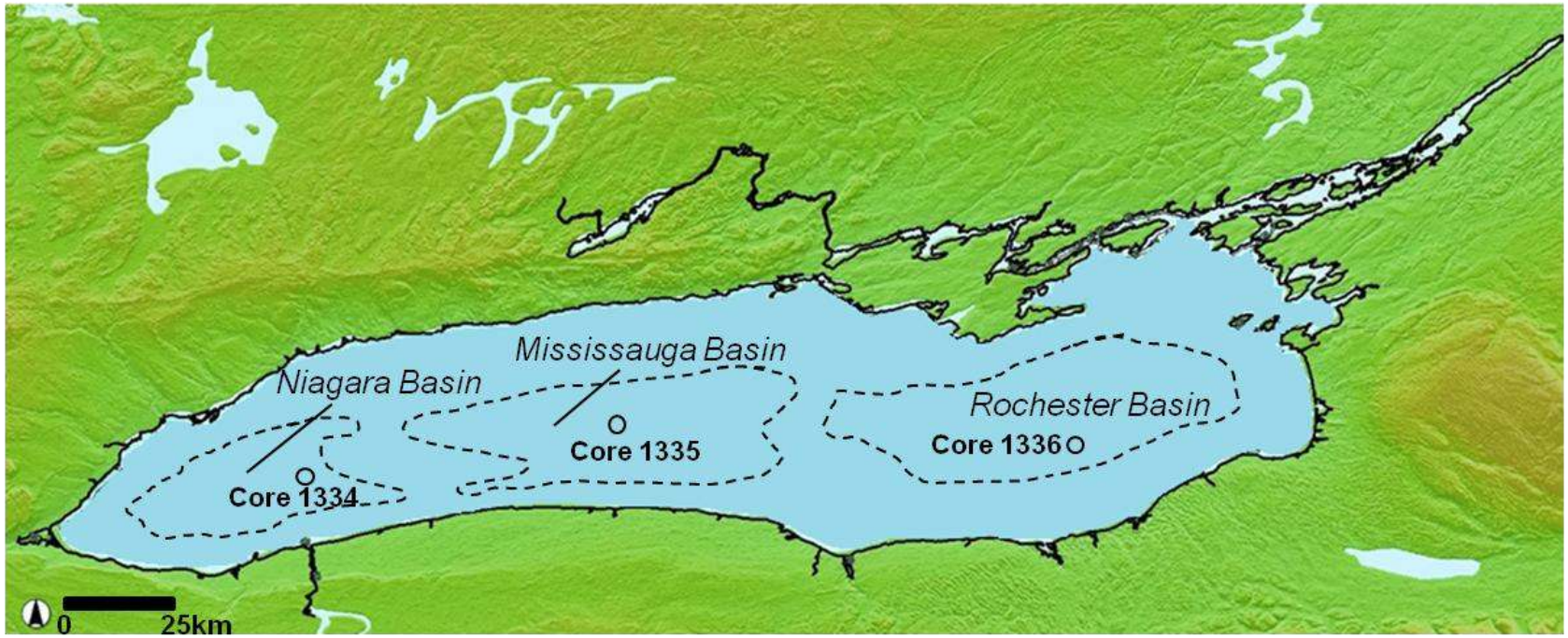

Figure 1.4. DEM of Lake Ontario. Core locations are denoted by circles and labeled respectively. Figure modified from the National Oceanic and Atmospheric Administration data center website (http://ngdc.noaa.gov/mgg/dem/).

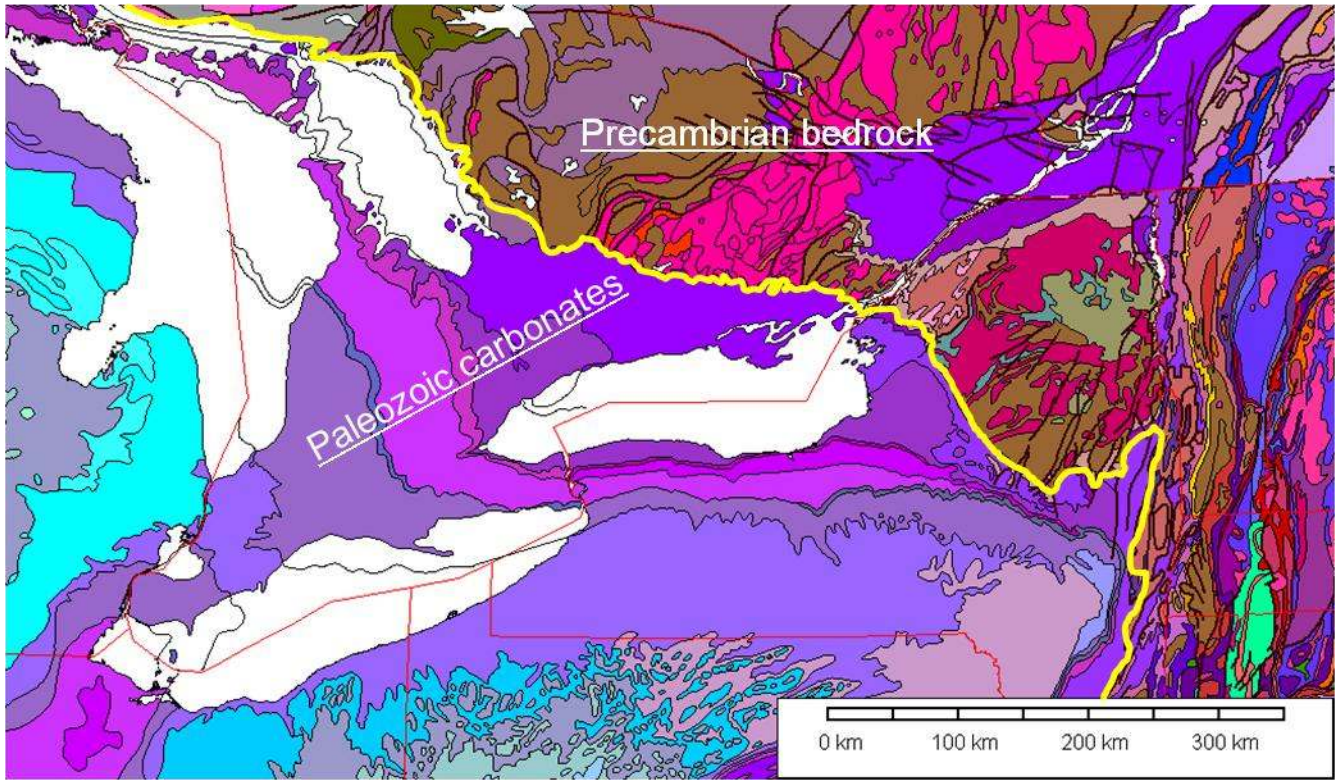

Figure 1.5. Geological map of southern Ontario. The yellow line defines the boundary between Paleozoic carbonates (to the southwest) and Precambrian bedrock (to the north). Lake Ontario's watershed contains both types of regional geology. Figure modified from Wheeler et al. (1997).

evaluated using the oxygen-isotope composition of biogenic carbonates (ostracode valves and clam shells). Spatial and temporal correlations are made across Lake Ontario using Cores 1334 (west), 1335 (central) and 1336 (east). The oxygen-isotope results are supplemented by mineralogical, grain size and ostracode assemblage data for the sediments of each core. Variations in ancient Lake Ontario's oxygen-isotope composition are compared with upstream source inputs (glacial Lakes Algonquin and Agassiz) and downstream outputs (Lake Vermont and the Champlain Sea). Lake Ontario's oxygen-isotope record is also compared with Greenland Ice Sheet ice core data to test for any matching meltwater signal.

Chapter 3 evaluates variations in primary lacustrine OM productivity and terrestrial OM inputs into Lake Ontario since the late Pleistocene. Traditional proxies including total organic carbon and nitrogen abundances, C/N ratios and the carbon- and nitrogen-isotope composition of bulk OM are used along with the carbon-isotope composition of ostracode valves to determine paleoproductivity. The carbon-isotope composition of ostracodes is also used to determine the sources of DIC in Lake Ontario, and how and why they varied temporally and spatially.

Chapter 4 compares results for the traditional lacustrine proxies, as described in Chapter 3, with *n*-alkane distributions and individual *n*-alkane carbon isotopic compositions. The *n*-alkane data are then used to refine and advance earlier work on organic matter sources and primary lacustrine productivity in ancestral Lake Ontario.

Several appendices are provided that supply supplementary information: (A1) core descriptions and images; (A2) isotopic standards, (A3) grain-size analysis; (A4) mineralogy; (A5) biogenic carbonate isotopic data; (A6) bulk OM chemical and isotopic compositions; (A7) n-alkane abundances and carbon-isotope compositions, and (A8) *n*-alkane gas-chromatograms.

1.5 References

Anderson, T.W., Lewis, C.F.M., 2012. A new water-level history for Lake Ontario basin:evidence for a climate-driven early Holocene lowstand. Journal of Paleolimology 47, 513–530.

Barnett, P.J., 1992. Quaternary geology of Ontario. in: Thurson, P.C., Williams, H.R., Sutcliffe, R.H., Stott, G.M., (Eds.), Geology of Ontario. Ontario Geological Survey Special Volume 4 (part 2), pp.1011–1088.

Broecker, W.S., Kennett, J.T., Flower, B.P., Teller, J.T., Trumbore, S., Bonani, G.,Wolfli, W., 1989. Routing of meltwater from the Laurentide Ice Sheet during the Younger Dryas cold episode. Nature 341, 318–320.

Coakley, J.P., Karrow, P.F., 1994. Reconstruction of post-Iroquois shoreline evolution in western Lake Ontario. Canadian Journal of Earth Sciences 31, 1618–1629.

Cronin, T.M., Manley, P.L., Brachfeld, S., Manley, T.O., Willard, D.A., Guilbault, J.P.,Rayburn, J.A., Thunell, R., Berke, M., 2008. Impacts of post-glacial lake drainage events and revised chronology of the Champlain Sea episode 13–9 ka. Palaeogeography, Palaeoclimatology, Palaeoecology 262, 46–60.

Dickson, B., Dye, S., 2007. Interrogating the "Great Ocean Conveyor". Oceanus Magazine.

Edwards, T.W.D., Wolfe, B.B., MacDonald, G.M., 1996. Influence of changing atmospheric circulation on precipitation δ18O–temperature relations in Canada during the Holocene. Quaternary Research 46, 211–218.

Eglinton, G., Hamilton, R.J., 1967. Leaf epicuticular waxes. Science 156, 1322–1335.

Eschman, D.F., Karrow, P.F., 1985. Huron basin glacial lakes: a review. in: Karrow, P.F., Calkin, P.E., (Eds.), Quaternary Evolution of the Great Lakes. Geological Association of Canada Special Paper 30, pp. 79–93.

Fisher, T.G., Waterson, N., Lowell, T.V., Hajdas, I., 2009. Deglaciation ages and meltwater routing in the Fort McMurray region, northeastern Alberta and northwestern Saskatchewan, Canada. Quaternary Science Reviews 28, 1608–1624.

Fisher, T.G., Lowell, T.V., 2006. Questioning the age of the Moorhead Phase in the glacial Lake Agassiz basin. Quaternary Science Reviews 25, 2688–2691.

Fritz, P., Anderson T.W., Lewis C.F.M., 1975. Late Quaternary climate trends and history of Lake Erie from stable isotope studies. Science 190, 267–269.

Google maps website (2014). Retrieved June 2, 2014 from http://www.google.ca/maps

Hutchinson, D.R., Lewis, C.F.M., Hund, G.E., 1993. Regional stratigraphic framework of surficial sediments and bedrock beneath Lake Ontario. Géographie physique et Quaternaire 47, 337–352.

Hyodo, A., Longstaffe, F.J., 2011. The palaeoproductivity of ancient Lake Superior. Quaternary Science Reviews 30, 2988–3000.

Larsen, C.E., 1985. Lake level, uplift, and outlet incision, The Nipissing and Algoma Great Lakes. in: Karrow, P.F., Calkin, P.E., (Eds.), Quaternary Evolution of the Great Lakes. Geological Association of Canada Special Paper 30, pp. 79–93.

Larson, G., Schaetzl, R., 2001. Origin and evolution of the Great Lakes. Journal of Great Lakes Research 27, 518–546.

Lewis, C.F.M., Moore Jr, T.C., Rea, D.K., Dettman, D.L., Smith, A.M., Mayer, L.A., 1994. Lakes of the Huron basin: their record of runoff from the Laurentide Ice Sheet. Quaternary Science Reviews 13, 891–922.

Longstaffe, F.J., Ayalon, A., Bumstead, N.L., Crowe, A.S., Hladyniuk, R., Hornibrook, P.A., Hyodo, A., Macdonald, R.A., 2011. The oxygen-isotope evolution of the North American Great Lakes. Northeastern (46th Annual) and North-Central (45th Annual) Joint Meeting of the Geological Society of America, Pittsburgh, Pennsylvania, USA, March 20-22, 2011, p. 57.

Lowell, T.V., Applegate, P.J., Fisher, T.G., Lepper, K., 2013. What caused the low-water phase of glacial Lake Agassiz? Quaternary Research 80, 370–382.

McFadden, M.A., Mullins, H.T., Patterson, W.P., Anderson, W.T., 2004. Paleoproductivity of eastern Lake Ontario over the past 10,000 years. Limnology and Oceanography 49, 1570–1581.

McFadden, M.A., Patterson, W.P., Mullins, H.T., Anderson, W.T., 2005. Multi-proxy approach to long-and short-term Holocene climate-change: evidence from eastern Lake Ontario. Journal of Paleolimnology 33, 371–391.

Muller, E.H., Prest, V.K., 1985. Glacial lakes in the Ontario basin. in: Karrow, P.F., Calkin, P.E., (Eds.), Quaternary Evolution of the Great Lakes. Geological Association of Canada Special Paper 30, pp.213–229.

Murton, J.B., Bateman, M.D., Dallimore, S.R., Teller, J.T., Yang, Z., 2010. Identification of Younger Dryas outburst flood path from Lake Agassiz to the Arctic Ocean. Nature 464, 740–743.

National Oceanic and Atmospheric Administration Digital Elevation Model (DEM) Discovery Portal website (2014). Retrieved June 2, 2014 from http://ngdc.noaa.gov/mgg/dem

National Science Foundation website (2014). Retrieved June 2, 2014 from http://www.nsf.gov

Rea, D.K., Moore Jr, T.C., Lewis, C.F.M., Mayer, L.A., Dettman, D.L., Smith, A.J., Dobson, D.M., 1994. Stratigraphy and paleolimnologic record of lower Holocene sediments in northern Lake Huron and Georgian Bay. Canadian Journal of Earth Sciences 31, 1586–1605.

Rieley, G., Collier, R.J., Jones, D.M., Eglinton, G., Eakin, P.A., Fallick, A.E., 1991. Sources of sedimentary lipids deduced from stable carbon-isotope analyses of individual compounds. Nature 352, 425–427.

Silliman, J.E., Meyers, P.A., Bourbonniere, R.A., 1996. Record of postglacial organic matter delivery and burial in sediments of Lake Ontario. Organic Geochemistry 24, 463–472.

Teller, J.T., 1985. Glacial Lake Agassiz and its influence on the Great Lakes, in: Karrow, P.F., Calkin, P.E., (Eds.), Quaternary Evolution of the Great Lakes. Geological Association of Canada Special Paper 30, pp.1–17.

Teller, J.T., 1987. Proglacial lakes and the southern margin of the Laurentide Ice Sheet, in: Ruddiman, W.F., Wright, H.E., (Eds.), North America and the Adjacent Oceans during the Last Deglaciation. Geological Society of America, The Geology of North America K-3, pp. 39–69.

Teller, J.T., 1990. Volume and routing of late glacial runoff from the southern Laurentide Ice Sheet. Quaternary Research 34, 12–23.

Teller, J.T., 1995. History and drainage of large ice-dammed lakes along the Laurentide Ice Sheet. Quaternary International 28, 83–92.

Teller, J.T., 2013. Lake Agassiz during the Younger Dryas. Quaternary Research 80, 361–369.

Wheeler, J.O., Hoffman, P.F., Card, K.D., Davidson, A., Sanford, B.V., Okulitch, A.V., and Roest, W.R. (comp.) 1997: Geological Map of Canada, Geological Survey of Canada, Map D1860A.

Wetzel, R.G., 2001. Limnology Lake and River Ecosystems, Third ed. Academic Press.

Chapter 2

2 The oxygen-isotope composition of ancient Lake Ontario

2.1 Introduction

The timing and volume of glacial meltwater outbursts from large glacial lakes in North America are crucial to understanding their potential role in initiating and/or enhancing climatic changes such as the Younger Dryas (YD), Pre-boreal Oscillation (PBO) and 8.2 ka events. In particular, it has been proposed that the onset of the YD (12,900 cal (calibrated years) [11,020 ^{14}C (radiocarbon)] BP was caused by a change in meltwater routing of glacial Lake Agassiz from a southern, Mississippi River outlet to an eastern outlet through the Great Lakes (Broecker et al., 1989) (Fig. 2.1). In this scenario, meltwater entering the North Atlantic Ocean via the St. Lawrence River suppressed an already weakened thermohaline circulation (THC) causing an abrupt change in global climate (Broecker et al., 1989). However, the lack of geomorphologic evidence such as flood deposits and down cut channels for an eastward routing of glacial Lake Agassiz has caused researchers to look for alternate pathways (Teller et al., 2005; Fisher and Lowell, 2006; Voytek et al., 2012). Identification of gravels and regional erosion surfaces throughout the Mackenzie River system led to the suggestion that glacial Lake Agassiz drained through a northwest outlet into the Arctic Ocean at the start of the YD (Murton et al., 2010; Condron and Winsor, 2012; Fahl and Stein, 2012). However, evidence concerning the position of ice margins and shorelines at this time caused Fisher and Lowell (2012) to reject the notion of glacial Lake Agassiz drainage via a northwest outlet during the YD. They noted that the Don's and Stony Mountain moraines prevented glacial Lake Agassiz meltwater from reaching the Clearwater-Athabasca Spillway and thus emptying into the Arctic Ocean. In short, the drainage history of glacial Lake Agassiz during the YD chronozone (12,900-11,700 cal [11,020-10,080 ^{14}C] BP) remains unclear.

Other large glacial lakes (Lake Algonquin and Lake Iroquois) also occupied the Great Lakes basin during the period of the YD. Their catastrophic drainage could also have contributed to suppression of the THC and aided in triggering the YD because of their

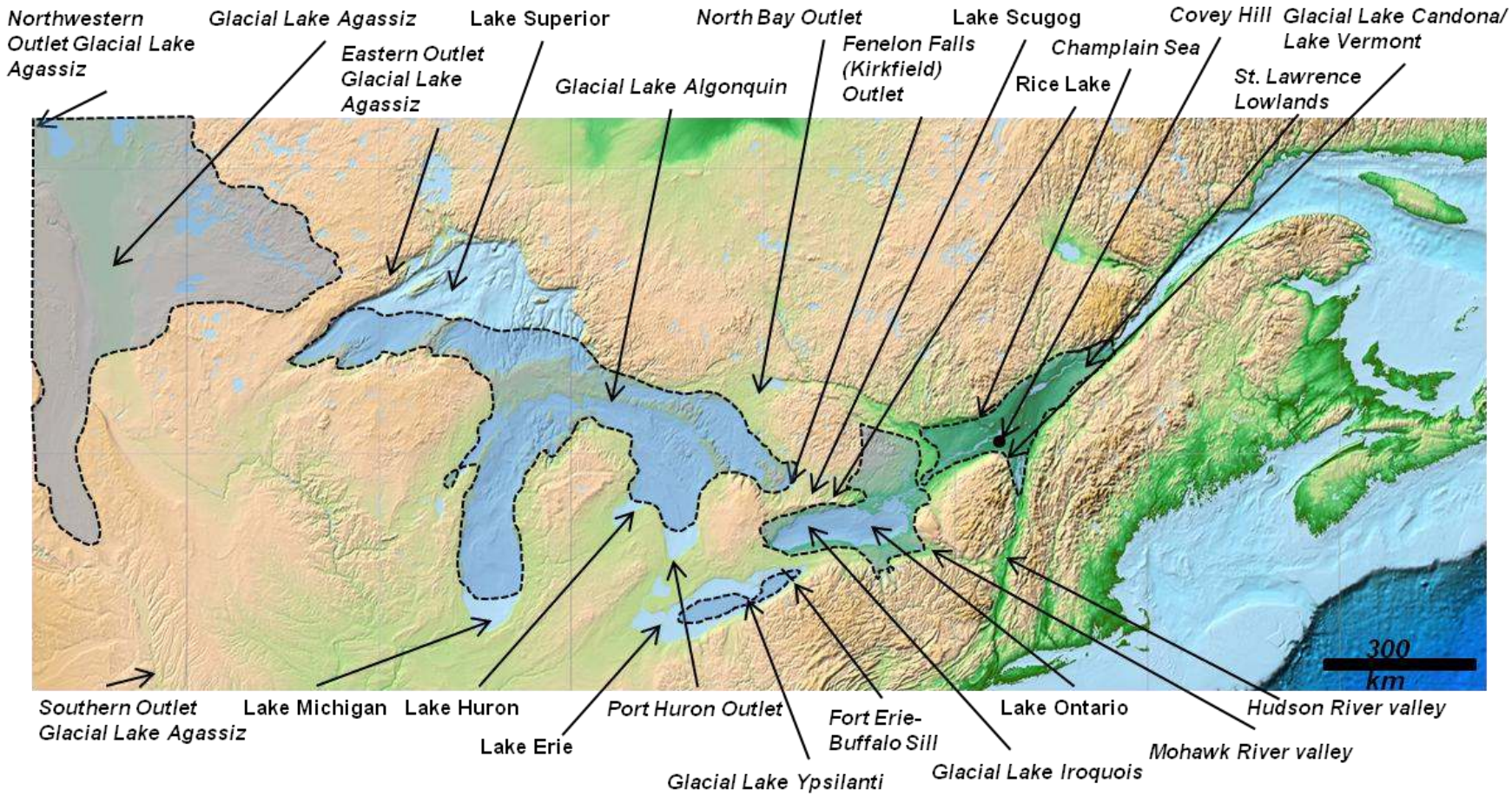

Figure 2.1. Digital Elevation Model (DEM) of the Great Lakes basin. Important outlets and locations are labeled. Figure modified from the National Oceanic and Atmospheric Administration data center website (http://ngdc.noaa.gov/mgg/dem/).

volume. Glacial lakes size and outlets were controlled by the retreating Laurentide Ice Sheet (LIS), ground topography and regional isostatic rebound. Lake Ontario sediments provide a special opportunity to revisit the timing and extent of eastward, glacial meltwater movement from various upstream sources (Fig. 2.1). With this objective in mind, we use the oxygen isotopic compositions of ostracodes valves and clam shells, together with sediment characteristics, to test for glacial meltwater contributions to Lake Ontario and its ancient equivalents since ~16,500 cal [~13,300 ^{14}C] BP. We also evaluate the role of this glacial meltwater in driving regional and/or global climate change during that time.

2.1.1 Oxygen-isotope compositions of ostracodes and clams

Environmental changes associated with deglaciation of the Ontario basin should be reflected in biostratigraphically recognizable faunal changes. Species emergence and changes in their populations, in particular, should provide a marker for variations in lake level and/or glacial meltwater input (Miller et al., 1985; Anderson and Lewis, 2012). Ostracode (*Candona subtriangulata* and *Fabaeformiscandona caudata*) and clam (*Pisidium* sp.) assemblages can be used for this purpose in Lake Ontario sediments. Increased productivity (as measured by the number of valves/shells per gram of sediment) should correlate with the absence of glacial meltwater (less turbidity) and more favourable climatic conditions. Lower lake levels during a period of increasing primary productivity could also favour an increased abundance of shallower water species of clams (Delorme, 1989).

The oxygen isotopic composition of biogenic calcium carbonate precipitated by ostracodes and clams ($\delta^{18}O_{carbonate}$) can provide detailed information about environmental conditions during their lifetimes. The $\delta^{18}O_{carbonate}$ values are determined by water temperature, water oxygen-isotope composition ($\delta^{18}O_{lakewater}$) and species-dependent isotopic vital effects at the time of shell formation (Holmes, 2001). The $\delta^{18}O_{lakewater}$ values reflect latitude- and altitude-dependent variations in $\delta^{18}O_{precipitation}$, watershed size, regional temperature and humidity (which regulate evaporation rates), groundwater input, glacial melting and lakewater residence time. Within this framework, biogenic

$\delta^{18}O_{carbonate}$ values can be used to infer changes in air-mass sources, hydrology and evaporation within the Great Lakes region (Fritz et al., 1975; Lewis and Anderson, 1992). Low values of biogenic $\delta^{18}O_{carbonate}$ (–18 ‰, VSMOW) in Lake Ontario, for example, are associated with a sizeable supply of glacial meltwater, whereas much higher values (–6 ‰) typically indicate more local recharge, warmer conditions, and/or increased evaporation (Yu et al., 1997). During glacial times, variations in ancient Lake Ontario $\delta^{18}O_{lakewater}$ values were largely determined by the balance between long-distance input of glacial meltwater and more local input from the watershed. When glacial meltwater input ended, variations in $\delta^{18}O_{lakewater}$ were more strongly controlled by regional climate conditions.

2.1.2 Sediment properties

Variations in the amount, grain-size and mineralogy of Lake Ontario sediments, together with the $\delta^{18}O_{carbonate}$ values of associated shelly fauna, carry information about the source(s), routing and transport energy of this detritus. Such data can be helpful in identifying glacial meltwater input via the Fenelon Falls (Kirkfield) versus the Port Huron outlets (Fig. 2.1) if differences existed between sediments transported using one versus the other route. Mineralogical and grain-size data are also useful for correlating lithological units and contacts among cores within the geophysical/seismic stratigraphic framework available for Lake Ontario sediments.

2.1.3 Late Quaternary history of the Ontario basin

The sediment record began with till deposition in the western half of the Ontario basin during retreat of the Port Huron ice lobe at ~16,500 cal [13,300 ^{14}C] BP (Hutchinson et al., 1993). Glaciolacustrine deposition began at ~14,000 cal [12,150 ^{14}C] BP when the LIS retreated northward, blocking the St. Lawrence River and impounding water in the Ontario basin. Glacial Lake Iroquois was formed and rose to ~35 (west) to 115 (east) m above present levels (Coakley and Karrow, 1994; Anderson and Lewis, 2012). Growth of glacial Lake Iroquois was regulated by drainage through the Rome Outlet to the Mohawk Valley, ultimately travelling to the Atlantic Ocean via the Hudson River valley

(Figs. 2.1, 2.2) (Muller and Prest, 1985). Continued retreat of the LIS also opened a gap at Covey Hill (Muller and Prest, 1985; Parent and Occhietti, 1988) (Fig. 2.1). This allowed glacial Lake Iroquois to expand eastward into the St. Lawrence valley, where it connected with glacial Lake Candona and glacial Lake Vermont (Fig. 2.1). Varved sediments containing *C. subtriangulata* characterize this time period in these localities.

Glacial Lake Iroquois and its successors persisted until ~13,000 cal [11,100 ^{14}C] BP, at which time further retreat of the LIS made eastward flow of the impounded water possible. Lake Iroquois' drawdown through several stages (Frontenac, Sydney '?', Belleville-Sandy Creek, Trenton-Skinner Creek) resulted finally in lake levels that were ~15 m above present lake level in the eastern section of the Ontario basin and below present levels in the west (Coakley and Karrow, 1994; Anderson and Lewis, 2012). The Belleville-Sandy Creek and Trenton-Skinner Creek lake levels were confluent with neighbouring Lake Vermont in the Champlain basin, which flowed to the Atlantic Ocean via the Hudson River valley (Rayburn et al., 2007; Anderson and Lewis, 2012) (Fig. 2.1). The last stage (Trenton), confluent with Lake Vermont and Lake Candona formed an extensive body of freshwater throughout the isostatically-depressed upper St. Lawrence River, Lake Champlain and lower Ottawa River valleys and the Lake Ontario basin (Parent and Occhietti, 1988; Rayburn et al., 2007). Additional ice retreat and removal of the ice dam from the lower St. Lawrence valley released this large volume of freshwater to the Gulf of St. Lawrence which was replaced with marine water of the Champlain Sea at ~13,000 cal [11,100 ^{14}C] BP (Richard and Occhietti, 2005; Rayburn et al., 2007). At this time early Lake Ontario was confluent with the Champlain Sea but eastward forcing of freshwater, aided by glacial meltwater input to Lake Ontario and perhaps isostatic rebound, are generally considered to have prevented invasion of saltwater into early Lake Ontario (Anderson and Lewis, 2012). A final pulse of glacial meltwater entered early Lake Ontario between ~13,000 cal [11,100 ^{14}C] BP and ~12,500 cal [10,500 ^{14}C] BP. This flow is postulated to include the discharge (overflow) (12,700 to 12,600 cal [10,800 to 10,650 ^{14}C] BP) of glacial Lake Algonquin (Fig. 2.1); the water is assumed to have travelled to Lake Ontario initially by a direct path via the Fenelon Falls outlet in the east and later by a circuitout route through glacial Lake Algonquin's Port Huron outlet in the west both by a more circuitous route through glacial Lake Algonquin's Port Huron Outlet

in the west (Figs. 2.1, 2.2) (Eschman and Karrow, 1985; Moore et al., 2000; Anderson and Lewis, 2012).

From 12,300-8,300 cal [(10,400-7,500 ^{14}C] BP, flow from the upper Great Lakes (Superior, Michigan, Huron) was diverted to the North Bay Outlet (Fig. 2.1), in response to isostatic rebound. The outflow then travelled onward via the Ottawa River valley system to the Atlantic Ocean. This rerouting led to hydrologic closure of the lower Great Lakes (Erie and Ontario) and Lake Ontario water levels dropped substantially – to the lowest level in its history (Lewis et al., 2012; Anderson and Lewis, 2012). Flow of upper Great Lakes water returned to the lower Great Lakes during the Nipissing rise at 5,800 cal [5,090 ^{14}C] BP. By then, isostatic rebound tilted the Lake Huron basin and lifted the North Bay outlet above the southern outlet at Port Huron, so glacial Lake Algonquin discharged via the Erie basin and Niagara River, and the Lake Ontario water surface began to ride towards present levels.

2.2 Materials and methods

Three piston cores and accompanying benthos cores (used for future studies) were collected from Lake Ontario during July 15-17, 2008 by the captain and crew of the Canadian Coast Guard Ship (CCGS) *Limnos*: Core 1335, Mississauga basin; Core 1336, Rochester basin, and Core 1334, Niagara basin (Fig. 2.2). The cores were cut into ~1 m sections onboard and stored in a refrigerator prior to delivery to the University of Rhode Island, where they were halved longitudinally and visible characteristics (colour, consistency, grain size, sedimentary structures including laminations) were noted (Appendix I). Sediment colour was described using the Munsell Soil Colour Charts and notation (2000). The cores were then shipped to the University of Western Ontario where they continue to be stored at 4°C.

A total of 219 ten-cm sections were extracted from the sampling half of the piston cores. The samples were wet-sieved using cold tap water and a combination of four sieve pans (1.00 mm, 500 μm, 250 μm, 125 μm) to recover ostracode valves and clam shells; visible organic matter was also collected. The air-dried fossil material was transferred into petri dishes, where the biogenic carbonates were identified and separated by species;

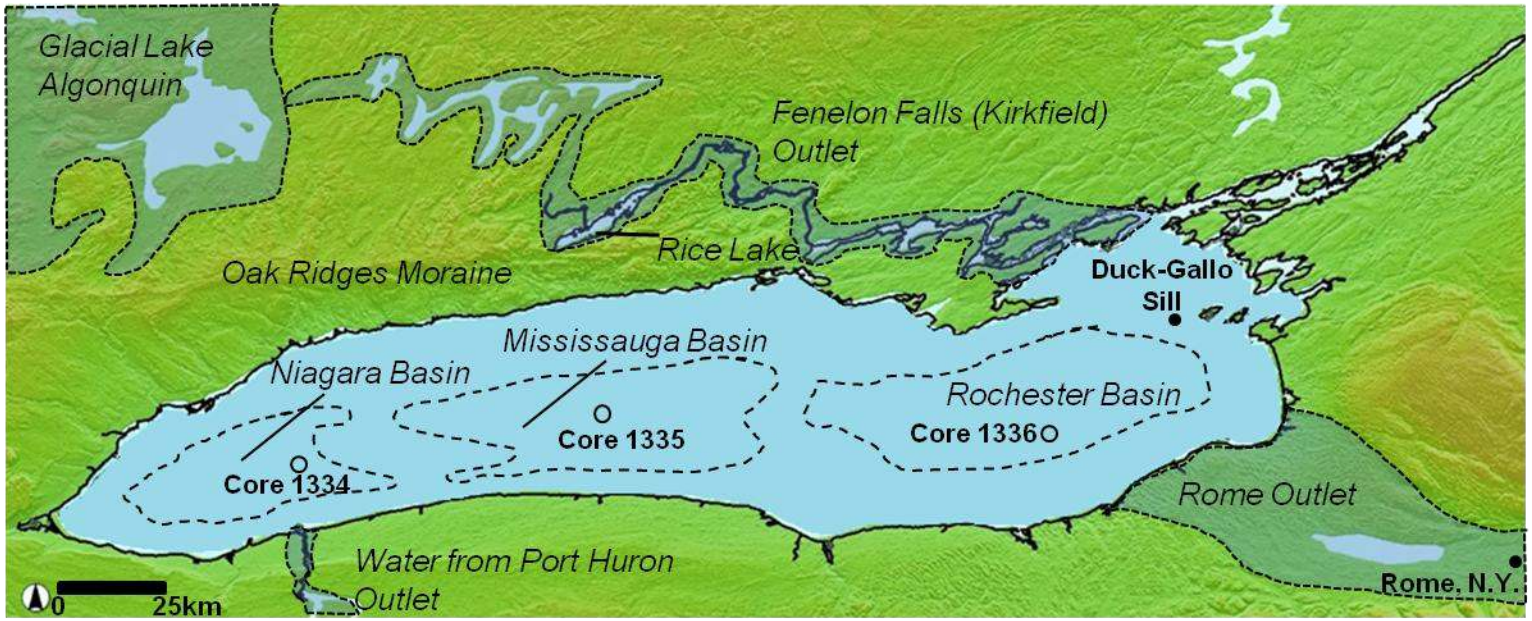

Figure 2.2. DEM Lake Ontario region showing the locations of sediment piston cores: Core 1334 (43° 24' 23" N and 79° 00' 05" W; water depth, 110.3 m; core length, 17.00 m), Core 1335 (43° 33' 19" N and 78° 09' 01" W; water depth, 192 m; core length, 18.20 m), Core 1336 (43° 30' 28" N and 76° 53' 07" W; water depth, 221.5 m; core length, 18.41 m). Several locations discussed in the text are also shown. Figure modified from the National Oceanic and Atmospheric Administration data center website (http://ngdc.noaa.gov/mgg/dem/).

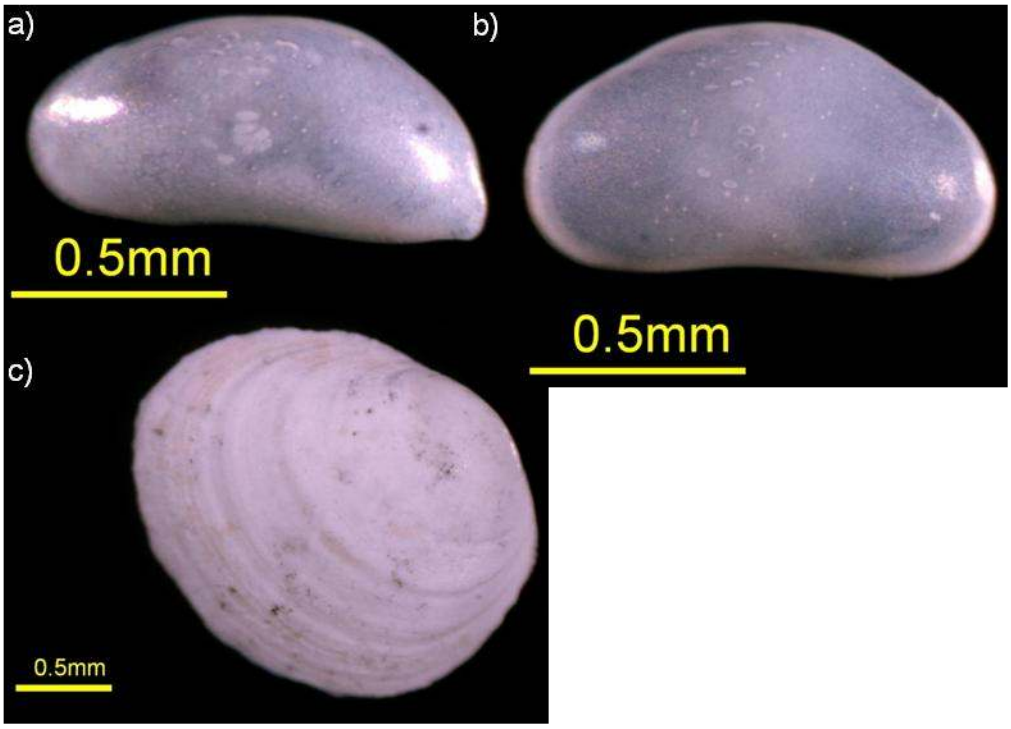

Figure 2.3. Photographs of: a) *Fabaeformiscandona caudata,* b) *Candona subtrigangulata* and c) *Pisidium* species clams.

ostracodes were counted from the >250 μm sieve material. Two species of ostracodes were identified in all three cores, *Candona subtriangulata* and *Fabaeformiscandona caudata* (Fig. 2.3); only adult ostracodes were used for abundance determinations. The ostracodes displayed no macroscopic or microscopic evidence of transport (e.g., broken/pitted valves), and hence are considered to be autochthonous. Whole clam shells of the *Pisidium* genus (Fig. 2.3) were present only in Cores 1334 and 1335 and were less abundant than clam fragments, which were present in all cores at various intervals. Approximately 0.05 mg of powdered biogenic carbonate was utilized for each oxygen isotopic measurement (five to six ostracode valves depending on individual weight, whole clam shells were homogenized when available and when only clam fragments were present, two to three clam shell fragments). Only undamaged, adult ostracodes valves were analyzed to ensure correct identification. The oxygen-isotope results are presented using the conventional δ-notation:

$$\delta^{18}O = [(R_{sample} - R_{standard})-1] \text{ (in ‰)}$$

where R_{sample} and $R_{standard} = {}^{18}O/{}^{16}O$ in the sample and standard, respectively. All δ-values are reported relative to VSMOW, unless otherwise stated. The oxygen-isotope measurements were made at the Laboratory for Stable Isotope Science (LSIS) at the University of Western Ontario, London, Ontario, and were obtained by reaction with orthophosphoric acid (H_3PO_4) at 90°C using a Micromass Multiprep autosampling device coupled to a VG Optima dual-inlet, stable-isotope-ratio mass spectrometer. International standards NBS-19 and NBS-18 were used to provide a two-point calibration curve for the oxygen-isotope compositions relative to VSMOW (Coplen, 1996). Two internal laboratory calcite standards were used to evaluate the accuracy and precision of the $\delta^{18}O$ values: WS-1 = +26.28 ± 0.15 ‰ (SD, n=9) and Suprapur = +13.20± 0.07 ‰ (SD, n=24); these results compare well with their accepted values of +26.23 ‰ and +13.20 ‰, respectively (Appendix II).

The $\delta^{18}O_{lakewater}$ values were calculated using: (1) the ostracode or clam $\delta^{18}O$ values, after first correcting for any vital effect (*C. subtriangulata* and *F. caudata*, +2.2 ‰; no vital effect correction for *Pisidium* sp. clams; von Grafenstein et al., 1999; Decrouy et al.,

2011a, b); (2) an assumed water temperature of 4 °C, and (3) the Friedman and O'Neil (1977) geothermometer for the low-Mg calcite – water system.

Mineralogy was determined by powder X-ray diffraction (pXRD) at LSIS, using a Rigaku, high brilliance, rotating-anode X-ray diffractometer equipped with a graphite monochromater and CoKα radiation produced at 45 kV and 160 mA. A total of 85 one-cm thick slices were obtained from the sampling portion of the cores. The samples were freeze-dried, finely ground using a mortar and pestle, and back-packed into an Al sample holder to achieve random orientation. Samples were scanned from 2° to 82° 2θ at a scanning rate of 10° 2θ/min. The abundance of each mineral was estimated using the background-subtracted peak height of its most intense diffraction, except where overlap with other phases existed. The form factor used to adjust for crystallinity differences among minerals was x1, except for the (001) diffractions of kaolinite (x2), chlorite (x2) and illite (x4).

Grain-size analysis was conducted using a Cilas 930e Laser Particle Size Analyzer at the Canada Center for Inland Waters (CCIW), Burlington, Ontario. Forty-six (46) one-cm thick slices from the sampling portion of the cores were freeze-dried and lightly broken apart using a mortar and pestle. The homogenized sample was then passed through a 500 μm sieve, and a 0.4 mg sub-sample ultrasonicated for 1 minute in 10 ml of a 0.05 % sodium hexametaphosphate solution in the Cilas sample bucket.

The age-depth model is anchored by three accelerator mass spectrometer (AMS) radiocarbon dates of terrestrial macrofossils and clam shells (Table 2.1). The analyses were performed at the University of Arizona's Accelerator Mass Spectrometer Laboratory, Tuscon, AZ. The date for the clam shell was corrected for the hard water effect by subtracting 535 ± 15 years (Anderson and Lewis, 2012). All radiocarbon dates have been converted to calibrated ages using INTCAL09 (Reimer et al., 2009). Information from previous Lake Ontario core studies was also used to help construct the age-depth model, including pollen stratigraphy (Carmichael et al., 1990; McAndrews, 1994; Pippert et al., 1996), seismic stratigraphy (Hutchinson et al., 1993), magnetic properties (Carmichael et al., 1990) and radiocarbon dates (Silliman et al., 1996;

Table 2.1. Radiocarbon dates were obtained at the University of Arizona AMS Laboratory in Tuscon, AZ, USA. The date for the *Pisidium* sp. clam shells was corrected for the hard water effect (HWE) by subtracting 535 ± 15 years (Anderson and Lewis, 2012) prior to converting it to a calibrated age. Radiocarbon dates were converted to calibrated ages using the computer program CLAM and INTCAL09 (Reimer et al., 2009; Blaauw, 2010). Calibrated ages represent the midpoint of the sampled interval; C1334 545 cm, C1335 525 cm and C1336 425 cm.

AA Lab #	Sample ID	Material	δ^{13}C (‰)	Radiocarbon age (^{14}C-year)	Calibrated age (midpoint between depths) (cal year BP)
AA97955	C1334 540-550 cm	*Pisidium* sp. clam shells	–0.2	9,640 ± 53	10,281 (HWE corrected age)
AA97956	C1335 520-530 cm	Wood and beetle	–25.5	9,987 ± 55	11,474
AA97957	C1336 420-430 cm	Wood	–25.3	9,397 ± 56	10,616

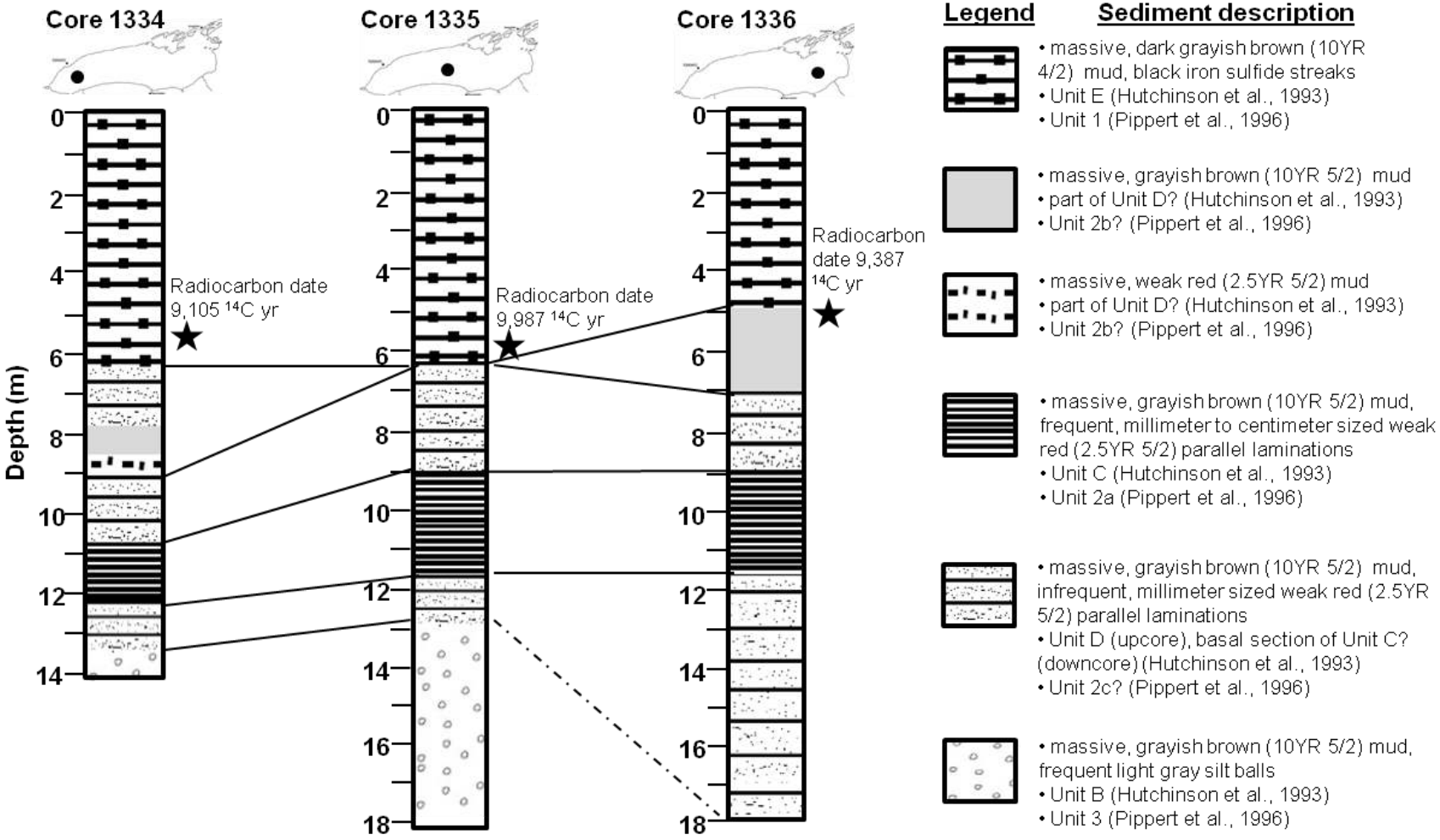

Figure 2.4. Generalized lithology of the Lake Ontario sediments in Cores 1334, 1335 and 1336. Locations of radiocarbon-dated material are denoted by stars.

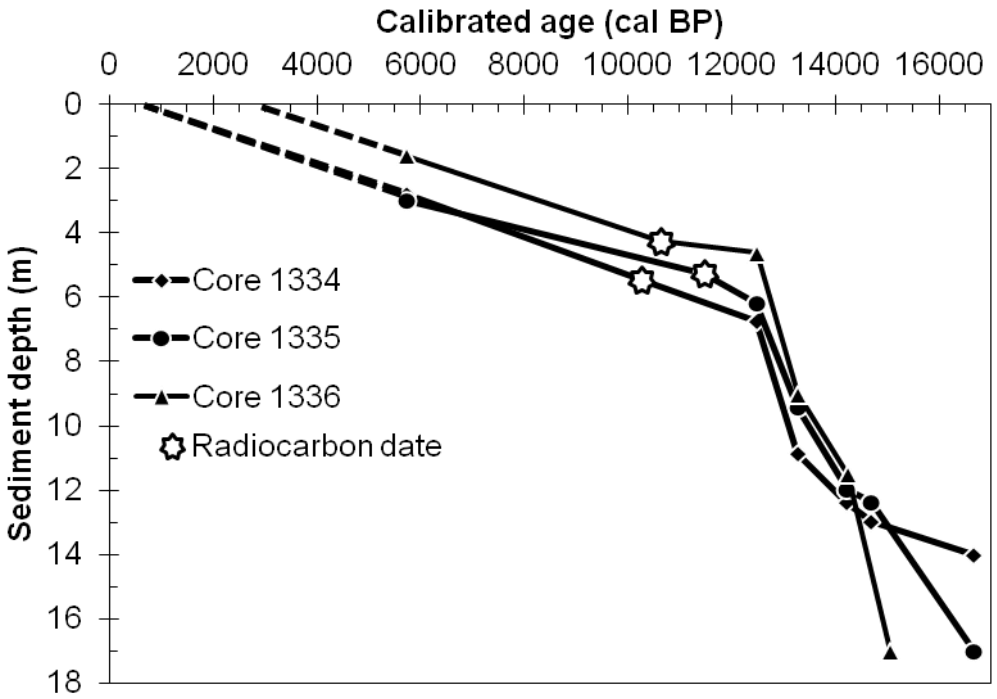

Figure 2.5. Non-Bayesian, linear interpolated, age-depth produced by CLAM (Blaauw, 2010). All radiocarbon dates were converted to calibrated ages by CLAM using INTCAL09 (Reimer et al., 2009). Three radiocarbon dates were used along with results from previous studies on Lake Ontario to establish the age-depth profiles (Schroeder and Bada, 1978; Carmichael et al., 1990; Hutchinson et al., 1993; McAndrews, 1994; Pippert et al., 1996; Silliman et al., 1996; Anderson and Lewis, 2012). See Table 2.1 for details.

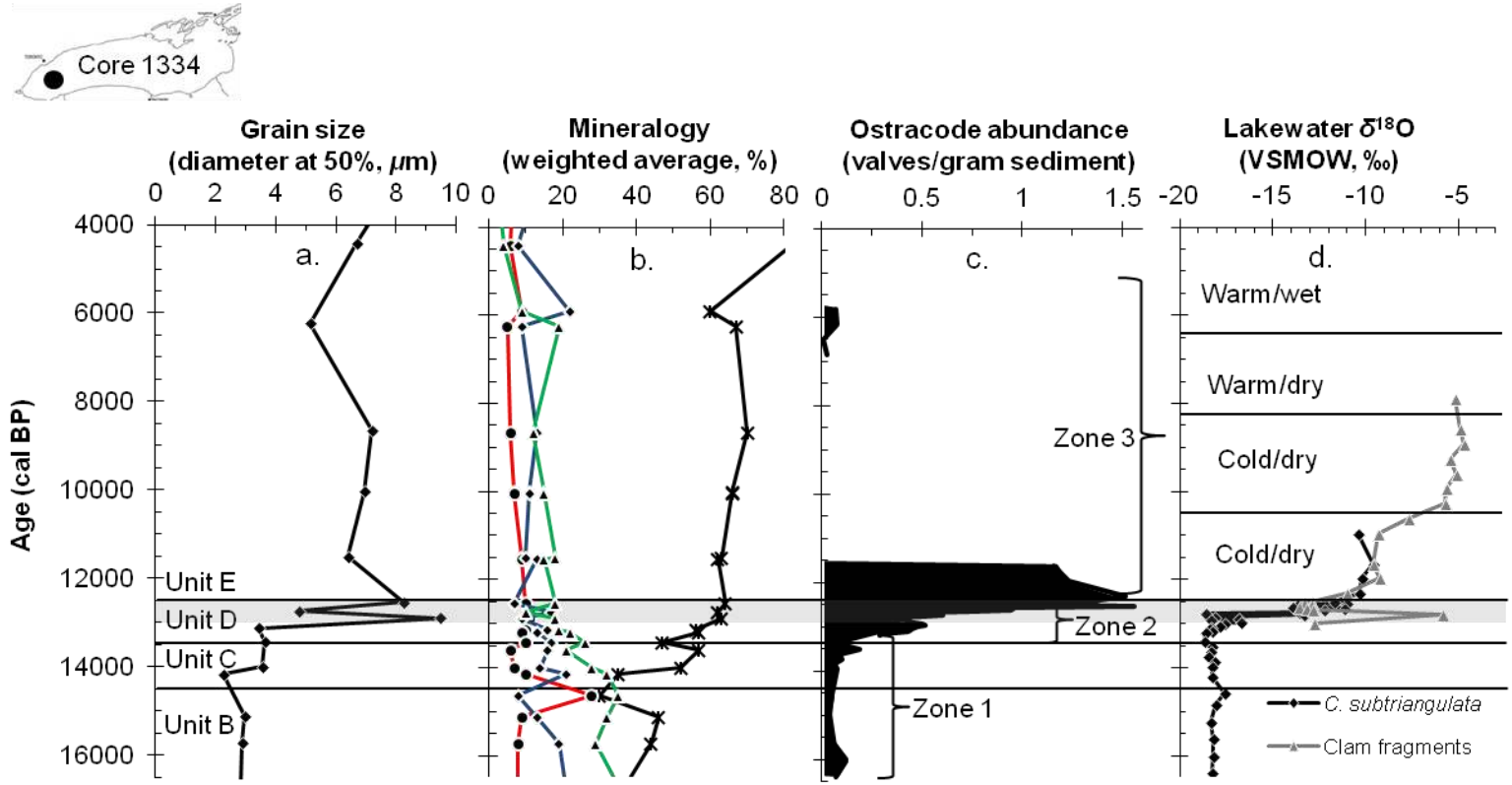

Figure 2.6. Data for Core 1334: (a) median grain size; (b) mineralogy (red line, feldspars; blue line, clays; green line, carbonates; black line, quartz) (c) ostracode abundances, valves per gram sediment (v/g), and (d) $\delta^{18}O_{lakewater}$ values inferred from ostracode valves and clam shells. Gray shaded area indicates a renewed period of glacial meltwater influx. Divisions between sediment units are denoted by continuous solid lines across (a), (b), (c) and (d). Biostratigraphic zonations are illustrated by braces in (c). Post-glacial isotopic changes are demarcated by solid lines that divide (d) and are placed at 10,500, 8,300 and 6,800 cal BP.

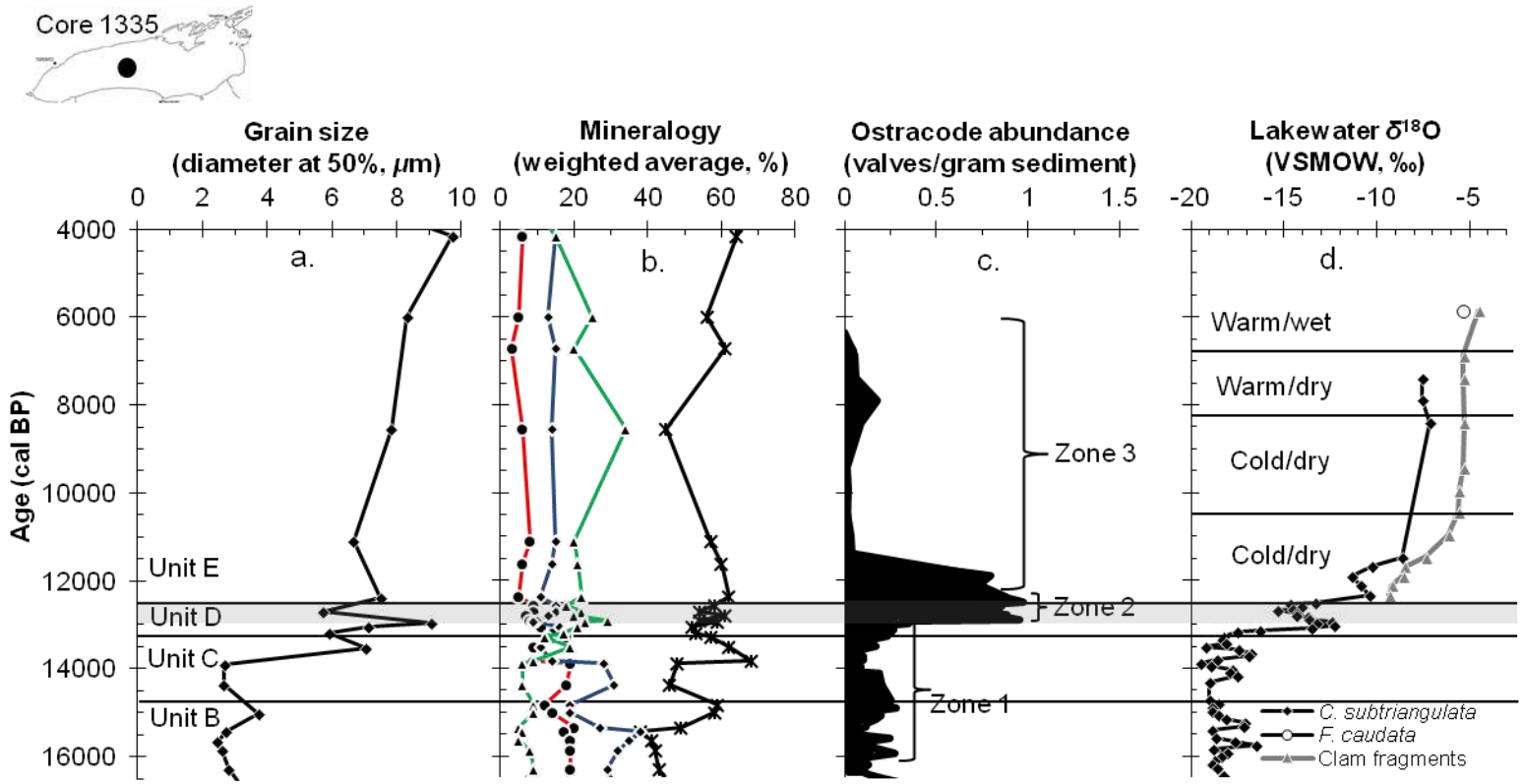

Figure 2.7. Data for Core 1335: (a) median grain size; (b) mineralogy (red line, feldspars; blue line, clays; green line, carbonates; black line, quartz) (c) ostracode abundances, valves per gram sediment (v/g), and (d) $\delta^{18}O_{lakewater}$ values inferred from ostracode valves and clam shells. Gray shaded area indicates a renewed period of glacial meltwater influx. Divisions between sediment units are denoted by continuous solid lines across (a), (b), (c) and (d). Biostratigraphic zonations are illustrated by braces in (c). Post-glacial isotopic changes are demarcated by solid lines that divide (d) and are placed at 10,500, 8,300 and 6,800 cal BP.

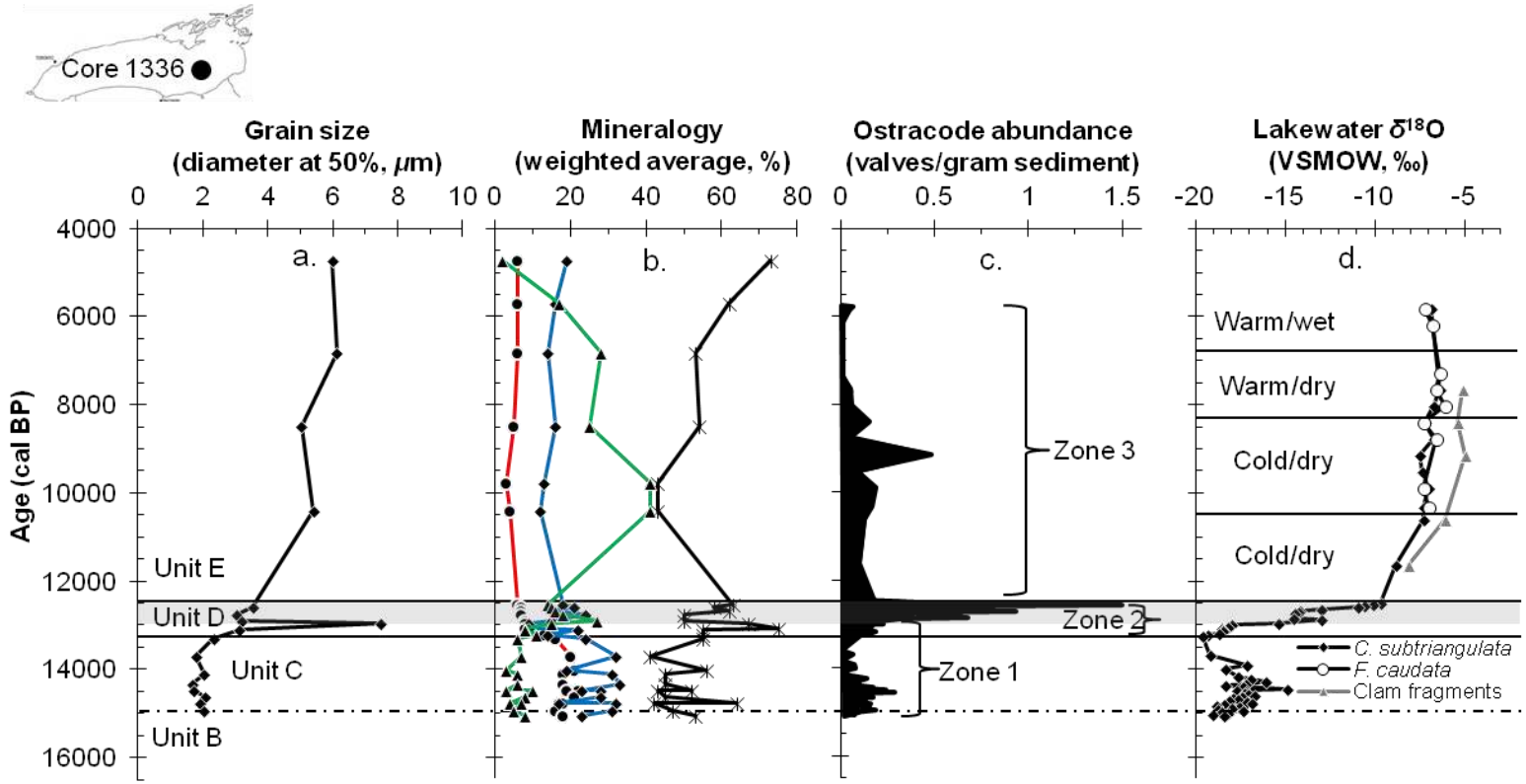

Figure 2.8. Data for Core 1336: (a) median grain size; (b) mineralogy (red line, feldspars; blue line, clays; green line, carbonates; black line, quartz) (c) ostracode abundances, valves per gram sediment (v/g), and (d) $\delta^{18}O_{lakewater}$ values inferred from ostracode valves and clam shells. Gray shaded area indicates a renewed period of glacial meltwater influx. Divisions between sediment units are denoted by continuous solid lines across (a), (b), (c) and (d). Biostratigraphic zonations are illustrated by braces in (c). Post-glacial isotopic changes are demarcated by solid lines that divide (d) and are placed at 10,500, 8,300 and 6,800 cal BP.

Anderson and Lewis, 2012). These data were combined to produce a non-Bayesian, linear interpolated age-depth model using the computer program CLAM (Blaauw, 2010), which provides a probabilistic age range for each depth.

2.3 Results

Descriptions of Cores 1334, 1335 and 1336 are summarized in Figure 2.4 and given in detail in Appendix I. Age-depth models are illustrated in Figure 2.5. Grain-size, mineralogy, ostracode abundances and $\delta^{18}O_{lakewater}$ values are summarized in Figure 2.6 (Core 1334), Figure 2.7 (Core 1335) and Figure 2.8 (Core 1336).

2.3.1 Core descriptions

The bottom sections (greater than 17.0 m) of Cores 1335 and 1336 contain minor and pronounced vertical streaking, respectively (Appendix I). These features suggest sediment disruption caused by lifting of the piston during withdrawal of the corer from the lakebed. These intervals may be disturbed in-place sediment, or sediment drawn up into the bottom of the core barrel during corer withdrawal; they are not described further.

The basal section in Cores 1334 (14.0-13.0 m) and 1335 (18.0-12.5 m) consist of massive, grayish-brown (10YR 5/2) sediment containing abundant light gray silt balls (Fig. 2.4; Appendix I). These sediments correspond to 'Unit B' of Hutchinson et al. (1993). A similar mud clast-bearing interval was described by Pippert et al. (1996), which they termed 'Unit 3'. The basal section of Core 1336 consists of a grayish-brown (10YR 5/2) sediment package containing weak red (2.5YR 5/2), infrequent, mm-thick, parallel laminations that can be correlated with sediments in Cores 1334 and 1335. The contact between the massive, grayish brown (10YR 5/2) unit in Cores 1334 and 1335 and the beginning of the mm-thick parallel laminations is gradational and marks the transition to 'Unit C' (Hutchinson et al., 1993).

Up-core in 'Unit C', there are local to abundant, mm- to cm-thick, weak red (2.5YR 5/2), parallel laminations that increase in thickness and abundance in the western half of the

lake (Appendix I). A sharp contact marks the appearance of thickly laminated sediments at 12.45 m in Core 1334, 11.97 m in Core 1335 and 11.50 m in Core 1336.

A massive, grayish brown (10YR 5/2) mud unit characterized by local, mm-thick, weak red (2.5YR 5/2) parallel laminations appears next in the stratigraphic section. Transition from underlying sediments characterized by cm-thick laminations to thinner, sparse laminations occurs at 10.84 m in core 1334, 9.43 m in core 1335 and 9.00 m in Core 1336. Hutchinson et al. (1993) classified such sediments as the earliest stage of 'Unit D' and noted that this unit characterizes post-Iroquois glacial lakes in the Ontario basin. The sediments exhibit major differences across Lake Ontario in the later stages of Unit D. In the west (Niagara basin), Core 1334 transitions from thinly laminated grayish brown (10YR 5/2) mud to massive, weak red (2.5YR 5/2) mud (9.10 m), overlain by featureless massive, grayish brown (10YR 5/2) mud (8.22-8.06 m). Thinly laminated grayish brown (10YR 5/2) mud (8.05-6.75 m) was deposited above these massive units. This latter unit was also deposited in the central, Mississauga basin (Core 1335) of Lake Ontario (9.43-6.20 m), but massive muds were not observed. In the east (Rochester basin), Core 1336 transitions from thinly laminated grayish brown (10YR 5/2) mud to a massive, featureless grayish brown (10YR 5/2) mud (7.00-4.62 m).

A conformable, sharp contact exists between Unit D and the overlying 'Unit E' of Hutchinson et al. (1993) ('Unit 1' of Pippert et al., 1996). Unit E is characterized by black, iron sulfide streaks intercalated with dark grayish brown (10YR 4/2) mud. Unit E occurs at 6.75 m in Core 1334, 6.20 m in Core 1335 and 4.62 m in Core 1336; its appearance marks the end of glacial influence on ancient Lake Ontario. Deposition of this unit continues to the present time.

2.3.2 Grain size and mineralogy

Median grain size (diameter at 50 %) generally increases upwards, but never exceeds ~ 10 μm (Figs. 2.6a, 2.7a, 2.8a; Appendix III). Unit B and the thinly laminated sediments of Unit C have a median grain size of <3.0 μm. The transition to Unit D is marked by a slight increase in median grain size across the lake, and occurs above 10.84 m in Core 1334, above 9.43 m in Core 1335 and above 9.00 m in Core 1336. There are sharp spikes

to higher grain size within Unit D in all three cores: at 8.90 m and 7.10 m in Core 1334, at 8.10 m in Core 1335, and at 7.30 m in Core 1336. Unit E sediment gradually increases in median grain size up-core to a maximum of 8.0, 9.5 and 6.0 μm from the Niagara to Rochester basin, respectively (Appendix III).

The sediment contains varying abundances of quartz, feldspar (plagioclase, potassium feldspar), clay minerals (kaolinite, illite, chlorite) and carbonates (calcite and dolomite) (Figs. 2.6b, 2.7b, 2.8b; Appendix IV). Quartz is generally the most abundant phase, varying in abundance from 30 to >80 %. Distinct mineralogical differences occur from west to east in Unit B and the basal section of Unit C. In Core 1334, carbonates are in high abundance (~30 %) from 14.00-13.00 m whereas in the same unit in Core 1335 (17.00-11.97 m) and Core 1336 (17.00-11.50 m), carbonate contents are much lower (~ <5 %). Feldspar and clay mineral abundances also vary from west to east in Unit B and the basal section of Unit C. In Core 1334, feldspar abundance increases sharply to ~25 % at 12.9 m from ≤5 % in the underlying interval (14.0-13.0 m). Feldspar abundances remain at ~15 % in Cores 1335 and 1336 during the same period. In Unit B and the basal section of Unit C, clay mineral contents increase from west (~20 %) to east (>30 %). Unit D in Core 1334 is marked by decreasing carbonate abundances from ~30 to 15 %, whereas in Cores 1335 and 1336 carbonate abundance increases from 15 to 30 %. Carbonate abundances in Unit E are variable across the lake. In Core 1334, carbonate content decreases relative to unit D (from 20 to <5 %), whereas in Cores 1335 and 1336, carbonate contents increase initially to a maximum of 40 % but then gradually decrease to <5 %. Clay and feldspar contents remain constant in Unit E whereas quartz abundances generally increase upwards.

2.3.3 Biostratigraphy

Two species of ostracodes, *Candona subtriangulata* and *Fabaeformiscandona caudata* and *Pisidium* sp. clams (whole) shells were present in Cores 1334 and 1335 and clam shell fragments were present in all cores (Figs. 2.6c, 2.7c, 2.8c). We have defined three biostratigraphic zonations. Zone 1 has *C. subtriangulata* abundances less than 0.2 valves per gram sediment (v/g), and occurs at >11.10 m in Core 1334, >9.65 m in Core 1335 and

>7.50 m in Core 1336. Zone 2 has higher *C. subtriangulata* abundances to a maximum of 1.56 v/g in Core 1334 (7.10 m), 0.96 v/g in Core 1335 (6.25 m) and 1.50 v/g in Core 1336 (5.05 m). Zone 3 contains both ostracode species and clams. There is a marked decline in the abundance of *C. subtriangulata* in Zone 3 along with the sporadic appearance of *F. caudata* (<0.08 v/g) in low abundances. Both whole and fragments of *Pisidium* sp. clam shells appear at 7.80 m in Core 1334 and 6.05 m in Core 1335. Only fragmented clam shells appear in Core 1336 – at 4.45 m. Ostracodes and clam species disappear from the sediment record at 2.8 m in Core 1334, 3.0 m in Core 1335 and 1.6 m in Core 1336.

2.3.4 Lakewater oxygen-isotope composition

The average $\delta^{18}O_{lakewater}$ value, as derived from ostracode compositions, is ~ –17.5±0.8 ‰ (SD; n=81) in sediments >10.84 m in Core 1334, >9.43 m in Core 1335 and >9.00 m in Core 1336 (Figs. 2.6d, 2.7d, 2.8d; Appendix V). Variation in the $\delta^{18}O_{lakewater}$ values appears to increase from east to west: Core 1334, –17.7±0.2 ‰ (SD; n=14); Core 1335, –17.8±0.7 ‰ (SD; n=36); Core 1336, –17.2±0.9 ‰ (SD; n=31). An analysis of variance (ANOVA) was performed on the $\delta^{18}O_{lakewater}$ values from these intervals. Significant variation exists among the three cores (F-value= 6, p-value=0.005). A post-hoc Tukey's test found significant variation between Core 1336 and the other two cores (Core 1334; p-value=0.03, Core 1335; p-value=0.02), but not between Cores 1334 and 1335 (p-value=0.1).

Subsets of the interval above were further analyzed for statistical significance and discussion. From 15,300 to 14,500 cal [12,975 to 12,410 ^{14}C] BP, the average lakewater oxygen-isotope composition in Core 1334 was –17.5±0.4 ‰ (SD; n=3) and Core 1335 was –17.9±0.6 ‰ (SD; n=7). From 14,000 to 13,000 cal [12,150-11,100 ^{14}C] BP the average lakewater compositions were; Core 1334, –17.8±0.3 ‰ (SD; n=12); Core 1335, –16.8±2.0 ‰ (SD; n=14); Core 1336, –18.1±0.7 ‰ (SD; n=10). An ANOVA determined no statistical variance (p-value >0.05) between the cores in any of the time intervals.

Above this interval, $\delta^{18}O_{lakewater}$ values increase by a maximum of ~7 ‰ from 10.45-7.65 m in Core 1334, 9.05-8.45 m in Core 1335, and 8.85-6.85 m in Core 1336. A decrease in

$\delta^{18}O_{lakewater}$ then interrupts the overall trend of increasing oxygen isotopic compositions, beginning at 7.45 m in Core 1334, 8.25 m in Core 1335 and 6.65 m in Core 1336.

The upward trend in $\delta^{18}O_{lakewater}$ values resumes following this brief downward excursion (Figs. 2.6d, 2.7d, 2.8d). For ostracodes, the calculated $\delta^{18}O_{lakewater}$ reaches values as high as –9.1 ‰ in Core 1334 (11,636 cal [10,077 ^{14}C] BP), –6.7 ‰ in Core 1335 (8,407 cal [7,609 ^{14}C] BP), and –5.9 ‰ in Core 1336 (7,662 cal [6,805 ^{14}C] BP). Still higher $\delta^{18}O_{lakewater}$ values are recorded by the clams: –4.2 ‰ in Core 1334 (8,906 cal [7,984 ^{14}C] BP), –4.0 ‰ in Core 1335 (5,850 cal [5,041 ^{14}C] BP), and –4.5 ‰ in Core 1336 (9,141 cal [8,224 ^{14}C] BP). Modern Lake Ontario, by comparison, has a $\delta^{18}O_{lakewater}$ value of –6.6 ‰ (Longstaffe et al., 2011). Clam shells and fragments in Core 1334 initially record similar $\delta^{18}O_{lakewater}$ values as ostracodes but trend toward more ^{18}O-rich compositions after the ostracodes disappear from the record. In Core 1335, there is an initial ~1 ‰ offset between clam and ostracode $\delta^{18}O_{lakewater}$ values. The offset increases up-core to ~2 ‰ at the time of the final appearance of both species. Clam shell fragments in Core 1336, which appear later than in Cores 1334 and 1335, exhibit a ~1 ‰ offset between clam and ostracode $\delta^{18}O_{lakewater}$ values.

2.4 Discussion

2.4.1 Glacial period (16,500-13,000 cal [13,300-11,100 ^{14}C] BP)

The lowermost portions of Cores 1334 and 1335 contain glacial sediments (Unit B or Unit 3, following Hutchison et al., 1993 and Pippert et al., 1996, respectively) that were deposited in the Niagara and Mississauga basins by retreating Port Bruce ice beginning at ~16,500 cal [13,300 ^{14}C] BP (Barnett, 1992). Age control for these sediments is difficult to establish because of the absence of dated pollen horizons and the paucity of dateable organic material. A depositional age (>14,655 cal [12,500 ^{14}C] BP) for this unit has therefore been inferred by linear extrapolation of sedimentation rates beyond the known contacts of Units B and C.

These sediments are characterized by low abundances of *C. subtriangulata*, a grain size <3 μm and low $\delta^{18}O_{lakewater}$ (<–17 ‰). There are noteworthy mineralogical differences

between the Niagara and Mississauga basin glacial sediments. Traditionally, these sediments have been interpreted as flow tills or the product of subglacial processes associated with the retreating LIS (Hutchinson et al., 1993). The sediments of Core 1335 may best represent such processes, given their higher proportions of feldspar and clay minerals, which likely originate from the Precambrian Canadian Shield. The higher carbonate abundances in Core 1334 (>30 %) relative to Core 1335 (<5 %) likely indicate an additional source. This carbonate may represent input from glacial Lake Ypsilanti, which was likely enriched in Paleozoic carbonate detritus originating in both the Erie and Huron basins. At 16,000-15,300 cal [13,140-12,975 ^{14}C] BP, the LIS retreated into the Ontario basin, which allowed glacial Lake Ypsilanti (Erie basin) to overflow its outlet at the Fort Erie-Buffalo sill (Fig. 2.1) (Lewis et al., 2012). This brief period of connectivity between the Erie and Ontario basins allowed ancestral Lake Ontario to receive glacial meltwater and sediment from the carbonate-rich Erie basin.

Ice readvanced during the Mackinaw interstadial, ending the glacial Lake Ypsilanti phase and severing connectivity between the Erie and Ontario basins (Calkin and Feenstra, 1985; Lewis et al., 2012). Ancestral Lake Erie rose to the Lake Whittlesey level and overflowed westward to the Michigan basin from 15,300-14,500 cal [12,975-12,410 ^{14}C] BP (Calkin and Feenstra, 1985; Lewis et al., 2012). Subglacial deposition became dominant in the Ontario basin during this period (Hutchinson et al., 1993). The increase in feldspar content in Core 1334 is consistent with glacial sediment from eastern sources. The variability in $\delta^{18}O_{lakewater}$ during this time interval may be related to instability of the LIS. The $\delta^{18}O_{lakewater}$ variability in Core 1335 (–17.9±0.6 ‰) may indicate incomplete mixing of an inconsistent meltwater flux from the LIS to the east and north. The short time scale (on the order of weeks) over which an ostracode acquires its oxygen isotope signal from lakewater makes the recording of such a signal possible. Lower $\delta^{18}O_{lakewater}$ variability in Core 1334 (–17.5±0.4 ‰) may suggest that these perturbation were more limited further from Core 1335. This remains speculative, as the differences in $\delta^{18}O_{lakewater}$ variance between Cores 1334 and 1335 are not statistically significant.

Retreat of the LIS following the Port Huron stadial initiated glacial Lake Iroquois while continuing to block Ontario basin's outlet to the St. Lawrence River (~14,000 cal [12,150

^{14}C] BP). Glacial Lake Iroquois sediments (Unit C) were observed in the cores from all three Lake Ontario basins. The near uniform abundances of *C. subtriangulata* indicate cold (~ 4 °C), dilute (<90 mg/l total dissolved solids), and oxygenated (>5.6 mg/l) benthic conditions (Delorme, 1978; 1989). The low median grain size (<3 μm) reflects deposition in a deep, low energy, lacustrine environment, which is consistent with glacial Lake Iroquois levels having been ~35 (west) to 115 (east) m higher than at present (Coakley and Karrow, 1994).

The relative contributions of different glacial meltwater sources (LIS, glacial Lake Algonquin) to glacial Lake Iroquois probably varied over time. From 14,000-13,000 cal [12,150-11,100 ^{14}C] BP, outflow from glacial Lake Algonquin bypassed the Erie basin and flowed directly into glacial Lake Iroquois via the Fenelon Falls outlet (Figs. 2.1, 2.2). Data for ostracodes from Lake Simcoe and Lake Huron sediments suggest that glacial Lake Algonquin $\delta^{18}O_{lakewater}$ input ranged from –19 to –17.5 ‰ (Bumstead et al., 2009; Macdonald and Longstaffe, 2008). This meltwater, which entered glacial Lake Iroquois via its eastern-central inlet, had a short and direct path to outflow through the Mohawk River valley (Figs. 2.1, 2.2). Core 1336 (–18.1±0.7 ‰) is situated very close to this pathway, unlike Core 1334 (–17.8±0.3 ‰) and to a lesser extent, Core 1335 (–16.8±2.0 ‰). The higher variance in $\delta^{18}O_{lakewater}$ recorded by Cores 1335 and 1336 and the overall lower $\delta^{18}O_{lakewater}$ values of Core 1336 relative to Core 1334 can be explained by their locations. In this scenario, the larger $\delta^{18}O_{lakewater}$ variations in Core 1335 reflects a dynamic lacustrine regime mostly resulting from fluctuating contributions from the west (regional precipitation ($\delta^{18}O_{precipitation}$ = –16.5 ‰; Edwards et al., 1996), from the east-central outlet of glacial Lake Algonquin (–19 to –17 ‰) and direct LIS runoff (–35 to –25 ‰) (Flower et al., 2004; Bumstead et al., 2009; Macdonald and Longstaffe, 2008) from immediately to the northeast. The lowest $\delta^{18}O_{lakewater}$ values in eastern glacial Lake Iroquois, in particular, likely reflect increased meltwater delivery directly from the LIS, an observation also consistent with higher feldspar and clay abundances in Core 1336 relative to Cores 1334 and 1335 at this time.

Similar isotopic fluctuations are recorded by Gulf of Mexico (GOM) foraminifers from 13,700-13,000 cal [11,800-11,100 ^{14}C] BP (Williams et al., 2010). There, lower GOM

foraminifer $\delta^{18}O$ values are interpreted to indicate episodic delivery of meltwater from glacial Lake Agassiz via the Mississippi drainage system (Williams et al., 2010; 2012). Similar to the GOM, isotopic fluctuations occur in Core 1335 at 13,650 cal [11,780 ^{14}C] BP and in Core 1336 at 14,000 cal [12,150 ^{14}C] BP. Collectively, these observations point to an unstable LIS, with irregular ablation reflected in pulses of low-^{18}O meltwater recorded in downstream sedimentary records.

As discussed earlier, the extensive LIS retreat into the St. Lawrence lowland shortly after ~13,260 cal [11,360 ^{14}C] BP led to the drainage of glacial Lake Iroquois to its low Lake Trenton phase that was characterized by slowdown and termination of the glacial meltwater supply to the distant Lake Ontario basin. These changes coincided with a regional cold/dry period (Lewis et al., 2008). The ensuing rapid increase in $\delta^{18}O_{lakewater}$ values from –19 to –12 ‰ (Figs. 2.6d, 2.7d, 2.8d) mostly reflects elimination of the low-^{18}O glacial meltwater input, although evaporative ^{18}O-enrichment likely also played some role.

At ~13,000 cal [11,100 ^{14}C] BP, it is impossible to rule out an ^{18}O-rich influx from the confluent Champlain Sea from isotopic data alone. However, there is no evidence for marine invasion of Lake Ontario, such as extirpation of the salinity-sensitive *C. subtriangulata* or appearance of marine foraminifera or ostracodes, as is discussed further below.

2.4.2 Final glacial meltwater influx (13,000-12,500 cal [11,100-10,500 ^{14}C] BP)

The rise in $\delta^{18}O_{lakewater}$ values that began at ~13,260 cal [11,360 ^{14}C] BP was not continuous. In particular, $\delta^{18}O_{lakewater}$ values in Core 1335 decreased from ~ –12 to –14 ‰ beginning at ~13,031 cal [11,100 ^{14}C] BP and remained low for ~500 years (Fig. 2.9a, b). The lowering could reflect a change in the oxygen isotopic composition of regional precipitation and/or a renewed influx of low-^{18}O glacial meltwater. The first possibility is unlikely. While pollen and wood cellulose records indicate cold and dry conditions at this time, cellulose-derived $\delta^{18}O_{precipitation}$ values nevertheless rose slightly from –17 to –

15 ‰ during this time period (Edwards and Fritz, 1986; Edwards and McAndrews, 1989; Edwards et al., 1996). In contrast, renewed glacial meltwater input would produce lower $\delta^{18}O_{lakewater}$, a scenario also supported by the spike in median sediment grain size (~2.5 to 9 μm) measured for this time (Fig. 2.7a). Similar decreases in $\delta^{18}O_{lakewater}$ and increases in median grain size are recorded at 12,657 cal [10,780 ^{14}C] in Core 1334 and 12,884 cal [11,000 ^{14}C] BP in Core 1336 (Figs. 2.6a, 2.6d, 2.8a, 2.8d). The differences in timing among the cores could indicate errors in the age-depth models or reflect variable meltwater delivery across the Ontario basin. The latter scenario is more likely given the common termination date for the low-^{18}O interval (12,500 cal [10,500 ^{14}C] BP) in all three cores.

Anderson and Lewis (2012) noted the inundation of ancient Lake Ontario with meltwater at 12,800 cal [10,965 ^{14}C] BP. However, its sources and routing into and out of Lake Ontario have been largely unexplored. Glacial meltwater input from glacial Lake Algonquin via Lake Erie, which established connectivity with the Ontario basin at 13,000 cal [11,110 ^{14}C] BP, and/or directly from glacial Lake Algonquin (Port Huron or Fenelon Falls outlets, respectively), could account for this interval of lower $\delta^{18}O_{lakewater}$ values.

Simple estimates suggest that the overall volume of water in ancient Lake Ontario increased by ~25 % during this meltwater influx, based on the 5 m increase in lake level reported by Anderson and Lewis (2012). This estimate allows us to test for possible contributions of meltwater to the Ontario basin from ancient Lake Erie versus directly from Lake Algonquin, assuming no outlet and no evaporation from ancient Lake Ontario. Ancient Lake Erie experienced a –3 ‰ shift in $\delta^{18}O_{lakewater}$ values to –16.8 ‰ at ~ 12,900-12,300 cal [11,020-10,400 ^{14}C] BP, which Lewis and Anderson (1992) attributed to increased glacial meltwater input. Simple mixing calculations indicate that such a flux from ancient Lake Erie can account for only ~50 % of the decrease in ancient Lake Ontario $\delta^{18}O_{lakewater}$ during this 500-year interval. However, ancient Lake Ontario was likely also receiving glacial meltwater from glacial Lake Algonquin via the Fenelon Falls outlet at this time (Lewis and Anderson, 1992). If glacial Lake Algonquin ($\delta^{18}O_{lakewater}$ = –19 to –17.5 ‰; Bumstead et al., 2009) was the sole contributor to Lake Ontario's ~25 % increase in volume, then ancient Lake Ontario would have acquired a $\delta^{18}O_{lakewater}$ value of

~ –14 ‰. These simple calculations support the suggestion that meltwater influx from glacial Lake Algonquin via the Fenelon Falls outlet was dominant at this time.

As discussed above, there is some variability in the timing of meltwater delivery to Lake Ontario during this interval. That the entry of this pulse of glacial meltwater was first recorded in Core 1335 hints at the possibility that meltwater originating from glacial Lake Algonquin, via the Fenelon Falls outlet, breached the Oak Ridges Moraine, thus entering early Lake Ontario at a central locality (Figs. 2.1, 2.2). One possible location, supported by channels between uplands, suggests a breach in the Oak Ridges Moraine at Lake Scugog (Fig. 2.1) (Sharpe et al., 2004). Another possible location is Rice Lake (Figs. 2.1, 2.2), the only lake that currently breaches the Oak Ridges Moraine (Fig. 2.2).

The ultimate source of glacial meltwater input into Lake Ontario beginning at ~13,000 cal [11,100 ^{14}C] BP is of interest, given that this time period coincides with the beginning of the YD cooling event. As described earlier, Broecker et al. (1989) hypothesized a change in meltwater routing out of glacial Lake Agassiz from southward (Gulf of Mexico) to eastward (Great Lakes Basin) during the YD. Geomorphological evidence for an eastern outlet to the Great Lakes, however, remains elusive (e.g., Teller et al., 2005; Fisher and Lowell, 2006; Voytek et al., 2012). Others have suggested drainage of glacial Lake Agassiz into the Arctic Ocean at this time (Murton et al., 2010; Fahl and Stein, 2012). Still others posit that glacial Lake Agassiz drained neither to the northwest nor to the east, but instead evaporated (e.g., Fisher and Lowell, 2012; Lowell et al., 2013). Unfortunately, oxygen isotopes do not provide for a clear distinction between meltwater contributions to Lake Ontario from glacial Lake Agassiz versus other glacial lake(s). First, the δ^{18}O values of glacial Lake Agassiz deep waters at this time, as inferred from ostracodes and porewater, ranged from –21 to –18 ‰ (Last et al., 1994; Birks et al., 2007), not all that dissimilar to Lake Algonquin. Second, Birks et al. (2007) have proposed that Lake Agassiz became isotopically stratified by ~13,000 cal [11,100 ^{14}C] BP. In the Birks et al. (2007) scenario, water enriched in ^{18}O by ~7 ‰ (cellulose inferred) had pooled at the surface of Lake Agassiz as the product of precipitation, surface runoff and evaporation under warmer climatic conditions. If this ^{18}O-enriched water in the epilimnion reached the southern Great Lakes (Erie and Ontario) it would

have imparted an oxygen isotopic signal similar to the observed values in Early Lake Ontario (–14 ‰). Nonetheless, this scenario remains unlikely in the absence of other evidence for eastern drainage of glacial Lake Agassiz into the Great Lakes during this time period (Voytek et al., 2012).

A putative outlet for the final pulse of glacial meltwater received by Lake Ontario is equally enigmatic. One possibility is an eastern outlet into the Champlain Valley. Near the onset of the YD (13,100 cal [11,170 ^{14}C] BP), Lake Vermont was transitioning to the Champlain Sea representing a shift from lacustrine to marine environments (Rayburn et al., 2011; Cronin et al., 2012). This transition involved complex hydrological changes which are recorded by shifting microfaunal assemblages (Rayburn et al., 2011; Cronin et al., 2012). The earliest part of the transition (Marine Phase I) is defined by the occurrence of foraminiferal species (Rayburn et al., 2011). Marine Phase I was followed by periods of abrupt freshening (Freshwater Phase) in which ostracodes assemblages emerge and the foraminiferal species disappear (Rayburn et al., 2011; Cronin et al., 2012). Lastly, a Transitional Phase occurs before the onset of Champlain Sea (Marine Maximum at 12,900 cal [11,020 ^{14}C] BP) in which both ostracodes and forminiferal assemblages co-exist (Rayburn et al., 2011; Cronin et al., 2012). The Lake Vermont-Champlain Sea sediments recorded signals of glacial meltwater floods, such as the lowering of δ^{18}O values of marine benthic foraminifera and appearance of freshwater ostracodes, both consistent with abrupt periods of glacial meltwater freshening (Rayburn et al., 2011; Cronin et al., 2012) (Fig. 2.9c). The $\delta^{18}O_{ostracode}$ values measured by Cronin et al. (2012) for the Freshwater and Transitional phases during the Lake Vermont-Champlain Sea transition are very similar to those recorded in Lake Ontario (Fig. 2.9b). These glacial meltwater floods have been attributed to drainage of glacial Lake Agassiz (Rayburn et al., 2011; Cronin et al., 2012) that occurred somewhat earlier than the meltwater pulse under discussion here.

The onset of the Marine Maximum phase of the Champlain Sea after 12,900 cal [11,020 ^{14}C] BP occurred as Lake Ontario began to receive a renewed glacial meltwater supply from glacial Lake Algonquin. In absence of continued evidence for meltwater induced freshening of the Champlain Sea, it is unlikely that drainage from glacial Lake Algonquin

via Lake Ontario played a role in disruption of the THC. Instead, this meltwater flow likely only pushed marine water somewhat eastward, inhibiting a marine incursion into Lake Ontario. The shift in Ontario basin $\delta^{18}O_{lakewater}$ from –12 to –14 ‰ continued until ~12,500 cal [10,500 ^{14}C] BP, whereas there is no record of meltwater entry into the Champlain Sea after 12,900 cal [11,020 ^{14}C] BP (Fig. 2.9c.)

It is nonetheless interesting to note that this period (13,000-12,500 cal [11,100-10,500 ^{14}C] BP) of meltwater influx into Lake Ontario coincides with a shift in Greenland Ice Sheet (GISP2) $\delta^{18}O$ values from –38 to –42 ‰ (Fig. 2.10). The hemispheric YD-related cooling recorded by GISP2 was almost certainly manifested in the Ontario basin, and perhaps even intensified by this final flux of glacial meltwater into the region (Lewis and Anderson, 1992). The simple water volume estimates described earlier assumed no outflow from the Ontario basin after 12,900 cal [11,020 ^{14}C] BP. Instead, water levels in the Ontario basin likely rose to accommodate the incoming glacial meltwater. The water level increase may have been attenuated by evaporation, as has been suggested for glacial Lake Agassiz by Birks et al. (2007), Fisher and Lowell (2012) and Lowell et al. (2013). However, the rapid increase in $\delta^{18}O_{lakewater}$ values that resumed towards the end of this 500-year interval (Figs. 2.6d, 2.7d, 2.8d) is most simply explained by cessation of low-^{18}O meltwater input than by any other mechanism.

A more robust age model, assisted by paleomagnetic secular variation records, would help to improve current age control on meltwater passage through the Ontario basin, and perhaps offer further possibilities for outlets from the lake at this time. Nonetheless, our current ideas correlate well with the lake-level history described by Anderson and Lewis (2012) (Fig. 2.11). In short, evidence for a large YD-age meltwater/flood routing event from the Ontario basin and adjacent confluent waters in the Lake Champlain, lower Ottawa and upper St. Lawrence valleys is the drawdown of glacial Lake Trenton which is recorded in Lake Ontario sediments beginning at ~13,260 cal [11,360 ^{14}C] BP by a sequence of increasingly positive $\delta^{18}O_{lakewater}$ values. The subsequent meltwater episode in the Ontario basin recorded from ~13,000 to 12,500 cal [11,100-10,500 ^{14}C] BP which is apparently is not represented in a downstream sediment sequence, would have little impact on the Atlantic THC/MOC.

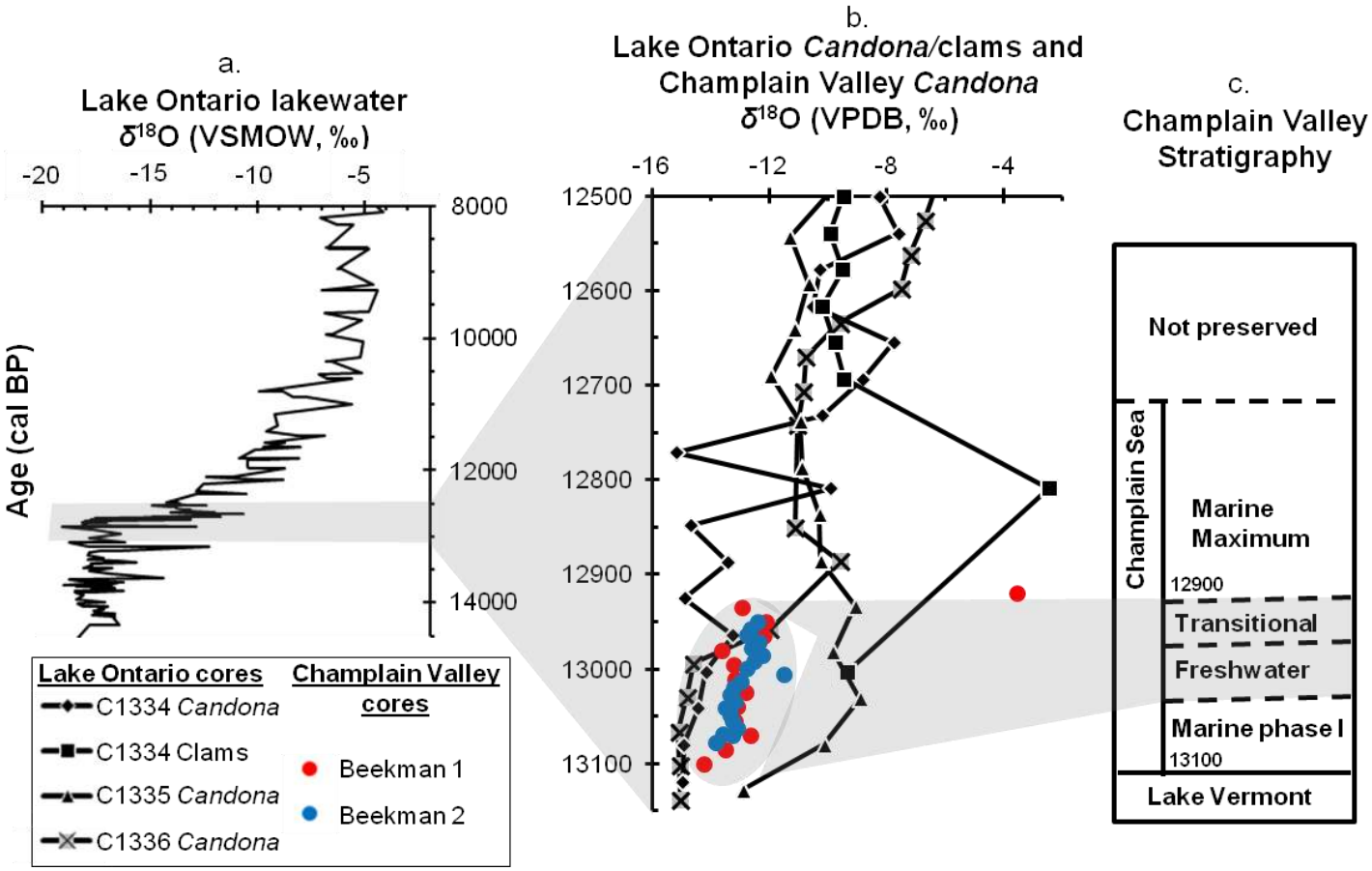

Figure 2.9. (a) Three-point running average of $\delta^{18}O_{lakewater}$ values for Cores 1334, 1335, and 1336. (b) Ostracode valve and clam shell oxygen isotope compositions (VPDB) (vital effect corrected, subtract 2.2 ‰ from VPDB data) for Lake Ontario. Red and blue dots represent Champlain valley *Candona* record from Beekmantown 1 and 2 cores, as outlined by Cronin et al. (2012). A generalized age for the Beekmantown cores was inferred from Rayburn et al. (2011). (c) Champlain Valley stratigraphy outlined by Cronin et al. (2012).

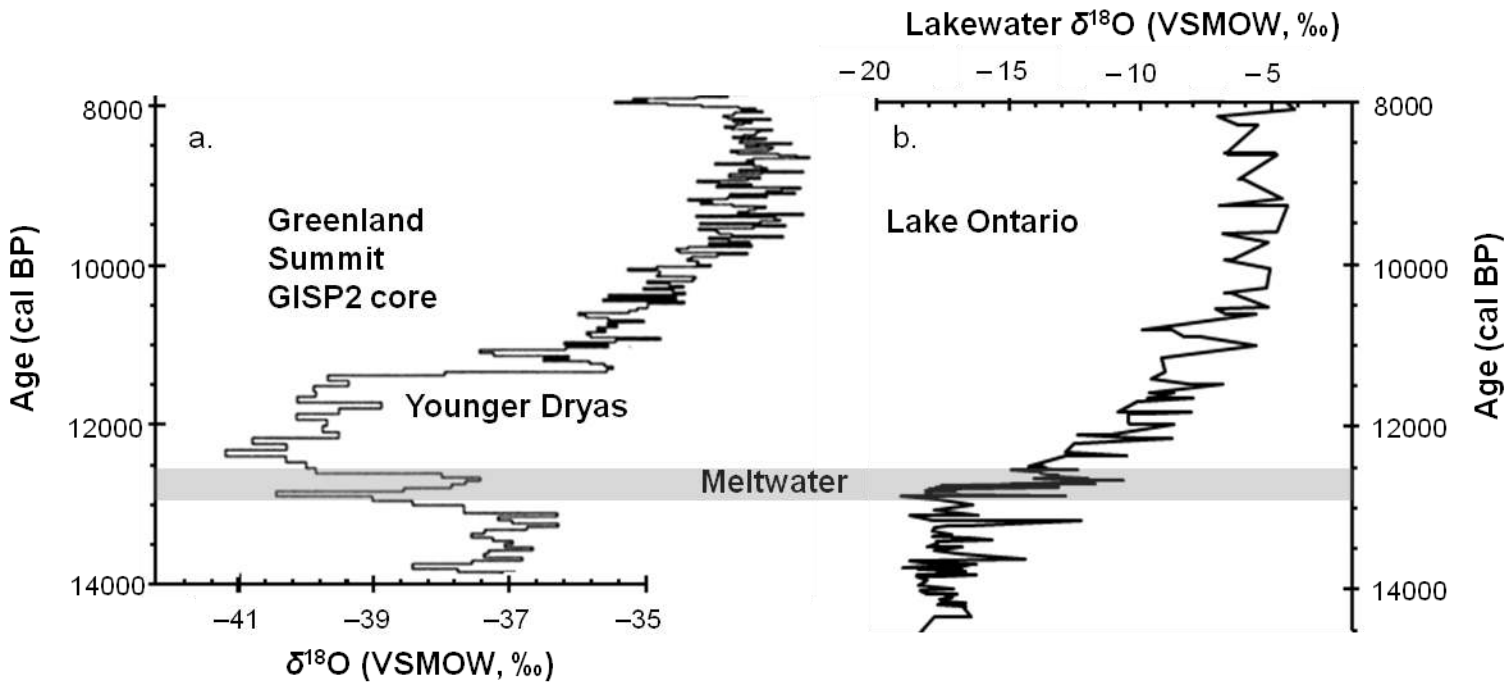

Figure 2.10. (a) GISP2 oxygen-isotope record illustrating the Younger Dryas event (Yu and Eicher, 1998). (b) Three-point running average of $\delta^{18}O_{lakewater}$ values for Cores 1334, 1335 and 1336. Gray shaded area indicates the period of the terminal glacial meltwater influx at 13,000-12,500 cal [11,100-10,500 ^{14}C] BP.

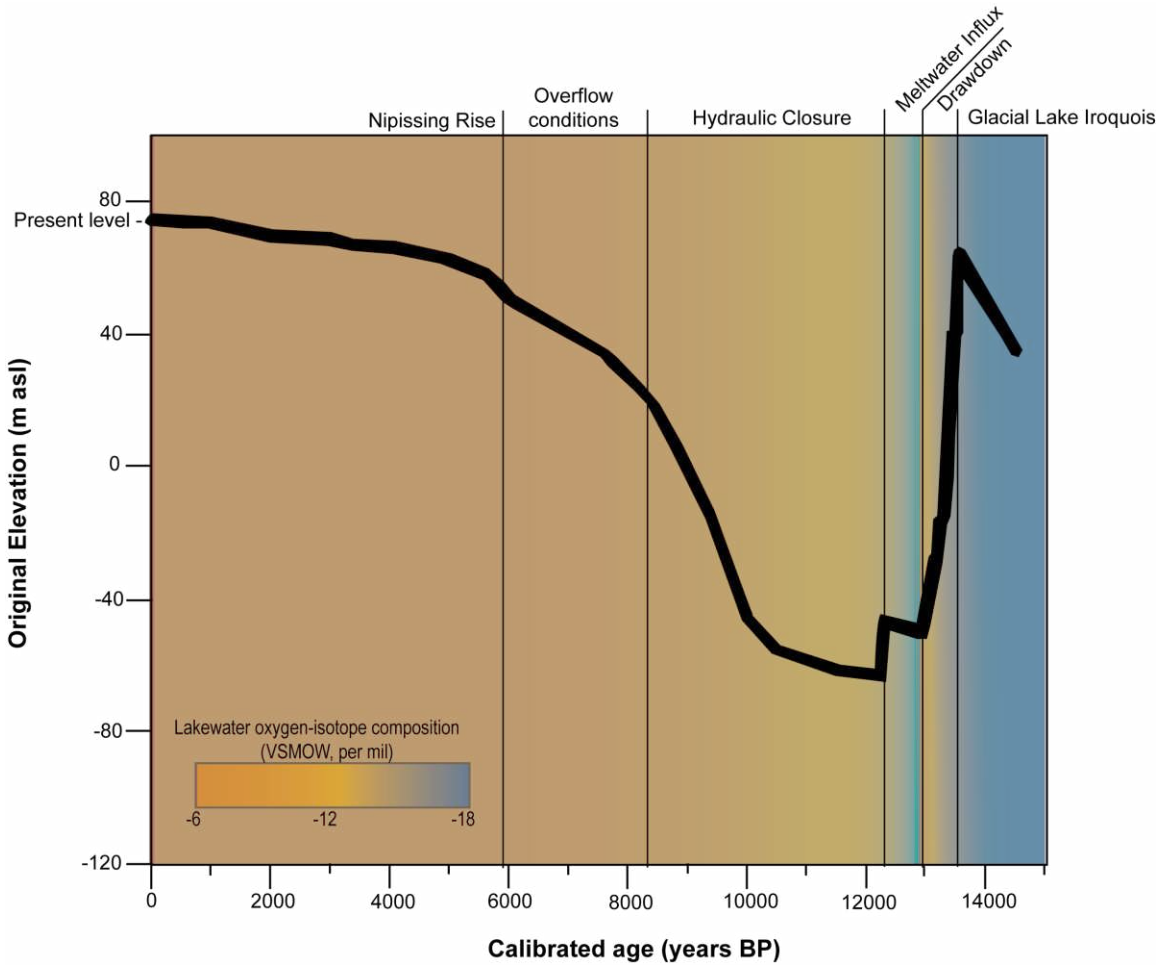

Figure 2.11. Lake elevation versus age in the main Ontario basin, as outlined by Anderson and Lewis (2012). The thick black line represents the inferred lake level. The $\delta^{18}O_{lakewater}$ values (inferred from ostracodes valves and clam shells) are demonstrated by the colour gradient –blue representing lower $\delta^{18}O_{lakewater}$ values, whereas orange represents higher $\delta^{18}O_{lakewater}$ values. Important lake phases are indicated at the top of the diagram.

Moore et al. (2000) and Cronin et al. (2008) proposed that meltwater flowed through the Erie-Ontario basins into the St. Lawrence-Champlain system during the main drawdown of glacial Lake Algonquin at 11,200 to 11,100 cal [9,750 to 9,640 ^{14}C] BP. Such routing is very unlikely. As is discussed below, Lakes Erie and Ontario were hydrologically closed during the main Algonquin drawdown; there is no low ^{18}O signal present in the ostracode record of Lake Ontario sediment for this time period (Anderson and Lewis; 2012; Lewis et al., 2012). Meltwater reaching the St. Lawrence-Champlain system from glacial Lake Algonquin would have required routing through the North Bay outlet, thus bypassing the lower Great Lakes.

2.4.3 Post-glacial transition and hydrologic closure (12,500-8,300 cal [10,500-7,500 ^{14}C] BP)

Following the final influx of glacial meltwater into Lake Ontario, glacial Lake Algonquin outlets at Port Huron and Fenelon Falls were abandoned and outflow diverted to a newly opened northern outlet near North Bay, Ontario (Eschman and Karrow, 1985; Karrow, 2004). The increase in Ontario basin $\delta^{18}O_{lakewater}$ resumed, largely because glacial meltwater input had ended; values inferred from ostracode compositions reached as high as –9.8 ‰ in Core 1334, –9.9 ‰ in Core 1335 and –9.0 ‰ in Core 1336 by 12,300 cal [10,400 ^{14}C] BP (Figs. 2.6d, 2.7d, 2.8d). At 12,300 cal [10,400 ^{14}C], Lake Ontario entered closed basin conditions according to Anderson and Lewis (2012); they noted that the lowest water levels were a product of evaporative stress, and lasted until about 10,000 cal [8,880 ^{14}C] BP. Water levels gradually rose after that time as evaporative stress eased, but hydrologic closure persisted until ~8,300 cal [7,500 ^{14}C] BP.

The $\delta^{18}O_{lakewater}$ values and biostratigraphy of Ontario basin sediments support Anderson and Lewis' (2012) model (Fig. 2.11). During the early Holocene (until ~ 8,300 cal [7,500 ^{14}C] BP), southern Ontario was influenced mainly by Arctic air masses over the northward-retreating LIS (Edwards et al., 1996). This Arctic influence produced a cold/dry period in southern Ontario, with relative humidity levels 20% lower than at present (Edwards et al., 1996). Over this time period, $\delta^{18}O_{precipitation}$ values in southern Ontario increased from –15 to –11 ‰ (Edwards et al., 1996). Such compositions for

precipitation in the regional watershed would be expected to yield $\delta^{18}O_{lakewater}$ values no higher than ~ –12.5 to – 8.5 ‰, based on the present spread of ~2.5 ‰ between modern Lake Ontario and precipitation in the region (Longstaffe et al., 2011). However, by 10,500 cal [9,280 ^{14}C], $\delta^{18}O_{lakewater}$ had already increased to a maximum of –7 ‰ (ostracodes) to –6 ‰ (clam shell fragments) (Figs. 2.6d, 2.7d, 2.8d, 2.11). As such, the $\delta^{18}O_{lakewater}$ values during this stage of hydrologic closure point to a greater role for evaporative ^{18}O-enrichment than is presently the case.

The rate of increase in $\delta^{18}O_{lakewater}$ values slowed considerably after ~10,500 cal [9,280 ^{14}C] BP (Figs. 2.6d, 2.7d, 2.8d) through to end of hydrologic closure at 8,300 cal [7,500 ^{14}C] BP. There is little change in $\delta^{18}O_{lakewater}$ recorded by ostracodes, including *F. caudata* that appeared in Core 1336, and <2 ‰ increase (to –5 ‰) in all cores, based on clams. These results are consistent with the easing of evaporative conditions in the Ontario basin proposed by Anderson and Lewis (2012) as humidity and precipitation levels gradually increased with the onset of warmer conditions.

Low water levels during hydrologic closure were accompanied by the appearance of *Pisidium* sp. clams (Cores 1334 and 1335; fragments only in Core 1336) and *F. caudata* in Core 1336. Their appearance marks a significant change in the benthic biological community. The change in the biological community coincides with hydrologic closure of the Ontario basin and a peak in ostracode productivity in Cores 1334 and 1335. However, clam fragments were not detected until ~1,500 years later in Core 1336 (Figs. 2.6d, 2.7d, 2.8d). Shallower water is likely responsible for the emergence of clams (Delorme, 1989). They appeared first in Cores 1334 and 1335, initially as shell fragments, likely transported from shallower water, then as whole shells presumed deposited *in situ* when the basins were at their shallowest (current water depths, 110 and 192 m, respectively).

Clam fragments, likely transported from shallower water, appear later at the deeper Core 1336 site (current depth, 222 m). Shallower water conditions developed later in the vicinity of Core 1336 (current depth, 222 m) than elsewhere in Lake Ontario (Anderson and Lewis, 2012). The appearance of *F. caudata (*and disappearance of *C.*

subtriangulata) in Core 1336 suggests that bottom waters in this deeper basin were becoming less oxygenated compared to the western portion of the lake. Although not likely anoxic, the Rochester basin was likely experiencing conditions similar to those found in present day Lake Erie (Delorme, 1978). Loss of *C. subtriangulata* typically occurs as dissolved oxygen concentrations fall below its threshold of 5.6 mg/l. Successive years of low dissolved oxygen lead to extirpation of *C. subtriangulata* because of its relatively long life cycle (1 year) and the inability to reach a maturity to lay eggs (Delorme, 1978). *F. caudata*, by comparison, has lower dissolved oxygen requirements (2.3 mg/l), thus allowing it to thrive under lower oxygen conditions. Its shorter life cycle (3 to 4 weeks), and associated egg production, ensures proliferation for several generations (Delorme, 1978).

In Core 1334, the first clams record $\delta^{18}O_{lakewater}$ values similar to coexisting ostracodes. Clams in Cores 1335 and 1336, however, indicate higher $\delta^{18}O_{lakewater}$ values (by 1 to 2 ‰) than ostracodes from the same intervals. These differences could point to development of monomictic conditions in ancient Lake Ontario. The clams may have grown in shallower waters enriched in ^{18}O by evaporation prior to lake overturn, prior to being transported to deeper in the basin after death, whereas the *in-situ* ostracode valves reflected deeper, bottom-water compositions characteristic of well-mixed conditions.

2.4.4 Post-hydrologic closure (since 8,300 cal [7,500 ^{14}C] BP)

With the continued retreat and eventual collapse of the LIS, southern Ontario became more strongly influenced by marine tropical air masses originating in the Gulf of Mexico. This caused the regional climate to shift from the cold and dry conditions described earlier, to warm and dry (~8,300 to 6,800 cal [7,500 to 6,000 ^{14}C] BP), and then to warm and wet (at ~6,800 cal [6,000 ^{14}C] BP) (Edwards et al., 1996). Lake levels began to increase at ~8,300 cal [7,500 ^{14}C] BP (Anderson and Lewis, 2012). The Nipissing Rise at ~5,800 cal [5,090 ^{14}C] BP is typically used to mark the return of upper Great Lakes drainage to the Lakes Erie and Ontario, as warm and wet conditions became fully established. Evaluating these changes isotopically, however, is difficult because samples suitable for analysis were not found younger than ~7,900 cal [7,030 ^{14}C] BP in Core

1334, 5,900 cal [5,100 ^{14}C] BP in Core 1335, and 5,800 cal [5,090 ^{14}C] BP in Core 1336. The ostracode record for Core 1336 suggests that $\delta^{18}O_{lakewater}$ values were virtually identical to the present value of –6.6 ‰ between ~8,300 and 7,300 cal [7,500 and 6,370 ^{14}C] BP but hints at a slight lowering of $\delta^{18}O_{lakewater}$ values to ~ –7 ‰ by 5,800 cal [5,090 ^{14}C] BP (Fig. 2.11). The limited record for Core 1335 indicates slightly lower $\delta^{18}O_{lakewater}$ values (~ –7.5 ‰) for about the same time interval (Figs. 2.6d, 2.7d, 2.8d). Clam shells continue to record higher $\delta^{18}O_{lakewater}$ values (~ –5 ‰) with perhaps even more ^{18}O-rich, shallow water conditions in Core 1335 at ~ 5,900 cal [5,100 ^{14}C] BP; notably, a coexisting *in situ F. caudata* valve also suggests $\delta^{18}O_{lakewater}$ values of at least –5.5 ‰.

The paucity of suitable samples makes it difficult to comment further except in the most general of terms. By the time of the Nipissing rise, climatic and hydrological conditions in the Ontario basin, at least those that are captured by the $\delta^{18}O_{lakewater}$ signal, were not significantly different from the present time. Further comment is not warranted, given that shelly fauna disappeared completely from the sediment records examined here by 4,500 cal [4,000 ^{14}C] BP in Core 1334 and by 6,000 cal [5,280 ^{14}C] BP in Cores 1335 and 1336 (Figs. 2.6c, 2.7c, 2.8c). Low sedimentation rates likely caused biogenic carbonates to be dissolved before they could be buried. This observation is supported by a decrease in detrital carbonate contents over this time period (Figs. 2.6b, 2.7b, 2.8b).

2.5 Conclusions

The oxygen isotopic compositions of ostracodes and clams, supplemented by mineralogical and grain-size information, provide key insights into the extent, duration and origin of glacial meltwater input into ancient Lake Ontario since ~16,500 cal [13,300 ^{14}C] BP. These data allow us to assess the role of glacial meltwater passage through Lake Ontario as a trigger for the Younger Dryas cooling event:

1. Ostracode proxies for $\delta^{18}O_{lakewater}$ (<–17 ‰) values from the lowermost sediments sampled in the western and central portions of Lake Ontario confirm substantial glacial meltwater presence between 16,000-15,300 cal [13,140-12,975 ^{14}C] BP. Variations in detrital carbonate, clay and feldspar contents between the western and central portions of the Ontario basin indicate connectivity with ancient Lake Erie

(glacial Lake Ypsilanti) at this time. Continued low $\delta^{18}O_{lakewater}$ values (<–17.5 ‰) but a shift in detrital mineralogy and increased variability in $\delta^{18}O_{lakewater}$ from 15,300-14,500 cal [12,975-12,410 ^{14}C] BP marked the end of connectivity with Lake Ypsilanti to the west and dominance of eastern glacial meltwater inputs to the Ontario basin.

2. Glacial meltwater originating both from glacial Lake Algonquin and directly from the LIS contributed to glacial Lake Iroquois and subsequent glacial lakes, which were established in the Ontario basin as the LIS retreated and continued to block the Ontario basin's outlet to the St. Lawrence River (14,000-13,260 cal [12,150-11,360 ^{14}C] BP). Generally lower $\delta^{18}O_{lakewater}$ values (–18.1±0.7 ‰) in the eastern portion of glacial Lake Iroquois indicate contributions of meltwater deriving from the LIS. More variable $\delta^{18}O_{lakewater}$ values (–16.8±2.0 ‰) in the central portion of glacial Lake Iroquois indicate variable mixing between contributions from the west, from the east-central outlet of glacial Lake Algonquin and direct LIS runoff.
3. Extensive retreat of the LIS from the Lake Ontario basin to the St. Lawrence valley shortly after 13,260 cal [11,360 ^{14}C] BP led to the final post-Iroquois stage (Lake Trenton) which was confluent with Lake Vermont in the Lake Champlain basin and Lake Candona in the upper St Lawrence and lower Ottawa River valleys. The Ontario basin was marked by an increase in $\delta^{18}O_{lakewater}$ values from –19 to –12 ‰, largely caused by the loss of glacial meltwater input from the more distant ice margin.
4. A large volume outflow of freshwater to the Gulf of St. Lawrence followed when the extensive confluent water body standing at ~15 m above sea level, consisting of Lakes Trenton, Vermont, and Candona, drained catastrophically to the Gulf of St. Lawrence and was replaced by marine water of the Champlain Sea. Further evaluation of this large freshwater outflow is required to assess its impact on the North Atlantic THC/MOC and possible contribution to the onset of the YD climate event.
5. A decrease in $\delta^{18}O_{lakewater}$ values from ~ –12 to –14 ‰ marked entry of a final inflow of glacial meltwater – likely from glacial Lake Algonquin – into the Ontario basin, beginning at ~13,031 cal [11,100 ^{14}C] BP and lasting for ~500 years. Its initial arrival was not synchronous across the lake, appearing first in the central portion of

the Ontario basin. This timing suggests that meltwater travelling from glacial Lake Algonquin may have breached the Oak Ridges Moraine, thus first entering the Ontario basin at a north-central location.

6. Glacial meltwater pulses that entered Lake Ontario from 12,900 to 12,500 cal [11,020 to 10,500 ^{14}C] BP cannot be traced isotopically eastward into the Champlain Sea, and instead were likely retained within Lake Ontario. Glacial meltwater transported through the Ontario basin is unlikely to have played a significant role in the YD cooling event.
7. The increase in $\delta^{18}O_{lakewater}$ values from ~ –14 to –9 ‰ from 12,500-12,300 cal [10,500-10,400 ^{14}C] BP marks the loss of glacial meltwater input and the hydrologic closure of Lake Ontario at 12,300 cal [10,400 ^{14}C] BP. This change in conditions and lower lake levels in particular were marked by appearance of *Pisidium* sp. clams and the ostracode species *F. caudata*. By ~10,500 cal [9,280 ^{14}C] BP, $\delta^{18}O_{lakewater}$ values as high as –6 ‰ reflect increases in evaporation under cold and dry conditions to a much larger extent than currently experienced by Lake Ontario. Evaporative conditions eased between ~10,500 cal [9,280 ^{14}C] BP (Figs. 2.6d, 2.7d, 2.8d) and the end of hydrologic closure at 8,300 cal [7,500 ^{14}C] BP with the onset of warmer conditions.
8. Throughout the subsequent period of warm/dry and then warm/wet climatic conditions, ostracode-derived $\delta^{18}O_{lakewater}$ values were similar to the previous period, with perhaps a slight lowering from ~ –6.5 to –7.5 ‰ between ~8,300 and 5,800 cal [7,500 and 5,090 ^{14}C] BP. Clam shells continued to record higher $\delta^{18}O_{lakewater}$ values (~ –5 ‰). In short, by the time of the Nipissing Rise, conditions in the Ontario basin that are captured by the $\delta^{18}O_{lakewater}$ signal were not significantly different from the present time (–6.6 ‰).

2.6 References

Anderson, T.W., Lewis, C.F.M., 2012. A new water-level history for Lake Ontario basin: evidence for a climate-driven early Holocene lowstand. Journal of Paleolimology 47, 513–530.

Barnett, P.J., 1992. Quaternary geology of Ontario. in: Thurson, P.C., Williams, H.R., Sutcliffe, R.H., Stott, G.M., (Eds.), Geology of Ontario. Ontario Geological Survey Special Volume 4 (part 2), pp.1011–1088.

Birks, S.J., Edwards, T.W.D., Remenda, V.H., 2007. Isotopic evolution of glacial Lake Agassiz: new insights from cellulose and porewater isotopic archives. Palaeogeography, Palaeoclimatology, Palaeoecolology 246, 8–22.

Blaauw, M., 2010. Methods and code for 'classical' age-modelling of radiocarbon sequences. Quaternary Geochronology 5, 512–518.

Broecker, W.S., Kennett, J.T., Flower, B.P., Teller, J.T., Trumbore, S., Bonani, G., Wolfli, W., 1989. Routing of meltwater from the Laurentide Ice Sheet during the Younger Dryas cold episode. Nature 341, 318–320.

Bumstead, N.L., Longstaffe, F.J., Macdonald, R.A., 2009. The paleolimnology of Lake Simcoe: oxygen-isotope compositions of ostracodes. 11th International Paleolimnology Symposium, Guadalajara, Mexico, December 15-18, 2009.

Calkin, P.E., Feenstra, B.H., 1985. Evolution of the Erie-basin Great Lakes. in: Karrow, P.F., Calkin, P.E., (Eds.), Quaternary Evolution of the Great Lakes. Geological Association of Canada Special Paper 30, pp. 149–170.

Carmichael, C.M., Mothersill, J.S., Morris W.A., 1990. Paleomagnetic and pollen chronostratigraphic correlations of the late glacial and postglacial sediments in Lake Ontario. Canadian Journal of Earth Sciences 27, 131–147.

Coakley, J.P., Karrow, P.F., 1994. Reconstruction of post-Iroquois shoreline evolution in western Lake Ontario. Canadian Journal of Earth Sciences 31, 1618–1629.

Condron, A., Winsor, P., 2012. Meltwater routing and the Younger Dryas. Proceedings of the National Academy of Sciences 109, 19928–19933.

Coplen, T.B., 1996. New guidelines for reporting stable hydrogen, carbon, and oxygen isotope ratio data. Geochimica et Cosmochimica Acta 17, 3359–3360.

Cronin, T.M., Manley, P.L., Brachfeld, S., Manley, T.O., Willard, D.A., Guilbault, J.P., Rayburn, J.A., Thunell, R., Berke, M., 2008. Impacts of post-glacial lake drainage events and revised chronology of the Champlain Sea episode 13–9 ka. Palaeogeography, Palaeoclimatology, Palaeoecology 262, 46–60.

Cronin, T.M., Rayburn, J.A., Guilbault, J.-P., Thunell, R., Franzi, D.A., 2012. Stable isotope evidence for glacial lake drainage through the St. Lawrence Estuary, eastern Canada, ~13.1–12.9 ka. Quaternary International 260, 55-65.

Decrouy, L., Vennemann, T.W., Ariztegui, D., 2011a. Controls on ostracod valve geochemistry, Part 1: Variations of environmental parameters in ostracod (micro-) habitats. Geochimica et Cosmochimica Acta 75, 7364–7379.

Decrouy, L., Vennemann, T.W., Ariztegui, D., 2011b. Controls on ostracod valve geochemistry: Part 2. Carbon and oxygen isotope compositions. Geochimica et Cosmochimica Acta 75, 7380–7399.

Delorme, L.D., 1978. Distribution of freshwater ostracodes in Lake Erie. Journal of Great Lakes Research 4, 216–220.

Delorme, L.D., 1989. Methods in Quaternary ecology #7. Freshwater ostracodes. Geoscience Canada 16, 85–90.

Edwards, T.W.D., Fritz, P., 1986. Assessing meteoric water composition and relative humidity from ^{18}O and ^{2}H in wood cellulose: paleoclimatic implications for southern Ontario. Applied Geochemistry 1, 715–723.

Edwards, T.W.D., McAndrews, J.H., 1989. Paleohydrology of a Canadian Shield lake inferred from ^{18}O in sediment cellulose. Canadian Journal of Earth Sciences 26, 1850–1859.

Edwards, T.W.D., Wolfe, B.B., MacDonald, G.M., 1996. Influence of changing atmospheric circulation on precipitation $\delta^{18}O$–temperature relations in Canada during the Holocene. Quaternary Research 46, 211–218.

Eschman, D.F., Karrow, P.F., 1985. Huron basin glacial lakes: a review. in: Karrow, P.F., Calkin, P.E., (Eds.), Quaternary Evolution of the Great Lakes. Geological Association of Canada Special Paper 30, pp. 79–93.

Fahl, K., Stein, R., 2012. Modern seasonal variability and deglacial/Holocene change of central Arctic Ocean sea-ice cover: new insights from biomarker proxy records. Earth and Planetary Science Letters 351–352, 123–133.

Fisher, T.G., Lowell, T.V., 2006. Questioning the age of the Moorhead Phase in the glacial Lake Agassiz basin. Quaternary Science Reviews 25, 2688–2691.

Fisher, T.G., Lowell, T.V., 2012. Testing northwest drainage from Lake Agassiz using extant ice margin and strandline data. Quaternary International 260, 106–114.

Flower, B.P., Hastings, D.W., Hill, H.W., Quinn, T., 2004. Phasing of deglacial warming and Laurentide Ice Sheet meltwater in the Gulf of Mexico. Geology 32, 597–600.

Friedman, I., O'Neil, J. R., 1977. Compilation of stable isotope fractionation factors of geochemical interest, in: Fleischer, M. (Ed.) US Geological Survey Professional Paper 440-KK. Data of geochemistry, US Government Print Office, Washington, DC, USA, pp. 1–12.

Fritz, P., Anderson T.W., Lewis C.F.M., 1975. Late Quaternary climate trends and history of Lake Erie from stable isotope studies. Science 190, 267–269.

Holmes, J. A., 2001. Ostracoda, in: Smol, J. P., Birks, H. J. B., Last, W. M. (Eds.), Tracking Environmental Change Using Lake Sediments Volume 4: Zoological Indicators. Dordrecht: Kluwer Academic Publishers, pp.125–152.

Hutchinson, D.R., Lewis, C.F.M., Hund, G.E., 1993. Regional stratigraphic framework of surficial sediments and bedrock beneath Lake Ontario. Géographie physique et Quaternaire 47, 337–352.

Karrow, P.F., 2004. Algonquin-Nipissin shorelines, North Bay, Ontario. Géographie physique et Quaternaire 58, 297–304.

Last, W.M., Teller, J.T., Forester, R.M., 1994. Paleohydrology and paleochemistry of Lake Manitoba, Canada: the isotope and ostracode records. Journal of Paleolimnology 12, 269–282.

Lewis, C.F.M., Anderson, T.W., 1992. Stable isotope (O and C) and pollen trends in eastern Lake Erie, evidence for a locally induced climatic reversal of Younger Dryas age in the Great Lakes basin. Climate Dynamics 6, 241–250.

Lewis, C.F.M., King, J.W., Blasco, S.M., Brooks, G.R., Coakley, J.P., Croley II, T.E., Dettman, D.L., Edwards, T.W.D., Heil Jr., C.W., Hubeny, J.B., Laird, K.R., McAndrews, J.H., McCarthy, F.M.G., Medioli, B.E., Moore Jr., T.C., Rea, D.K., Smith, A.J., 2008. Dry climate disconnected the Laurentian Great Lakes. EOS, Transactions American Geophysical Union 89, 541–542.

Lewis, C.F.M., Cameron, G.D.M., Anderson T.W., Heil Jr., C.W., Gareau, P.L., 2012. Lake levels in the Erie Basin of the Laurentian Great Lakes. Journal of Paleolimnology 47, 493–511.

Longstaffe, F.J., Ayalon, A., Bumstead, N.L., Crowe, A.S., Hladyniuk, R., Hornibrook, P.A., Hyodo, A., Macdonald, R.A., 2011. The oxygen-isotope evolution of the North American Great Lakes. Northeastern (46th Annual) and North-Central (45th Annual) Joint Meeting of the Geological Society of America, Pittsburgh, Pennsylvania, USA, March 20-22, 2011, p. 57.

Lowell, T.V., Applegate, P.J., Fisher, T.G., Lepper, K., 2013. What caused the low-water phase of glacial Lake Agassiz? Quaternary Research 80, 370–382.

McAndrews, J.H., 1994. Pollen diagrams for southern Ontario applied to archeology, in: MacDonald, R.I. (Ed.) Great Lakes Archeology and Paleoecology: Exploring Interdisciplinary Initiatives for the Nineties. Quaternary Sciences Institute, University of Waterloo, Waterloo, pp 179–195.

Macdonald, R.A., Longstaffe, F.L., 2008. The Late Quaternary oxygen-isotope composition of southern Lake Huron. Aquatic Ecosystem Health and Management 11, 137–143.

Miller, B.B., Karrow, P.F., Mackie, G.L. 1985. Late Quaternary molluscan faunal changes in the Huron basin, in: Karrow, P.F., Calkin, P.E., (Eds.), Quaternary Evolution of the Great Lakes. Geological Association of Canada Special Paper 30, pp.211–229.

Moore, T.C.J., Walker, J.C.G., Rea, D.K., Lewis, C.F.M., Shane, L.C.K., Smith, A.J., 2000. Younger Dryas interval and outflow from the Laurentide Ice Sheet. Paleoceanography 15, 4–18.

Muller, E.H., Prest, V.K., 1985. Glacial lakes in the Ontario basin, in: Karrow, P.F., Calkin, P.E., (Eds.), Quaternary Evolution of the Great Lakes. Geological Association of Canada Special Paper 30, pp.211–229.

Munsell Color. 2000. Munsell Soil Color Charts Year 2000 Revised Washable Edition. GretagMacbeth, New Windsor, NY.

Murton, J.B., Bateman, M.D., Dallimore, S.R., Teller, J.T., Yang, Z., 2010. Identification of Younger Dryas outburst flood path from Lake Agassiz to the Arctic Ocean. Nature 464 (7289), 740–743.

National Oceanic and Atmospheric Administration Digital Elevation Model (DEM) Discovery Portal website (2014). Retrieved February 14, 2014 from http://ngdc.noaa.gov/mgg/dem/

Parent, M., Occhietti, S., 1988. Late Wisconsinan deglaciation and Champlain Sea invasion in the St. Lawrence Valley, Quebec. Géographie physique et Quaternaire 42, 215–246.

Pippert, R.G., Brown, G.R., Morris, W.A., 1996. Palaeomagnetic chronostratigraphy of Holocene sediments, Niagara basin, Lake Ontario, Canada. Journal of Quaternary Science 11, 217–231.

Rayburn, J.A., Franzi, D.A., Knuepfer, P.L.K., 2007. Evidence from the Lake Champlain Valley for a later onset of the Champlain Sea and implications for late glacial meltwater routing to the north Atlantic. Palaeogeography, Palaeoclimatology, Palaeoecology 246, 62–74.

Rayburn, J.A., Cronin, T.M., Franzi, D.A., Knuepfer, P.L.K., Willard, D.A., 2011. Timing and duration of North American glacial lake discharges and the Younger Dryas climate reversal. Quaternary Research 75, 541–551.

Reimer, P.J., Baillie, M.G.L., Bard, E., Bayliss, A., Beck, J.W., Blackwell, P.G., Bronk Ramsey, C., Buck, C.E., Burr, G.S., Edwards, R.L., Friedrich, M., Grootes, P.M., Guilderson, T.P., Hajdas, I., Heaton, T.J., Hogg, A.G., Hughen, K.A., Kaiser, K.F., Kromer, B., McCormac, F.G., Manning, S.W., Reimer, R.W., Richards, D.A., Southon, J.R., Talamo, S., Turney, C.S.M., van der Plicht, J., Weyhenmeyer, C.E., 2009. IntCal09 and Marine09 radiocarbon age calibration Curves, 0–50,000 Years cal BP. Radiocarbon 51, 1111–1150.

Richard, P.J.H., Occhietti, S., 2005. ^{14}C chronology for ice retreat and inception of Champlain Sea in the St. Lawrence Lowlands, Canada. Quaternary Research 63, 353–358.

Schroeder, R.A., Bada, J.L., 1978. Aspartic acid racemization in Late Wisconsin Lake Ontario sediments. Quaternary Research 9, 193–204.

Sharpe, D., Pugin, A., Pullan, S., Shaw, J., 2004. Regional unconformities and the sedimentary architecture of the Oak Ridges Moraine area, southern Ontario. Canadian Journal of Earth Sciences 41, 183–198.

Silliman, J.E., Meyers, P.A., Bourbonniere, R.A., 1996. Record of postglacial organic matter delivery and burial in sediments of Lake Ontario. Organic Geochemistry 24 (4), 463–472.

Teller, J.T., Boyd, M., Yang, Z., Kor, P.S.G., Fard, A.M., 2005. Alternative routing of Lake Agassiz during the Younger Dryas: new dates, paleotopography and a re-evaluation. Quaternary Science Reviews 24, 1890–1905.

von Grafenstein, U., Erlernkeuser, H., Trimborn, P., 1999. Oxygen and carbon isotopes in modern fresh-water ostracod valves: assessing vital offsets and autecological effects of interest for palaeoclimate studies. Palaeogeography, Palaeoclimatology, Palaeoecology 148, 133–152.

Voytek, E.B., Colman, S.M., Wattrus, N.J., Gary, J.L., Lewis, C.F.M., 2012. Thunder Bay, Ontario, was not a pathway for catastrophic floods from Glacial Lake Agassiz. Quaternary International 260, 98–105.

Williams, C., Flower, B.P., Hastings, D.W., Guilderson, T.P., Quinn, K.A., Goddard, E.A., 2010. Deglacial abrupt climate change in the Atlantic Warm Pool: A Gulf of Mexico perspective. Paleoceanography 25, PA4221.

Williams, C., Flower, B.P., Hastings, D.W., 2012. Seasonal Laurentide Ice Sheet melting during the “Mystery Interval” (17.5-14.5 ka). Geology 40, 955–958.

Yu, Z., McAndrews, J.H., Eicher, U., 1997. Middle Holocene dry climate caused by change in atmospheric circulation patterns: evidence from lake levels and stable isotopes. Geology 25 (3), 251–254.

Yu, Z., Eicher, U., 1998. Abrupt climate oscillations during the last deglaciation in central North America. Science 282, 2235–2238.

Chapter 3

3 Late Quaternary paleoproductivity of Lake Ontario and its sources of organic matter

3.1 Introduction

Variations in aquatic productivity and source input to Lake Ontario provide clues as to how regional climate and environmental conditions evolved as the Laurentide Ice Sheet (LIS) retreated from the region. Lake Ontario, in particular, offers a unique opportunity to investigate a substantial period of hydrologic closure during its history, and to test the robustness of traditional lacustrine paleoproductivity proxies under a wide range of environmental conditions.

The water-level history of Lake Ontario and its predecessors since the latest Pleistocene have been described in detail by Anderson and Lewis (2012), thus making it possible to correlate ancient lake levels with organic productivity and changes in water sources. In brief, the water-level history is as follows. The recorded history of the Ontario basin began at ~16,000 cal BP when the LIS partially retreated from the Lake Ontario basin during the Mackinaw interstadial. This facilitated sediment deposition in the central and western portions of the lake. Ice readvance shortly thereafter resulted in subglacial sedimentation in the Ontario basin until 14,500 cal BP. During the Late Pleistocene (shortly after 14,500 cal BP), retreating Wisconsinan ice dammed the outlet at the St. Lawrence River (Fig. 3.1) allowing glacial Lake Iroquois to fill an isostatically depressed Ontario basin at ~14,000 cal BP. Glacial Lake Iroquois water levels and drainage were controlled by retreating ice; drainage occurred southeastward first through the Mohawk and Hudson River valleys to the Atlantic Ocean, then through the Lake Champlain basin to the Hudson River valley and Atlantic Ocean (Fig. 3.1) (Muller and Prest, 1985). Glacial Lake Iroquois terminated at 13,260 cal BP, draining in a series of lake stages (Frontenac, Sydney '?', Belleville-Sandy Creek, and Trenton-Skinner Creek) as the impounding ice retreated northward out of the St. Lawrence River valley (Pair and Rodrigues, 1993; Anderson and Lewis, 2012). The latter lake level stages were confluent with Lake Vermont in the Lake Champlain basin (Fig. 3.1), which continued to drain

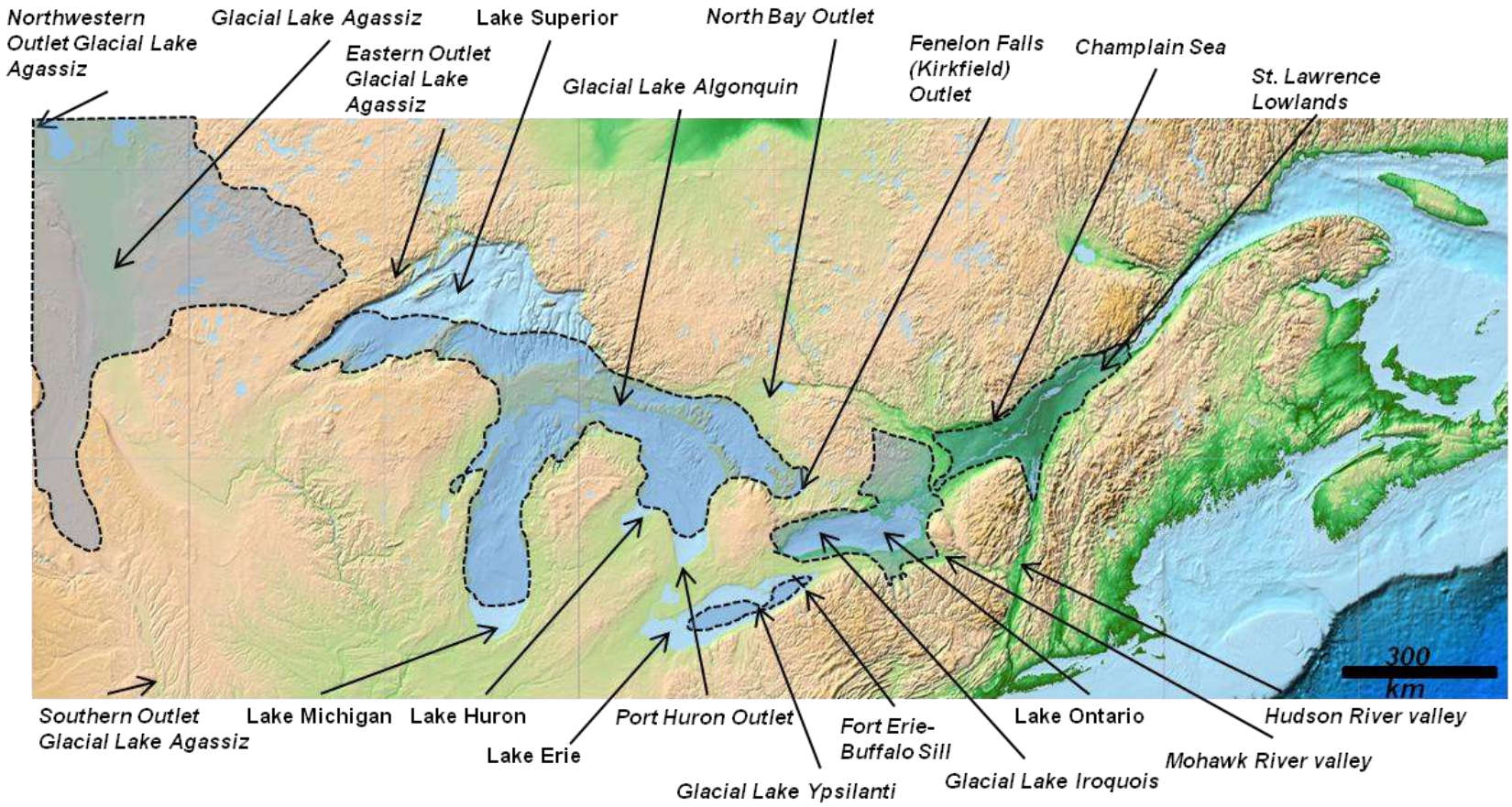

Figure 3.1. Digital Elevation Model (DEM) of the Great Lakes basin. Important outlets and locations are denoted in italics. Figure modified from the Nation Oceanic and Atmospheric Administration data center website (http://ngdc.noaa.gov/mgg/dem/).

through the Hudson River Valley (Anderson and Lewis, 2012). Continued retreat of the LIS from the St. Lawrence valley allowed invasion of seawater, thus forming the Champlain Sea (Fig. 3.1) at 12,900 cal BP (Anderson and Lewis, 2012). Early Lake Ontario was confluent with the Champlain Sea during a near stillstand period, while both basins and their water levels were rising (Anderson and Lewis, 2012). Early Lake Ontario was not inundated by seawater because of increased precipitation and meltwater inflow, most likely from glacial Lake Algonquin from 13,000 to 12,500 cal BP (Chapter 2, this thesis). Hydrologic closure of Lake Ontario began at 12,300 cal BP when the upper Great Lakes drainage pattern switched from the southern Port Huron outlet to the North Bay outlet (Fig. 3.1) (Anderson and Lewis, 2012). Hydrologic closure continued until 8,300 cal BP when increased precipitation caused the lake to reach overflow conditions. From 8,300 to 5,200 cal BP, lake level rise was synchronous with increased precipitation in southern Ontario. By 5,800 cal BP, the Nipissing rise marks the return of upper Great Lakes drainage to Lake Ontario.

The composition of lacustrine organic matter (OM) can provide insight into shifts in vegetation and aquatic productivity driven by changes in regional climate. In particular, the $\delta^{13}C$ values of biogenic carbonates, percentages of organic carbon (OC) and total nitrogen (TN), and the carbon/nitrogen (C/N) ratios and stable carbon-isotope ($\delta^{13}C_{OM}$) and nitrogen-isotope ($\delta^{15}N_{OM}$) values of bulk sediment organic matter (OM) provide useful measures of primary productivity and/or OM source changes to the lake. McFadden et al. (2004) and (2005) reported data for such parameters for the easternmost portion of Lake Ontario from 10,000 cal BP to 1850 AD. They showed, in general, that most proxies showed a shift at 9,400 cal BP, which is defined as the onset of Holocene warming in the region. These proxies also suggested that the Holocene Thermal Maximum (HTM; 9,400 to 5,300 cal BP) was the warmest and wettest period during the Holocene. Interrupting regional warming were two cold periods: the '8.2 ka' event and the Nipissing rise (6,800 to 5,000 cal BP). From 5,300 cal BP to 1850 AD, the region was cooler and drier, but more stable than during the HTM.

In addition, Silliman et al. (1996) described a record of postglacial OM delivery to Lake Ontario using C/N ratios and $\delta^{13}C_{OM}$ values. They found that C/N ratios increased from 4 (glacial) to 8 (postglacial) from the base of their core to ~300 cm. They interpreted the low C/N ratios to indicate that lacustrine algae was the dominant OM source, but suggested that the upward increase marked a shift to more terrigenous input following deglaciation. Silliman et al. (1996) reported $\delta^{13}C_{OM}$ values that varied between –28.0 and –25.5 ‰ throughout the record. They noted that such compositions span the range of both lacustrine algae and C_3 land plants, and thus do not discriminate between the two sources. They suggested that the $\delta^{13}C_{OM}$ values reflected the combined effects of lower atmospheric pCO_2 during the latest Pleistocene and perhaps recycled OM from the erosion of the Paleozoic carbonates.

In this paper, we build on these studies by examining similar proxies that extend back in time to ~16,000 cal BP and span the entire Lake Ontario basin from west to east. In particular, we report on and evaluate the overall significance of such proxies as measures of environmental change in this region over that time period.

3.1.1 Carbon-isotope composition of biogenic carbonates

The carbon isotopic compositions of ostracodes valves ($\delta^{13}C_{ostracode}$) and clam shells ($\delta^{13}C_{clam}$) have been largely ignored in lake sediments when interpreting climate histories because of the complexity of the lacustrine dissolved inorganic (DIC) pool. The $\delta^{13}C_{ostracode}$ and $\delta^{13}C_{clam}$ values mostly reflect the isotopic composition of the DIC ($\delta^{13}C_{DIC}$) from which the carbonate formed (Holmes, 2001). These measures can be used to evaluate lacustrine productivity changes, if the factors controlling the DIC pool can be determined, and can also be used to determine source inputs of DIC when $\delta^{13}C_{ostracode}$ and $\delta^{13}C_{clam}$ values vary within the lake (Fig. 3.2) (Schwalb et al., 2002; 2013). The complexity of this system reflects the various conditions under which biogenic carbonate can precipitate. DIC content and isotopic composition in lakewater are a function of the degree of CO_2 exchange with the atmosphere, the uptake rate of dissolved CO_2 during photosynthesis, rates of decay of organic matter, microbial

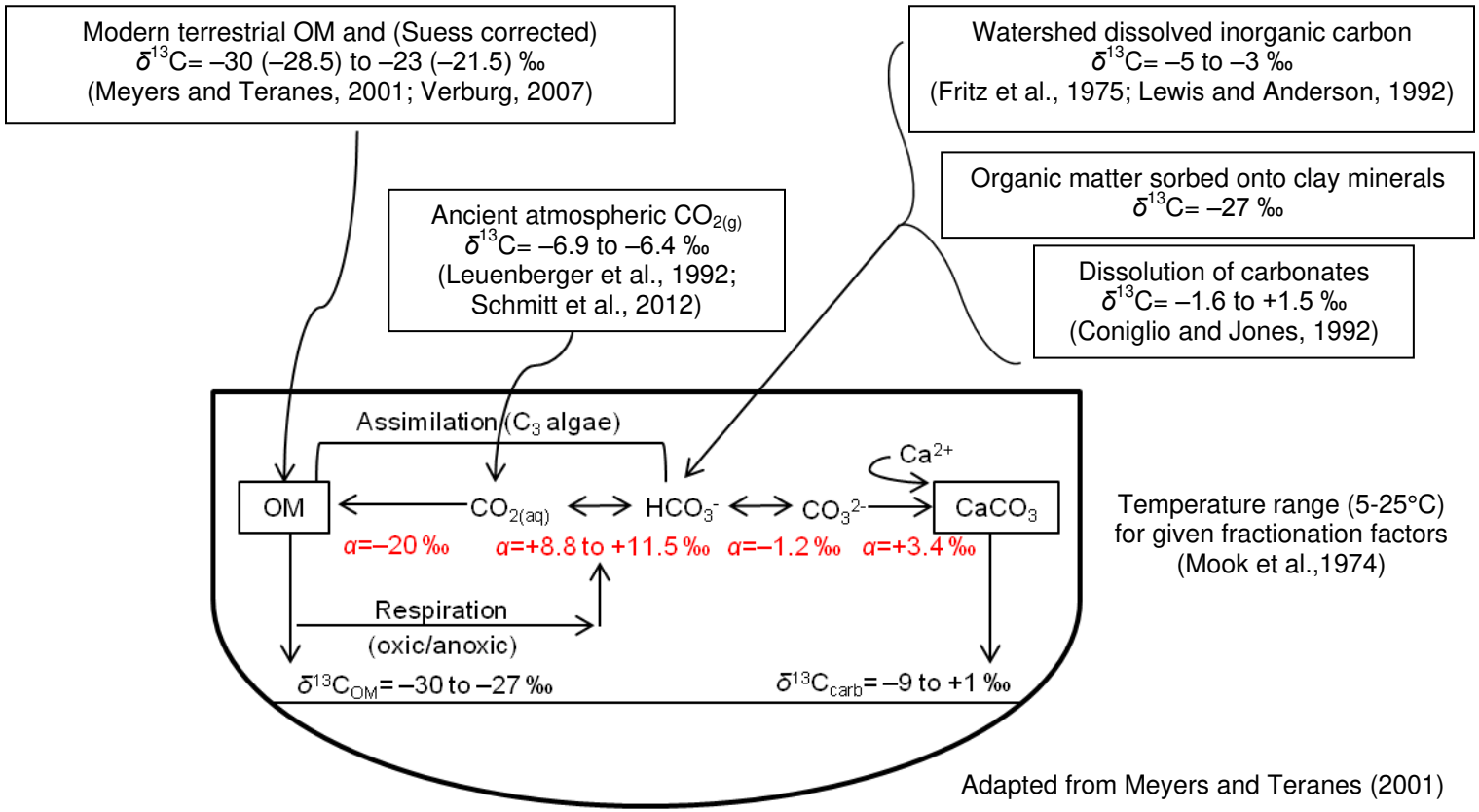

Figure 3.2. Carbon isotope systematics and sources of DIC to Lake Ontario. Figure modified from Meyers and Teranes (2001).

processes, micro-habitat conditions, and the composition and rate of dissolution of carbonate rocks and minerals within the catchment (Talbot and Kelts, 1990; von Grafenstein et al., 1999). Recent literature suggests that relative changes in $\delta^{13}C_{ostracode}$ (in our case, *Candona subtriangulata, Fabaeformiscandona caudata*) and $\delta^{13}C_{clam}$ values (in our case, *Pisidium* sp.) can be used as a measure of $\delta^{13}C_{DIC}$. These organisms exhibit no vital effects/offsets from the DIC pool and hence are a robust proxy for assessing historical lake conditions (von Grafenstein et al., 1999; Decrouy et al., 2011).

3.1.2 Organic carbon, total nitrogen and carbon/nitrogen ratio

OC and TN are useful proxies for assessing variations in the amount of OM input to lacustrine systems (Meyers and Teranes, 2001). Although OC and TN abundances cannot, in and of themselves, serve to distinguish between allocthonous and autocthonous OM input to a lake, they still provide a good first-order measure of general (perhaps regional) organic productivity. When comparing glacial and post-glacial sediments, differences in sedimentation rates and densities can be normalized using mass accumulation rates (MARS). MARS provide a better measure of delivery and preservation of OM than bulk OC and TN contents (Meyers and Lallier-Verges, 1999). In Great Lakes sediments, MARS are especially useful for determining changes in delivery rates and sources of OM to the lake, particularly when assessing the impact of glacially derived OM input to the lake.

Traditionally, the C/N ratio is also very important because it can help identify the proportions of aquatic (algal) non-vascular plants to terrestrial, vascular plants in a way not immediately obvious from direct measurements of bulk OC and TN concentrations. Non-vascular plants are protein-rich and cellulose-poor and will typically yield a C/N ratio between 4 and 10 (Meyers, 1994). Vascular terrestrial plants are protein-poor and cellulose-rich and have a C/N ratio of >20 (Meyers, 1994). These original ratios are generally preserved in lake sediment OM, with minor exceptions. C/N ratios >20 are traditionally interpreted as indicating dominance of terrestrial plants in lacustrine OM. This can indicate higher local terrestrial productivity related to warmer temperatures

and/or increased precipitation, and hence increased run-off and terrestrial OM transport to the lake. C/N ratios between 4 and 10 are traditionally interpreted to indicate dominance of lacustrine algal productivity. This can indicate increased autocthonous OM production in the lake and/or hydrologic closure of the lake basin, which is associated with reduced run-off and hence lower terrestrial OM input. In this paper, we evaluate whether or not this simple model is applicable to the interpretation of results for glacial and postglacial sediments from Lake Ontario.

3.1.3 Carbon-isotope composition of bulk sediment organic matter

Values of $\delta^{13}C_{OM}$ can be a useful aid in determining changes in primary productivity and OM sources (Hodell and Schelske, 1998). A systematic increase in $\delta^{13}C_{OM}$ values during periods of higher lacustrine productivity arises from preferential uptake of ^{12}C during photosynthesis; increased productivity reduces this discrimination resulting in higher $\delta^{13}C_{OM}$ values (McKenzie, 1985). The $\delta^{13}C_{OM}$ values can also be used to identify changes in terrestrial plant communities, if a significant proportion of OM entering the lake is of terrestrial origin. Most photosynthetic plants incorporate carbon into OM using the C_3 – Calvin – pathway, which preferentially takes up ^{12}C with an isotopic discrimination yielding an average $\delta^{13}C_{OM} = -25$ ‰ presently (O'Leary, 1988). Fewer plants use the C_4 – Hatch-Slack – pathway ($\delta^{13}C_{OM} = -10$ ‰), and still fewer the CAM – Crassulacean Acid Metabolism – pathway ($\delta^{13}C_{OM} = -25$ to -10 ‰) (O'Leary, 1988), especially in the Great Lakes region. Freshwater algae (C_3 pathway) use dissolved CO_2 in isotopic equilibrium with the atmosphere and are isotopically indistinguishable from OM produced by C_3 plants from the surrounding watershed (–29 to –25 ‰) (Meyers and Ishiwatari, 1993; Meyers, 1997; Meyers and Teranes, 2001).

3.1.4 Nitrogen-isotope compositions of bulk sediment organic matter

Nitrogen occurs in fresh waters in numerous forms including dissolved molecular nitrogen, amino acids, amines, proteins, humic compounds, ammonia, nitrite and nitrate. Sources of nitrogen include nitrogen fixation both in the water and sediments, inputs from surface and ground water, and precipitation (Wetzel, 2001). Values of $\delta^{15}N_{OM}$ can assist in identifying aquatic versus terrestrial sources and in reconstructing

paleoproductivity rates (Meyers, 2003). Inorganic nitrogen reservoirs for land and aquatic plants are quite different; dissolved nitrate (NO_3^-) has mean $\delta^{15}N_{OM}$ range of +7 to +10 ‰, and atmospheric molecular nitrogen (N_2) has a $\delta^{15}N$ value of +0.5 ‰ (Peters et al., 1978; Wada, 1980). Hence, algae $\delta^{15}N_{OM}$ are normally around +8.5 ‰, typically higher than C_3 land plants (average $\delta^{15}N$ = +1 ‰) (Meyers and Lallier-Verges, 1999; Meyers, 2003). That said – the complex nature of the nitrogen cycle and isotopic discrimination of nitrogen during biological uptake introduces variability to any generalized $\delta^{15}N$ values for the OM system (Fogel and Cifuentes, 1993). Deviations from the $\delta^{15}N_{OM}$ values expected in lake sediment records can challenge the utilization of bulk $\delta^{15}N$ values (which can include nitrogen from both organic and inorganic sources) as a proxy for changes in OM sources and allocthonous production (Meyers and Lallier-Verges, 1999).

3.2 Materials and methods

Three piston cores, along with accompanying benthos cores, were collected from Lake Ontario during July 15-17, 2008 by the captain and crew of the Canadian Coast Guard Ship (CCGS) *Limnos*: Core 1335, Mississauga basin; Core 1336, Rochester basin, and Core 1334, Niagara basin (Fig. 3.3). The cores were cut into ~1 m sections onboard and stored in a refrigerator prior to delivery to the University of Rhode Island, where they were halved longitudinally and their visible characteristics noted (colour, consistency, grain size, sedimentary structures including laminations; Chapter 2, this thesis). Sediment colour was described using the Munsell Soil Colour Charts and notation (2000). The cores were then shipped to the University of Western Ontario where they continue to be stored at 4°C.

The age-depth model (Fig. 3.4) was anchored using three accelerator mass spectrometer (AMS) radiocarbon dates of terrestrial macro-fossils and clam shells (Chapter 2, this thesis; Table 2.1). The clam shell date was corrected for the hard water effect by subtracting 535 ± 15 years (Anderson and Lewis, 2012). All radiocarbon dates were converted to calibrated ages using INTCAL09 (Reimer et al., 2009). Additional information used to construct the age-depth model included pollen stratigraphy (Carmichael et al., 1990; McAndrews, 1994; Pippert et al., 1996), seismic stratigraphy

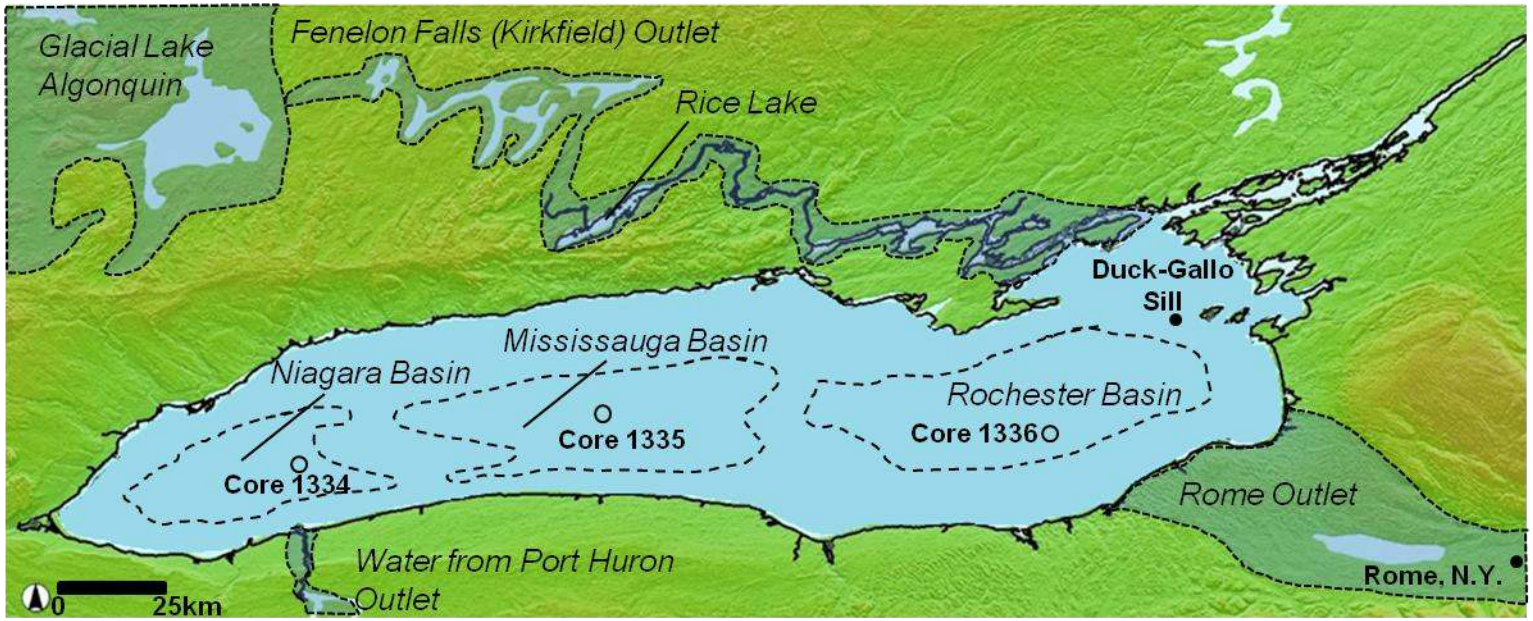

Figure 3.3. DEM Lake Ontario region showing the locations of sediment piston cores: Core 1334 (43° 24' 23" N and 79° 00' 05" W; water depth, 110.3 m; core length, 17.00 m), Core 1335 (43° 33' 19" N and 78° 09' 01" W; water depth, 192 m; core length, 18.20 m), Core 1336 (43° 30' 28" N and 76° 53' 07" W; water depth, 221.5 m; core length, 18.41 m). Several locations discussed in the text are also shown. Figure modified from the National Oceanic and Atmospheric Administration data center website (http://ngdc.noaa.gov/mgg/dem/).

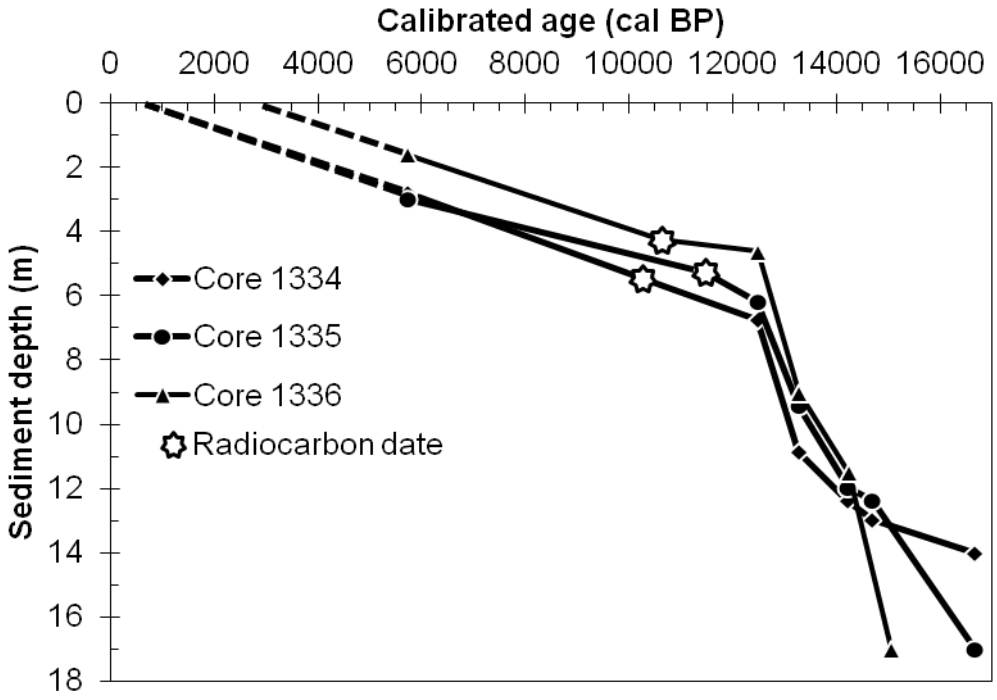

Figure 3.4. Non-Bayesian, linear interpolated, age-depth model for Cores 1334, 1335 and 1336 produced using CLAM (Blaauw, 2010). All radiocarbon dates were converted to calibrated ages by CLAM using INTCAL09 (Reimer et al., 2009). Three radiocarbon dates were used along with additional information from previous studies on Lake Ontario to establish the chronology (Schroeder and Bada, 1978; Carmichael et al., 1990; Hutchinson et al., 1993; McAndrews, 1994; Pippert et al., 1996; Silliman et al., 1996; Anderson and Lewis, 2012).

(Hutchinson et al., 1993), magnetic properties (Carmichael et al., 1990) and radiocarbon dates (Silliman et al., 1996; Anderson and Lewis, 2012). These data were combined to produce a non-Bayesian, linear interpolated age-depth model using the computer program CLAM (Blaauw, 2010), which provides a probabilistic age range for each depth.

A total of 219 ten-cm sections were extracted from the sampling half of the piston cores. The samples were wet-sieved using cold tap water and a combination of four sieve pans (1.00 mm, 500 μm, 250 μm, 125 μm) to recover ostracodes valves and clams shells; visible organic matter was also collected. The air-dried fossil material was then transferred into petri dishes, where the biogenic carbonates were identified, ostracodes retained on sieves >250 μm were counted, and isolated for isotopic analysis. Two species of ostracodes were identified in all three cores, *Candona subtriangulata* and *Fabaeformiscandona caudata*; only adult ostracodes were counted to determine their abundances in each sample. No evidence of transportation (e.g., broken/pitted valves) was observed microscopically for the ostracodes, and hence they are considered to indicate autochthonous conditions. Bivalves identified as freshwater clams from the *Pisidium* genus were also present in various intervals.

All carbon-isotope results, including those for the ostracode valves and clam shells, are presented using the conventional δ-notation relative to the Vienna PDB standard (VPDB) (Coplen, 1996):

$$\delta^{13}C = [(R_{sample} - R_{standard})\text{-}1] \text{ (in ‰)}$$

where R_{sample} and $R_{standard} = {}^{13}C/{}^{12}C$ in the sample and standard, respectively. For each measurement, approximately 0.05 mg of powdered carbonate was utilized (five to six ostracode valves depending on their individual weight; typically, two to three small clam shell fragments). Only undamaged, adult ostracode valves were analyzed to ensure correct identification. The carbon-isotope compositions of the biogenic carbonates were measured in the Laboratory for Stable Isotope Science (LSIS) at the University of Western Ontario, London, Ontario, and were obtained by reaction with orthophosphoric acid (H_3PO_4) at 90°C using a Micromass Multiprep autosampling device coupled to a VG

Optima dual inlet mass spectrometer. The $\delta^{13}C$ values were calibrated to VPDB using NBS-19 (+1.95 ‰) and Suprapur (–35.3 ‰). NBS-18 and internal laboratory standard WS-1 were used to evaluate accuracy and precision of the analyses. For NBS-18, the average $\delta^{13}C$ value was –4.98±0.08 ‰ (SD, n=27), and for WS-1 +0.79±0.06 ‰ (SD, n=7), in close agreement with accepted values of –5.00 and +0.76 ‰, respectively.

One-centimetre-thick samples of bulk sediment were freeze-dried and ground by hand using a ceramic mortar and pestle in preparation for measurements of OC, TN and their respective isotopic compositions. Prior to measuring the total OC and $\delta^{13}C_{OM}$ values, inorganic carbonates were removed by acid fumigation (Harris et al., 2001). Thirty milligrams (mg) of sediment were weighed into silver capsules and placed into a sample tray. Two drops of deionised water were added to each capsule and then the samples were carefully stirred. Approximately 500 mL of concentrated, 12 N, hydrochloric acid (HCl) was then added to the bottom of a glass dessicator, insuring maximum surface area for the HCl to fumigate. The sample tray was then placed in the dessicator on an elevated ceramic holder above the acid and left overnight with the lid half off. Acid fumes dissolved into the water that had been added to the samples, creating an acidic solution that dissolved any carbonate (Harris et al., 2001; Komada et al., 2008; Brodie et al., 2011). The samples were then dried in an oven at 50 °C for ~16 hours. The dried samples were then crimped and wrapped in tin to maximize flash combustion in the elemental analyser. Separate ~30 mg samples that were not subjected to acid-treatment were loaded into tin capsules for determination of total nitrogen contents and nitrogen-isotope compositions. Untreated samples were used for nitrogen analyses because acid-treatment can change original $\delta^{15}N$ values by as much as 8 ‰ (Teranes and Bernasconi, 2000; Harris et al., 2001).

TN and OC concentrations were measured using a Fisons 1108 Elemental Analyzer and calibrated using Low Organic Content Soil (OC 1.52 wt. %, TN 0.13 wt. %) and High Organic Content Soil (OC 6.10 wt. %, TN 0.46 wt. %). The precision of duplicate analyses for samples (n=20) was better than 0.01 wt. % for OC and 0.001 wt. % for TN. The results were used to calculate atomic C/N ratios (Meyers, 1994).

A Costech Elemental Combustion System coupled to a Thermo Finnigan Delta^{PLUS} XL mass spectrometer in continuous-flow (He) mode was used to determine the carbon and nitrogen isotopic compositions of organic matter. The $\delta^{13}C$ values were calibrated to VPDB using USGS-40 (–26.39 ‰) and USGS-41 (+37.63 ‰) (accepted values in parentheses). The accuracy of this calibration curve was checked using IAEA-CH-6; the measured $\delta^{13}C$ value of –10.45±0.13 ‰ (SD, n=12) compared well with its accepted value of –10.45 ‰. Laboratory standard keratin was also analyzed to evaluate accuracy and precision within and among the analytical sessions. The average $\delta^{13}C$ value of keratin was –24.08±0.08 ‰ (SD, n=17) across all sessions, and compared well with its accepted value of –24.08 ‰. The absolute difference in $\delta^{13}C$ values between duplicate analyses of the same sample averaged 0.17±0.15 ‰ (n=6).

The nitrogen-isotope results ($^{15}N/^{14}N$) are also presented in the normal δ-notation relative to the accepted standard AIR (Mariotti, 1983); $\delta^{15}N$ values were calibrated to AIR using USGS-40 (–4.52 ‰) and USGS-41 (+47.57 ‰) (accepted values in parentheses). The accuracy of this calibration curve was checked using IAEA-N2; the measured $\delta^{15}N$ value of +20.39±0.08 ‰ (SD, n=2) compared well with its accepted value of +20.3 ‰. Laboratory standard keratin was also analyzed to evaluate accuracy and precision within and among the analytical sessions. The average $\delta^{15}N$ value of keratin was +6.57±0.05 ‰ (SD, n=5), which compared well with its accepted value of +6.36 ‰. The absolute difference in $\delta^{15}N$ values between duplicate analyses of the same sample averaged 0.19±0.25 ‰ (n=3). The nitrogen measured here is assumed to represent organic matter ($\delta^{15}N_{OM}$) values because the y-intercept (<0.01%) on a total nitrogen versus organic carbon plot indicates minimal contribution from inorganic sources. Low TN contents of glacial sediments in all three cores precluded measurement of their nitrogen-isotope compositions.

3.3 Results

3.3.1 Ostracode valves and clam shell carbon-isotope compositions

Two ostracode species are present in the Lake Ontario sediments analyzed here, which range in age from ~16,000 to 5,500 cal BP. *Candona subtriangulata* is present from

~16,000 to 7,000 cal BP. *Fabaeformiscandona caudata* was found in Cores 1335 and 1336 in sediments younger than ~10,500 cal BP. *Pisidium* sp. clam shells coexist with ostracode valves in the sediment record beginning at ~13,200 cal BP. Ostracodes in glacial sediments older than 15,000 cal BP were found only in Cores 1334 and 1335. Lake-wide, the biogenic carbonate record disappears between 4,500 (Core 1334) and 6,000 cal BP (Cores 1335 and 1336).

The $\delta^{13}C$ values obtained for the ostracode valves and clam shells are listed in Appendix V. For samples >15,000 cal BP, the average $\delta^{13}C_{ostracode}$ value for Core 1334 is –3.9±0.4 ‰ (SD; n=4) and for Core 1335, –5.7±1.1 ‰ (SD; n=18). From 15,000 to 13,250 cal BP, there is increasing variability in $\delta^{13}C_{ostracode}$ values within each core and significant differences in the average $\delta^{13}C_{ostracode}$ values among the cores: Core 1334, –3.6±0.4 ‰ (SD; n=9), Core 1335, –4.8±0.7 ‰ (SD; n=18), and Core 1336, –6.0±1.2 ‰ (SD; n=28) (one-way ANOVA: p-value <0.05). A Tukey's post-hoc test indicates significant differences (p-value<0.05) in $\delta^{13}C_{ostracode}$ values among all sediment cores over this interval.

Between 13,250 to 12,500 cal BP, the $\delta^{13}C_{ostracode}$ values stabilized across the lake, averaging –3.8±0.9 ‰ (SD; n=51). Average $\delta^{13}C_{ostracode}$ values for each core over this time period are: Core 1334, –3.4±0.7 ‰ (SD; n=19), Core 1335, –4.0±0.8 ‰ (SD; n=14) and Core 1336, –4.1±1.0 ‰ (SD; n=18). A one-way ANOVA test (p-value=0.02) indicates variation in $\delta^{13}C_{ostracode}$ values among the three cores, but a post-hoc Tukey's test suggests that these differences exist only between Cores 1334 and 1336 (p-value=0.04).

Lake Ontario sediments from 12,500 to 11,000 cal BP also have near uniform $\delta^{13}C_{ostracode}$ values across the lake, averaging –4.2±0.7 ‰ (SD; n=11). Over this time, the average $\delta^{13}C_{ostracode}$ values for each core are: Core 1334, –3.7±0.2 ‰ (SD; n=3), Core 1335, –4.8±0.3 ‰ (SD; n=6) and Core 1336, –3.8±1.2 ‰ (SD; n=2). While a one-way ANOVA test (p-value=0.04) indicates variation in $\delta^{13}C_{ostracode}$ values among the three cores, a post-hoc Tukey's test revealed no significant differences among any combinations of Cores 1334, 1335 and 1336, which likely arises from the small sample population. After 11,000

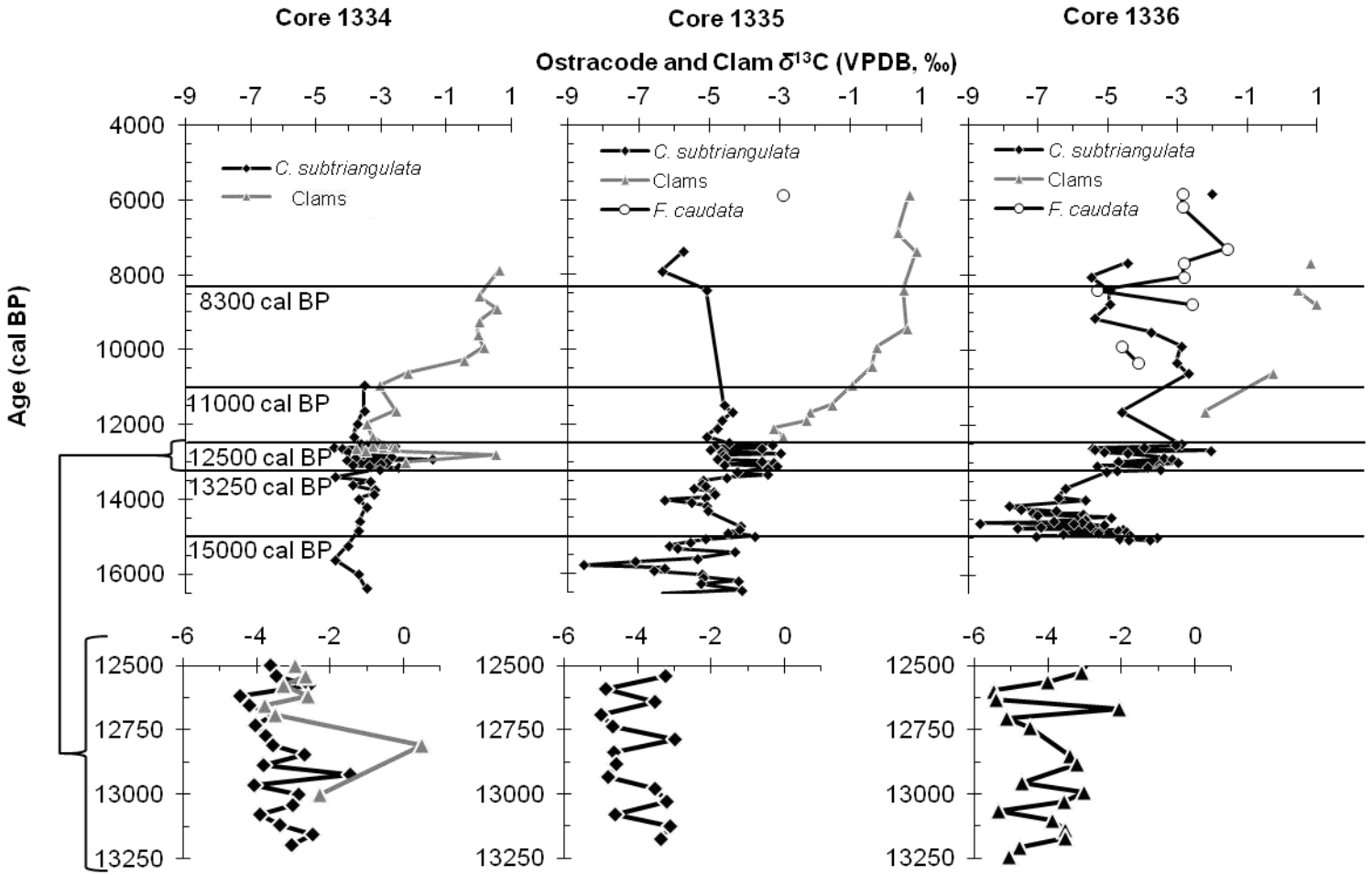

Figure 3.5. Ostracode valve and clam shell carbon isotope compositions for the period ~16,000 to 6,000 cal BP.

cal BP ostracodes disappear from the sediment record in Core 1334, and a general trend to more negative $\delta^{13}C_{ostracode}$ values begins in Cores 1335 and 1336. By ~7,500 cal BP, *C. subtriangulata* abundances become too low for isotopic analysis. *Pisidium* sp. clams emerge in the sediment record at different times throughout the lake (Fig. 3.5). In Core 1334, the clam fossil record starts at 13,000 cal BP; in Core 1335, it begins ~500 years later. Clams appear even later in Core 1336, at 11,500 cal BP, and at relatively low abundances compared to Cores 1334 and 1335. *Pisidium* sp. clams almost always coexist with ostracode species. Upon their first appearance, the clams usually record slightly higher $\delta^{13}C$ values than ostracodes, a gap in isotopic composition that widens upwards in the cores. Between 13,000 and 12,500 cal BP, $\delta^{13}C_{clam}$ values in Core 1334 average –2.6±1.3 ‰ (SD; n=8). The increase in $\delta^{13}C_{clam}$ values relative to $\delta^{13}C_{ostracode}$ becomes more pronounced in sediments younger than 12,500 cal BP. In Core 1335, the $\delta^{13}C_{ostracode}$ values trend downwards toward –6 ‰ from 12,500 to 6,000 cal BP whereas the $\delta^{13}C_{clam}$ values increase toward +1 ‰. A similar divergence in $\delta^{13}C$ values between clams and ostracodes begins later in Core 1334, at ~11,000 cal BP. While clams are more limited in abundance in Core 1336, their $\delta^{13}C$ values also increase upwards in the section (to +1 ‰). *F. caudata* is the most abundant in Core 1336, appearing at ~10,500 cal BP and generally trending up-section towards higher $\delta^{13}C_{ostracode}$ values (–3 ‰) by 5,500 cal BP – just before its disappearance. The one interval containing *F. caudata* in Core 1335 also has a $\delta^{13}C_{ostracode}$ value of –3 ‰.

3.3.2 Carbon (C) and nitrogen (N) mass accumulation rates (MARS) of bulk organic matter and C/N ratios

The C-MARS and N-MARS for Cores 1334, 1335 and 1336 are illustrated in Figures 3.6, 3.7 and 3.8, respectively, and were calculated following Yu et al. (2007) as follows:

$$\text{(C or N)-MARS} = [\text{wt. \% (C or N)}] \times [\text{LSR}] \times [\text{DBD}] \times 1000,$$

where LSR is the linear sedimentation rate and DBD is the dry bulk density.

Systematic patterns are present in the C- and N-MARS and C/N ratios of the Lake Ontario sediments, both spatially (i.e., west to east) and temporally. For sediment older

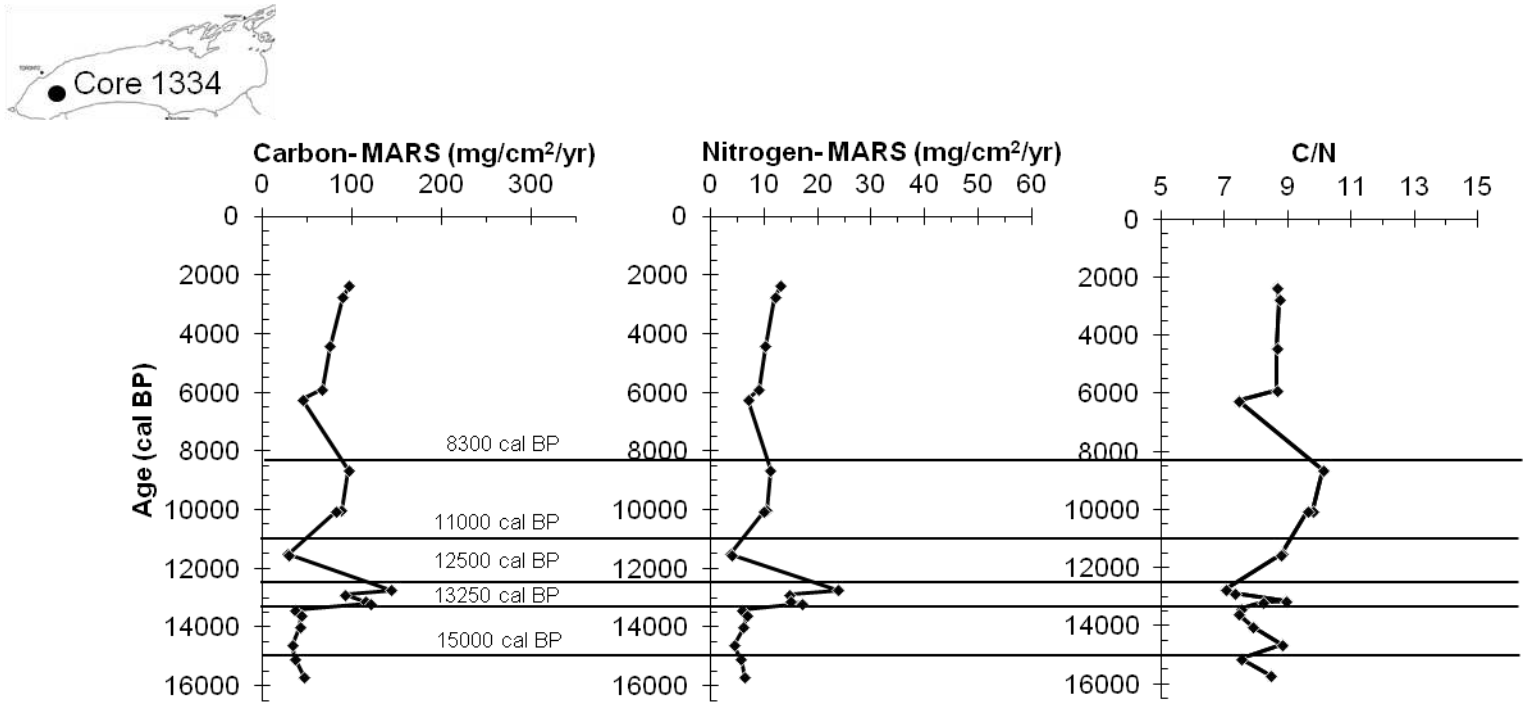

Figure 3.6. Carbon mass accumulation rates, nitrogen mass accumulation rates and C/N ratios for Core 1334.

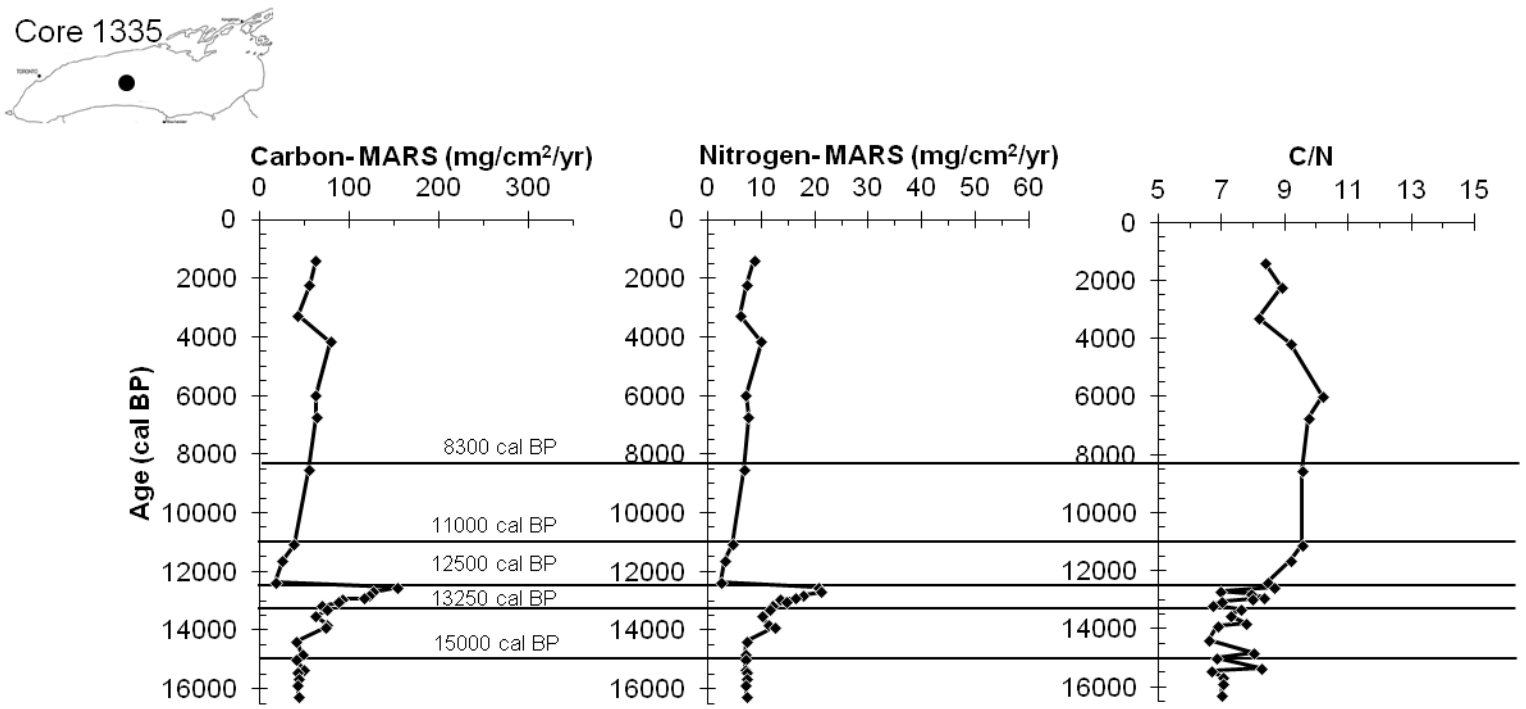

Figure 3.7. Carbon mass accumulation rates, nitrogen mass accumulation rates and C/N ratios for Core 1335.

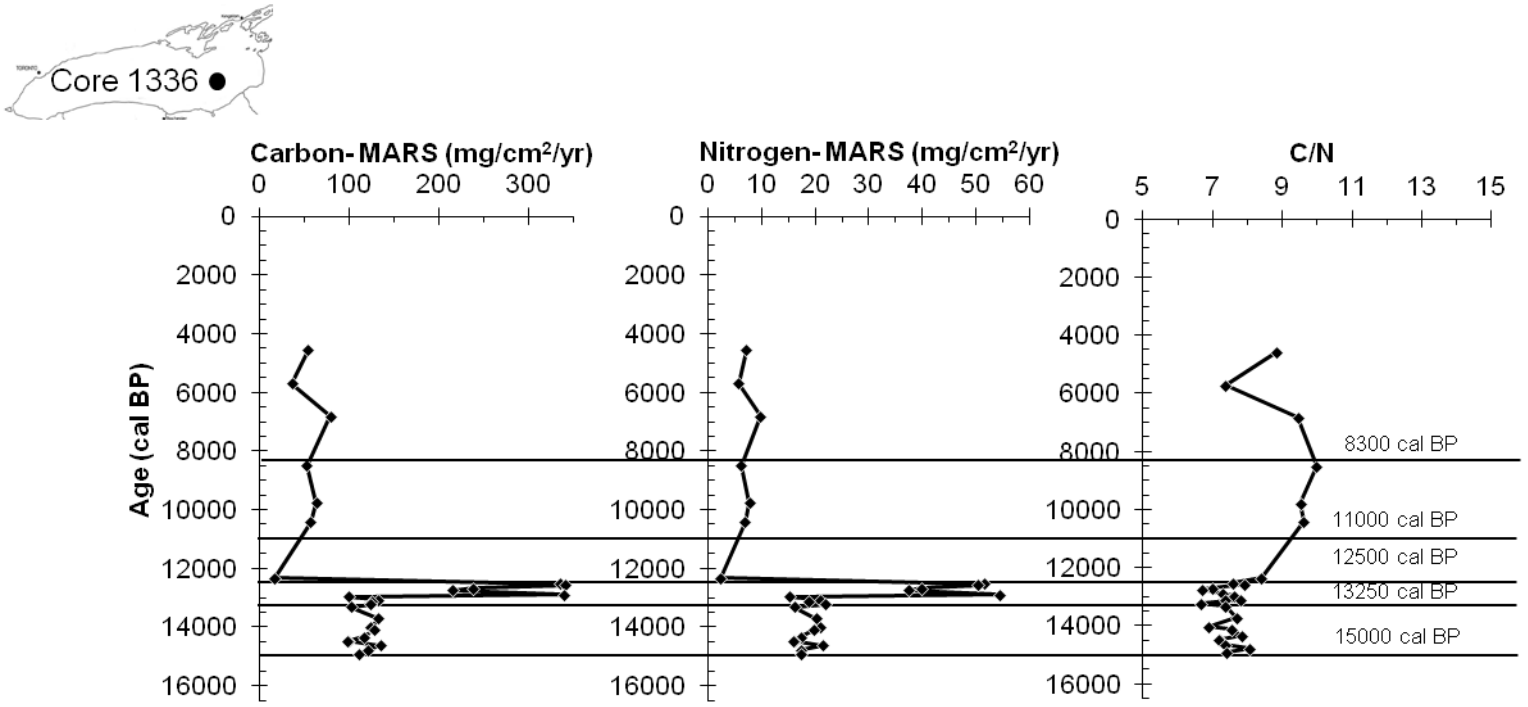

Figure 3.8. Carbon mass accumulation rates, nitrogen mass accumulation rates and C/N ratios for Core 1336.

than 13,250 cal BP, the C- and N-MARS are higher in the eastern portion of the lake than in the west. Core 1336 has an average C- and N-MARS of 116±13 (SD; n=10) and 18±2 (SD; n=10) mg/cm^2/yr, respectively, whereas the average C- and N-MARS of Cores 1334 and 1335 are much lower (39±5 [SD; n=8] and 5.6±0.9 [SD; n=8], and 53±14 [SD; n=12] and 9±2 [SD; n=12] mg/cm^2/yr, respectively). In sediments older than 13,250 cal BP, the C/N ratios average 7.3. Saying that, the C/N ratios in Cores 1335 and 1336 are slightly higher than in Core 1334, averaging 7.9. The overall percentages of carbon and nitrogen in these sediments are very low, less than 0.3 and 0.05 %, respectively.

There is a three-fold increase in the C- and N-MARS across the lake from ~13,000 to 12,500 cal BP. At 12,300 cal BP, C- and N-MARS in all cores decrease to their low of 15 and 5 mg/cm^2/yr, respectively. Concurrently, a general increase begins in the C/N ratios from ~8.5 to a maximum of 10. Generally, throughout the Holocene, the C- and N-MARS slowly increase (C-MARS from 15 to 60 and N-MARS from 5 to 10 mg/cm^2/yr). At 4,000 cal BP, the C- and N-MARS are greater in the western portion of the lake (100 and 13 mg/cm^2/yr) than in the east (60 and 10 mg/cm^2/yr). The C/N ratio also fluctuates during the Holocene. The increase in C/N ratios that began at 12,300 cal BP continues to shortly after 8,500 cal BP, at which time the C/N ratios then decrease to 7.5. Lake-wide stabilization of C/N ratios to ~8.5 occurs after 6,000 cal BP.

3.3.3 Bulk sediment organic matter carbon- and nitrogen-isotopic compositions

Sediments ranging in age from 15,000 to 13,250 cal BP show different trends in $\delta^{13}C_{OM}$ values across the lake (Fig. 3.9). In the central and eastern basins of Lake Ontario, the $\delta^{13}C_{OM}$ values average –27.3 and –27.7 ‰, respectively. Concurrently, the $\delta^{13}C_{OM}$ values in the western portion of the lake increase from –28.8 ‰ in the oldest sediments to –27.8 ‰ by 13,250 cal BP. The paucity of samples limits statistical examination of carbon isotopic variation during this time interval. Between 13,250 and 12,500 cal BP, the $\delta^{13}C_{OM}$ values across the lake vary by <1‰ averaging –27.6 ‰ in Core 1334, –28.2‰ in Core 1335 and –28.3 ‰ in Core 1336. A one-way ANOVA indicates no statistical differences among the $\delta^{13}C_{OM}$ values across the lake (p-value=0.2). A lake-wide

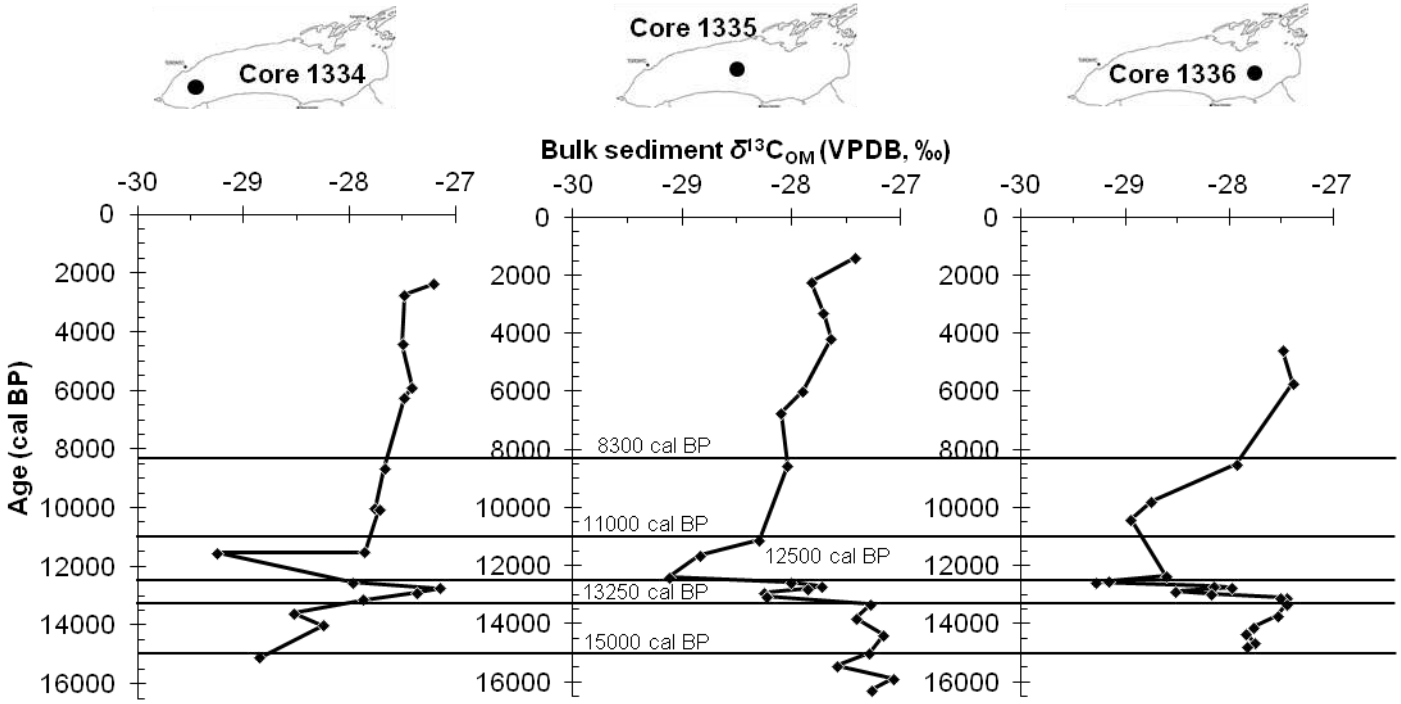

Figure 3.9. Bulk sediment organic matter carbon isotope compositions Cores 1334, 1335 and 1336.

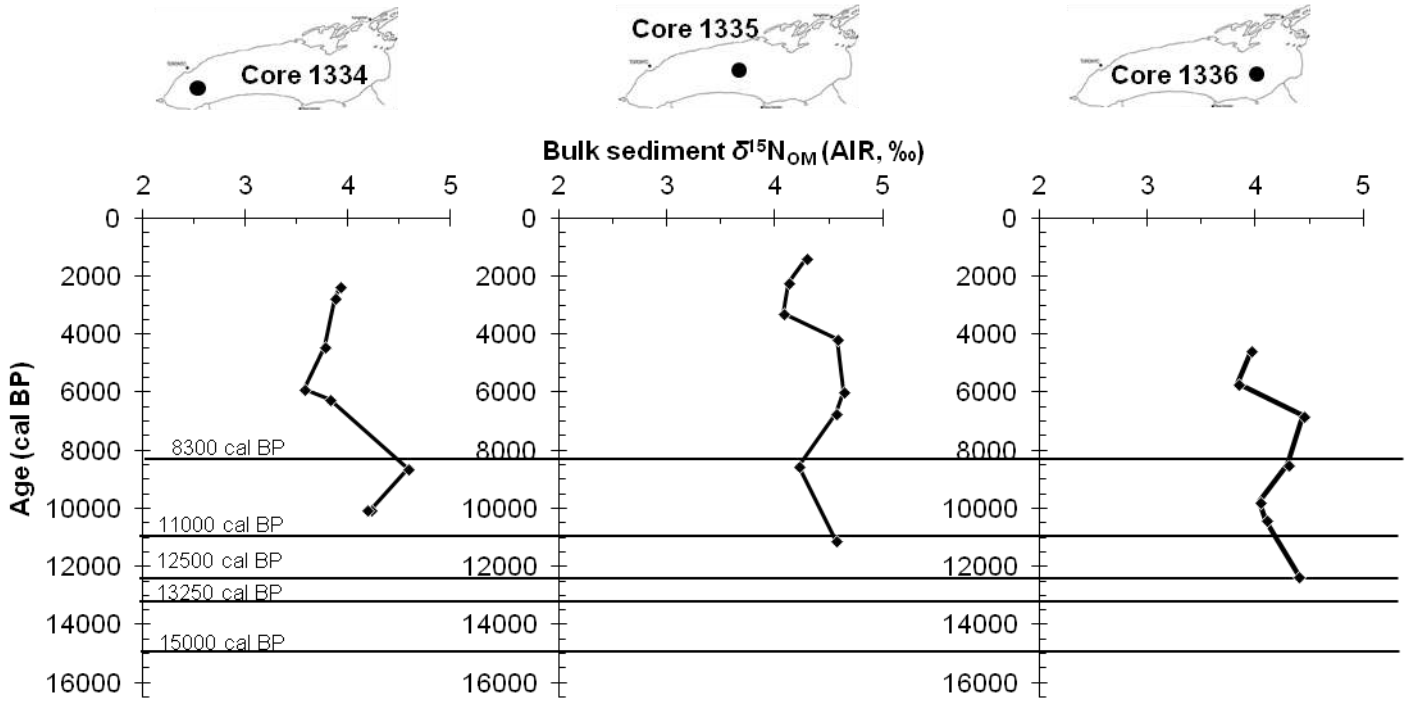

Figure 3.10. Bulk sediment organic matter nitrogen isotope compositions for Cores 1334, 1335 and 1336

decrease in $\delta^{13}C_{OM}$ values is observed at about 12,250 cal BP to about –29 ‰. The $\delta^{13}C_{OM}$ values then steadily increase (to –27.5 ‰) until the last recorded sample at 1,300 cal BP.

Total nitrogen isotopic compositions were measured only for sediments younger than 12,500 cal BP (Fig. 3.10). In general, there is little change in $\delta^{15}N_{OM}$ values from 12,500 to 1,500 cal BP: Niagara basin (+3.5 to +4.7 ‰); Mississauga basin (+4.0 to +4.7 ‰), and Rochester basin (+3.3 to +4.5 ‰).

3.4 Discussion

3.4.1 Glacial sediments in Lake Ontario (16,000-12,300 cal BP)

We use the $\delta^{13}C_{ostracode}$ values (Fig. 3.5) here to assess the relative contributions of DIC entering the lake from different sources during glacial times. Potential contributions to the overall lacustrine DIC pool during the last deglaciation of Lake Ontario are summarized in Figure 3.2. At this time, the $\delta^{13}C$ values of atmospheric CO_2 were likely –6.9 to –6.4 ‰ (Leuenberger et al., 1992; Schmitt et al., 2012). If dissolved atmospheric CO_2 was in equilibrium with water and it was the only contributor to the DIC pool, then $\delta^{13}C_{ostracode}$ values should be ~ +6 ‰ (calculated using the fractionation factors for the carbonate system of an idealized lake at temperatures ranging from 5 to 25 °C; Mook et al., 1974; Meyers and Teranes, 2001) (Fig. 3.2). However, the DIC pool of ancestral Lake Ontario is also affected by the dissolution of surrounding Paleozoic carbonate bedrock. The $\delta^{13}C$ values of Paleozoic carbonates in the region lie mostly between –1.6 and +1.5 ‰ (Coniglio and Williams-Jones, 1992). Ostracodes utilizing only DIC from this source would have a mean $\delta^{13}C$ value of ~ +2 ‰. In addition, Silliman et al. (1996) suggested that Lake Ontario $\delta^{13}C_{DIC}$ values could be affected by older recycled OM obtained from the glacial erosion of the carbonate bedrock; this source would decrease the $\delta^{13}C_{DIC}$ values. Terrestrial OM also contributes to the lacustrine DIC pool. Southern Ontario is dominated by C_3 photosynthetic plants, which presently have $\delta^{13}C$ values ranging from –30 to –23 ‰ (Meyers and Teranes, 2001). These values are lower than plants growing prior to the Industrial Revolution, because of the CO_2 contribution from the burning of fossil fuels. Hence, a so-called ‘Suess correction’ is needed to estimate the

$\delta^{13}C$ values of ancient terrestrial OM preserved in Lake Ontario (Verburg, 2007). Assuming a Suess correction factor of +1.5 ‰, the expected range of $\delta^{13}C$ values for ancient C_3 plants shifts to –28.5 to –21.5 ‰. OM transported to Lake Ontario from the periglacial environment via glacial processes – for example, *Sphagnum* mosses and other bog plants ($\delta^{13}C$ values= –31 to –27 ‰; Hornibrook et al., 2000) also could have contributed to lake OM. Suess-corrected $\delta^{13}C$ values for ancient mosses would shift to –29.5 to –25.5 ‰. DIC formed by oxidation of such OM would yield $\delta^{13}C_{ostracode}$ values of ~ –15 ‰ (assuming a temperature range of 5 to 25 °C). Hyodo and Longstaffe (2011) have suggested that OM fixed to glacially transported soil clay minerals also comprises a significant fraction of the very low OM contents (<0.2 % carbon) in many Great Lakes glacial sediments. However, such OM is likely to be very recalcitrant with respect to oxidation, and not a significant direct contributor to DIC.

Perhaps the most important control on $\delta^{13}C_{DIC}$ variations in Lake Ontario and its precursors is the changing DIC contributions from its varied watershed over the lake's history. Watershed DIC varies with outlet control and source of origin. The hydrologic budget (inputs and outputs) and water level history of Lake Ontario have been described by Anderson and Lewis (2012). Understanding this dynamic hydrologic history of Lake Ontario allows us to control for certain factors affecting the lacustrine DIC pool, as is described below.

At 16,000 cal BP, half of present-day Lake Ontario was ice-covered (Mackinaw interstadial). Sediment deposition along the ice margin (Mississauga basin) would have been largely from subglacial flow, whereas in the western portion of the lake, ice-free deposition would have been controlled both by subglacial processes and input from glacial Lake Ypsilanti in the Erie basin (Fig. 3.11a). The average $\delta^{13}C_{ostracode}$ values for sediments older than 15,300 cal BP in Cores 1334 (–3.9 ‰) and 1335 (–5.7 ‰) (Fig. 3.5) likely indicate differences in DIC input sources. There are two likely ways in which this spatial variability in $\delta^{13}C_{ostracode}$ values could arise. One possibility is that an increase in pelagic productivity caused the benthic carbon pool to become enriched in ^{12}C as algal organic matter sank to the lake bottom and was oxidized (McKenzie, 1985). A modern analog is provided by Lake Constance in the Swiss Alps; it is a monomictic lake

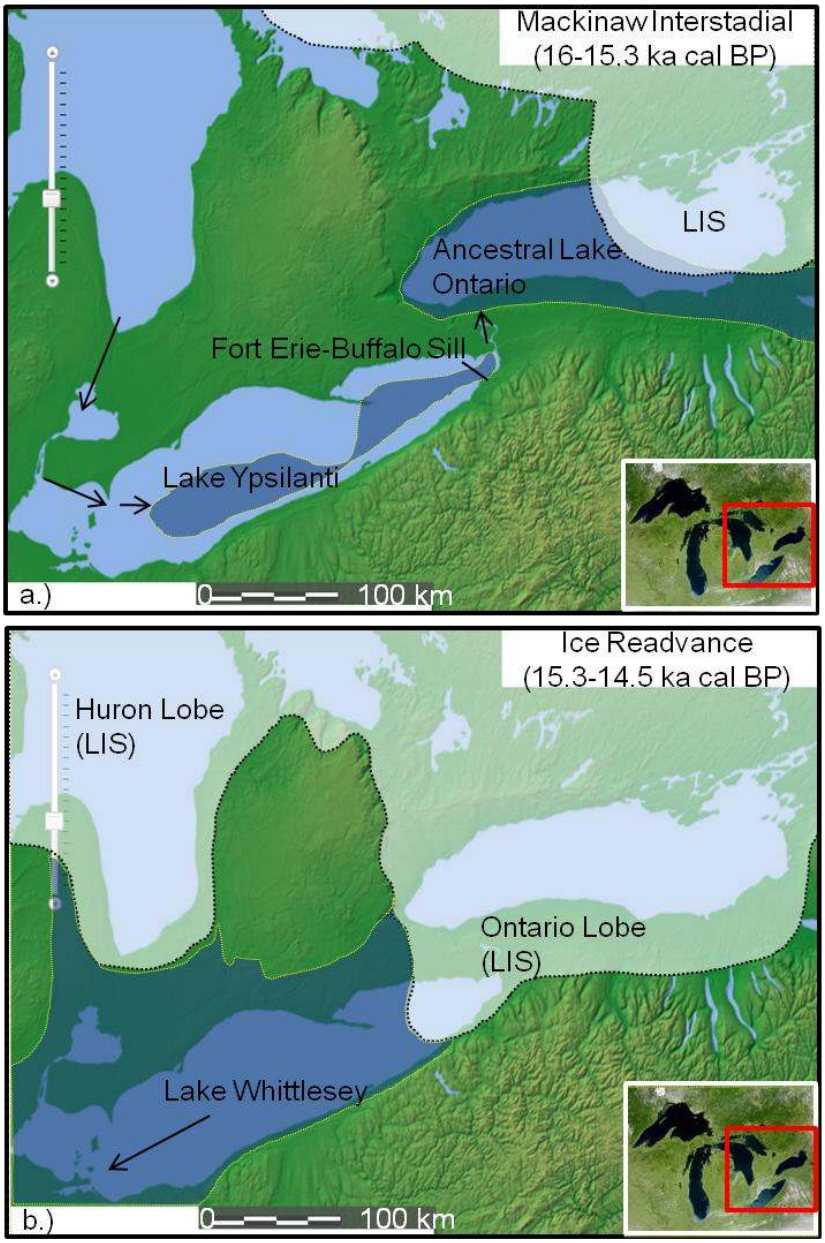

Figure 3.11. DEM overlain by the LIS margin and glacial lakes in the Great Lakes basin: (a) Mackinaw Interstadial from 16,000 to 15,300 cal BP. Drainage of Lake Ypsilanti is indicated by the arrow; (b) Ice readvance from 15,300 to 14,500 cal BP. Lake Whittlesey drainage is indicated by the arrow.

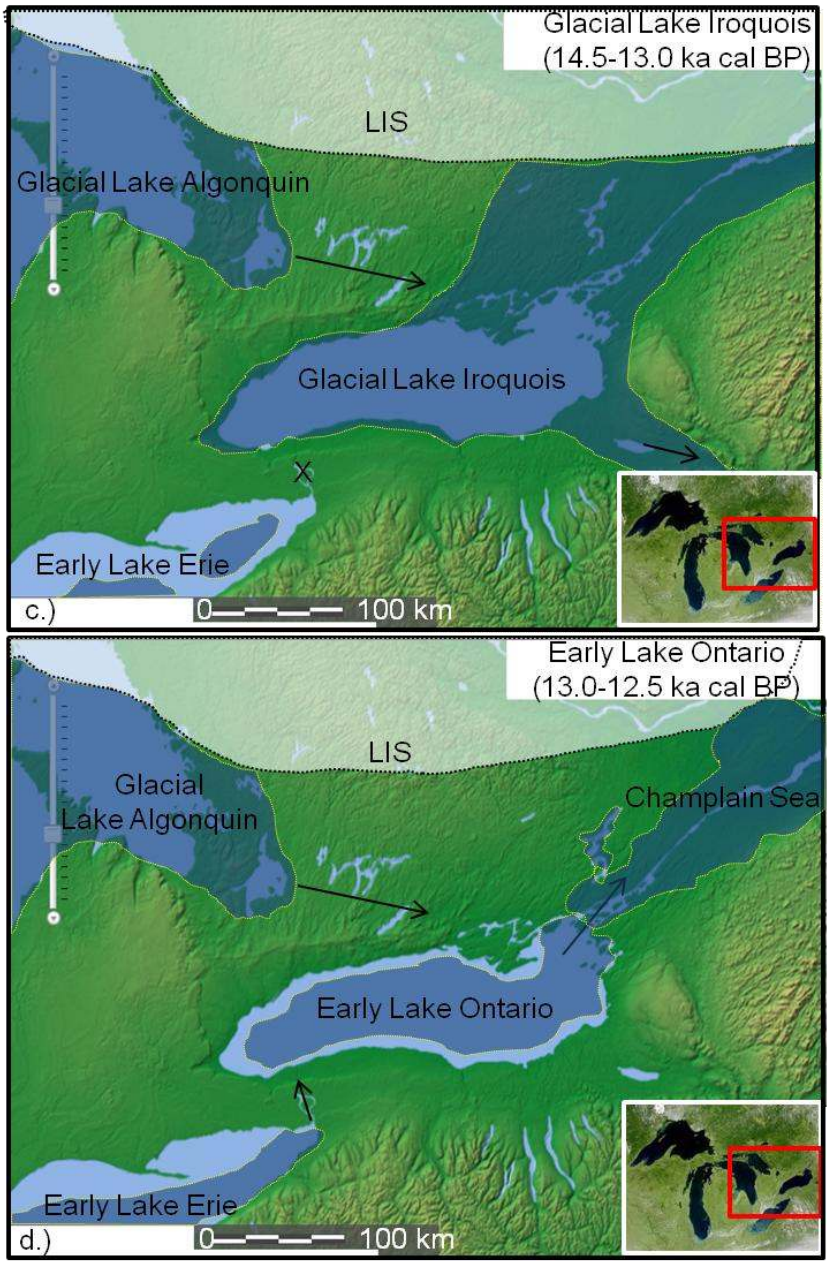

Figure 3.11 (continued). DEM overlain by the LIS margin and glacial lakes in the Great Lakes basin: c) Rise of glacial Lake Iroquois from 14,500 to 13,000 cal BP. Drainage into glacial Lake Iroquois from glacial Lake Algonquin is indicated by the arrow. Water from Erie basin did not enter the Ontario basin at this time; (d) Fall of glacial Lake Iroquois and formation of early Lake Ontario from 13,000 to 12,500 cal BP. Drainage into Lake Ontario occurred through both active outlets of glacial Lake Algonquin as indicated by the arrows. Increased meltwater supply inhibited the marine invasion of the Champlain Sea into the Ontario basin. Figures adapted from Lewis et al. (1994), Calkin and Feenstra (1985), Karrow (1989) and the National Oceanic and Atmospheric Administration data center website (http://ngdc.noaa.gov/mgg/dem/).

containing Pleistocene tills and meltwater deposits, with a maximum water depth of 254 m. The carbon productivity pump in Lake Constance leads to a decrease of 1.5 ‰ in bottom water $\delta^{13}C_{DIC}$ relative to source water $\delta^{13}C_{DIC}$ (Schwalb et al., 2013). Such a productivity pump could account for the spatial variability in $\delta^{13}C_{ostracode}$ values of 1.8 ‰ across the Ontario basin. However, it is unlikely that increases in primary productivity were sufficient under glacial conditions to force such changes; organic carbon (<0.05 %) and nitrogen (<0.01 %) contents in the sediments are very low during this time period.

Another way to account for the variability in $\delta^{13}C_{ostracode}$ values is through differences among the sources of DIC entering the lake. Two such contributors to the DIC pool during this time period were: (i) water from the Erie basin, and (ii) meltwater delivered directly from the LIS. During the period of glacial Lake Ypsilanti in the Erie basin (16,000-15,300 cal BP), water entered ancestral Lake Ontario when the glacial Lake Ypsilanti overflowed its outlet at the Fort Erie-Buffalo sill (Fig. 3.11a). Water from this source likely had a different $\delta^{13}C_{DIC}$ than meltwater entering the Ontario basin directly from the LIS. Meltwater entering the Ontario basin from Erie basin would likely have contained a much greater fraction of DIC derived from Paleozoic bedrock ($\delta^{13}C \approx 0$ ‰), thus giving rise to higher $\delta^{13}C_{ostracode}$ values in the western portion of the lake. Notably, the abundance of detrital carbonate is higher in Core 1334 (~30 %) than Core 1335 (~5 %) for this time period (Chapter 2, this thesis).

Meltwater delivered directly into the Ontario basin from the LIS at this time would have had different $\delta^{13}C_{DIC}$ values, reflecting a different mix of contributions to DIC. In particular, glacial detritus originating directly from the LIS would have contained larger contributions of OM (vegetation, soils) derived from the aggressive denudation of the Canadian Shield by direct glacial action. OM from this source would have a bulk carbon-isotope composition of ~ –25 ‰, much like present Arctic permafrost, and be available for oxidation upon release from the LIS (Dutta et al., 2006). The C-MARS data demonstrate a larger carbon influx into the Mississauga basin than the Niagara basin at this time, and clay mineral abundances, presumably of soil origin, are much higher (38 %) in the former than the latter (19 %) (Chapter 2, this thesis). Thus, this DIC pool

should yield lower $\delta^{13}C_{ostracode}$ values than further to the west, assuming that Lake Ontario was not well mixed year-round at this time.

After the Mackinaw interstadial (15,300-14,500 cal BP), the Ontario lobe of the LIS readvanced into the eastern Erie basin blocking any connection to the Ontario basin (Fig. 3.11b). The only source of DIC entering an ice-covered Ontario basin was through subglacial processes. Primary productivity would have remained low and any algal growth would have had to occur largely under the advancing ice sheet for ~800 years. In Core 1334 (Niagara basin), the $\delta^{13}C_{ostracode}$ values remained similar to those of the Mackinaw interstadial at the same location (Fig. 3.5); this suggests entry of DIC from sub-glacial processes and perhaps connectivity to the Erie basin. Eastward (Cores 1335 and 1336), there is significant variability in $\delta^{13}C_{ostracode}$ values over this time interval; the trend to lower $\delta^{13}C_{ostracode}$ values likely reflects addition of DIC directly from the LIS via flowtill deposition.

An ice dam remained at the present-day St. Lawrence River outlet from Lake Ontario upon the complete retreat of the LIS from the Ontario basin at 14,500 cal BP (Fig. 3.11c). The ice dam maintained glacial Lake Iroquois (~14,000 cal BP). Outlet control was to the southeast, via Rome, NY, with drainage through the Mohawk River valley (Fig. 3.1). From 14,500 to 13,250 cal BP, input to glacial Lake Iroquois and its precursors was via the Fenelon Falls outlet from glacial Lake Algonquin; no water entered glacial Lake Iroquois via the Erie basin. This meltwater input extended past glacial Lake Iroquois' termination at 13,260 cal BP until ~13,000 cal BP. Significant differences in the average $\delta^{13}C_{ostracode}$ values existed across the lake at this time (Core 1334 = –3.6 ‰, Core 1335 = –4.8 ‰, Core 1336 = –6.0 ‰; Fig. 3.5), with variability over the interval increasing eastward (SD=0.4 ‰, 0.7 ‰ and 1.2 ‰, respectively). The differences and variability in $\delta^{13}C_{ostracode}$ values almost certainly reflect the varying influence of LIS and glacial Lake Algonquin input. Clay deposition, which is a good marker for deposition directly from the LIS, was highest in the Rochester basin (closest to the inlet from glacial Lake Algonquin; Figs. 3.1 and 3.11c), whereas there is a step-wise decrease in relative clay abundance moving west (away from the inlet, the LIS and the sources of meltwater) (Chapter 2, this thesis).

Some of the differences in the $\delta^{13}C_{ostracode}$ values could also arise from the timing of variable meltwater delivery to Lake Ontario during this interval (Chapter 2, this thesis). It is possible that, at times, meltwater originating from glacial Lake Algonquin breached the Oak Ridges Moraine, thus entering Lake Ontario at a more central location (Chapter 2, this thesis). If this is the case, some of the observed variability in the $\delta^{13}C_{ostracode}$ values for Core 1335 could be attributed to the contribution of DIC from other sources such as meltwater pathways that connect present day Lake Scugog and Rice Lake to Lake Ontario.

Following the last major inundation of meltwater from upstream glacial Lake Algonquin at 13,000 cal BP (Fig. 3.11d), as inferred from decreasing $\delta^{18}O_{ostracode}$ values (Chapter 2, this thesis), the connection between Lake Erie and early Lake Ontario was also re-established, allowing uniform average $\delta^{13}C_{ostracode}$ values (~ –4.1 ‰) to develop across the lake under presumably well-mixed conditions. The DIC pool of early Lake Ontario at this time therefore largely reflected upstream sources – ancestral Lake Erie, Lake Simcoe and Lake Huron, all of which have similar $\delta^{13}C_{ostracode}$ values (–4 ‰) (Lewis and Anderson, 1992; Bumstead et al., 2009; Macdonald, 2012).

Variations in the C-MARS, N-MARS, C/N and $\delta^{13}C_{OM}$ values in the glacial sediments provide complementary information to that inferred from $\delta^{13}C_{ostracode}$ values and the information about DIC sources that they carry. In the oldest sediments (>15,300 cal BP), the C-MARS for Cores 1334 and 1335 are nearly equal (also true for N-MARS) indicating that the OM flux to the lake was the same in its western and central portions. A small apparent difference in average C/N ratios between Core 1334 (8.4; n=1) and Core 1335 (7.2±0.7; SD, n=4) hints at a small difference in OM sources between these localities, as was also inferred for DIC based on $\delta^{13}C_{ostracode}$ values. The average $\delta^{13}C_{OM}$ (–27.3 ‰; Core 1335 only) is not particularly diagnostic of OM source however, beyond being within the range characteristic of C_3 terrestrial and lacustrine vegetation.

The period of ice readvance at 15,300 to 14,500 cal BP may provide some insight into sources of OM in the lake. Perhaps the biggest difference is the C- and N-MARS in Core 1336 as compared to Cores 1334 and 1335 during this time interval. The C- and N-

MARS in the eastern portion of the lake are about three times higher (113, 17, respectively; Fig. 3.8) than in the central (44, 7, respectively; Fig. 3.7) and western portions (34, 5, respectively; Fig. 3.6). Differences in the C/N ratios and $\delta^{13}C_{OM}$ values across the lake are more subtle than apparent from the MARS. The increased flux of OM, indicated by higher MARS in the east, reflects the advancing position of the LIS. Readvancing ice would have deposited the greatest fraction of its terrestrially derived detritus in the Rochester basin before expanding across the central and western portions of the lake.

The source of the OM is more enigmatic. Traditionally, C/N ratios of ~7.5, as measured here and for the older glacial sediments, would indicate OM arising from predominantly lacustrine algal productivity. That scenario, however, seems unlikely under the glacial conditions that dominated this time period. We suggest instead that most of the OM entering the lake was carried there sorbed on soil clay minerals. Wang et al. (2013) have shown that mineral (clay)-bound organic matter typically has a C/N of ~9 and that this ratio decreases as it is transformed into more stable residues. It follows that if the dominant source of OM entering ancestral Lake Ontario was bound to clay minerals then Core 1336 should have the highest clay mineral abundance at this time, which is the case (up to 33% versus 13% in the west) (Chapter 2, this thesis). We posit that the C/N ratio must be used with caution as a lacustrine paleoproductivity indicator in such glacial environments.

LIS retreat at 14,500 cal BP allowed glacial Lake Algonquin to flow directly into glacial Lake Iroquois. With the outlet at Port Huron inactive until 13,000 cal BP, water used the Fenelon Falls outlet to travel to glacial Lake Iroquois, and exited from the lake through the Mohawk River valley in the southeast (Chapter 2, this thesis). C- and N-MARS are highest in the eastern portion of the lake, consistent with the Fenelon Falls flow path. Some variation exists in the average C/N ratios (8.0, 7.1, 7.3) and average $\delta^{13}C_{OM}$ (–28.2, –27.5, –27.6 ‰) from west to east among the three cores, but the differences cannot be tested for statistical significance because of low sample size.

Upon the termination of glacial Lake Iroquois and its successors at 13,000 cal BP, early Lake Ontario was established; it was confluent with the neighbouring Champlain Sea shortly thereafter (12,900 cal BP) (Fig. 3.1). Re-activation of the Port Huron outlet at ~13,000 cal BP allowed glacial Lake Algonquin to flow into early Lake Ontario from both the Fenelon Falls and Port Huron outlets. Higher C- and N-MARS in Cores 1334 and 1335 indicate increased OM deposition in the western and central portions of the lake (Figs. 3.6, 3.7). The still higher C- and N-MARS in Core 1336 (Fig. 3.8), however, indicate that most detritus entered the lake via the Fenelon Falls pathway. Once connectivity to early Lake Erie was established, a gradient appears in $\delta^{13}C_{OM}$ from –27.5 ‰ in the west to –28.5 ‰ in the east (Fig. 3.9). The values in the eastern portion of the lake compare well with those reported by Silliman et al. (1996). This pattern is accompanied by an increase in carbonate and a decrease in clay abundances in all three cores. This change in $\delta^{13}C_{OM}$ is consistent with the shift in $\delta^{13}C_{DIC}$ described above for the same period. It is also interesting to note that the C/N ratios of the Niagara and Rochester basin are virtually the same (7.2), whereas in the central portion of the lake the C/N ratio is higher (8.0), perhaps owing to variable meltwater delivery across the Oak Ridges Moraine to a central locality as posited above.

3.4.2 Lake Ontario hydrologic closure (12,300-8,300 cal BP)

The period of hydrologic closure beginning at 12,300 cal BP provides a unique opportunity to assess $\delta^{13}C_{ostracode}$ and $\delta^{13}C_{OM}$ values as measures of primary lacustrine productivity in Lake Ontario. The emergence of *Pisidium* sp. clams was a clear response to the change in the environmental setting; their initial co-existence with *C. subtriangulata* and similar $\delta^{13}C$ values likely reflected a nearly uniform $\delta^{13}C_{DIC}$ pool in the spring and summer. The subsequent divergence between clam and ostracode $\delta^{13}C$ values – *Pisidium* sp. clams trending towards +1 ‰ and *C. subtriangulata* towards –6 ‰ – is more challenging to explain (Fig. 3.5). One possibility is a difference in the growth patterns of the organisms, in association with differences in the spring versus summer DIC pools. Clam shells form continuously throughout life but growth is most rapid during the spring season (von Grafenstein et al., 1999), and hence $\delta^{13}C_{clam}$ should largely reflect the spring DIC pool. Conversely, ostracodes molt new carapaces in the summer,

offering a snapshot of the summer DIC pool (Boomer, 2002). We posit that the divergence in $\delta^{13}C$ values between the bottom-water dwelling clam shells and ostracode valves could indicate onset of warm monomictic conditions. During winter overturn, lake water enriched in $^{13}C_{DIC}$ and $^{18}O_{H2O}$ by the biological pump and evaporation would be mixed with lower $^{13}C_{DIC}$ and $^{18}O_{H2O}$ bottom waters. These signals would be transferred to clam shells during spring growth. Re-development of stratification by summer would again lead to lower bottom-water $\delta^{13}C_{DIC}$ and $\delta^{18}O_{H2O}$ relative to surface water, with this signal being transferred to ostracode valves.

The progressively stronger divergence in $\delta^{13}C$ values from 12,500 to 11,000 cal BP between clam shells and ostracode valves in the Mississauga basin (Core 1335) versus the Niagara basin (Core 1334) may be related to the formers's greater depth (presently 191.5 m versus 110.3 m); deeper water environments are more likely to facilitate pronounced stratification and hence isotopic differentiation between clams and ostracodes. Progressive warming in southern Ontario and lowering of lake levels during hydrologic closure would also have contributed to these processes. Notably, the ostracode record in Core 1334 effectively disappeared at 11,000 cal BP when conditions in the shallowest Lake Ontario basin became unfavourable (too warm, salinity too high) for growth of *C. subtriangulata*. The deep Rochester basin (presently 221.5 m) shows a similar divergence between clam and *C. subtriangulata* $\delta^{13}C$ values as in Core 1335. Higher in the section, towards the end of the period of hydrologic closure, a second species of ostracode, *F. caudata,* also commonly demonstrates enrichment in ^{13}C relative to *C. subtriangulata,* albeit to a lesser extent than the clams (Fig. 3.5). We attribute this difference to somewhat different moulting cycles for the two ostracodes as well as position of growth in the water column (i.e., growth of *F. caudata* in shallower water).

The variations in C-MARs, N-MARs, C/N ratios and $\delta^{13}C_{OM}$ values also convey important information concerning primary lacustrine productivity during the hydrologic closure of Lake Ontario. OC input, once derived almost solely from glacial processes, is now more strongly influenced by autochthonous production. Lower sedimentation rates in Lake Ontario during post-glacial periods are reflected in a sharp decrease in the C- and N-MARS (Figs. 3.6-3.8). There is also a sharp initial lowering in $\delta^{13}C_{OM}$ to values as

low as –29.5 ‰, which is attributed to the first significant production of lacustrine algae. These rapid responses emphasize the sensitivity of Lake Ontario to changes in hydrologic regime. Throughout the period of hydrologic closure, until 8,300 cal BP, the $\delta^{13}C_{OM}$ values steadily increase across the basin to a maximum of –27.5 ‰. This ^{13}C-enrichment is likely productivity-related, reflecting increased competition for ^{12}C by a progressively increasing lacustrine biomass.

During hydrologic closure, C/N ratios gradually increase upwards from ratios of 7-8 that typify the underlying glacial sediments to progressively higher values of ~8 to 10. The C/N ratios measured by Silliman et al. (1996) for the Rochester basin also increase over this time period, but from values as low as 4 to as high as 8. Why C/N ratios as low as 4 were not observed in the present study is unclear, but is likely related to differences between the coring sites. This suggests some heterogeneity in the OM record. As reviewed earlier, C/N values of 4-10 are normally associated with lacustrine algal matter, and almost certainly reflect a significant contribution from this source during hydrologic closure. Silliman et al. (1996) note that the bulk of the OM originated from lacustrine algae, but also interpret the upward increasing C/N ratios to signify a modest increase in terrestrial OM contribution. However, as previously discussed, we suggest that the C/N ratios (7-8) of the glacial sediments originated in some other fashion, and are not diagnostic of lacustrine algal production. Therefore, in the case of Core 1336, we suggest that the modest upward trend in C/N ratios during transition from glacial sedimentation to hydrologic closure (Figs. 3.6-3.9) reflects a decreasing contribution of allochthonous organic matter of glacial, terrestrial origin having 'anomalous' C/N ratios coupled with an increase in autochthonous algal production and perhaps also additional 'normal' terrestrial OM.

The $\delta^{15}N_{OM}$ values show little variation across Lake Ontario during this time period (average +4.3±0.2 ‰; SD, n=9). There are no systematic changes that might be attributed to major changes in OM sources, or nitrogen limitation of productivity during hydrologic closure of Lake Ontario. Pang and Nriagu (1976) showed that modern sediments in areas of Lake Ontario receiving larger proportions of terrestrial OM have lower $\delta^{15}N_{OM}$ values (+3.7 ‰) than areas with higher aquatic OM (+4.9 ‰). Assuming

similar compositions for the period of hydrologic closure, such $\delta^{15}N_{OM}$ values would indicate relatively equal proportions of terrestrial and aquatic OM input into Lake Ontario. McFadden et al. (2005) reported similar findings ($\delta^{15}N_{OM}$ ~+4.0 ‰ and C/N ratios of ~10), which indicate a mixture of terrestrial and aquatic OM sources.

3.4.3 Overflow conditions (8,300-1,000 cal BP)

At 8,300 cal BP, the climate in southern Ontario shifted from cold and dry, to warm and dry (Anderson and Lewis, 2012). This change was accompanied by an increase in annual precipitation, which caused Lake Ontario to overflow its outlet (Anderson and Lewis, 2012). During this period, $\delta^{13}C_{ostracode}$ and $\delta^{13}C_{clam}$ values continued to reflect differing summer and spring DIC pools, which persisted until the biogenic carbonate record disappeared at ~4,500 (Core 1334) and 6,000 cal BP (Cores 1335 and 1336) because of conditions favouring biogenic carbonate dissolution during the Nipissing rise (Fig. 3.5).

The gradual increase in $\delta^{13}C_{OM}$ values over this time period (Fig. 3.9) is likely a signal of increasing terrestrial OM input. The pre-existing shoreline of Lake Ontario would have been drowned by the gradual increase in water level and this, coupled with increased runoff from precipitation, would increase terrestrial OM contributions to Lake Ontario. A similar trend in $\delta^{13}C_{OM}$ values was observed by McFadden et al. (2005) and attributed to the same causes. The small and gradual increases in C- and N-MARS also support this observation. However, C/N ratios over this time period measured in the present study generally remain stable or show a small decrease. This result contrasts with the large increase in C/N ratios observed by McFadden et al. (2005). The stable (or small decrease) in C/N ratios observed in this study may indicate that increasing amounts of terrestrial OM are counterbalanced by an overwhelming supply of lacustrine algae, as observed by Silliman et al. (1996). During this time period, there is no evidence for a significant contribution of terrestrially derived carbon with anomalous C/N ratios, such as that associated with soil clays.

As noted earlier for the period of hydrologic closure, there is little change in the $\delta^{15}N_{OM}$ values throughout this time interval (Fig. 3.10). There is little difference in average $\delta^{15}N_{OM}$ values from west to east across Lake Ontario (Core 1334: +3.8±0.1 ‰, n=5; Core

1335: +4.3±0.2 ‰, n=5; Core 1336: +4.1±0.3 ‰, n=3). McFadden et al. (2005) also observed minimal changes in the $\delta^{15}N_{OM}$ values (<1 ‰) during this interval.

3.4.4 Overview: Source versus productivity and environmental conditions in Lake Ontario

During glacial periods, changes in OM source inputs (i.e., directly from the LIS or from up-stream glacial Lake Algonquin and ancient Lake Erie), controlled the DIC pool in ancestral Lake Ontario. Cold/dry conditions in southern Ontario, coupled with the retreat of the LIS, limited primary productivity in the Ontario basin. Primary production ceased in the subglacial lake during the Port Huron advance. Still, small amounts of OM were delivered to the lake sediments from the LIS. Increased contributions of glacial meltwater from glacial Lake Algonquin during the latter stages of deglaciation in the area provided a consistent and steady supply of DIC not only to ancestral Lake Ontario but also to the lakes then occupying the Huron and Erie basins. This regional influence of the LIS on the Great Lakes system allowed for a 'stabilization' of the DIC pool by large volumes of glacial meltwater gathered upstream. During glacial periods, OM entering the lake may have been associated with (soil?) clay minerals.

It was not until hydrologic closure of early Lake Ontario at the onset of post-glacial conditions that unambiguous changes in primary lacustrine productivity could be detected. In the benthic environment, differences between the summer and spring DIC pools appear to be recorded in the $\delta^{13}C_{ostracode}$ and $\delta^{13}C_{clam}$ values of their valves/shells. This seasonal pattern likely reflects the timing of lake thermal stratification (Hodell and Schelske, 1998). Increases in $\delta^{13}C_{OM}$ values during post-glacial times generally support an increase in primary lacustrine productivity, although this signal may also reflect an increase in the terrestrial OM contribution associated with the onset of warmer conditions in the Ontario basin at 8,300 cal BP.

3.5 Conclusions

In the Ontario basin, competition between direct meltwater inflow from the LIS and inflow from upstream large accumulations of ponded glacial meltwater (e.g., Lake Agassiz, ancestral Lake Superior, Lake Algonquin, etc.) were the main controls on DIC

and hence the $\delta^{13}C$ values of ostracode valves. When significant quantities of upstream DIC was available to the benthic environment, $\delta^{13}C_{ostracode}$ values were higher than when the DIC pool was controlled more directly by the advancing/retreating LIS. Meltwater directly derived from the LIS appears to have had more negative $\delta^{13}C_{DIC}$ values reflecting a greater contribution of oxidized organic matter, whereas water received from the Erie basin had higher $\delta^{13}C_{DIC}$ values, likely arising from greater contributions of inorganic carbonate bedrock. Individual basins within Lake Ontario preserved somewhat unique $\delta^{13}C_{ostracode}$ values until the last significant input glacial meltwater occurred from ~13,000 to 12,500 cal BP. At that time, a consistent benthic DIC pool was established across all of ancestral Lake Ontario.

The low C/N ratios of OM preserved in the glacial sediments are not a reliable proxy for algal productivity in Lake Ontario, and instead are more likely the signature of autochthonous material delivered by glaciation. Upon hydrologic closure of Lake Ontario at 12,300 cal BP, however, the initial increase in C/N marks a transition from atypical ratios of allochthonous OM imported during glacial times to ratios representative of lacustrine algal productivity in post-glacial times. The abrupt shift to low $\delta^{13}C_{OM}$ values upon hydrologic closure, followed by a gradual enrichment in ^{13}C, is also a pattern expected for increasing primary lacustrine productivity. Rising lacustrine productivity and biodiversity is also signaled by the emergence of clams. Furthermore, comparison of clam and ostracode $\delta^{13}C$ values suggests a significant difference between summer and spring DIC pools arising from the timing of thermal stratification associated with onset of warm monomictic conditions.

Changing environmental conditions from cold/dry to warm/dry to warm/wet in southern Ontario brought hydrologic closure to an end in Lake Ontario and it returned to overflow conditions. C/N ratios and slowly rising $\delta^{13}C_{OM}$ values generally support increasing primary lacustrine productivity during this time. Onset of warmer conditions at 8,300 cal BP, with associated rising water levels and drowning of Lake Ontario shorelines, may also have led to increased contribution of terrestrial OM to Lake Ontario sediments.

3.6 References

Anderson, T.W., Lewis, C.F.M., 2012. A new water-level history for Lake Ontario basin evidence for a climate-driven early Holocene lowstand. Journal of Paleolimnology 47, 513–530.

Blaauw, M., 2010. Methods and code for 'classical' age-modelling of radiocarbon sequences. Quaternary Geochronology 5, 512–518.

Boomer, I., 2002. Environmental applications of marine and freshwater ostracoda. in: Haslett, S.K., (Ed.), Quaternary Environmental Micropalaeontology. Arnold: London, pp. 115–138.

Brodie, C.R., Leng, M.J., Casford, J.S.L., Kendrick, C.P., Lloyd, J.M., Yongqiang, Z., Bird, M.I., 2011. Evidence for bias in C and N concentrations and $\delta^{13}C$ composition of terrestrial and aquatic organic materials due to pre-analysis acid preparation methods. Chemical Geology 282, 67–83.

Bumstead, N.L., Longstaffe, F.J., Macdonald, R.A., 2009. The paleolimnology of Lake Simcoe: oxygen-isotope compositions of ostracodes. 11th International Paleolimnology Symposium, Guadalajara, Mexico, December 15-18, 2009.

Carmichael, C.M., Mothersill, J.S., Morris W.A., 1990. Paleomagnetic and pollen chronostratigraphic correlations of the late glacial and postglacial sediments in Lake Ontario. Canadian Journal of Earth Sciences 27, 131–147.

Calkin, P.E., Feenstra, B.H., 1985. Evolution of the Erie-Basin Great Lakes. in: Karrow, P.F., Calkin, P.E., (Eds.), Quaternary Evolution of the Great Lakes. Geological Association of Canada Special Paper 30, pp. 149–170.

Coniglio, M., Williams-Jones, A.E., 1992. Diagenesis of Ordovician carbonates from the north-east Michigan Basin, Manitoulin Island area, Ontario: evidence from petrography, stable isotopes and fluid inclusions. Sedimentology 39, 813–836.

Coplen, T.B., 1996. New guidelines for reporting stable hydrogen, carbon, and oxygen isotope ratio data. Geochimica et Cosmochimica Acta 17, 3359–3360.

Decrouy, L., Vennemann, T.W., Ariztegui, D., 2011. Controls on ostracod valve geochemistry: Part 2. Carbon and oxygen isotope compositions. Geochimica et Cosmochimica Acta. 75, 7380–7399.

Dutta, K., Schuur, E.A.G., Neff, J.C., Zimov, S.A., 2006. Potential carbon release from permafrost soils of Northeastern Siberia. Global Change Biology 12, 2336–2351.

Fritz, P., Anderson, T.W., Lewis, C.F.M., 1975. Late-Quaternary climatic trends in history of Lake Erie from stable isotope studies. Science 190, 267–269.

Fogel, M.L., Cifuentes, L.A., 1993. Isotope fractionation during primary production. in: Engel, M.H., Macho, S.A. (Eds.), Organic Geochemistry Plenum Press, NewYork, pp. 73–98.

Harris, D., Horwath, W.R., van Kessel, C., 2001. Acid fumigation of soils to removecarbonates prior to total organic carbon or carbon-13 analysis. Soil Society of America Journal 65, 1853–1856.

Hodell, D.A., Schelske, C.L., 1998. Sedimentation, and isotopic composition of organic matter in Lake Ontario. American Society of Limnology and Oceanography 43, 200–214.

Holmes, J. A., 2001. Ostracoda, in: Smol, J. P., Birks, H. J. B., Last, W. M. (Eds.), Tracking Environmental Change Using Lake Sediments Volume 4: Zoological Indicators. Dordrecht: Kluwer Academic Publishers, pp. 125–152.

Hornibrook, E.R., Longstaffe, F.J., Fyfe, W.S., Bloom, Y., 2000. Carbon-isotope ratios and carbon, nitrogen and sulfur abundances in flora and soil organic matter from a temperate-zone bog and marsh. Geochemical Journal of Japan 34, 237–245.

Hutchinson, D.R., Lewis, C.F.M., Hund, G.E., 1993. Regional stratigraphic framework of surficial sediments and bedrock beneath Lake Ontario. Géographie physique et Quaternaire 47, 337–352.

Hyodo, A., Longstaffe, F.J., 2011. The palaeoproductivity of ancient Lake Superior. Quaternary Science Reviews 30, 2988–3000.

Karrow, P.F., 1989. Quaternary geology of the Great Lakes subregion. in: Fulton, R.J. (ed.), Quaternary geology of Canada and Greenland. Geol. Survey of Canada, Geology of Canada, pp. 326–350.

Komada, T., Anderson, M.R., Dorfmeier, C.L., 2008. Carbonate removal from coastalsediments for the determination of organic carbon and its isotopic signatures, $\delta^{13}C$ and $\Delta^{14}C$: comparison of fumigation and direct acidification by hydrochloric acid. Limnology and Oceanography: Methods 6, 254–262.

Leuenberger, M., Siegenthaler, U., Langway, C.C., 1992. Carbon isotope composition of atmospheric CO_2 during the last ice age from an Antarctic ice core. Science 357, 488–490.

Lewis, C.F.M., Anderson, T.W., 1992. Stable isotope (O and C) and pollen trends in eastern Lake Erie, evidence for a locally induced climatic reversal of Younger Dryas age in the Great Lakes basin. Climate Dynamics 6, 241–250.

Lewis, C.F.M, Moore Jr, T.C., Rea, D.K., Dettman, D.L., Smith, A.M., Mayer, L.A., 1994. Lakes of the Huron basin: their record of runoff from the Laurentide Ice Sheet. Quaternary Science Reviews 13, 891–922.

Macdonald, R.A., 2012. Late Quaternary histories of Lakes Huron and Michigan: A stable isotope investigation of sediment cores and modern biogenic carbonates. Ph.D. thesis, The University of Western Ontario, London, pp. 314.

Mariotti, A. 1983. Atmospheric nitrogen is a reliable standard for natural ^{15}N abundance measurements. Nature 303, 685-687.

McAndrews, J.H., 1994. Pollen diagrams for southern Ontario applied to archeology, in: MacDonald, R.I. (Ed.) Great Lakes Archeology and Paleoecology: Exploring Interdisciplinary Initiatives for the Nineties. Quaternary Sciences Institute, University of Waterloo, Waterloo, pp. 179–195.

McFadden, M.A., Mullins, H.T., Patterson, W.P., Anderson, W.T., 2004. Paleoproductivity of eastern Lake Ontario over the past 10,000 years. Limnology and Oceanography 49, 1570–1581.

McFadden, M.A., Patterson, W.P., Mullins, H.T., Anderson, W.T., 2005. Multi-proxy approach to long-and short-term Holocene climate-change: evidence from eastern Lake Ontario. Journal of Paleolimnology 33, 371–391.

McKenzie, J.A., 1985. Carbon isotopes and productivity in the lacustrine and marine environment. in: Stumm, W. (Ed.), Chemical Processes in Lakes. Wiley, New York, pp. 99–118.

Meyers, P.A., 1994. Preservation of elemental and isotopic source identification of sedimentary organic matter. Chemical Geology114, 289–302.

Meyers, P.A., 1997. Organic geochemical proxies of paleoceanographic, paleolimnologic, and paleoclimatic processes. Organic Geochemistry 27, 213–250.

Meyers, P.A., 2003. Applications of organic geochemistry to paleolimnological reconstructions: a summary of examples from the Laurentian Great Lakes. Organic Geochemistry 34, 261–289.

Meyers, P.A., Ishiwatari, R., 1993. Lacustrine organic geochemistry–an overview of indicators of organic matter sources and diagenesis in lake sediments. Organic Geochemistry 20, 867–900.

Meyers, P.A., Lallier-Verges, E., 1999. Lacustrine sedimentary organic matter records of Late Quaternary paleoclimates. Journal of Paleolimnology 21, 345–372.

Meyers, P.A., Teranes, J.L., 2001. Sediment organic matter. in: Last, W.M., Smol, J.P. (Eds.), Tracking Environmental Change Using Lake Sediments: Physical and Geochemical Methods. Developments in Paleoenvironmental Research, vol. 2. Kluwer Academic Publishers, Dordrecht, pp. 239–269.

Muller, E.H., Prest, V.K., 1985. Glacial lakes in the Ontario basin, in: Karrow, P.F., Calkin, P.E., (Eds.), Quaternary Evolution of the Great Lakes. Geological Association of Canada Special Paper 30, pp. 211–229.

Munsell Color. 2000. Munsell Soil Color Charts Year 2000 Revised Washable Edition. GretagMacbeth, New Windsor, NY.

Mook, W.G., Bommerson, J.C., Staverman, W.H., 1974. Carbon isotope fractionation between dissolved bicarbonate and gaseous carbon dioxide. Earth and Planetary Science Letters 22, 169–176. Munsell Color. 2000. Munsell Soil Color Charts Year 2000 Revised Washable Edition. Gretag Macbeth, New Windsor, NY.

National Oceanic and Atmospheric Administration Digital Elevation Model (DEM) Discovery Portal website (2014). Retrieved February 14, 2014 from http://ngdc.noaa.gov/mgg/dem/

O'Leary, M.H., 1988. Carbon isotopes in photosynthesis. Bioscience. 38, 328–336.

Pair, D.L., Rodrigues, C.G., 1993. Late Quaternary deglaciation of the southwestern St. Lawrence Lowland, New York and Ontario. Geological Society of America Bulletin 105, 1151–1164.

Pang, P.C., Nriagu, J.O., 1976. Distribution and isotope composition of nitrogen in Bay of Quinte (Lake Ontario) sediments. Chemical Geology 18, 93–105.

Peters, K.E., Sweeney, R.E., Kaplan, I.R., 1978. Correlation of carbon and nitrogen stable isotope ratios in sedimentary organic matter. Limnology and Oceanography 23, 598–604.

Pippert, R.G., Brown, G.R., Morris, W.A., 1996. Palaeomagnetic chronostratigraphy of Holocene sediments, Niagara basin, Lake Ontario, Canada. Journal of Quaternary Science 11, 217–231.

Reimer, P.J., Baillie, M.G.L., Bard, E., Bayliss, A., Beck, J.W., Blackwell, P.G., Bronk Ramsey, C., Buck, C.E., Burr, G.S., Edwards, R.L., Friedrich, M., Grootes, P.M., Guilderson, T.P., Hajdas, I., Heaton, T.J., Hogg, A.G., Hughen, K.A., Kaiser, K.F., Kromer, B., McCormac, F.G., Manning, S.W., Reimer, R.W., Richards, D.A., Southon, J.R., Talamo, S., Turney, C.S.M., van der Plicht, J., Weyhenmeyer, C.E., 2009. IntCal09 and Marine09 radiocarbon age calibration Curves, 0–50,000 Years cal BP. Radiocarbon 51, 1111–1150.

Schmitt, J., Schneider, R., Elsig, J., Leuenberger, D., Lourantou, A., Chappellaz, J., Köhler, P., Joos, F., Stocker, T.F., Leuenberger, M., Fischer, H., 2012. Carbon isotope constraints on the deglacial CO_2 rise from ice cores. Science 336, 175–182.

Schroeder, R.A., Bada, J.L., 1978. Aspartic acid racemization in Late Wisconsin Lake Ontario sediments. Quaternary Research 9, 193–204.

Schwalb, A., Burns, S.J., Cusminsky, G., Kelts, K., Markgraf, V., 2002. Assemblage diversity and isotopic signals of modern ostracodes and host waters from Patagonia, Argentina. Palaeogeography, Palaeoclimatology, Palaeoecolology 187, 323–339.

Schwalb, A., Dean, W., Güde, H., Hanisch, S., Sobek, S., Wessels, M., 2013. Benthic ostracode $\delta^{13}C$ as sensor for early Holocene establishment of modern circulation patterns in Central Europe. Quaternary Science Reviews 66, 112–122.

Silliman, J.E., Meyers, P.A., Bourbonniere, R.A., 1996. Record of postglacial organic matter delivery and burial in sediments of Lake Ontario. Organic Geochemistry 24, 463–472.

Talbot, M.R., Kelts, K., 1990. Paleolimnological signatures from carbon and oxygen isotopic ratios in carbonates from organic carbon-rich lacustrine sediments. in: Katz BJ (Ed.), Lacustrine Basin Exploration: Case Studies and Modern Analogs. The American Association of Petroleum Geologists Memoir 50. Tulsa, OK, pp. 99–112.

Teranes, J.L., Bernasconi, S.M., 2000. The record of nitrate utilization and productivity limitation provided by $\delta^{15}N$ values in lake organic matter- A study of sediment trap and core sediments from Baldeggersee, Switzerland. Limnology and Oceanography 45, 801–813.

Verburg, P., 2007. The need to correct for the Suess effect in the application of $\delta^{13}C$ in sediment of autotrophic Lake Tanganyika, as a productivity proxy in the Anthropocene. Journal of Paleolimnology 37, 591–602.

von Grafenstein, U., Erlernkeuser, H., Trimborn, P., 1999. Oxygen and carbon isotopes in modern fresh-water ostracod valves: assessing vital offsets and autecological effects of interest for palaeoclimate studies. Palaeogeography, Palaeoclimatology, Palaeoecolology 148, 133–152.

Wada, E., 1980. Nitrogen isotope fractionation and its significance in biogeochemical processes occurring in marine environments. in: Goldberg, E.D., Horibe, Y., Sarunhashi, K. (Eds.), Isotope marine chemistry. Tokyo: Uchida Rokakuho, pp. 375–398.

Wetzel, R.G., 2001. Limnology Lake and River Ecosystems, Third ed. Academic Press.

Wang, Z., Govers, G., Oost, K.V., Clymans, W., den Putte, A.V., Merckx, R., 2013. Soil organic carbon mobilization by interrill erosion: Insights from size fractions. Journal of Geophysical Research: Earth Surface 118, 348–360.

Yu, S., Berglund, B.E., Sandgren, P., Colman, S.M., 2007. Holocene organic carbon burial rates in the southeastern Swedish Baltic Sea. Holocene 17, 673–681.

Chapter 4

4 *n*-Alkane evidence for the origin of organic matter in Lake Ontario since the Late Pleistocene

4.1 Introduction

Organic matter (OM) preserved in lake sediments comprises a complex mixture of watershed detritus (allocthonous) and in-lake (autocthonous) productivity. As such, differentiating between source changes and changes in primary productivity in lake sediment archives can prove challenging (Silliman et al., 1996; McFadden et al., 2004; 2005; Hyodo and Longstaffe, 2011; Chapter 3, this thesis). In this regard, the lipid fraction of OM, specifically *n*-alkanes, which are typically well preserved in lake sediments (Meyers, 1997), can record many aspects of OM depositional history, and lend insight into both sources of organic detritus and changes in primary terrestrial and lacustrine productivity (Meyers and Ishiwatari, 1993; Brincat et al., 2000).

Previous studies of the Rochester basin in Lake Ontario have attempted to link the OM depositional history to changing environmental conditions since deglaciation. Silliman et al. (1996) used grain size, C/N ratios, bulk OM carbon-isotope compositions and abundances of *n*-alkanes to examine OM accumulation since the retreat of the Laurentide Ice Sheet (LIS). They determined that fine-grained sediments deposited during glacial periods represented a blend of contemporaneous OM and much older recycled OM obtained from the glacial erosion of the surrounding Paleozoic bedrock (Silliman et al., 1996). As the LIS retreated, Silliman et al. (1996) attributed the increasing grain size, C/N ratios and $\delta^{13}C_{OM}$ values of postglacial sediments to increased delivery of terrestrial OM to Lake Ontario under warmer and wetter conditions; the progressive increase in terrestrial/aquatic *n*-alkane ratios also hinted at changes in watershed vegetation and subsequent delivery of terrestrial OM to Lake Ontario.

McFadden et al. (2004) and (2005) used a multi-proxy study (C/N ratios, abundances of carbon and nitrogen, $\delta^{13}C_{OM}$ values among others) of Rochester basin sediments to characterize regional climate since 10,000 cal BP. The start of Holocene warming at ~9,400 cal BP was demarcated by increases in C/N ratios, %C, %N and $\delta^{13}C_{OM}$ values.

McFadden et al. (2004) and (2005) linked these changes to Holocene Thermal Maximum (HTM) warming (9,400 to 5,300 cal BP), during which southern Ontario summer temperatures were ~2-4 °C higher than today. They also linked this warmest and wettest period in Lake Ontario's history to increased terrestrial OM input, as indicated by higher C/N ratios and increases in % total carbon. Beginning at 5,300 cal BP, McFadden et al. (2004) and (2005) noted decreases in sedimentation rates, terrestrial OM input and lower C/N ratios, which they associated with a gradual cooling, a trend also observed by Silliman et al. (1996). These changes were interpreted to denote establishment of a cooler, more stable climate in southern Ontario following the HTM.

In this study, we build upon the previous work in Lake Ontario's Rochester basin sediments by providing a combined *n*-alkane abundance and carbon-isotope record extending to ~15,000 cal BP. We use this record, together with other proxy data (Chapter 3, this thesis), to examine in more detail the relative contributions of autochthonous and allocthonous OM to Lake Ontario sediments as the region responded to environmental changes during and since the last deglaciation. In particular, we use the variation in the abundances and $\delta^{13}C$ values of *n*-alkanes over time to reconstruct terrestrial vegetation shifts, changing inputs of terrestrial OM to the lake, and changes in lacustrine algae productivity. A stronger understanding of allochthonous and autochthonous OM production and delivery in the Lake Ontario basin while the LIS was present and following its retreat will aid the interpretation of regional ecological changes during this dynamic time, and provide a historical baseline for future vegetation responses to changing climatic conditions.

4.1.1 Geological history of Lake Ontario

A detailed late Quaternary history of the Lake Ontario basin is provided in Chapters 1 and 2 (this thesis). Briefly, ancestral Lake Ontario was largely ice free at ~14,500 cal BP. Blocked by the LIS at the St. Lawrence valley, water levels rose in the Lake Ontario basin, forming glacial Lake Iroquois from 14,500 to 13,250 cal BP. Cold and dry conditions characterized southern Ontario during the glacial period (Anderson and Lewis, 2012). Continual northward retreat of the LIS then opened an outlet at the St. Lawrence River, causing drainage of glacial Lake Iroquois. Early Lake Ontario then became

hydrologic closed from 12,300 to 8,300 cal BP when upper Great Lakes drainage was routed through the newly opened North Bay outlet (Anderson and Lewis, 2012). Hydrologic closure of Lake Ontario coincided with the period of maximum dryness (10,100 to 8,900 cal BP) in southern Ontario, which enhanced evaporative loss from the lake (Anderson and Lewis, 2012). Increased precipitation beginning at ~8,300 cal BP caused Lake Ontario to overflow its outlet at the eastern end of the lake, thus ending hydrologic closure (Anderson and Lewis, 2012). Lake levels then steadily rose over the centuries until connectivity to the upper Great Lakes was re-established from ~6,300 to 5,200 cal BP during the Nipissing rise (Anderson and Lewis, 2012). The climate transitioned from warm/dry to warm/wet beginning at ~6,800 cal BP, which also contributed to higher water levels in Lake Ontario (Edwards et al., 1996).

4.1.2 *n*-Alkanes

Eglinton and Hamilton (1967) provide an excellent description of the biosynthesis of *n*-alkanes in plants. Briefly, biosynthesis of *n*-alkanes begins with a precursor molecule, palmitic acid, which is a C_{16} *n*-alkanoic acid. The palmitic acid is progressively elongated by addition of two carbon atoms to form a longer chain *n*-acid. This long chain *n*-acid, for example C_{30} acid, is decarboxylated (loss of carboxyl group, R-COOH) to yield an odd-chain *n*-alkane (C_{29}). The strong odd over even predominance of primary *n*-alkanes in plants reflects this primary process. Furthermore, bacterial reworking or diagenetic alteration of OM can be identified by diminishment or disappearance of odd-dominated *n*-alkanes in the sediment record (Meyers and Ishiwatari, 1993).

The *n*-alkane fraction contains the most abundant lipid molecules biosynthesized by terrestrial and aquatic plants, and certain algae (Chikarashi and Naraoka, 2003). Lipid molecules assist the plant leaf in controlling water balance and mechanical damage, inhibiting pests and protecting against harmful radiation (Eglinton and Hamilton, 1963). The production of *n*-alkanes of specific length also makes it possible to distinguish among terrestrial and aquatic plants, and algae in the lake sediment record. The relative abundances of various *n*-alkanes in a plant family or genus are not consistent but appear to be fairly consistent at the species level (Smith et al., 2007). Of most importance to

paleoenvironmental applications is that *n*-alkanes in the fossil record typically preserve the original signal of the living species (Meyers and Ishiwatari, 1993).

The *n*-alkanes produced by terrestrial, higher plant species are characterized by a strong odd predominance of long-chain (C_{25} to C_{35}) lengths (Eglinton and Hamilton, 1967; Rieley et al., 1991). Tundra-type vegetation (e.g., grasses and herbs) is dominated by C_{31} *n*-alkanes, whereas boreal forest vegetation (e.g., birch) is characterized by elevated abundances of C_{27} *n*-alkanes (Cranwell, 1973; Schwark et al., 2002). The shift from boreal to pine-dominated forests is accompanied by increased abundances of C_{29} and C_{31} *n*-alkanes; transition to a deciduous forest is marked by C_{29} dominance (Schwark et al., 2002). Other long-chain *n*-alkanes, such as C_{33} and C_{35}, are also produced by terrestrial vegetation but are usually low in abundance (Maffei et al., 2004).

Aquatic plants, such as macrophytes, are characterized by *n*-alkanes ranging from C_{21} to C_{25} and in some cases C_{29} and C_{31} (Ficken et al., 2000; Sachse et al., 2004). The complicated nature of *n*-alkane distributions observed in macrophyte species reflects the varying environments they inhabit. Macrophytes can be classified as emergent, submergent or floating. Emergent macrophytes have similar *n*-alkane distributions as terrestrial plants, maximising at C_{29} or C_{31} (Ficken et al., 2000). Submergent and floating macrophyte species maximise at C_{23} and to a lesser extent C_{25}, with some exceptions outlined by Ficken et al. (2000). Complexity also arises when categorizing the *n*-alkane C_{25}. Contributions of C_{25} to the sediment record can be associated with increases in terrestrial OM, *Sphagnum* mosses and/or macrophytes. Hence, care must be taken when linking changes in abundances and carbon-isotope compositions of C_{25} *n*-alkanes to environmental parameters.

Further complexity arises in interpreting the *n*-alkane record from lakes, especially during glacial periods, because of the overlapping *n*-alkane patterns of moss and macrophyte species. Bog-forming vegetation, such as *Sphagnum* mosses, generally contains high abundances of C_{23} and to a lesser extent C_{25} and C_{31} (Bingham et al., 2010). The predominance of relatively shorter-chain *n*-alkanes in higher plants is an unusual property (Eglinton and Hamilton, 1967). The ability to distinguish between *n*-alkane signatures of

macrophytes and moss species is crucial in interpreting the source(s) of OM delivered to Lake Ontario under glacial conditions.

Short-chain *n*-alkanes (C_{17}, C_{19}, C_{21}) are produced by aquatic algae (Gelpi et al., 1970; Han and Calvin, 1970; Cranwell et al., 1987). While algal lipid matter is preferentially degraded during the sinking of particulate OM because of the freshness of the material (Meyers, 1997), the presence of short-chain *n*-alkanes is generally reliable as an indicator of aquatic algal growth (Sachse et al., 2004). While shorter chain algal *n*-alkanes are more susceptible to degradation than their longer-chain counterparts, rapid sinking and lateral transport improves preservation of algal OM in deep, off-shore environments such as Lake Ontario's Rochester basin (Meyers and Eadie, 1993).

The carbon isotopic compositions of *n*-alkanes ($\delta^{13}C_{n\text{-alkane}}$) can also serve as an indicator of source inputs, productivity and environmental conditions. Values of $\delta^{13}C_{n\text{-alkane}}$ depend on: (i) the carbon source utilized, (ii) isotope effects associated with assimilation of carbon by the plant, (iii) isotope effects associated with biosynthesis, and (iv) cellular carbon budgets (Hayes, 1993). Plant water-use efficiency is a related and important physiological factor that can affect $\delta^{13}C_{n\text{-alkane}}$ values (Sun et al., 2013). Likewise, negative correlations have been reported between water availability (amount of precipitation) and the $\delta^{13}C_{n\text{-alkane}}$ values (Stevenson et al., 2005; Sun et al., 2013).

First and foremost, the $\delta^{13}C_{n\text{-alkane}}$ values of land plants track the carbon-isotope composition of atmospheric CO_2, as fractionated by the various photosynthetic pathways of different plant classes (C_3, C_4 and CAM) (Chikaraishi and Naraoka, 2007). Small increases in $\delta^{13}C_{n\text{-alkane}}$ values can arise from increases in terrestrial production because of competition related availability of ^{12}C. In C_3 plants, larger increases in $\delta^{13}C_{n\text{-alkane}}$ values are likely associated with water availability. During periods of water stress, diffusion of CO_2 into the leaf is limited because of stomatal closure (Farquhar et al., 1989). In this case, the overall CO_2 uptake rate is limited by the initial diffusion process (associated with a fractionation of –4 ‰) and the internal CO_2 concentration is low (O'Leary, 1993). During stomatal closure, the leaf acts as a closed system and all of the available CO_2 is used, and thus the carboxylation isotope fractionation (–29 ‰) is not expressed (O'Leary,

1993). The C_3 plant in this scenario should approach higher $\delta^{13}C$ values (O'Leary, 1993). In terrestrial environments, relative changes in $\delta^{13}C_{n\text{-alkane}}$ values may hence be driven in part by shifts between more arid and more humid climatic conditions. In aquatic systems, the carbon cycle and the carbon sources available for algal assimilation are more complex (see Chapter 3, this thesis). Nonetheless, changes in algae $\delta^{13}C_{n\text{-alkane}}$ values provide a useful signal of changes in productivity or sources of carbon in the lake.

4.2 Materials and methods

Core 1336 was collected from the Rochester Basin in Lake Ontario on July 16, 2008 by the captain and crew of the Canadian Coast Guard Ship (CCGS) *Limnos* (Fig. 4.1). The cores were cut into ~1 m sections onboard and stored in a refrigerator prior to delivery to the University of Rhode Island, where they were halved longitudinally and visible characteristics (colour, consistency, grain size, sedimentary structures including laminations) noted (see Appendix I). Sediment colour was described using the Munsell Soil Colour Charts and notation (2000). The cores were then shipped to the University of Western Ontario where they continue to be stored at 4°C.

Total lipid extracts (TLEs) for 18 samples from Core 1336 were obtained from 15 g of freeze-dried, powdered and sieved sediment intervals. Soxhlet extraction was performed in the Laboratory for Stable Isotope Science (LSIS) at the University of Western Ontario (London, Ontario, Canada) for 24 hours with a 2:1 (v/v) mixture of dichloromethane (DCM) and methanol (MeOH). TLEs were treated with activated copper for 24 hours in order to remove elemental sulphur. After rotary-evaporation, 20 μL of an internal standard made from 5α-androstane and 2-hexadecanol was added. Liquid to liquid chromatography was performed using a disposable glass pipette packed with 4 cm (in height) of silica. The hydrocarbon fractions were eluded using 3 mL of hexane, whereas the alcohol fractions were eluded using 5 mL of DCM followed by 3 mL of DCM:MeOH (1:1, v/v) and the most polar fractions were collected using 3 mL of MeOH. The alcohol and most polar fractions were retained for future analysis.

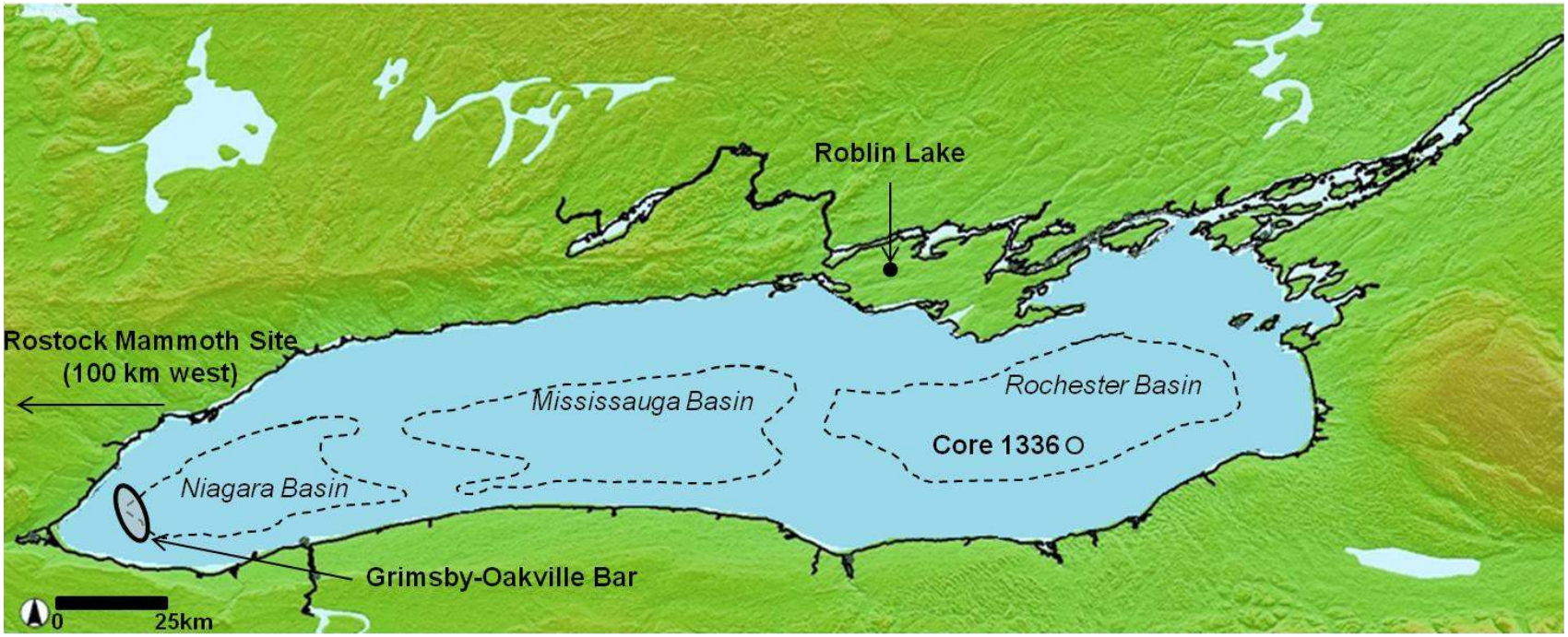

Figure 4.1. Digital elevations model (DEM) of Lake Ontario region showing the location of sediment piston Core 1336 obtained by the CCGS *Limnos* in July 2008: 43° 30' 28" N and 76° 53' 07" W; water depth, 221.5 m; core length, 18.41 m. Figure modified from the National Oceanic and Atmospheric Administration data center website (http://ngdc.noaa.gov/mgg/dem/).

Gas chromatography (GC) was performed in the Workentin Laboratory in the Department of Chemistry at the University of Western Ontario (London, Ontario, Canada) using an Aglient 6890N GC fitted with a DB5-MS (30 m x 0.25 mm, film thickness 0.25 μm) capillary column and a flame ionisation detector (FID). Helium was used as a carrier gas. The GC temperature program used was 70 to 130°C at 10°C/min followed by 130 to 300°C at 40°C/min with a 15 minute hold. GC-mass spectrometry (MS) was performed in the CFI-Common laboratory in the Department of Chemical and Biochemical Engineering at the University of Western Ontario (London, Ontario, Canada) using an Aglient 7890A GC-MS fitted with a mass selective detector (model 5975C) with the same column and operated using the same temperature program as the Aglient 6890N GC. The instrument was operated over a scan range of *m/z* 50-550 amu with an ionization energy of 70 eV. Identification of *n*-alkanes was made by comparison of retention times and spectra reported in the literature for the conditions used here. Quantification of *n*-alkane abundances was performed by integration of peak areas relative to the internal standard (5α-androstane). The GC and GC-MS data were acquired and edited using Chemstation software.

The carbon-isotope results are presented using the conventional δ-notation:

$$\delta^{13}C = [(R_{sample} - R_{standard})-1] \text{ (in ‰)}$$

where R_{sample} and $R_{standard} = {}^{13}C/{}^{12}C$ in the sample and standard, respectively. All δ-values are reported relative to VPDB. The $\delta^{13}C_{n\text{-alkane}}$ values were determined in LSIS using an Aligent 6890N GC/C coupled to a Thermo Finnigan DeltaPlus XL stable-isotope-ratio-mass-spectrometer (IRMS) running ISODAT (version 3.0). All $\delta^{13}C_{n\text{-alkane}}$ values reported here are averages of two or more measurements (Appendix VII). The same column type and temperature program as described above was also used for these analyses. For *n*-alkane identification, the chromatograms for 1-2 μL of sample dissolved in hexane were compared to the GC-MS results described above. Instrument performance was monitored daily and the calibration of the sample results was achieved using a C_{16} to C_{30} *n*-alkane standard known as 'Mixture A' (prepared by A. Schimmelmann) with known isotopic compositions acquired from Indiana University,

USA. The difference (SD) between offline carbon-isotope compositions (obtained from Indiana University) and online values measured in this study ranged from 0.01 to 0.20 ‰ (n=8). Accuracy was assessed by comparing the measured offline carbon isotopic composition of a co-injected 5α-androstane standard (–31.66 ±0.16 ‰; SD, n=7) to the measured online results (–31.20 ±0.14 ‰; SD, n=8).

As described in Chapter 2 of this thesis, the age-depth model of Core 1336 (Fig. 4.2) is anchored using an accelerator mass spectrometer (AMS) radiocarbon date (University of Arizona, Tuscon, AZ) of 9,397±56 years (10,619 cal BP using INTCAL09; Reimer et al., 2009) for a terrestrial macro-fossil (wood) obtained at a depth of 420-430 cm. Additional information from previous studies of Lake Ontario sediments were also used to construct the age-depth model, including pollen stratigraphy (Carmichael et al., 1990; McAndrews, 1994; Pippert et al., 1996), seismic stratigraphy (Hutchinson et al., 1993), magnetic properties (Carmichael et al., 1990) and radiocarbon dates (Silliman et al., 1996; Anderson and Lewis, 2012). These data were combined to produce a non-Bayesian, linear interpolated age-depth model using the computer program CLAM (Blaauw, 2010).

4.3 Results

The *n*-alkanes identified throughout the sediment record have carbon chain lengths ranging from C_{17} to C_{35} (Table 4.1). The amount of C_{35} *n*-alkanes was too small for isotopic analysis and is not considered further. Subordinate amounts of even-numbered *n*-alkanes were also observed in the GC-MS spectra, but are not considered further (Appendix VIII, Fig. 4.3).

Average *n*-alkane chain length (ACL) was calculated as follows:

$$ACL= (\Sigma C_n \bullet n)/ (\Sigma C_n)$$

where C_n is the concentration of *n*-alkane containing *n* carbon atoms (Fig. 4.4a) (Chikaraishi and Naraoka, 2003). The terrigenous to aquatic (TAR) *n*-alkane ratio (Fig. 4.4b) was adapted from Silliman et al. (1996) as follows:

$$TAR= (C_{27}+C_{29}+C_{31})/(C_{17}+C_{19}+C_{21})$$

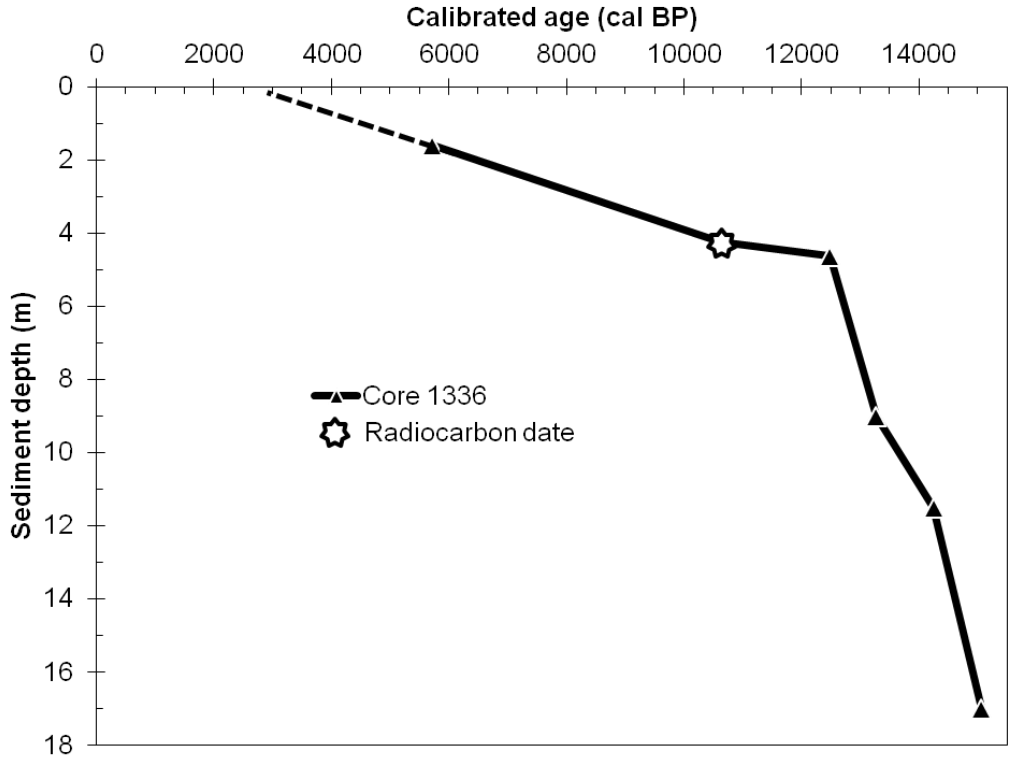

Figure 4.2. Non-Bayesian, linear interpolated age-depth model for Core 1336 produced by CLAM (Blaauw, 2010). The radiocarbon date was converted to calibrated ages by CLAM using INTCAL09 (Reimer et al., 2009). Results from previous studies of Lake Ontario were also used to establish chronology (Schroeder and Bada 1978; Anderson and Lewis, 2012; Carmichael et al., 1990; Hutchinson et al., 1993; McAndrews, 1994; Pippert et al., 1996; Silliman et al., 1996).

Table 4.1. Abundances of *n*-alkanes in Lake Ontario Core 1336, reported in absolute (μg/g) and relative abundances (%) (C_{35} is omitted) by depth (meters) and age (calibrated years BP). Bold and italicized values represent the highest *n*-alkane abundance for a given sample.

Depth	Age	Abundance C_{17}		C_{19}		C_{21}		C_{23}		C_{25}		C_{27}		C_{29}		C_{31}		C_{33}		C_{35}
(m)	(cal BP)	(μg/g)	(%)	(μg/g)	(%)	(μg/g)	(%)	(μg/g)	(%)	(μg/g)	(%)	(μg/g)	(%)	(μg/g)	(%)	(μg/g)	(%)	(μg/g)	(%)	(μg/g)
0.515	3583	***0.52***	***16***	0.33	10	0.38	12	0.34	11	0.31	10	0.35	11	0.47	15	0.36	11	0.13	4	0.08
1.38	5289	0.23	8	0.32	12	0.36	13	0.31	11	0.29	11	0.35	13	***0.42***	***15***	0.34	12	0.14	5	0.07
1.91	6294	0.25	8	***0.51***	***16***	0.34	11	0.34	11	0.28	9	0.36	12	0.47	15	0.38	12	0.23	7	0.05
2.315	7033	0.13	4	0.18	5	0.30	9	0.41	12	0.39	11	***1.02***	***29***	0.52	15	0.38	11	0.14	4	0.05
2.715	7773	0.18	6	0.22	7	0.35	11	0.44	14	0.34	10	0.42	13	***0.63***	***20***	0.45	14	0.19	6	0.06
3.105	8512	0.26	10	0.25	10	0.30	12	***0.37***	***15***	0.26	10	0.30	12	***0.38***	***15***	0.29	12	0.11	4	0.04
4.31	10922	0.30	11	***0.45***	***17***	0.27	10	0.32	12	0.25	10	0.37	14	0.33	12	0.23	9	0.13	5	0.03
5.13	12577	0.31	10	***0.45***	***15***	***0.46***	***15***	0.44	14	0.32	10	0.34	11	0.30	10	0.23	8	0.20	7	0.14
5.51	12645	0.35	12	***0.47***	***16***	0.44	15	0.38	13	0.30	10	0.31	11	0.29	10	0.23	8	0.19	6	0.06
5.99	12731	***0.48***	***16***	***0.46***	***16***	0.44	15	0.35	12	0.29	10	0.29	10	0.26	9	0.21	7	0.17	6	0.04
6.97	12908	0.27	11	***0.32***	***14***	0.27	11	0.26	11	0.22	10	0.26	11	0.26	11	0.23	10	0.25	11	0.08
7.51	13005	0.27	12	***0.30***	***13***	***0.30***	***13***	***0.31***	***13***	0.27	11	0.27	12	0.26	11	0.20	9	0.16	7	0.04
7.96	13086	0.19	9	0.22	10	0.24	11	***0.28***	***14***	0.25	12	0.27	13	0.25	12	0.20	10	0.19	9	0.03
8.99	13271	0.08	4	0.17	8	0.21	10	0.33	15	0.32	15	***0.38***	***17***	0.32	15	0.25	12	0.10	5	0.04
9.99	13659	0.15	11	0.18	13	0.18	13	***0.23***	***16***	0.18	13	0.18	13	0.14	10	0.09	7	0.04	3	0.01
10.99	14049	0.15	7	0.21	10	0.25	11	***0.39***	***17***	0.35	16	0.35	16	0.27	12	0.19	8	0.08	3	0.03
11.99	14320	0.16	9	0.19	10	0.22	12	***0.30***	***17***	0.26	14	0.26	14	0.21	11	0.15	8	0.06	3	0.02
14.93	14752	0.18	9	0.24	12	0.25	13	***0.30***	***15***	0.25	13	0.27	13	0.22	11	0.17	8	0.12	6	0.04
16.51	14984	0.37	12	0.39	13	0.39	13	***0.43***	***14***	0.37	12	0.40	13	0.34	11	0.26	8	0.13	4	0.05

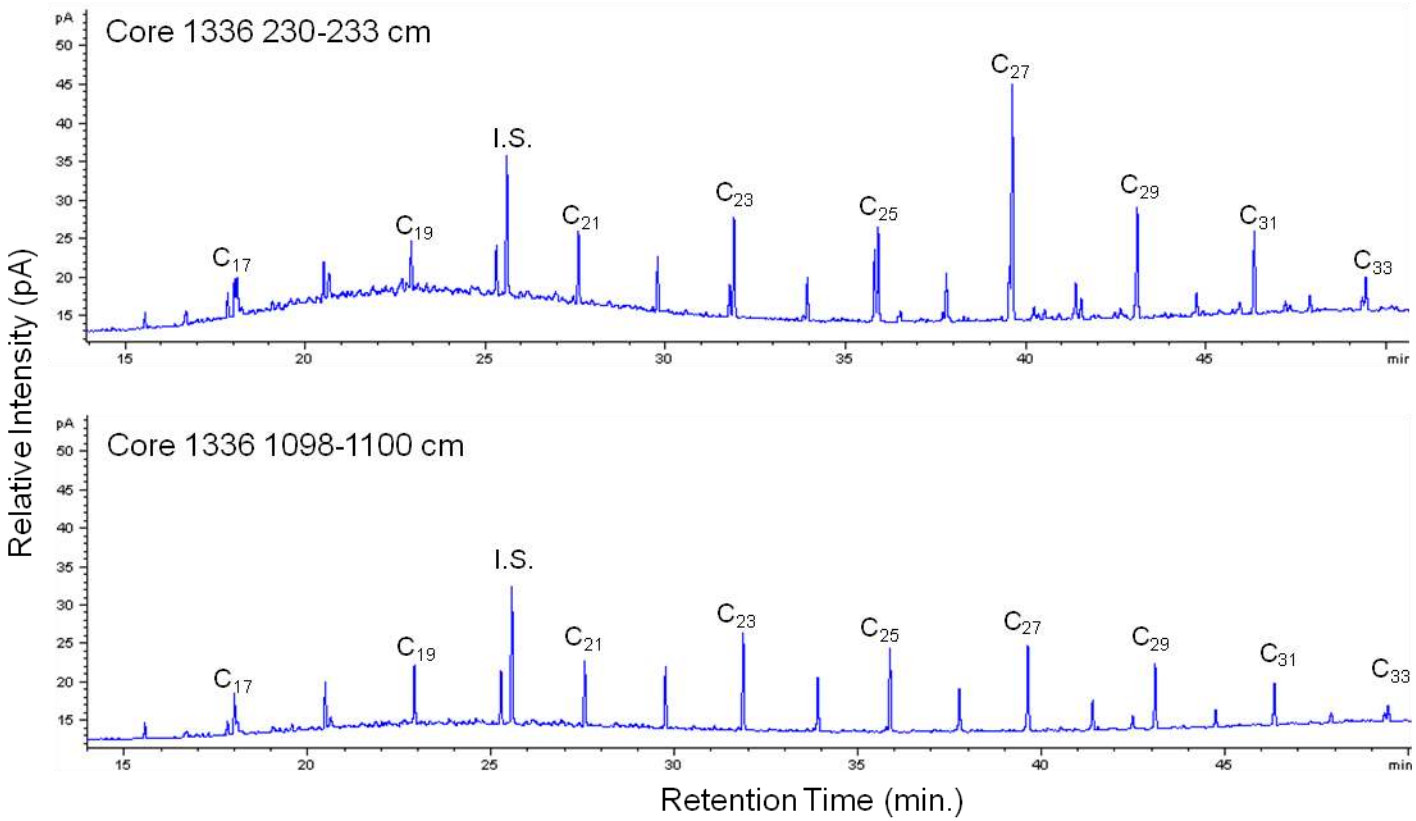

Figure 4.3. Gas chromatograms for the non-polar lipid fraction from Core 1336 sediments. Molecular weights of odd-chain *n*-alkanes and the internal standard (I.S.) 5α-androstane are annotated. (a) Typical chromatogram for post-glacial sediments. (b) Typical chromatogram for glacial sediments.

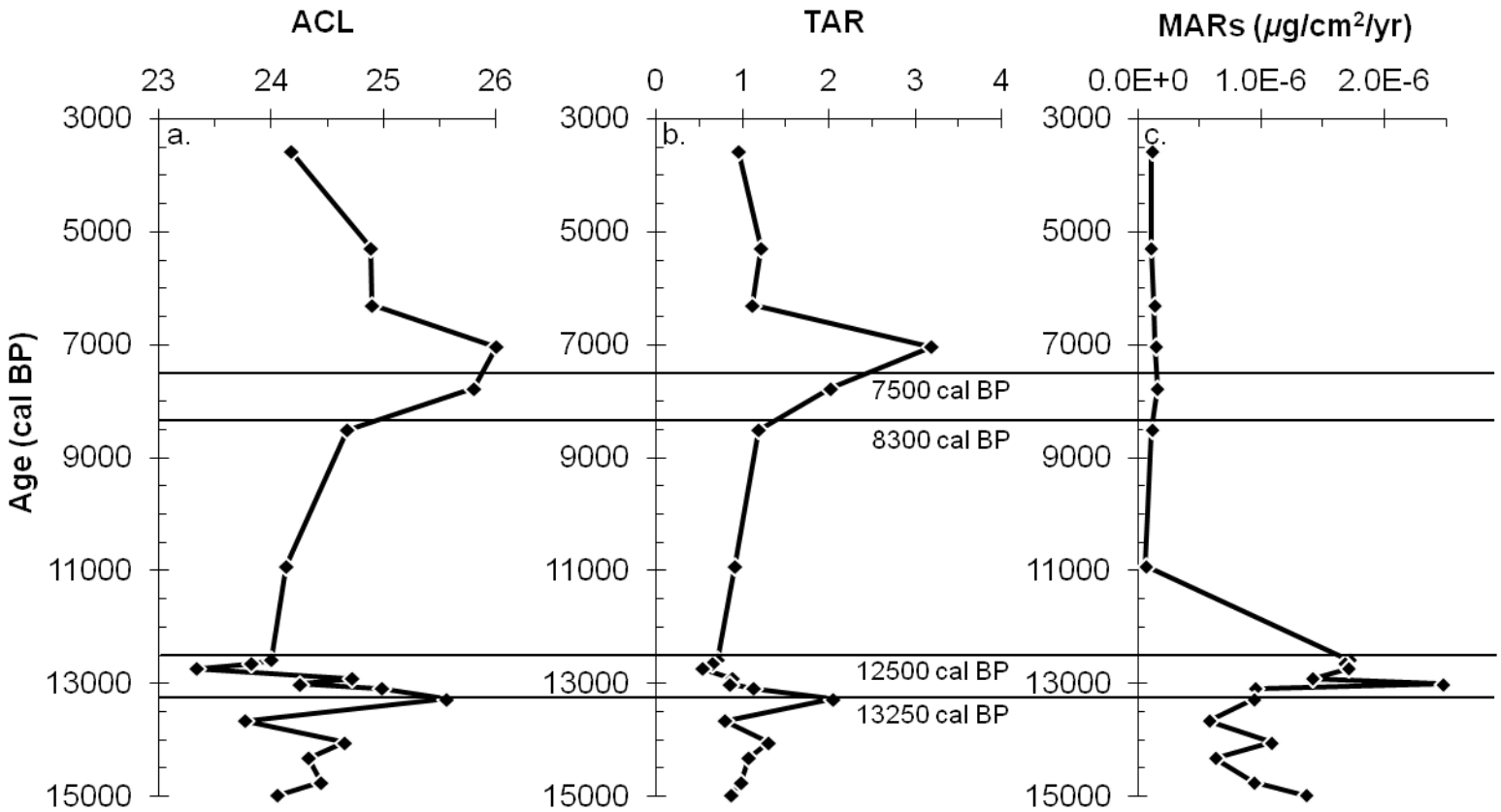

Figure 4.4. (a) Average chain length of *n*-alkanes calculated using ACL = $(\Sigma C_n \bullet n)/(\Sigma C_n)$, where C_n is the concentration of *n*-alkane containing *n* carbon atoms (Chikaraishi and Naraoka, 2003). (b) The terrestrial to aquatic (TAR) *n*-alkane ratio was calculated using TAR= $(C_{27}+C_{29}+C_{31})/(C_{17}+C_{19}+C_{21})$, adapted from Silliman et al. (1996). (c) *n*-Alkane mass accumulation rates (MARs) calculated using MARs= concentration of total *n*-alkanes • linear sedimentation rates • dry bulk density • 10^{-6}.

In our application of the TAR, the denominator was changed from Silliman et al. (1996) (C_{15}+C_{17}+C_{19}) because no C_{15} *n*-alkanes were observed in the sediment record. The short-chain *n*-alkanes C_{17}, C_{19} and C_{21} used here are also all associated with aquatic algae production.

n-Alkane mass accumulation rates (MARs) (Fig. 4.4c) were calculated as follows:

$$\text{MARs= total } n\text{-alkane concentration } (\mu g) \bullet \text{LSR (cm/yr)} \bullet \text{DBD } (g/cm^3) \bullet 10^{-6},$$

where LSR is the linear sedimentation rate and DBD is dry bulk density.

4.3.1 The *n*-alkane abundances

In sediments ranging from ~15,000 to 13,260 cal BP, there is a broadly symmetrical distribution of *n*-alkanes, with the highest abundances generally being in the C_{23} to C_{27} range – typically peaking at C_{23} – and decreasing most strongly towards higher, and less strongly, towards lower chain lengths (Table 4.1, Figs. 4.5, 4.6). During this time period, the average relative abundance of C_{23} is 15 % (Fig. 4.6), the mean ACL is 24.5±0.6 (SD, n=6), TAR is 1.2±0.5 (SD, n=6) and MARs average $9.2x10^{-7}$±$3.0x10^{-7}$ $\mu g/cm^2/yr$ (SD, n=6) (Fig. 4.4a,b,c).

A (positively) right-skewed pattern of *n*-alkane abundances towards increased quantities of short-chains becomes apparent from ~13,260 to 12,500 cal BP when the ACL decreases to 24.2±0.6 (SD, n=6) (Figs. 4.4a, 4.5, 4.6). The dominant *n*-alkanes during this time interval (specifically12,908 to 10,922 cal BP) are ≤C_{23}, with the highest abundances generally occurring for C_{19} (avg. ~16 %; Fig. 4.6). TAR also decreases during this time period, averaging 0.8±0.2 (SD, n=6) (Fig. 4.4b). MARs increase ~two-fold during this interval and average $1.7x10^{-6}$±$4.9x10^{-7}$ $\mu g/cm^2/yr$ (SD, n=6) (Fig. 4.4c).

A broad bimodal distribution of *n*-alkanes exists from ~12,500 to 8,300 cal BP (Fig. 4.5). The less skewed pattern (i.e., flatter distribution) of *n*-alkane abundances from C_{17} to C_{31} signals a shift to higher relative abundances of long-chain *n*-alkanes (C_{27}-C_{31}), beginning after 10,922 cal BP and continuing through to 7,773 cal BP (Fig. 4.6). Saying that, the dominant *n*-alkane during this interval is C_{19} (avg. ~14 %). The shift to higher relative

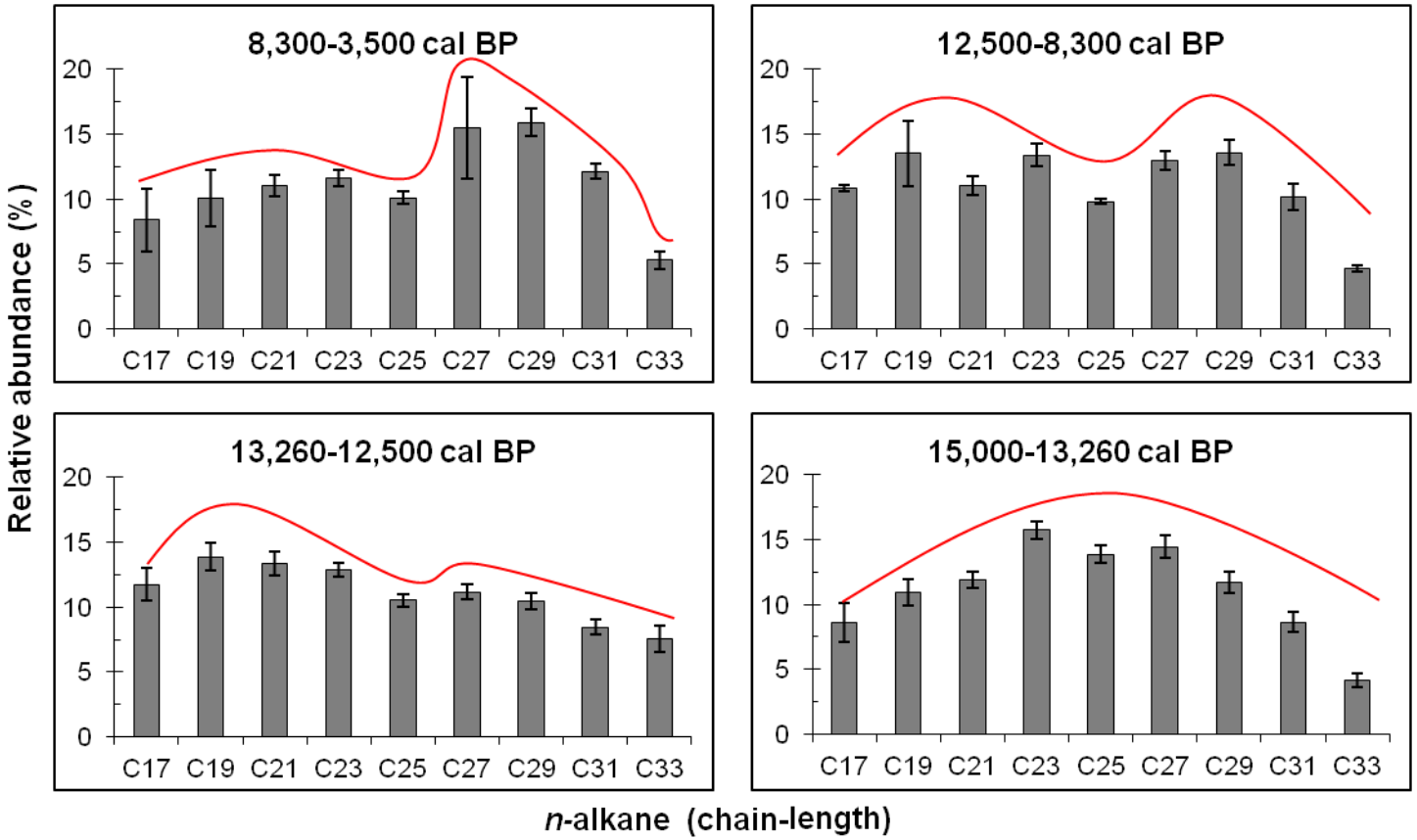

Figure 4.5. Standard *n*-alkane chain-length distributions for various time intervals. The average relative abundance for a given time interval is represented by the height of the individual column and the standard deviation is shown by error bars. The general distribution for each time interval is shown by the red trace above the bar graph.

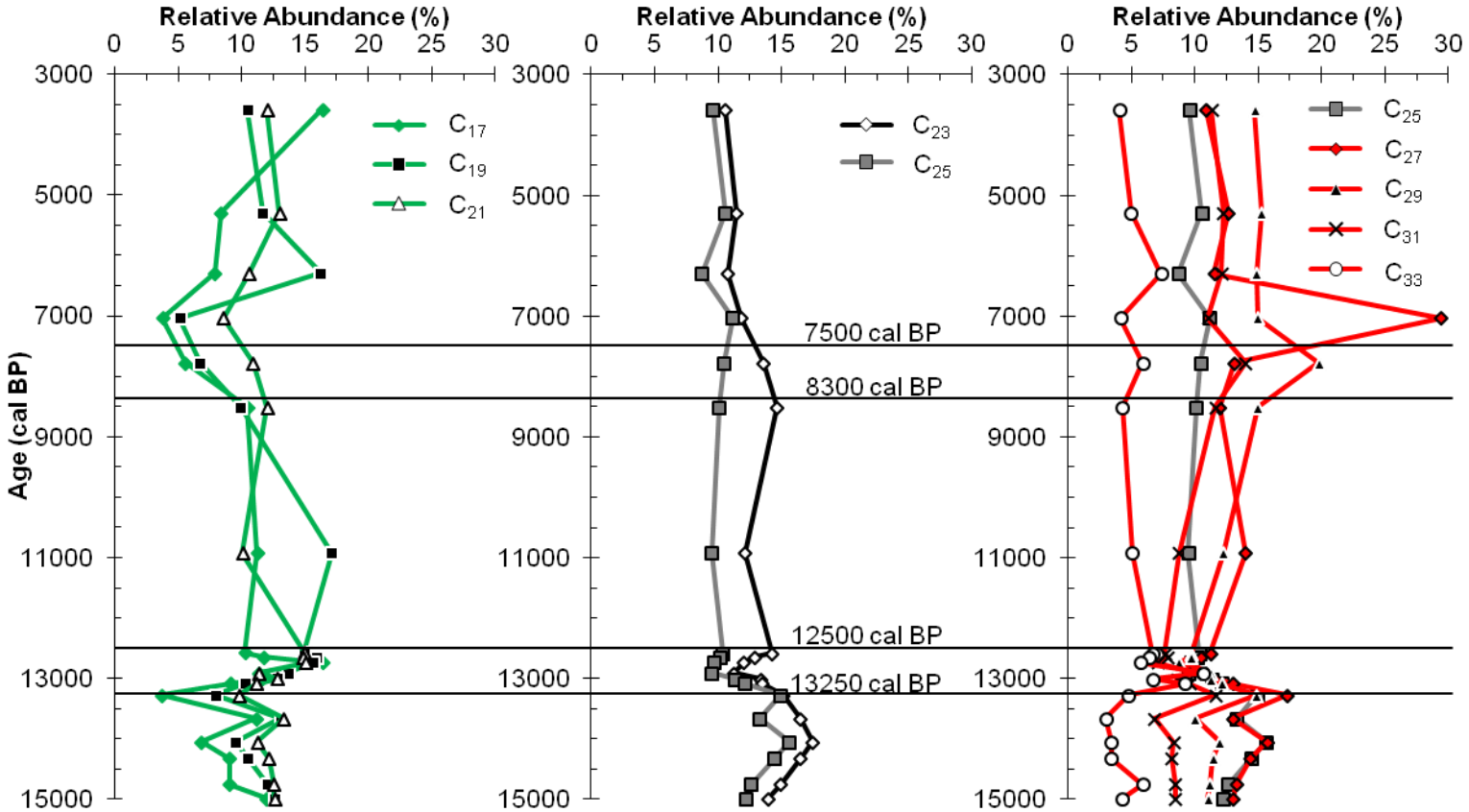

Figure 4.6. The *n*-alkane relative abundances (%) organized by sediment age (cal BP). The abundances of *n*-alkanes are divided into short-, mid-, and long-chain lengths for easier comparison within a group.

abundances of long-chain *n*-alkanes is also illustrated by increases in ACL (25.2±0.8 (SD, n=2)) and TAR (1.6±0.6 (SD, n=2)) (Fig. 4.4a,b). MARs decrease sharply to $8.8x10^{-8}$±$3.6x10^{-8}$ $\mu g/cm^2/yr$ (SD, n=2) during this interval (Fig. 4.4c).

From 8,300 to 3,500 cal BP there is a shift to a (negatively) left-skewed pattern of *n*-alkane abundances peaking at C_{27} and C_{29} (Fig. 4.5). The average relative abundance of C_{29} during this time interval is 16 % (Fig. 4.6). An increase in ACL (to 26.0) and TAR (to 3.2) occurs from 8,300 to ~7,000 cal BP (Fig. 4.4a,b). After ~7,000 cal BP, both ACL and TAR decrease to 24.2 and 1.0, respectively, for the youngest measured sample (3,583 cal BP) (Fig. 4.4a,b). MARs remain low during this time interval and averages $1.3x10^{-7}$±$2.1x10^{-8}$ $\mu g/cm^2/yr$ (SD, n=5) during this interval (Fig. 4.4c).

4.3.2 Carbon isotopic composition of *n*-alkanes

In sediments ranging from ~15,000 to 13,260 cal BP, there is only limited variation in $\delta^{13}C_{n\text{-alkane}}$ values among short-, mid- and long-chain *n*-alkanes: short-chain (C_{17}, C_{19}, C_{21}), –30.2±0.9 ‰ (SD, n=18); mid-chain (C_{23}, C_{25}), –31.9±0.6 ‰ (SD, n=12), and long-chain (≥C_{27}),–32.2±0.7 ‰ (SD, n=24). All $\delta^{13}C_{n\text{-alkane}}$ values show a slight (up to 2 ‰), up-core increase (Table 4.2; Fig. 4.7).

Between ~13,260 to 12,500 cal BP, the trend of increasing $\delta^{13}C_{n\text{-alkane}}$ values continues, albeit of smaller magnitude. There is little variation in C_{17}, C_{19} and C_{21} $\delta^{13}C_{n\text{-alkane}}$ values, which average –30.5±0.8 ‰ (SD, n=18). The mid-chain *n*-alkanes C_{23} and C_{25} have nearly equal $\delta^{13}C_{n\text{-alkane}}$ values of –31.8 ‰. Long-chain *n*-alkanes (≥C_{27}) have an average $\delta^{13}C_{n\text{-alkane}}$ value of –32.0±0.6 ‰ (SD, n=24) (Table 4.2; Fig. 4.7).

Between 12,500 and 8,300 cal BP, the mid-chain *n*-alkane $\delta^{13}C_{n\text{-alkane}}$ values deviate from each other by up to ~5 ‰ (avg. C_{23} = –33.6±0.6 ‰, SD, n=2; avg. C_{25} = –28.4±0.3 ‰, SD, n=2; Table 4.2; Fig. 4.7). For C_{21} and ≥C_{25}, there is an increasing up-core trend in the $\delta^{13}C_{n\text{-alkane}}$ values, which is most pronounced for the mid- to long-chain *n*-alkanes C_{25} and C_{27}. Long-chain (≥C_{27}) $\delta^{13}C_{n\text{-alkane}}$ values average –30.7±0.7 ‰ (SD, n=8). Short-chain $\delta^{13}C_{n\text{-alkane}}$ values (C_{17}, C_{19}, C_{21}) remain largely unchanged from previous intervals and average –30.1±0.4 ‰ (SD, n=6).

Table 4.2. Carbon-isotope compositions (VPDB, ‰) of *n*-alkanes in Lake Ontario Core 1336, reported by depth (meters) and age (calibrated years BP).

Depth (m)	Age (cal BP)	$\delta^{13}C$ (VPDB,‰) C_{17}	C_{19}	C_{21}	C_{23}	C_{25}	C_{27}	C_{29}	C_{31}	C_{33}
0.515	3583	–34.0	–31.4	–32.3	–33.4	–30.5	–30.7	–31.1	–31.1	–30.4
1.38	5289	–31.6	–31.2	–32.0	–31.7	–30.1	–30.1	–30.9	–30.9	–30.8
1.91	6294	–31.8	–32.5	–32.5	–31.4	–29.7	–30.4	–31.0	–31.4	–30.9
2.315	7033	–30.3	–30.8	–31.8	–32.4	–28.3	–33.0	–29.9	–30.3	–29.4
2.715	7773	–29.6	–31.3	–29.9	–30.9	–25.1	–26.8	–28.9	–30.3	–30.1
3.105	8512	–29.6	–30.3	–30.0	–33.6	–28.2	–29.3	–30.8	–30.9	–30.0
4.31	10922	–29.7	–30.0	–30.8	–32.8	–28.6	–31.1	–30.5	–31.5	–31.2
5.13	12577	–29.8	–30.4	–31.8	–32.4	–31.2	–31.8	–31.2	–31.2	–31.1
5.51	12645	–30.7	–30.7	–31.4	–31.8	–31.7	–31.5	–31.9	–32.8	–32.3
5.99	12731	–29.9	–29.2	–31.2	–31.2	–32.9	–31.2	–31.8	–32.4	–31.4
6.97	12908	–29.3	–29.8	–31.3	–31.5	–31.5	–32.0	–32.2	–32.4	–32.0
7.51	13005	–30.3	–30.5	–31.5	–32.3	–31.7	–31.6	–32.4	–33.2	–33.3
7.96	13086	–29.5	–30.0	–31.5	–31.5	–31.6	–31.5	–32.0	–32.8	–32.2
8.99	13271	–29.7	–30.0	–30.5	–31.6	–31.7	–31.5	–31.9	–32.0	–32.0
9.99	13659	–29.1	–30.3	–30.4	–31.2	–31.9	–31.4	–31.8	–32.3	–31.7
10.99	14049	–29.9	–29.5	–30.0	–31.4	–31.2	–31.4	–32.2	–31.7	–31.5
11.99	14320	–29.1	–29.4	–30.3	–32.0	–32.2	–31.9	–32.3	–32.7	–31.3
14.93	14752	–29.8	–30.2	–31.6	–31.7	–31.9	–32.0	–32.6	–33.2	–32.5
16.51	14984	–30.2	–29.8	–32.8	–32.9	–33.3	–32.6	–33.2	–33.4	–33.6

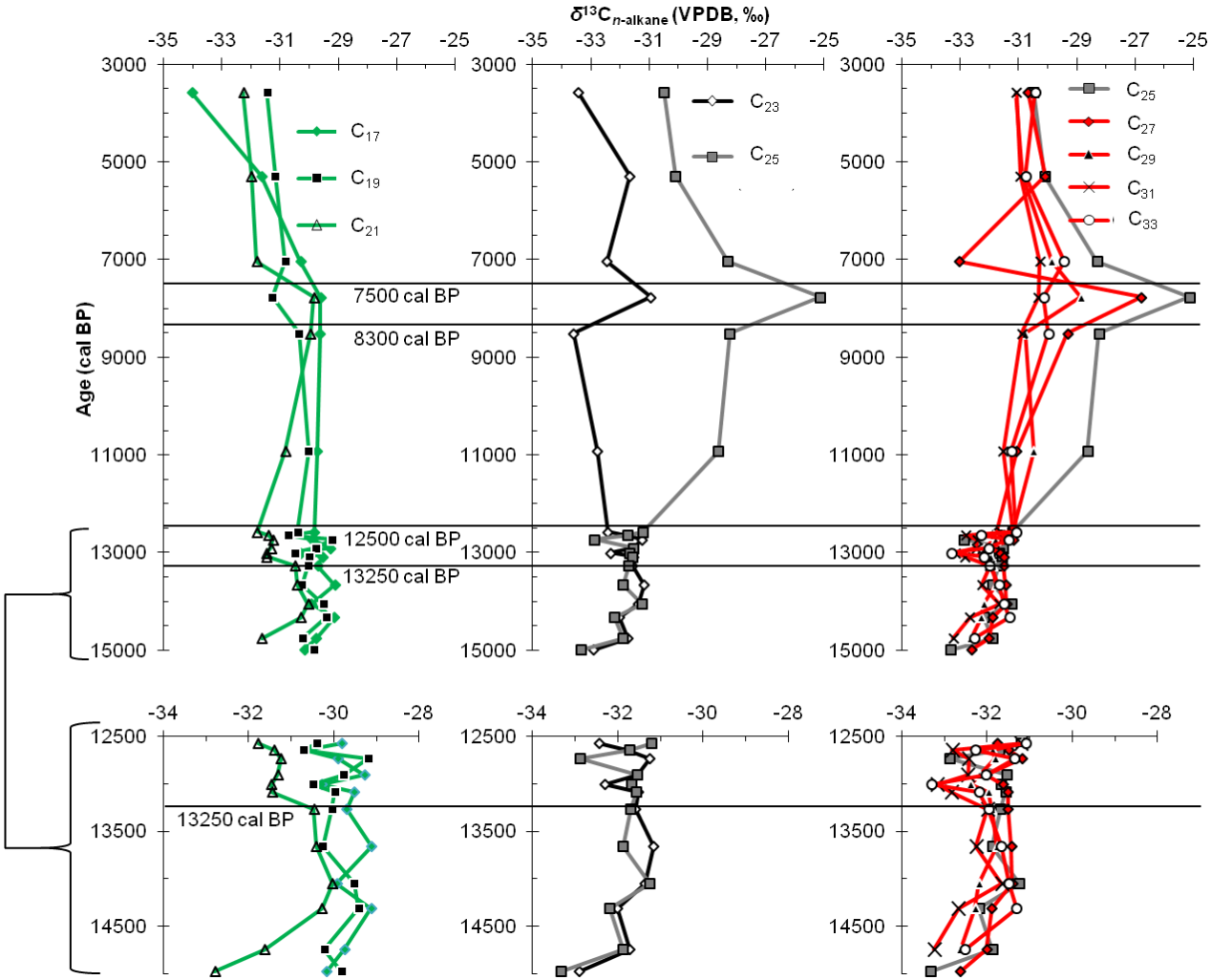

Figure 4.7. Age (cal BP) versus $\delta^{13}C$ values for each *n*-alkane.

From 8,300 to 7,500 cal BP, there is an increase in the $\delta^{13}C_{n\text{-alkane}}$ values of mid- to long-chain *n*-alkanes (Table 4.2; Fig. 4.7). In particular, the $\delta^{13}C_{n\text{-alkane}}$ values of C_{23}, C_{25} and C_{27} increase by ~3 ‰ between 8,512 and 7,773 cal BP, which coincides with higher values of ACL and TAR (Fig. 4.4a,b). From ~7,500 to 3,500 cal BP, there is then a progressive decrease in the $\delta^{13}C_{n\text{-alkane}}$ values of short- and mid-chain *n*-alkanes, whereas most long-chain *n*-alkane $\delta^{13}C_{n\text{-alkane}}$ values decrease only slightly. Over this entire interval (8,300 to 3,500 cal BP), the average $\delta^{13}C_{n\text{-alkane}}$ value for short-chain *n*-alkanes C_{17}, C_{19} and C_{21} is –31.9±0.9 ‰ (SD, n=12); mid-chain *n*-alkane C_{23} is –32.2±0.9‰ (SD, n=4) and C_{25} is –29.6±0.9‰ (SD, n=4); and long-chain *n*-alkanes $\geq C_{27}$ is –30.8±0.8 ‰ (SD, n=16) (Table 4.2; Fig. 4.7).

4.4 Discussion

4.4.1 Glacial periods in early Lake Ontario (15,500-13,260 cal BP)

Perhaps the best record of vegetation history in southern Ontario has been developed for the Rostock Mammoth Site (Fig. 4.8, adapted from McAndrews, 1994). Its pollen record reveals that prior to 15,500 cal BP, southern Ontario vegetation resembled a polar desert (McAndrews, 1994). This landscape must have been highly unstable, with wind eroding fine material from till and frost shattering local bedrock (Spear, 1989). Low pollen counts indicate that vegetation was sparse (McAndrews, 1994). Silliman et al. (1996) reported TAR values ≤1 for Rochester basin *n*-alkanes older than 15,500 cal BP. This ratio likely reflects the combination of extremely low abundances of higher terrestrial plants in the polar desert and enhanced preservation of algal *n*-alkanes during this period of high sedimentation rates.

Evaluating the sources of OM in Lake Ontario's glacial sediments from 15,500 to 13,260 cal BP requires an understanding of regional climatic conditions and vegetation at that time. Warming beginning at 15,500 cal BP led to establishment of a tundra-woodland environment (Fig. 4.8, adapted from McAndrews, 1994). This period (15,500 to 15,300 cal BP) correlates with the Mackinaw interstadial phase of the LIS. Such conditions would favour increased aquatic productivity, and indeed TAR ratios reported by Silliman et al. (1996) show a slight decrease beginning at 15,500 cal BP. On land, ablation of the

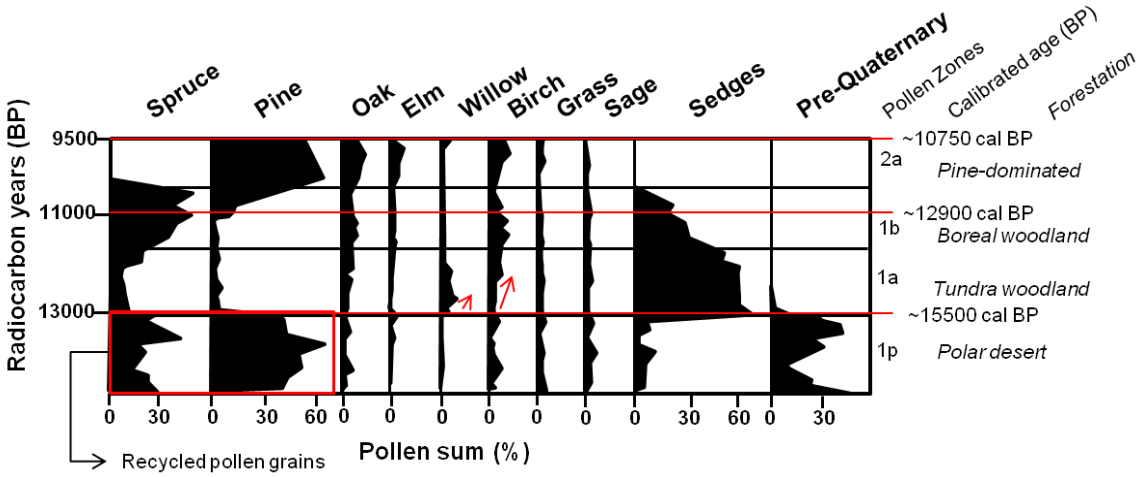

Figure 4.8. Pollen diagram for Rostock mammoth site (redrawn from McAndrews, 1994). See Figure 1 for location. Pollen zone 1p represents a polar desert. The high abundances of spruce and pine pollen likely represent recycled pollen grains. A transition from tundra woodland to boreal woodland occurs in pollen zone 1a. A pine-dominated forest was established at ~12,900 cal BP. Red arrows indicate the timing of increased abundances of birch and willow pollen.

ice sheet and associated ponding of meltwater would have been ideal for peat bog formation, much like present-day northernmost Canada. The tundra ecosystem would have consisted of sedge meadows and/or peat bogs, and included *Sphagnum* species (sp.) mosses in abundance (Davis and Webb, 1975).

Ice readvance at 15,300 cal BP scraped the landscape clean yet again, delivering its OM to the Lake Ontario basin (Fig. 4.9a). The sediment record captured by Core 1336 begins at ~15,000 cal BP, which is nearly contemporaneous with the advancing ice. High abundances of C_{23} and C_{25} *n*-alkanes in these sediments are best attributed to terrestrial OM originating from the tundra. *Sphagnum* sp. generally contains high abundances of C_{23} and to a lesser extent C_{25} while other bog-forming species are dominated by C_{31} (Bingham et al., 2010). As a cautionary note, such an *n*-alkane signature can be confounded by C_{23} and C_{25} *n*-alkanes from submergent and floating macrophytes (Ficken et al., 2000). However, there was little likelihood of highly productive macrophyte growth in ancient Lake Ontario at 15,000-14,500 cal BP. First, the Lake Ontario basin was covered by the LIS. Limited light penetration and very cold water under an ice sheet would have severely limited macrophyte sustainability. Second, macrophyte growth requires a stable littoral habitat. Littoral zones provide optimal conditions for submergent (2-4 m water depth) and emergent (~2 m water depth) macrophytes (Dale, 1986; Sifeddine et al., 2011). Given the ice readvance after the Mackinaw interstadial, much of the littoral habitat would have been destroyed. The low average $\delta^{13}C_{n\text{-alkane}}$ value (~ –32.5±0.8 ‰, SD, n=4; Fig. 4.7) of the mid-chain *n*-alkanes (C_{23} and C_{25}) from 15,000-14,500 cal BP compares well with contemporaneous (15,000-14,500 cal BP) terrestrial vegetation ($\geq C_{27}$), which has an average $\delta^{13}C_{n\text{-alkane}}$ value of –32.9±0.5 ‰ (SD, n=8). This suggests a similar carbon substrate available for photosynthesis (atmospheric CO_2).

C/N ratios, *n*-alkane patterns and TAR values for this OM show that *Sphagnum* sp. mosses were by no means the only organic input between 15,000 and 14,500 cal BP. First, bulk C/N ratios of lake sediment OM during this time interval averaged ~7.5 (Chapter 3, this thesis). Whole-plant *Sphagnum* sp. from bogs and wetlands, by

comparison, commonly have C/N ratios >45 (Hornibrook et al., 2000). As discussed in Chapter 3, C/N ratios ≤ 10 are traditionally interpreted to indicate aquatic algal OM rather than terrestrial input (C/N >10), although recycled, degraded terrestrial OM including that sorbed on soil clays (Hyodo and Longstaffe, 2011) may comprise an important exception. Second, abundant short-chain *n*-alkanes (C_{17}; 10 %, C_{19}; 12 %, C_{21}; 13 %) indicate a contribution from algae sources. It appears that algae grew in the lake at this time, perhaps near to the LIS margin and within the ice sheet, much like present-day Antarctica (Gibson et al., 1999). Third, the TAR ratio at this time in Core 1336 was ~1.0 (Fig. 4.4b; see also Silliman et al., 1996), indicating that OM from terrestrial higher plants was equally as abundant as lacustrine algae.

The average short-chain $\delta^{13}C_{n\text{-alkane}}$ value is –30.7±1.2 ‰ (SD, n=6; C_{17}, C_{19}, C_{21}). Within that range, the average C_{21} $\delta^{13}C_{n\text{-alkane}}$ value is ~1.5 ‰ lower than for C_{17} and C_{19}. This may reflect OM from dinoflagellates (Sun et al., 2013), which are common in Great Lakes sediments (McCarthy et al., 2011). The lower C_{21} $\delta^{13}C_{n\text{-alkane}}$ values may indicate some differences in dinoflagellate carbon sources within the water column relative to other algae (diatoms, chrysophytes, blue-green algae). Saying that, the average short-chain $\delta^{13}C_{n\text{-alkane}}$ value remains higher than measured for C_{23} and C_{25} (–32.5±0.8 ‰, SD, n=4; Fig. 4.7). Algae would have assimilated usable sources of DIC in the lake, mainly $CO_{2(aq)}$ originating from dissolved atmospheric CO_2 ($CO_{2(atm)}$). The predicted $\delta^{13}C_{n\text{-alkane}}$ value for algal *n*-alkanes primarily using this source of DIC is ~ –27.5 ‰, assuming atmospheric $\delta^{13}C_{(CO2)}$ = –6.5 ‰ (Schmitt et al., 2012) and the following C-isotope fractionations: $CO_{2(aq)}$–$CO_{2(atm)}$ = –1 ‰, bulk algal tissue–$CO_{2(aq)}$ = –19 ‰, and *n*-alkanes–bulk algal tissues = –1 ‰ (Hecky and Hesslein, 1995; Schouten et al., 1998; Mook, 2000). Instead, the algal $\delta^{13}C_{n\text{-alkane}}$ values (avg. –30.7±1.2 ‰, SD, n=6) lie between the predicted $\delta^{13}C_{n\text{-alkane}}$ values (–27.5 ‰) and the $\delta^{13}C_{n\text{-alkane}}$ values (avg. –32.9±0.5 ‰, SD, n=8) of terrestrial OM that entered the lake. When the advancing LIS covered the lake, other sources of DIC such as bicarbonate (HCO_3^-), carbonate (CO_3^{2-}) and oxidation of organic matter likely increased in importance. On one hand, algal incorporation of bicarbonate and carbonate (from Suess-corrected atmospheric CO_2; +3.5 and +2.5 ‰, respectively; Mook, 2000) would have increased algal $\delta^{13}C_{n\text{-alkane}}$ values. On the other hand, CO_2 produced by oxidation of glacially transported terrestrial OM

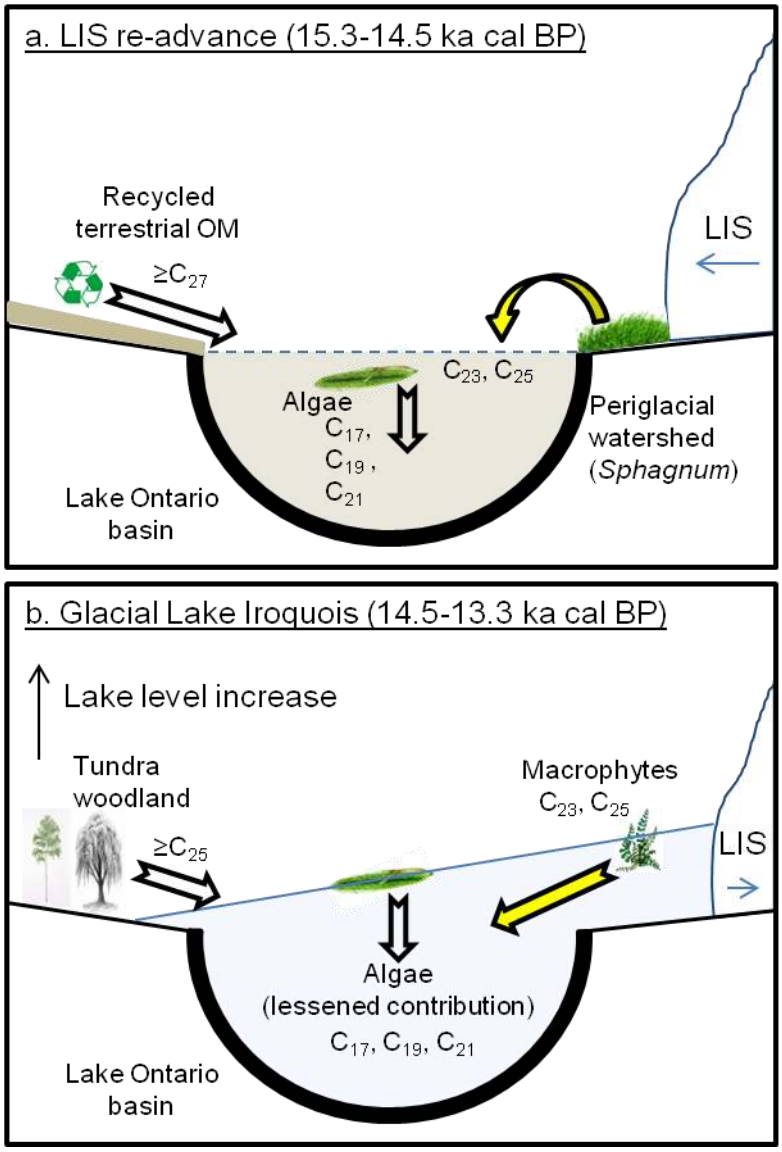

Figure 4.9. Schematic diagram illustrating potential sources of OM entering ancient Lake Ontario. The yellow arrow indicates the most important source of OM during a given time period. (a) Re-advance of the LIS from 15,300 to 14,500 cal BP transported detritus from the periglacial environment to ancient Lake Ontario. *Sphagnum* mosses were the primary source of OM. Significant amounts of long-chain *n*-alkanes ($\geq C_{27}$) also entered the lake, and likely included recycled and degraded terrestrial vegetation. (b) During formation of glacial Lake Iroquois, aquatic macrophytes were the major source of OM in lake sediments. *Sphagnum* mosses were likely less important.

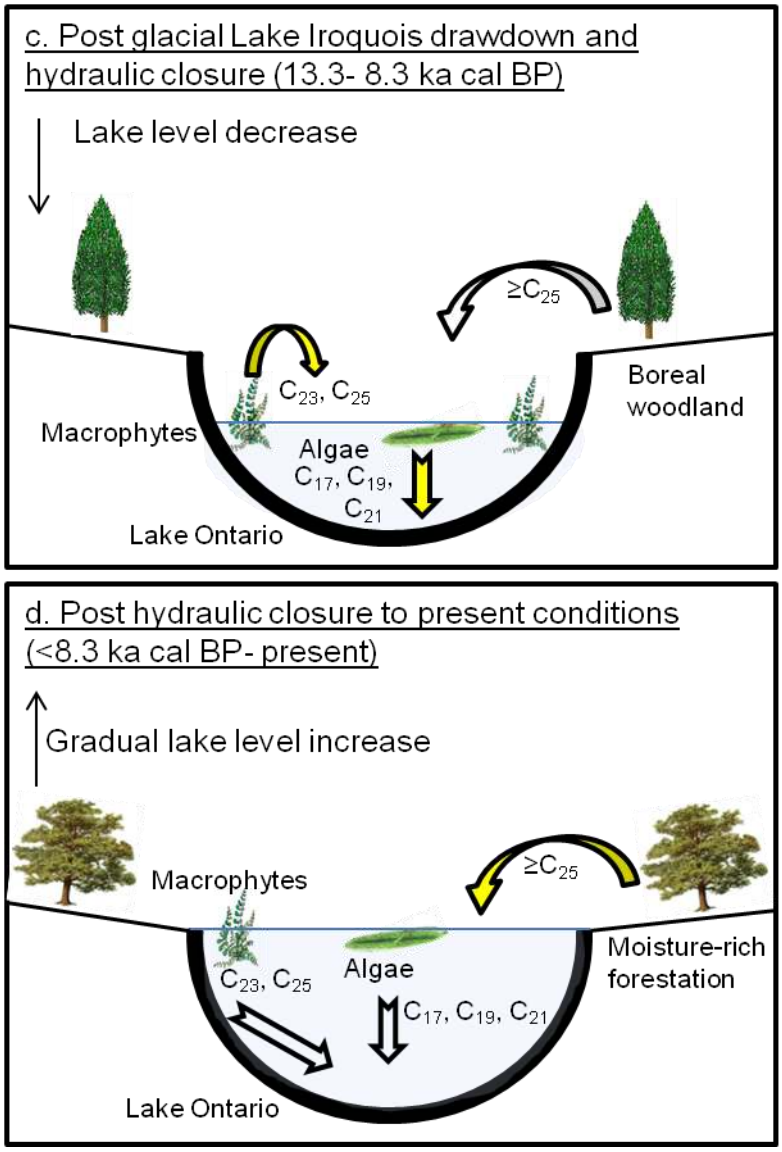

Figure 4.9 (continued). (c) Lower lake levels of post-glacial Lake Iroquois were associated with increased abundances of algal biomarkers (C_{17}, C_{19}); hydrologic closure also favoured growth of aquatic macrophytes. There was also some OM contribution from the coniferous-forested watershed to the lake sediments. (d) Increased precipitation caused Lake Ontario to rise. The forested watershed, now dominated by angiosperms, was a major contributor to the lake sediment OM record, particularly through drowned shorelines. OM contributions from algal and aquatic macrophytes continued to be significant.

(avg. –25 ‰, Suess corrected; O'Leary, 1988) would have assumed much greater importance, as direct access to atmospheric CO_2 became limited in the ice-covered lake. The DIC pool available for algal assimilation would therefore acquire lower $\delta^{13}C$ values, as is observed.

The long-chain *n*-alkanes (C_{27}, C_{29} and C_{31}), especially C_{27}, have only slightly lower relative abundances than the most dominant *n*-alkane (C_{23}), and can be used to evaluate, to a certain degree, the relative proportions of birch *(Betula)*, pine *(Pinus)* and grasses entering the lake (Schwark et al., 2002). The relative abundance of C_{27} (13 %) is slightly higher than that of C_{29} (11 %) and correlates well with increases in birch and poplar *(Populus)* pollen at the Rostock Mammoth site (McAndrews, 1994). Pine pollen entering the lake at this time (C_{29}) likely was recycled from glacial till (McAndrews, 1994). The lower relative amount of C_{31} (8 %) suggests insufficient soil development to support grasses in abundance, likely because of the readvance of glacial ice (Schwark et al., 2002). All long-chain *n*-alkanes (C_{27}, C_{29} and C_{31}) have very similar $\delta^{13}C_{n\text{-alkane}}$ values (avg. –32.9±0.5 ‰, SD, n=8), which are very similar to those of the mid-chain *n*-alkanes (C_{23}, C_{25}), as discussed earlier, and suggest a similar source of CO_2.

Shortly after 14,500 cal BP, ice retreated from the Lake Ontario basin and glacial Lake Iroquois formed (Chapter 2, this thesis and references therein) (Fig. 4.9b). From 14,500 to 13,000 cal BP, the ice dam across the St. Lawrence River valley held up a series of glacial lakes starting initially with high-level glacial Lake Iroquois up to ~35 (east) and 115 (west) m higher than at present (higher at the east end of the lake because of differential rebound) (Coakley and Karrow, 1994; Anderson and Lewis, 2012). As ice retreated towards a position across the lower St. Lawrence River valley and opened lower outlets, the glacial water levels fell through the Frontenac, Sydney '?', Belleville and Trenton stages (Coakley and Karrow, 1994; Anderson and Lewis, 2012). Overall increases in ACL (24.5 to 25.5) and TAR (0.9 to 2.0) over this period indicate higher terrestrial OM contributions (Fig. 4.4a,b). Gradual warming associated with deglaciation again allowed for tundra-woodland development (tundra sedge, willow *(Salix)*, birch and poplar (McAndrews, 1994). Its appearance is marked by higher abundances of long-

chain *n*-alkanes (C_{25}, C_{27}, C_{29}, C_{31}) in the lake sediment OM (Fig. 4.6), again consistent with the Rostock Mammoth site pollen record (McAndrews, 1994). This change is accompanied by an average ~1 ‰ increase in long-chain $\delta^{13}C_{n\text{-alkane}}$ values (avg. –31.8±0.4 ‰, SD, n=20) (Fig. 4.7). This upward shift may be related to increased water stress related to cold and dry climate conditions at this time or perhaps also a slight increase in the concentration of atmospheric CO_2 (Schmitt et al., 2012). The increasing relative abundance of C_{29} during this time period likely reflects a general increase in terrestrial biomass rather than only inherited contributions from earlier pine forests.

The most abundant *n*-alkane, C_{23}, occurs in similar abundances (~15 %) as in the older sediments (>14,500 cal BP) (Fig. 4.6). Its origin, however, is more enigmatic. While continued retreat of the LIS would have created abundant, meltwater-fed bogs, a mechanism is lacking for significant transport of *Sphagnum*-moss C_{23} *n*-alkanes to the lake. Aquatic macrophytes were more likely the main contributor of C_{23} (and perhaps C_{25}) *n*-alkanes. The decline in water level of glacial Lake Iroquois occurred through a series of stages over ~1500 years from 14,500-13,000 cal BP and uplift of the basin relative to lake level occurred after the controlling outlet sill for the lower stages became established at the southern end of the Lake Champlain valley, thus allowing for development of extensive littoral zones and healthy macrophyte (i.e., C_{23}) populations. The abundance of mid-chain *n*-alkane C_{25} also increased during this time. However, C_{25} is also present in terrestrial plants, and thus is an inconclusive indicator for macrophyte production. From 14,500 to 13,260 cal BP, the average $\delta^{13}C_{n\text{-alkane}}$ value for C_{23} (~ –31.5±0.4 ‰, SD, n=4) is slightly higher (by ~1 ‰) than during the previous time period (Fig. 4.7). In this case, however, C_{23} *n*-alkanes originated from macrophyte production, whereas earlier (>14,500 cal BP), C_{23} originated from *Sphagnum* moss species. The $\delta^{13}C_{n\text{-alkane}}$ value suggests that atmospheric CO_2 and dissolved atmospheric CO_2 were the primary DIC sources for floating and submerged macrophytes, respectively. The ~1 ‰ increase from the previous time period may be explained by differences in the *n*-alkane–bulk tissue C-isotope fractionation, which is ~ –6 ‰ for *Sphagnum* moss (Conte et al., 2003), much like terrestrial vegetation, versus ~ –4 ‰ for macrophytes (average from Ficken et al., 2000). Submergent macrophytes can also utilize bicarbonate as a carbon substrate, which would result in a further increase in $\delta^{13}C_{n\text{-alkane}}$ values. By comparison,

the C_{23} $\delta^{13}C_{n\text{-alkane}}$ value is slightly lower than that of the algae (C_{17}, C_{19}, and C_{21}) (–29.9±0.5 ‰, SD, n=12) during this time period. This difference may arise from their differing environments. Oxidative decay of macrophytes in the littoral zone is capable of lowering the DIC $\delta^{13}C$ values of the surrounding water (Keough et al., 1998).

The decrease in abundance of short-chain *n*-alkanes (C_{17}, C_{19}, and C_{21}) from 14,500 to 13,260 cal BP relative to >14,500 cal BP, especially for C_{17} (~10 to 5 %), simply reflects the relative increase in addition of terrestrial OM to the lake (Table 1; Fig. 4.6). The C_{17} and C_{19} $\delta^{13}C_{n\text{-alkane}}$ values are unchanged from the earlier period (Fig. 4.7), indicating no significant change in algal carbon sources.

4.4.2 Post glacial Lake Iroquois drawdown and meltwater influx (13,260-12,500 cal BP)

Soon after ~13,260 cal BP, the LIS withdrew from the St. Lawrence lowland, leading to drainage of glacial Lake Iroquois (Chapter 2, this thesis and references therein). Continued warming caused spruce *(Picea)* to spread across the landscape, forming a boreal woodland (McAndrews, 1994) (Figs. 4.8, 4.9c). For the first time, early Lake Ontario was not influenced by the retreating LIS and associated meltwater, except for a final, brief influx shortly after 13,000 cal BP (Chapter 2, this thesis).

Between 13,260 and ~12,700 cal BP, there are marked decreases in ACL (from 25.5 to 23.5) and TAR (from 2.0 to 0.5) (Fig. 4.4a,b), which were also observed by Silliman et al. (1996). These changes are associated with increased algal production relative to terrestrial, allochthonous OM input and occurred even though mass accumulation rates (MARs) for carbon and nitrogen also increased ~three-fold during this time period (Chapter 3, this thesis). While terrestrial organic detritus continued to enter the eastern portion of the lake from the active Fenelon Falls outlet, autochthonous input must have been still greater to explain the decreasing ACL and TAR values.

The shift to higher relative abundances of short-chain *n*-alkanes (C_{17}, C_{19}, C_{21}) reached a maximum at ~12,700 cal BP (Fig. 4.6). The strong C_{21} peak may reflect OM from dinoflagellates as discussed earlier. The $\delta^{13}C_{n\text{-alkane}}$ values of C_{17} and C_{19} increase by only ~1‰ (–30 to –29 ‰), and C_{21} decreases by only ~1 ‰ (–30.5 to –31.5 ‰) during this

interval (Fig. 4.7), signaling only minor change in carbon source/availability or environmental conditions.

A relative increase in C_{23} abundance relative to higher chain *n*-alkanes also contributed to the decreasing ACL during this time period (Figs. 4.4a, 4.6). Given the waning influence of the LIS and the gradual warming in the watershed, this *n*-alkane is unlikely to have been derived from *Sphagnum* moss species. Instead, lower lake levels and a larger littoral zone would have encouraged aquatic macrophyte growth (Fig. 4.9c). However, the limited variation in C_{23} $\delta^{13}C_{n\text{-alkane}}$ values (Fig. 4.7) suggests that the macrophyte carbon reservoir was not sensitive to changes in sources or aquatic productivity during this time.

The final influx of glacial meltwater into Lake Ontario from 13,000 (earliest) to 12,500 cal BP was accompanied by a slight increase in ACL and TAR values (Fig. 4.4a,b), an approximately two-fold increase in *n*-alkane mass accumulation rates (Fig. 4.4c) and no change in the $\delta^{13}C_{n\text{-alkane}}$ record relative to the immediately preceding time period (Fig. 4.7). This suggests either that the LIS-associated meltwater contained large quantities of *n*-alkanes (with similar isotopic compositions to Lake Ontario) or that *n*-alkanes were accumulated in greater proportions when compared to other glacial sediments. This pattern correlates well with the three-fold increase in C-MARs and N-MARs previously documented for this period of time (Chapter 3, this thesis).

4.4.3 Hydrologic closure of Lake Ontario (12,300-8,300 cal BP)

The time period beginning at 12,300 cal BP is a very dynamic part of Lake Ontario's history. Not only was the lake hydrologically closed – input from the upper Great Lakes into Lakes Erie and Ontario had ceased – but the region, while initially still cold and dry, was beginning to warm while remaining quite dry (Anderson and Lewis, 2012). As a result, Lake Ontario water levels fell to well below its outlet at the St. Lawrence River. Lower lake levels and low precipitation limited input from its watershed (leading to increased water clarity and greater light penetration) and warming likely favoured macrophyte growth in Lake Ontario's littoral zone (Fig. 4.7c). The slight increase in ACL (24.0 to 24.7) and TAR (0.7 to 1.2) from 12,300 to 8,300 cal BP (Fig. 4.4a,b) may

indicate more abundant emergent macrophytes, perhaps in combination with some increase in terrestrial OM input. Silliman et al. (1996) attributed an increase in TAR after ~10,500 cal BP to increased contributions of tree and shrub litter to the lake.

Both algae and macrophytes are well represented in the *n*-alkane distributions of the few samples analyzed from this time interval (Fig. 4.6). The relative abundances of C_{17} and C_{21} *n*-alkanes remain nearly constant during this time, whereas C_{19} contents decrease by the end of hydrologic closure (~8,300 cal BP) (Fig. 4.6). This decrease, coupled with a slight increase in the relative abundance of C_{23} between ~10,900 and 8,500 cal BP hints at a reduction in algal production relative to macrophyte growth (Fig. 4.6). Macrophytes can outcompete algae in the photic zone in such environments (Nakai et al., 1999). All macrophyte types (submergent, floating, emergent) likely were important contributors to the OM budget of the lake at this time. Ficken et al. (2000) described a proxy ratio (P_{aq}=C_{23}+C_{25}/C_{23}+C_{25}+C_{29}+C_{31}) for assessing the relative contributions of macrophyte types, where P_{aq} = 0.1 to 0.4 indicate greater abundances of emergent macrophytes, and P_{aq} = 0.4 to 1.0 indicate more abundant submergent/floating macrophytes. During this time interval, P_{aq} remains largely unchanged (avg. 0.5), and suggests that submergent/floating macrophtyes were favoured slightly.

The limited change in C_{17}, C_{19} and C_{21} $\delta^{13}C_{n\text{-alkane}}$ values (avg. ~ –30.1±0.4 ‰, SD, n=6) within this interval (or from earlier times) indicates that the carbon reservoir utilized by the algal biomass was not perturbed by shifting ecological conditions (Fig. 4.7). Comparison of the C_{23} and C_{25} $\delta^{13}C_{n\text{-alkane}}$ values over this time interval suggest that these *n*-alkanes are derived from different vegetation types (Fig. 4.7). Near the beginning of hydrologic closure (12,300 cal BP) the $\delta^{13}C_{n\text{-alkane}}$ values of C_{23} (–32.4 ‰) and C_{25} are nearly equal (–31.2 ‰) (Fig. 4.7). By 10,900 cal BP, there is a ~4 ‰ difference between C_{23} (–32.8 ‰) and C_{25} (–28.6 ‰), which becomes even more pronounced (~5.5 ‰) towards the end of hydrologic closure at 8,300 cal BP (C_{23}, –33.6 ‰; C_{25}, –28.2 ‰; Fig. 4.7). Such a large difference is most unlikely to arise through natural fractionation within the same macrophyte (Hayes et al., 1990; Collister et al., 1994). Instead, it appears that C_{25} behaves like the higher chain terrestrial $\delta^{13}C_{n\text{-alkane}}$ values during the period of

hydrologic closure. We suggest that C_{25} is more closely associated with emergent/floating macrophytes than with submergent macrophytes.

During hydrologic closure, Lake Ontario dropped to the lowest water levels in its history. Low water levels created new embayments favourable to macrophyte growth, especially in the eastern portion of the lake (Thousand Island area). Emergent and floating macrophytes were likely influenced by different carbon uptake processes than submergent macrophytes. Emergent and floating macrophytes utilize atmospheric CO_2 as their carbon source. In general, higher transpiration rates are observed in emergent macrophytes when compared to terrestrial flora (Wetzel, 2001). Under increased water stressed conditions, the stomata of emergent macrophytes may close to a further extent when compared to terrestrial vegetation. This may explain why the C_{25} $\delta^{13}C_{n\text{-alkane}}$ values are even higher than terrestrial vegetation during the dry conditions associated with hydrologic closure. By comparison, submergent macrophytes use only dissolved CO_2 as their carbon substrate, and are largely unaffected by terrestrial water stress. Notably, the C_{23} $\delta^{13}C_{n\text{-alkane}}$ values, which we attribute to submergent macrophytes, remain largely unchanged during hydrologic closure (Fig. 4.7).

Proliferation of pine *(Pinus)* during the period of hydrologic closure and the emergence of hemlock *(Tsuga)* at 8,400 cal BP, as recorded at Roblin Lake (Figs. 4.1, 4.10) (Terasmae, 1980), are consistent with rising terrestrial productivity. A concomitant increase in terrestrial OM contribution to the lake during this time interval is consistent with the findings of Silliman et al. (1996), McFadden et al. (2004), (2005) and Chapter 3 (this thesis) (increasing total organic matter, C/N ratios, $\delta^{13}C_{OM}$ values and TAR). The progressive increase in C_{29} and C_{31} *n*-alkane abundances –compared to the relative constant C_{25}, C_{27} and C_{33} *n*-alkane contents during hydrologic closure (Fig. 4.6) – suggests that emergent macrophytes, pine and/or grasses were responsible for the additional terrestrial OM detritus. Nonetheless, the relative contribution of terrestrial OM ($\geq C_{25}$) to the lake remained lower than input from lacustrine productivity (C_{17}, C_{19}, C_{21}, C_{23}) (Fig. 4.6). The increase in average $\geq C_{27}$ $\delta^{13}C_{n\text{-alkane}}$ values from –31 to –30 ‰ over this time interval (Fig. 4.7) likely reflects increasing aridity during hydrologic closure (Anderson and Lewis, 2012).

4.4.4 Post hydrologic closure to present condition in Lake Ontario (8,300-3,500 cal BP)

Edwards et al. (1996) suggest that climatic conditions in southern Ontario transitioned from cold and dry to warm and dry at ~8,300 cal BP. According to Anderson and Lewis (2012), the period of maximum dryness (11,500 to 6,800 cal BP) overlapped the Holocene Thermal Maximum (HTM) (~9,400 to 5,300 cal BP). The HTM was likely brought on by long-term changes in insolation (average summer temperature increased by ~2 to 4 °C) (McFadden et al., 2005). Although the region remained dry, warmer conditions were accompanied by some increase in annual precipitation (Edwards et al., 1996; Lewis et al., 2008), which is reflected in increased abundances of moisture-loving vegetation such as hemlock, beech (*Fagus)* and maple *(Acer)* pollen (Shuman et al., 2002) (Fig. 4.10). Rising water levels associated with increased precipitation brought hydrologic closure of Lake Ontario to an end (Anderson and Lewis, 2012) (Fig. 4.9d). Oxygen-isotope records for cellulose show that, by ~6,800 cal BP, warm and dry conditions in the region were fully replaced by warm and wet conditions (Edwards et al., 1996).

From the end of hydrologic closure to ~7,000 cal BP, there is a significant increase in both ACL (24.7 to 26.0) and TAR (1.2 to 3.2) (Fig. 4.4a,b). The higher relative abundances of long-chain *n*-alkanes reflect increased transport of terrestrial OM to the lake in runoff and from drowned shorelines. By 7,033 cal BP, the relative abundance of C_{27} had increased three-fold (Fig. 4.6). Macrophyte *n*-alkane C_{23} remained an important contributor to OM, but the relative importance of algal *n*-alkanes declined (Fig. 4.6), perhaps because of macrophyte competition and/or increasing turbidity in the rising waters. An increase in the $\delta^{13}C_{n\text{-alkane}}$ values of long-chain *n*-alkanes ($\geq C_{25}$) is evident at 7,773 cal BP; their $\delta^{13}C_{n\text{-alkane}}$ values also decrease systematically with increasing chain length, from –25.1 ‰ (C_{25}) to –30.4 ‰ (C_{33}) (Table 2; Fig. 4.7). Such a pattern is characteristic of angiosperms whereas the opposite distribution is known for coniferous gymnosperms (Chikarashi and Naraoka, 2003; Smith et al., 2007). The Roblin Lake pollen record (Fig. 10) supports a decrease in spruce and pine, and their replacement by birch, lilac *(Fraxinus),* elm *(Ulmus),* maple, hickory (*Carya)* and beech (Terasmae,

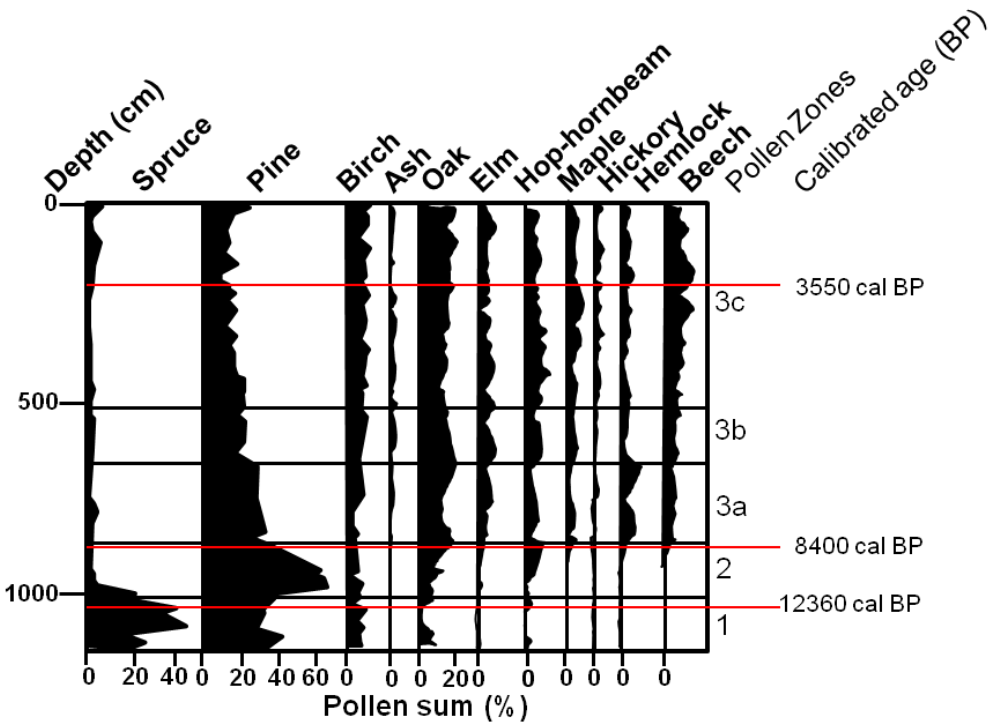

Figure 4.10. Roblin Lake pollen record, as adapted from Terasmae (1980) and re-drawn for this thesis.

1980). However, angiosperms generally have lower overall $\delta^{13}C_{n\text{-alkane}}$ values than gymnosperms, which were not observed in the Lake Ontario record. Also, a systematic increase in $\delta^{13}C_{n\text{-alkane}}$ values with increasing *n*-alkane chain length was not observed during time periods when coniferous gymnosperms dominated. Given these ambiguities, it is simplest to attribute the general increase in $\delta^{13}C_{n\text{-alkane}}$ values at 7,773 cal BP to aridity-related water stress, as discussed earlier. The differences among the long-chain *n*-alkane $\delta^{13}C_{n\text{-alkane}}$ values may be related to angiosperm development but could also reflect a mixture of terrestrial and emergent/floating macrophyte (C_{25}) OM sources.

The C_{23} $\delta^{13}C_{n\text{-alkane}}$ values remain similar to those of the short chain *n*-alkanes at this time, largely reflecting their common lacustrine DIC source, and are much lower than those of C_{25} (Fig. 4.7). However, both C_{23} and C_{25} $\delta^{13}C_{n\text{-alkane}}$ values increase by ~3 ‰ from 8,512 to 7,773 cal BP (Fig. 4.7). By comparison, there is much less change in the algal $\delta^{13}C_{n\text{-alkane}}$ values, although both C_{17} and C_{21} also reach their maximum ^{13}C-enrichments relative to the previous time interval. The cause of this behaviour remains enigmatic but perhaps arises from lacustrine habitat. Algae are most abundant in the pelagic zone, whereas submergent macrophytes are mostly located in the littoral zone. Given enhanced competition for dissolved CO_2 in the littoral zone, the submergent macrophytes (e.g., C_{23}) may have also utilized bicarbonate, which would increase their $\delta^{13}C_{n\text{-alkane}}$ values (Mook, 2000).

Peak ACL and TAR values at 7,033 cal BP (Fig. 4.4a,b) likely point to higher terrestrial productivity related to warmer and wetter conditions at this time (Smith et al., 2007). Lower ACL after 7,033 cal BP signals a progressive increase in the relative abundance of OM derived from aquatic productivity versus terrestrial detritus (Fig. 4.4a). By this time, lacustrine algae, macrophytes and terrestrial plants were sub-equal contributors to the OM preserved in Lake Ontario sediments (Fig. 4.6). When considered together with the gradual change in ACL, the sharp drop in TAR after 7,033 cal BP, and steady TAR ratio of ~1 thereafter, point to an ecosystem in which algae were once again out-competing macrophytes. This likely reflects higher water levels and stabilization of the lake water budget by the return of inflow from the upper Great Lakes. By 5,289 cal BP, the lower

Great Lakes (Erie and Ontario) were receiving water from the upper Great Lakes during the Nipissing rise (Chapter 2, this thesis; Anderson and Lewis 2012).

The decline in ACL and TAR beginning after 7,033 cal BP is preceded by a decrease in all $\delta^{13}C_{n\text{-alkane}}$ values after 7,773 cal BP (Fig. 4.7). This shift is more pronounced for C_{27} and C_{25} (3 to 5 ‰) and more subdued for other *n*-alkanes (<2 ‰). For the higher chain *n*-alkanes, the lower $\delta^{13}C_{n\text{-alkane}}$ values are likely a consequence of the regional shift to warm and wet conditions (6,800 cal BP) (Edwards et al, 1996). Increased warmth and moisture availability during the HTM after 7,773 cal BP drove a rapid change from a mixed gymnosperm (conifer) and angiosperm forest to an almost exclusively angiosperm forest (Fig. 4.9d). Smith et al. (2007) attributed such changes in $\delta^{13}C_{n\text{-alkanes}}$ values during the Paleocene-Eocene Thermal Maximum (PETM) in the Bighorn Basin, Wyoming, to such a floral community transition. Following Flanagan et al. (1997) and Chikaraishi and Naraoka (2003), Smith et al. (2007) noted that angiosperms exhibit a larger discrimination against ^{13}C than conifers growing in the same region. Warmer temperatures also likely contributed to increased discrimination against ^{13}C, albeit at a smaller scale (~ –0.15 ‰/°C; Edwards et al., 2000).

The gradual lowering of $\delta^{13}C_{n\text{-alkane}}$ values of the shorter chain *n*-alkanes, especially for C_{17}, from 7,773 to 3,583 cal BP (C_{17}–C_{23}) suggests a change in the relative contributions of different carbon sources (Fig. 4.7). An increased supply of carbon dioxide from oxidation of terrestrial OM detritus could have lowered the $\delta^{13}C$ values of the available DIC pool (Keough et al., 1998). Why the shift to lower $\delta^{13}C_{n\text{-alkane}}$ values is larger for C_{17} versus other short-chain *n*-alkanes, and more generally, why short-chain *n*-alkane isotopic compositions are variable from each other within a sample, is not fully understood. Such differences are suggestive of compound-specific carbon-isotope fractionations at the biochemical level, variations in individual short-chain *n*-alkane abundances from one aquatic species to another, and/or the timing of growth of various aquatic species; the $\delta^{13}C_{DIC}$ of modern Lake Ontario, for example, varies seasonally by up to 2 ‰ (Hodell and Schelske, 1998).

4.5 Conclusions

The *n*-alkane abundances and carbon isotopic compositions of OM in Lake Ontario sediments can be used to distinguish variations in sources from changes in lacustrine productivity when these data are interpreted in concert with information on historic lake levels, regional paleoclimatic conditions and pollen records.

During the late Pleistocene, the source of abundant C_{23} and C_{25} *n*-alkanes was likely *Sphagnum* mosses transported to the lake from the periglacial environment. Their average $\delta^{13}C_{n\text{-alkane}}$ values reflect composition of atmospheric CO_2 at that time. In addition, short-chain (algae) and long-chain (terrestrial, perhaps recycled) *n*-alkane abundances mark major OM contributions from these sources. Low bulk C/N ratios during the glacial period are likely the signature both of abundant short- and mid-chain *n*-alkanes and diagenetically altered, allochthonous terrestrial organic matter delivered to Lake Ontario. As gradual warming took hold shortly after 14,500 cal BP, a tundra woodland developed in the Lake Ontario region. The most abundant *n*-alkane (C_{23}) – and perhaps also C_{25} – in the sediments marks prolific growth of macrophytes in the lake's littoral zone, as opposed to *Sphagnum* mosses, as was earlier the case.

During hydrologic closure of Lake Ontario (12,300- 8,300 cal BP), low lake levels associated with high aridity favoured proliferation of algae and aquatic macrophytes, as indicated by the sub-equal abundances of short- and mid-chain n-alkanes (C_{17}-C_{23}). Towards the end of hydrologic closure, macrophyte production appears to have exceeded algal production. Increased contributions of terrestrial OM detritus were marked in particular by rising abundances of C_{29} and C_{31} n-alkanes, which characterize pine and/or grass. During hydrologic closure, there was little change in algal $\delta^{13}C_{n\text{-alkane}}$ values, suggesting that the lacustrine DIC reservoir was well-mixed and largely unaffected by increased biological demands from algal and submergent/floating macrophyte growth. By comparison, strong ^{13}C-enrichment of the long-chain *n*-alkanes, especially C_{25} and C_{27}, relative to C_{17}-C_{23} $\delta^{13}C_{n\text{-alkane}}$ values, provides a clear signal of dry terrestrial conditions during the period of hydrologic closure.

The time period following hydrologic closure of Lake Ontario (8,300 cal BP to the end of our record at 3,583 cal BP) was characterized first by full entry into warm and dry climatic conditions, followed by the transition to warm and wet conditions by ~6,800 cal BP. A sharp increase in the abundance of terrestrial OM, especially C_{27} n-alkanes, was likely associated with rising water levels and the drowning of vegetated shorelines. Further increases in long-chain *n*-alkane $\delta^{13}C_{n\text{-alkane}}$ values, especially C_{25} and C_{27}, up to 7,773 cal BP reflect water stress in the terrestrial environment during the warm and dry period. With the subsequent shift to warm but wet conditions, the long-chain $\delta^{13}C_{n\text{-alkane}}$ values decreased (especially C_{25} and C_{27}) largely in response to decreased water stress but perhaps also in part because of a terrestrial ecosystem shift favouring angiosperms. As lake levels stabilized at new, higher levels, the spike in C_{27} n-alkane abundance disappeared, and a nearly equal balance of OM contributions from lacustrine algae, macrophytes and terrestrial plants was established. The gradual lowering of $\delta^{13}C_{n\text{-alkane}}$ values in short-chain, algal *n*-alkanes, especially C_{17}, during this time suggests a shift in DIC composition/source(s), perhaps related to niche-specialization in the now much larger pelagic environment associated with higher lake levels.

4.6 References

Anderson, T.W., Lewis, C.F.M., 2012. A new water-level history for Lake Ontario basin: evidence for a climate-driven early Holocene lowstand. Journal of Paleolimology 47, 513–530.

Bingham, E.M., McClymont, E.L., Väliranta, M., Mauquoy, D., Roberts, Z., Chambers, F.M., Pancost, R.D., Evershed, R.P., 2010. Conservative composition of *n*-alkane biomarkers in *Sphagnum* species: Implications for palaeoclimate reconstruction in ombrotrophic peat bogs. Organic Geochemistry 41, 214–220.

Blaauw, M., 2010. Methods and code for 'classical' age-modelling of radiocarbon sequences. Quaternary Geochronology 5, 512–518.

Brincat, D., Yamada, K., Ishiwatari, R., Uemura, H., Naraoka, H., 2000. Molecular-isotopic stratigraphy of long-chain *n*-alkanes in Lake Baikal Holocene and glacial age sediments. Organic Geochemistry 31, 287–294.

Carmichael, C.M., Mothersill, J.S., Morris W.A., 1990. Paleomagnetic and pollen chronostratigraphic correlations of the late glacial and postglacial sediments in Lake Ontario. Canadian Journal of Earth Sciences 27, 131–147.

Chikaraishi, Y., Naraoka, H., 2003. Compound-specific δD–δ^{13}C analyses of *n*-alkanes extracted from terrestrial and aquatic plants. Phytochemistry 63, 361–371.

Chikaraishi, Y., Naraoka, H., 2007. δ^{13}C and δD relationships among three *n*-alkyl compound classes (*n*-alkanoic acid, *n*-alkane and *n*-alkanol) of terrestrial higher plants. Organic Geochemisty 38, 198–215.

Coakley, J.P., Karrow, P.F., 1994. Reconstruction of post-Iroquois shoreline evolution in western Lake Ontario. Canadian Journal of Earth Sciences 31, 1618–1629.

Collister, J., W., Rieley, G., Stern, B., Eglinton, G., Fry, B., 1994. Compound-specific δ^{13}C analyses of leaf lipids from plants with differing carbon dioxide metabolisms. Organic Geochemistry 21, 619–627.

Conte, M., Weber, J., Carlson, P., Flanagan, L., 2003. Molecular and carbon isotopic composition of leaf wax in vegetation and aerosols in a northern prairie ecosystem. Oecologia 135, 67–77.

Cranwell, P.A., 1973. Chain-length distribution of *n*-alkanes from lake sediments in relation to post-glacial environmental change. Freshwater Biology 3, 259–265.

Cranwell, P.A., Eglinton, G., Robinson, N., 1987. Lipids of aquatic organisms as potential contributors to lacustrine sediments—II. Organic Geochemistry 11, 513–527.

Dale, H., 1986. Temperature and light: The determining factors in maximum depth distribution of aquatic macrophytes in Ontario, Canada. Hydrobiologia 133, 73–77.

Davis, R.B., Webb III, T., 1975. The contemporary distribution of pollen in Eastern North America: A comparison with the vegetation. Quaternary Research 5, 395–434.

Edwards, T.W.D., Wolfe, B.B., MacDonald, G.M., 1996. Influence of changing atmospheric circulation on precipitation δ^{18}O–temperature relations in Canada during the Holocene. Quaternary Research 46, 211–218.

Edwards, T.W.D., Graf, W., Trimborn, P., Stichler, W., Lipp, J., Payer, H.D., 2000. δ^{13}C response surface resolves humidity and temperature signals in trees. Geochimica et Cosmochimica Acta 64, 161–167.

Eglinton, G., Hamilton, R.J., 1963. The distribution of alkanes. in: Swain, T., (Ed.), Chemical Plant Taxonomy. Academic Press, London and NewYork, pp. 187–217.

Eglinton, G., Hamilton, R.J., 1967. Leaf epicuticular waxes. Science 156, 1322–1335.

Farquhar, G.D., Ehleringer, J.R., Hubick, K.T., 1989. Carbon isotope discrimination and photosynthesis. Annual Review of Plant Physiology and Plant Molecular Biology 40, 503–537.

Ficken, K.J., Li, B., Swain, D.L., Eglinton, G., 2000. An *n*-alkane proxy for the sedimentary input of submerged/floating freshwater aquatic macrophytes. Organic Geochemistry 31, 745–749.

Flanagan, L.B., Brooks, J.R., Ehleringer, J.R., 1997. Photosynthesis and carbon isotope discrimination in boreal forest ecosystems: A comparison of functional characteristics in plants from three mature forest types. Journal of Geophysical Research 102, 28861–28869.

Gelpi, E., Schneider, H., Mann, J., Oro, J., 1970. Hydrocarbons of geochemical significance in microscopic algae. Phytochemistry 9, 603–612.

Gibson, J.A.E., Trull, T., Nichols, P.D., Summons, R.E., McMinn, A., 1999. Sedimentation of ^{13}C-rich organic matter from Antarctic sea-ice algae: A potential indicator of past sea-ice extent. Geology 27, 331–334.

Han, J., Calvin, C., 1970. Branched alkanes from blue-green algae. Journal of the Chemical Communications 1490–1491.

Hayes, J.M., 1993. Factors controlling ^{13}C contents of sedimentary organic compounds: Principles and evidence. Marine Geology 113, 111–125.

Hayes, J.M., Freeman, K.H., Popp, B.N., Hoham, C.H., 1990. Compound-specific isotopic analyses: A novel tool for reconstruction of ancient biogeochemical processes. Organic Geochemistry 16, 1115–1128.

Hecky, R.E., Hesslein, R.H., 1995. Contributions of benthic algae to lake food webs as revealed by stable isotope analysis. Journal of the North American Benthological Society 14, 631–653.

Hodell, D.A., Schelske, C.L., 1998. Sedimentation, and isotopic composition of organic matter in Lake Ontario. American Society of Limnology and Oceanography 43, 200–214.

Hornibrook, E.R., Longstaffe, F.J., Fyfe, W.S., Bloom, Y., 2000. Carbon-isotope ratios and carbon, nitrogen and sulfur abundances in flora and soil organic matter from a temperate-zone bog and marsh. Geochemical Journal 34, 237–245.

Hutchinson, D.R., Lewis, C.F., Hund, G.E., 1993. Regional stratigraphic framework of surficial sediments and bedrock beneath Lake Ontario. Géographie physique et Quaternaire 47, 337–352.

Hyodo, A., Longstaffe, F.J., 2011. The palaeoproductivity of ancient Lake Superior. Quaternary Science Reviews 30, 2988–3000.

Keough, J.R., Hagley, C.A., Ruzycki, E., Sierszen, M., 1998. $\delta^{13}C$ composition of primary producers and role of detritus in a freshwater coastal ecosystem. Limnology and Oceanography 43, 737–740.

Lewis, C.F.M., King, J.W., Blasco, S.M., Brooks, G.R., Coakley, J.P., Croley II, T.E., Dettman, D.L., Edwards, T.W.D., Heil Jr., C.W., Hubeny, J.B., Laird, K.R., McAndrews, J.H., McCarthy, F.M.G., Medioli, B.E., Moore Jr., T.C., Rea, D.K., Smith, A.J., 2008. Dry climate disconnected the Laurentian Great Lakes. EOS, Transactions American Geophysical Union 89, 541–542.

Maffei, M., Badino, S., Bossi, S., 2004. Chemotaxonomic significance of leaf wax *n*-alkanes in the Pinales (Coniferales). Journal of Biological Research 1, 3–19.

McAndrews, J.H., 1994. Pollen diagrams for southern Ontario applied to archeology, in: MacDonald, R.I. (Ed.) Great Lakes Archeology and Paleoecology: Exploring Interdisciplinary Initiatives for the Nineties. Quaternary Sciences Institute, University of Waterloo, Waterloo, pp 179–195.

McCarthy, F.M.G., Mertens, K.N., Ellegaard, M., Sherman, K., Pospelova, V., Ribeiro, S., Blasco, S., Vercauteren, D., 2011. Resting cysts of freshwater dinoflagellates in southeastern Georgian Bay (Lake Huron) as proxies of cultural eutrophication. Review of Palaeobotany and Palynology 166, 46–62.

McFadden, M.A., Mullins, H.T., Patterson, W.P., Anderson, W.T., 2004. Paleoproductivity of eastern Lake Ontario over the past 10,000 years. Limnology and Oceanography 49, 1570–1581.

McFadden, M.A., Patterson, W.P., Mullins, H.T., Anderson, W.T., 2005. Multi-proxy approach to long-and short-term Holocene climate-change: evidence from eastern Lake Ontario. Journal of Paleolimnology 33, 371–391.

Meyers, P.A., 1997. Organic geochemical proxies of paleoceanographic, paleolimnologic, and paleoclimatic processes. Organic Geochemistry 27, 213–250.

Meyers, P.A., Eadie, B.J., 1993. Sources, degradation and recycling of organic matter associated with sinking particles in Lake Michigan. Organic Geochemistry 20, 47–56.

Meyers, P.A., Ishiwatari, R., 1993. Lacustrine organic geochemistry – an overview of indicators of organic matter sources and diagenesis in lake sediments. Organic Geochemistry 20, 867–900.

Mook, W.G., 2000. Environmental Isotopes in the Hydrological Cycle: Principles and applications. Volume 1: Introduction, Theory, Methods, Review. International

Hydrological Programme IHP-V. Technical Documents in Hydrology, No. 39, UNESCO, Paris.

Nakai, S., Inoue, Y., Hosomi, M., Murakami, A., 1999. Growth inhibition of blue-green algae by allelopathic effects of macrophytes. Water Science Technology 39, 47–53.

National Oceanic and Atmospheric Administration Digital Elevation Model (DEM) Discovery Portal website (2014). Retrieved June 2, 2014 from http://ngdc.noaa.gov/mgg/dem

O'Leary, M.H., 1988. Carbon isotopes in photosynthesis. Bioscience 38, 328–336.

O'Leary, M.H., 1993. Biochemical basis of carbon isotope fractionation, in: Ehleringer, J.R., Hall, A.E., Farquhar, G.D., (Eds.), Stable isotopes and plant carbon-water relations. Academic Press, San Diego, California, USA, pp.19–26.

Pippert, R.G., Brown, G.R., Morris, W.A., 1996. Palaeomagnetic chronostratigraphy of Holocene sediments, Niagara basin, Lake Ontario, Canada. Journal of Quaternary Science 11, 217–231.

Rieley, G., Collier, R.J., Jones, D.M., Eglinton, G., Eakin, P.A., Fallick, A.E., 1991. Sources of sedimentary lipids deduced from stable carbon-isotope analyses of individual compounds. Nature 352, 425–427.

Reimer, P.J., Baillie, M.G.L., Bard, E., Bayliss, A., Beck, J.W., Blackwell, P.G., Bronk Ramsey, C., Buck, C.E., Burr, G.S., Edwards, R.L., Friedrich, M., Grootes, P.M., Guilderson, T.P., Hajdas, I., Heaton, T.J., Hogg, A.G., Hughen, K.A., Kaiser, K.F., Kromer, B., McCormac, F.G., Manning, S.W., Reimer, R.W., Richards, D.A., Southon, J.R., Talamo, S., Turney, C.S.M., van der Plicht, J., Weyhenmeyer, C.E., 2009. IntCal09 and Marine09 radiocarbon age calibration Curves, 0–50,000 Years cal BP. Radiocarbon 51, 1111–1150.

Sachse, D., Radke, J., Gleixner, G., 2004. Hydrogen isotope ratios of recent lacustrine sedimentary n-alkanes record modern climate variability. Geochimica et Cosmochimica Acta 68, 4877–4889.

Schwark, L., Zink, K., Lechterbeck, J., 2002. Reconstruction of postglacial to early Holocene vegetation history in terrestrial Central Europe via cuticular lipid biomarkers and pollen records from lake sediments. Geology 30, 463–466.

Schmitt, J., Schneider, R., Elsig, J., Leuenberger, D., Lourantou, A., Chappellaz, J., Kohler, P., Joos, F., Stocker, T.F., Leuenberger, M., Fischer, H., 2012. Carbon Isotope Constraints on the Deglacial CO2 Rise from Ice Cores. Science 336, 711–714.

Schouten, S., Klein Breteler, W., Blokker, P., Schogt, N., Rijpstra, W.I.C., Grice, K., Baas, M., Sinninghe Damsté, J.S., 1998. Biosynthetic effects on the stable carbon

isotopic compositions of algal lipids: Implications for deciphering the carbon isotopic biomarker record. Geochimica et Cosmochimica Acta 62, 1397–1406.

Schroeder, R.A., Bada, J.L., 1978. Aspartic acid racemization in Late Wisconsin Lake Ontario sediments. Quaternary Research 9, 193–204.

Shuman, B., Bartlein, P., Logar, N., Newby, P., Webb, T., 2002. Parallel climate and vegetation responses to the early Holocene collapse of the Laurentide Ice Sheet. Quaternary Science Reviews 21, 1793–1805.

Sifeddine, A., Meyers, P.A., Cordeiro, R.C., Albuquerque, A.L.S., Bernardes, M., Turcq, B., Abrão, J.J., 2011. Delivery and deposition of organic matter in surface sediments of Lagoa do Caçó (Brazil). Journal of Paleolimology 45, 385–396.

Silliman, J.E., Meyers, P.A., Bourbonniere, R.A., 1996. Record of postglacial organic matter delivery and burial in sediments of Lake Ontario. Organic Geochemistry 24, 463–472.

Smith, F., Wing, S., Freeman, K., 2007. Magnitude of the carbon isotope excursion at the Paleocene–Eocene thermal maximum: The role of plant community change. Earth Planetary Science Letters 262, 50–65.

Spear, R.W., 1989. Late-Quaternary history of high-elevation vegetation in the White Mountains of New Hampshire. Ecological Monographs 125–151.

Stevenson, B.A., Kelly, E.F., McDonald, E.V., Busacca, A.J., 2005. The stable carbon isotope composition of soil organic carbon and pedogenic carbonates along a bioclimatic gradient in the Palouse region, Washington State, USA. Geoderma 124, 37–47.

Sun, Q., Xie, M., Shi, L., Zhang, Z., Lin, Y., Shang, W., Wang, K., Li, W., Liu, J., Chu, G., 2013. Alkanes, compound-specific carbon isotope measures and climate variation during the last millennium from varved sediments of Lake Xiaolongwan, northeast China. Journal of Paleolimnology 50, 331–344.

Terasmae, J., 1980. Some problems of Late Wisconsin history and geochronology in southeastern Ontario. Canadian Journal of Earth Sciences 17, 361–381.

Wetzel, R., G., 2001. Limnology Lake and River Ecosystems, 3rd ed. Academic Press, London, England.

Chapter 5

5 Conclusions

This thesis investigated the late Quaternary paleolimnology of Lake Ontario and its precursors. Many ideas have been presented aimed at filling voids in our understanding of ancestral Lake Ontario, the signals of regional climatic and environmental change contained in its sediments, and the putative connection of Lake Ontario – and the Great Lakes more broadly – to early to mid Holocene global climate change. This chapter summarizes and discusses the broader implications of the results presented in this thesis, and offers some suggestions for new avenues of research.

5.1 Meltwater routing through the Great Lakes

The timing and extent of glacial meltwater input to ancestral Lake Ontario was assessed in this thesis using the oxygen-isotope composition of ostracode valves and clam shells. The goal was to determine the extent of glacial meltwater routing through ancestral Lake Ontario and to suggest whether the quantity of glacial meltwater was sufficient to perturb THC in the Atlantic Ocean.

The results suggest that the final stage of freshwater impounded by the LIS was an extensive confluent water body comprising Lake Trenton in the Ontario basin, Lake Vermont in the Lake Champlain valley, and Lake Candona in the St. Lawrence and Ottawa river valleys. Standing about 15 m above sea level drainage of these lakes would likely have been rapid and catastrophic once the ice dam in the lower St. Lawrence River valley was breached at about 13,000 cal [11,100 ^{14}C] BP (Richard and Occhietti, 2005; Rayburn et al., 2011). This large freshwater outflow to the Gulf of St. Lawrence and beyond is a prime candidate as a contributing factor for perturbation of THC/MOC in the Atlantic Ocean, provided the waters were adequately distributed to areas of oceanic convection. An extension of the Atlantic Ocean, the Champlain Sea, rapidly replaced the foregoing freshwater impoundment, except for the Ontario basin.

While glacial meltwater was present in ancestral Lake Ontario from ~13,000 to 12,500 cal [11,100 to 10,500 ^{14}C] BP, its presence was not recorded for the complete duration of

this time period in the neighbouring Champlain Sea. Thus, the volume was insufficient to trigger a change in THC/MOC, if indeed any of this water reached the Atlantic Ocean. Rather, it seems that ponding of glacial meltwater that entered Early Lake Ontario at this time simply filled the basin to slightly higher levels and increased the freshwater outflow from the basin, providing the forcing that resisted and prevented inflow of Champlain Sea water. The discovery of a continuous sequence of benthic ostracodes of the *C. subtriangulata* species which is intolerant of dissolved solids > 92 mg/L provides definite evidence that sea water in significant amounts did not enter the bottom waters of Early Lake Ontario (Delorme, 1978).

A comparison of the Lake Ontario sediment records reported here with global climate records (e.g. Greenland ice cores, speleothem records) produced equivocal results. This effort was made in order to evaluate how the Great Lakes – Lake Ontario in particular – responded to global climate perturbations, on one hand, and affected global climate on the other hand. It is common to compare regional (and sometimes local) climate records from lake sediments with larger climate records across continents. Connections on these scales are often broad. Local and regional climate signals preserved in the lake sediments can be dampened in this interpretive process. While some possible connections between meltwater influx into Lake Ontario and GISP2 could be suggested from the oxygen isotopic records, the most useful information reported in Chapter 2 lay in smaller isotopic fluctuations that characterized regional rather than global climate change. It is important to take into consideration the size of the Great Lakes watershed and the many factors that can influence change in this lacustrine system. Once the complete hydrologic history – including robust chronological control since the latest Pleistocene – for each Great Lake is fully understood and then integrated as a whole across this freshwater system, attempts to make connections to global climate variations are likely to be more successful.

Although the origin of glacial meltwater entering ancestral Lake Ontario from ~13,000 to 12,500 cal [11,100-10,500 ^{14}C] BP cannot be ascertained using the oxygen-isotope compositions of shelly fauna, I should comment further on the possible routing of meltwater from glacial Lake Agassiz. Without evidence for eastern drainage to Lake Superior (Voytek et al., 2012), southern drainage to the Gulf of Mexico (Broecker et al.,

1989; Williams et al., 2010) and apart from a theoretical drought lowstand with no drainage (Lowell et al., 2013), two possible routing pathways remain: (i) a northwestern outlet to the Arctic Ocean (Murton et al., 2010; Fahl and Stein, 2012), and/or (ii) subglacial drainage elsewhere along the LIS margin. Although Fisher and Lowell (2012) hypothesized that there was no connectivity between glacial Lake Agassiz and the Clearwater-Athabasca drainage divide (which would have been necessary for a northwest passage), there is some geomorphological evidence in the northwest that suggests drainage of a sizeable amount of water (Teller et al., 2005; Murton et al., 2010). Saying that, glacial meltwater entering the Arctic Ocean via this route should be recorded further downstream in the Fram Strait as a result of the Beaufort Gyre. Evidence from radiogenic isotopes and ice rafted debris located in these distal locations support a meltwater drainage hypothesis via a northwest outlet (Hillaire-Marcel et al., 2013). Perhaps glacial Lake Agassiz drained subglacially and left no geomorphological evidence of water movement. Subglacial routing of meltwater to the Arctic Ocean would also have produced a glacial meltwater signal in a variety of proxies. There is still much debate and a lack of overwhelming evidence in support of one hypothesis versus another for glacial Lake Agassiz drainage. However, I believe that ocean records, such as those reported by Lewis et al. (2012) and Hillaire-Marcel et al. (2013), may prove to be our best option when searching for the dominant meltwater drainage pathway and that our answer to glacial Lake Agassiz outflow is unlikely to be found in Great Lakes sediments. Nonetheless, outflows from deglacial impoundments in the Laurentian Great Lakes drainage system have been substantial and should be assessed further.

5.2 Organic matter sources and primary productivity in Lake Ontario

Deconvoluting changing lacustrine productivity from mixing of multiple terrestrial and aquatic sources using bulk OM proxies has proven to be a problem in Lake Ontario sediments. Complexity arises because of the low abundances of total OM, the absence of visible OM, and the overlapping carbon-isotope compositions of terrestrial OM sources and aquatic algae. Low abundances of OM and the absence of visible OM made it difficult to reach unambiguous conclusions based on bulk isotopic measurements. It is

also difficult to ascertain the fate of the majority of terrestrial vegetation scraped away during glacial processes. In particular, there seems to be a paucity of OM deposition and/or poor OM preservation within sediments from the deepest portions of the Great Lakes (Fritz et al., 1975; Silliman et al., 1996; McFadden et al., 2004; 2005; Hyodo and Longstaffe, 2011; Chapter 3, this thesis). In the absence of visible OM and contradictory results from bulk OM proxies in Lake Ontario sediments during glacial periods, more unusual sources for the OM need to be considered. One possibility is that most of the OM recorded in Great Lakes glacial sediments was highly degraded, and carried there sorbed on soil clay minerals. Testing this hypothesis is an important subject for future work.

Because of Lake Ontario's well-known hydrologic history (Anderson and Lewis, 2012), it was easier to discriminate between changes in OM sources and varying lacustrine productivity during post-glacial periods – especially during hydrologic closure. Echoing the words of Lewis et al. (2011), this episode of hydraulic closure and coincidental Holocene warming "will provide new evidence of climate-hydrology sensitivity, and add confidence to modeled projections of future lake conditions". The onset of hydraulic closure was part of a continental-scale shift in atmospheric (jet stream) circulation and climate zones, owing to the residual presence of the LIS (Shuman et al., 2002). What this period of hydraulic closure does provide is an example of the sensitivity of even a large lake such as Lake Ontario to climates different than present.

The abundances and compound-specific carbon-isotope compositions of *n*-alkanes, complemented by pollen records from McAndrews (1994) and Terasmae (1980), has provided a better understanding of lacustrine paleoproductivity and source changes affecting ancestral Lake Ontario. The *n*-alkane data suggest that OM in the glacial sediments likely arose from *Sphagnum* moss production, transported along with other detritus to Lake Ontario by the LIS. In the absence of glacial deposition, a high proportion of Lake Ontario's OM consisted of aquatic macrophytes. In addition, during hydrologic closure – a period during which one might expect increased aquatic algal production – the *n*-alkane record shows only a modest enrichment in ^{13}C that can be associated with increased algal production. More generally, unambiguous trends in the

carbon isotopic composition of OM related to aquatic productivity, commonly described in studies of other lacustrine systems (e.g., Meyers and Ishiwatari, 1993; Meyers, 1994; Meyers, 1997), have proven difficult to identify in these Lake Ontario sediments.

Perhaps the most fascinating story concerning OM source inputs arises from the terrestrial vegetation preserved in these Lake Ontario sediments. Terrestrial *n*-alkanes entering Lake Ontario are characterized by increasing ^{13}C-enrichment during periods of drought (water stress under cold/dry and warm/dry climatic conditions). Upon establishment of wetter climatic conditions, the carbon-isotope compositions of *n*-alkanes most characteristic of terrestrial vegetation decrease almost immediately. This signal may prove useful for identifying aridity and drought in other regions in the past.

5.3 Concluding remarks and future directions

Interpretation of paleolimnological data relies on a multi-proxy approach. As apparent throughout this thesis, confounding results can arise when using only a single proxy for an environmental parameter. A clearer view of how lakes change under varying environmental parameters requires the use of multiple proxies within a tightly defined chronology.

Within this conceptual framework, I suggest several immediate directions for future research:

- For the Lake Ontario sediments, and indeed those from the other Great Lakes, it is important to establish a secure chronology not solely based on limited radiocarbon dating and stratigraphic information. Additional approaches could include paleosecular variation (PSV), natural-, remnant- and inherent-magnetism, pollen, and U/Th disequilibrium dating of shelly fauna. Compound-specific ^{14}C-dating of *n*-alkanes and other biomolecules could also be attempted to establish the age of OM preserved in these sediments. A robust chronology is needed before further efforts to draw connections between the Great Lakes region and global climate records are made.

- The final glacial lake impounded by the LIS, including Lake Trenton in the Ontario basin, released a large volume of freshwater to the Gulf of St. Lawrence with break-up of the LIS ice dam across the lower St. Lawrence River valley. This drainage occurred about 13,000 cal BP and was replaced by marine water to form the Champlain Sea (Richard and Occhietti, 2005, Rayburn et al., 2011). The downstream effects of this catastrophic freshwater discharge should be evaluated as possibly contributing to the onset of suppression of Atlantic THC/MOC and the Younger Dryas cold event.

- The nature of glacial meltwater delivery to ancestral Lake Ontario after ~13,000 cal [11,100 ^{14}C] BP should be investigated further. Oxygen-isotope records of shelly fauna from piston cores of lakes in the Fenelon Falls region could provide important information concerning the pathways and volume of glacial meltwater transported to Lake Ontario.

- The hydrogen isotopic compositions of *n*-alkanes could provide insight into the isotopic composition of the water involved in their biosynthesis. For the Lake Ontario system, this should provide an opportunity to confirm glacial meltwater involvement in aquatic vegetation, to test for extreme evaporation in lacustrine water bodies, and to identify water stress in terrestrial vegetation.

- The composition (macromolecular, chemical, isotopic) of OM associated with glacial and post-glacial clay minerals contained in Lake Ontario sediments should be determined, and compared with the results obtained for the whole sediment. Comparison with appropriate soil clays from tills and related glacial deposits should also be made. Further afield, one might also examine sediments found in the Orca basin of the Gulf of Mexico. Williams et al. (2012) used clay mineralogy to suggest that these sediments originated in the Great Lakes region, and were transported southward by meltwater routed through the Mississippi River. Isotopic examination of these clays and the OM they retain could provide a more robust test of this idea.

- Macrophytes represent a significant category of aquatic plants that played a large role in the OM history of the Lake Ontario sediments described here. A systematic study of the *n*-alkane compositions and carbon- and hydrogen-isotope compositions of individual *n*-alkanes from submergent, floating and emergent macrophytes would provide a much firmer baseline for paleolimnological interpretation of such data.

5.4 References

Anderson, T.W., Lewis, C.F.M., 2012. A new water-level history for Lake Ontario basin: evidence for a climate-driven early Holocene lowstand. Journal of Paleolimnology 47, 513–530.

Broecker, W.S., Kennett, J.P., Flower, B.P., Teller, J.T., Trumbore, S., Bonani, G., Wolfli, W., 1989. Routing of meltwater from the Laurentide Ice Sheet during the Younger Dryas cold episode. Nature 341, 318–321.

Cronin, T.M., Rayburn, J.A., Guilbault, J.-P., Thunell, R., Franzi, D.A., 2012. Stable isotope evidence for glacial lake drainage through the St. Lawrence Estuary, eastern Canada, ~13.1–12.9 ka. Quaternary International 260, 55-65.

Delorme, L.D., 1978. Distribution of freshwater ostracodes in Lake Erie. Journal of Great Lakes Research 4, 216–220.

Fahl, K., Stein, R., 2012. Modern seasonal variability and deglacial/Holocene change of central Arctic Ocean sea-ice cover: New insights from biomarker proxy records. Earth and Planetary Science Letters 351-352, 123–133.

Fisher, T.G., Lowell, T.V., 2012. Testing northwest drainage from Lake Agassiz using extant ice margin and strandline data. Quaternary International 260, 106–114.

Fritz, P., Anderson, T.W., Lewis, C.F.M., 1975. Late-Quaternary climatic trends in history of Lake Erie from stable isotope studies. Science 190, 267–269.

Hillaire-Marcel, C., Maccali, J., Not, C., Poirier, A., 2013. Geochemical and isotopic tracers of Arctic sea ice sources and export with special attention to the Younger Dryas interval. Quaternary Science Reviews 79, 184–190.

Hyodo, A., Longstaffe, F.J., 2011. The palaeoproductivity of ancient Lake Superior. Quaternary Science Reviews 30, 2988–3000.

Lewis, C.F.M., Rea, D.K., Hubeny, J.B., Thompson, T.A., Blasco, S.M., King, J.W., Reddin, M., Moore, T.C., 2010. Using geological history of the Laurentian Great Lakes to better understand their future. Aquatic Ecosystem Health & Management 13, 118–126.

Lewis, C.F.M., Miller, A.A.L., Levac, E., Piper, D.J.W., Sonnichsen, G.V., 2012. Lake Agassiz outburst age and routing by Labrador Current and the 8.2 cal ka cold event. Quaternary International 260, 83–97.

Lowell, T.V., Applegate, P.J., Fisher, T.G., Lepper, K., 2013. What caused the low-water phase of glacial Lake Agassiz? Quaternary Research 80, 370–382.

McAndrews, J.H., 1994. Pollen diagrams for southern Ontario applied to archeology, in: MacDonald, R.I. (Ed.) Great Lakes Archeology and Paleoecology: Exploring Interdisciplinary Initiatives for the Nineties. Quaternary Sciences Institute, University of Waterloo, Waterloo, pp 179–195.

McFadden, M.A., Mullins, H.T., Patterson, W.P., Anderson, W.T., 2004. Paleoproductivity of eastern Lake Ontario over the past 10,000 years. Limnology and Oceanography 49, 1570–1581.

McFadden, M.A., Patterson, W.P., Mullins, H.T., Anderson, W.T., 2005. Multi-proxy approach to long-and short-term Holocene climate-change: evidence from eastern Lake Ontario. Journal of Paleolimnology 33, 371–391.

Meyers, P.A., 1994. Preservation of elemental and isotopic source identification of sedimentary organic matter. Chemical Geology 114, 289–302.

Meyers, P.A., 1997. Organic geochemical proxies of paleoceanographic, paleolimnologic, and paleoclimatic processes. Organic Geochemistry 27, 213–250.

Meyers, P.A., Ishiwatari, R., 1993. Lacustrine organic geochemistry–an overview of indicators of organic matter sources and diagenesis in lake sediments. Organic Geochemistry 20, 867–900.

Murton, J.B., Bateman, M.D., Dallimore, S.R., Teller, J.T., Yang, Z., 2010. Identification of Younger Dryas outburst flood path from Lake Agassiz to the Arctic Ocean. Nature 464, 740–743.

Rayburn, J.A., Cronin, T.M., Franzi, D.A., Knuepfer, P.L.K., Willard, D.A., 2011. Timing and duration of North American glacial lake discharges and the Younger Dryas climate reversal. Quaternary Research 75, 541–551.

Richard, P.J.H., Occhietti, S., 2005. ^{14}C chronology for ice retreat and inception of Champlain Sea in the St. Lawrence Lowlands, Canada. Quaternary Research 63, 353–358.

Shuman, B., Bartlein, P., Logar, N., Newby, P., Webb, T., 2002. Parallel climate and vegetation responses to the early Holocene collapse of the Laurentide Ice Sheet. Quaternary Science Reviews 21, 1793–1805.

Silliman, J.E., Meyers, P.A., Bourbonniere, R.A., 1996. Record of postglacial organic matter delivery and burial in sediments of Lake Ontario. Organic Geochemistry 24, 463–472.

Teller, J.T., Boyd, M., Yang, Z., Kor, P.S.G., Mokhtari Fard, A., 2005. Alternative routing of Lake Agassiz overflow during the Younger Dryas: new dates, paleotopography, and a re-evaluation. Quaternary Science Reviews 24, 1890–1905.

Terasmae, J., 1980. Some problems of Late Wisconsin history and geochronology in southeastern Ontario. Canadian Journal of Earth Sciences 17, 361–381.

Voytek, E.B., Colman, S.M., Wattrus, N.J., Gary, J.L., Lewis, C.F.M., 2012. Thunder Bay, Ontario, was not a pathway for catastrophic floods from Glacial Lake Agassiz. Quaternary International 260, 98–105.

Williams, C., Flower, B.P., Hastings, D.W., Guilderson, T.P., Quinn, K.A., Goddard, E.A., 2010. Deglacial abrupt climate change in the Atlantic Warm Pool: A Gulf of Mexico perspective. Paleoceanography 25, PA4221.

Williams, C., Flower, B.P., Hastings, D.W., Brown, E., Lowell, T.V., Shevenell, A., 2012. Deglacial meltwater input to Gulf of Mexico: A marine-based record for Laurentide Ice Sheet chronology. Geological Society of American fall meeting, Charlotte, N.C., Nov. 4–7.

Appendices

Appendix I provides digital images of each core (Core 1334; Niagara basin, Core 1335; Mississauga basin, and Core 1336; Rochester basin), divided into ~1 m intervals. Core descriptions include general commentary, grain-size measurements, Munsell Soil Colour Charts (2000) classifications and correlations to other studies (Hutchinson et al., 1993; Pippert et al., 1996).

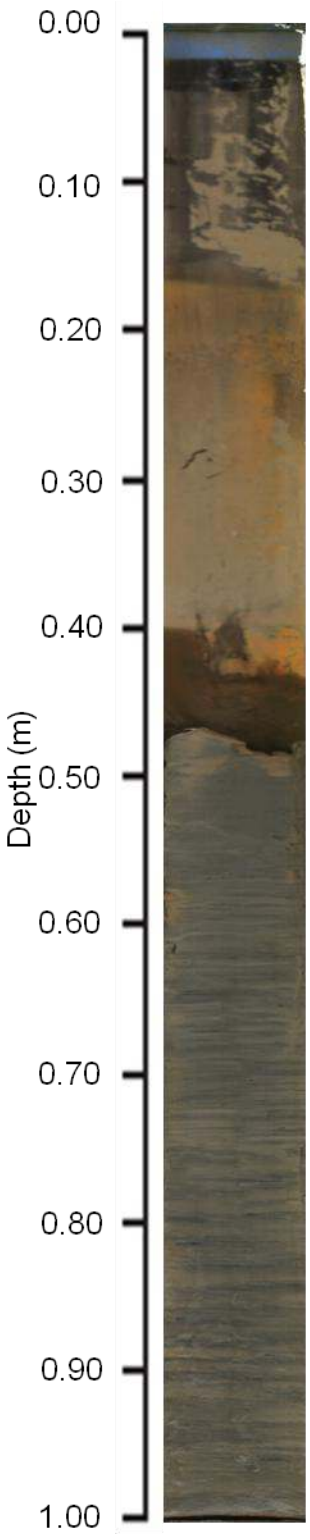

Core 1334: 0.00-1.00 m

- No sediment from 0.00 to 0.48 m
- Some oxidized iron sulfide, yellowish red (5Y 5/8)
- Massive, dark grayish brown (10YR 4/2) throughout section
- Unit E (Hutchinson et al., 1993), Unit 1 (Pippert et al., 1996)

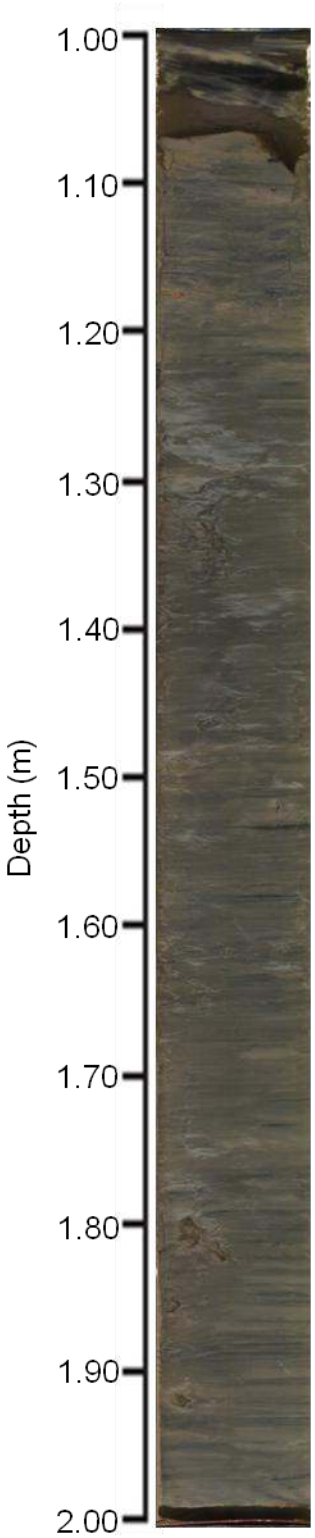

Core 1334: 1.00-2.00 m

- No sediment from 1.00 to 1.07 m
- Very watery
- Some oxidized iron sulfide, yellowish red (5Y 5/8)
- Massive, dark grayish brown (10YR 4/2) throughout section
- Grain size at 1.205 m (diameter 50 %) is 8.23 μm
- Unit E (Hutchinson et al., 1993), Unit 1 (Pippert et al., 1996)

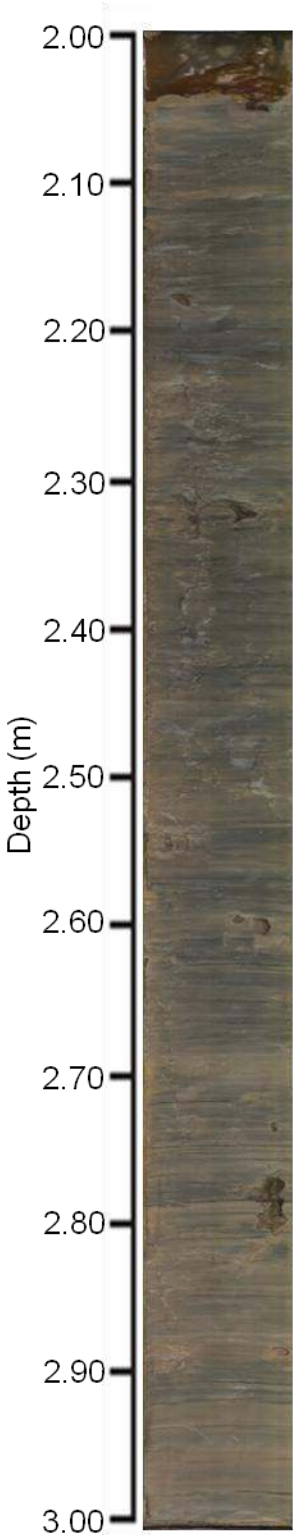

Core 1334: 2.00-3.00 m

- No sediment from 2.00 to 2.04 m
- Very watery
- Iron sulfide, yellowish red (5Y 5/8)
- Black banding millimeters in size throughout section
- Massive, dark grayish brown (10YR 4/2) throughout section
- Grain size at 2.105 m (diameter 50 %) is 6.67 μm
- Unit E (Hutchinson et al., 1993), Unit 1 (Pippert et al., 1996)

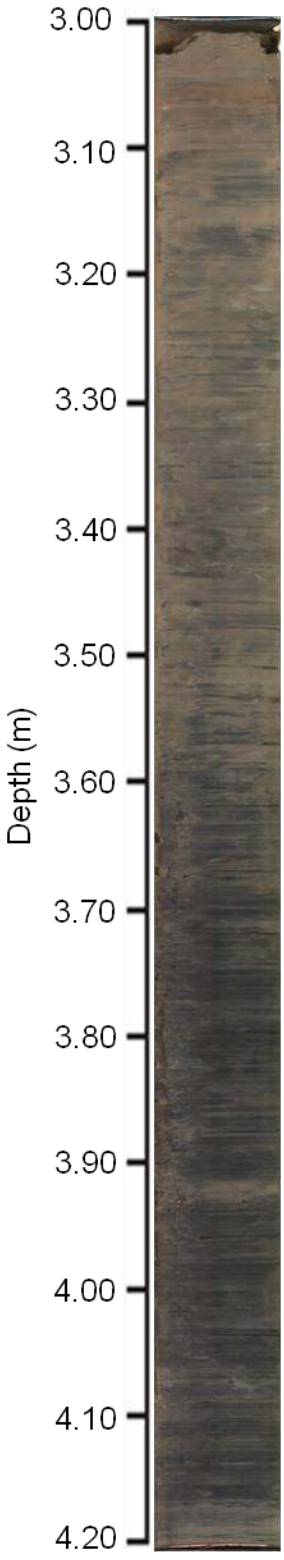

Core 1334: 3.00-4.21 m

- Abundance of iron sulfide, black
- Black banding millimeters to centimeters in size throughout section
- Massive, dark grayish brown (10YR 4/2) throughout section
- Some oxidized iron sulfide spheres, yellowish red (5Y 5/8)
- Grain size at 3.105 m (diameter 50 %) is 5.13 μm
- Unit E (Hutchinson et al., 1993), Unit 1 (Pippert et al., 1996)

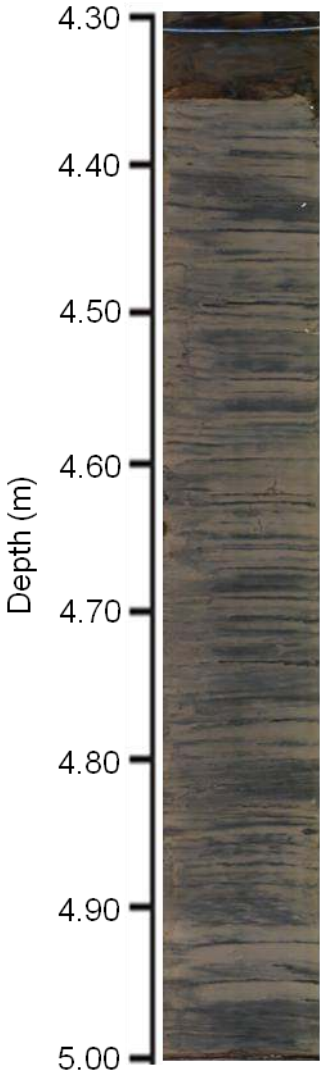

Core 1334: 4.34-5.00 m

- No sediment from 4.00 to 4.04 m
- Exposed shelly material
- Oxidized iron sulfide banding millimeters to centimeters in size, yellowish red (5Y 5/8), most likely black, reduced upon core splitting
- Massive, dark grayish brown (10YR 4/2) throughout section
- Grain size at 4.505 m (diameter 50 %) is 7.20 μm
- Unit E (Hutchinson et al., 1993), Unit 1 (Pippert et al., 1996)

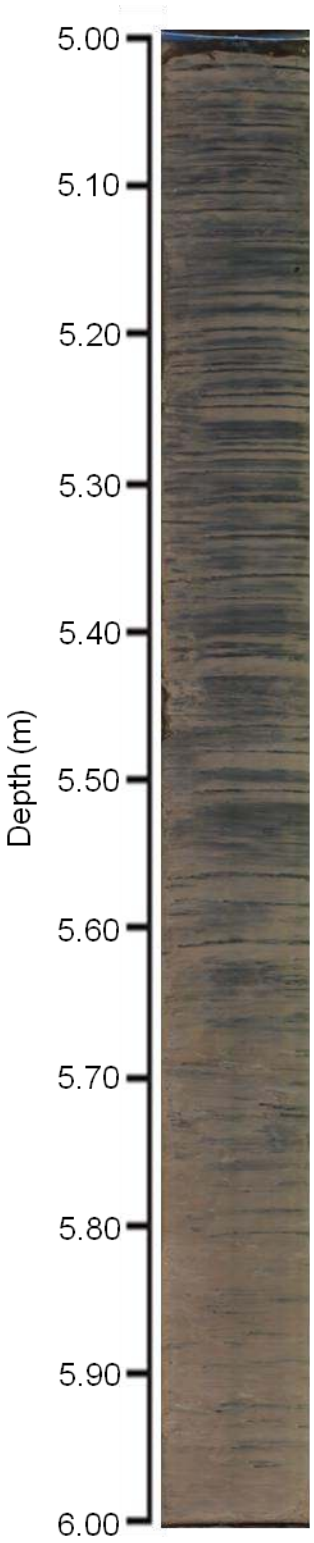

Core 1334: 5.00-6.00 m

- Exposed shelly material
- Oxidized iron sulfide banding millimeters to centimeters in size, yellowish red (5Y 5/8), most likely black, reduced upon core splitting
- Massive, dark grayish brown (10YR 4/2) throughout section
- Bottom of the core section (5.80-6.00 m) looks denser than the top
- Grain size at 5.315 m (diameter 50 %) is 6.92 μm
- Unit E (Hutchinson et al., 1993), Unit 1 (Pippert et al., 1996)

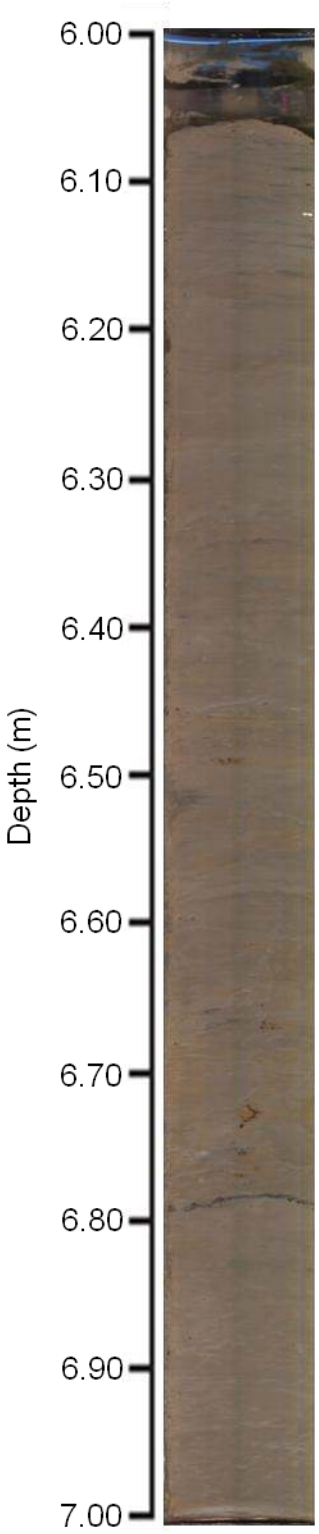

Core 1334: 6.00-7.00 m

- No sediment from 6.00 to 6.06 m
- Banding centimeters in size at 6.79 m, appears to be an increase in grain-size in banding
- Some oxidized iron sulfide at 6.75 m, yellowish red (5YR 5/8)
- Massive, dark grayish brown (10YR 4/2) throughout section
- Section is very dense with respect to the other sediment core sections
- Grain size at 6.185 m (diameter 50 %) is 6.40 μm
- Transition from Unit E (Hutchinson et al., 1993), Unit 1 (Pippert et al., 1996) at 6.75 m to Unit D (Hutchinson et al., 1993), Unit 2c? (Pippert et al., 1996)

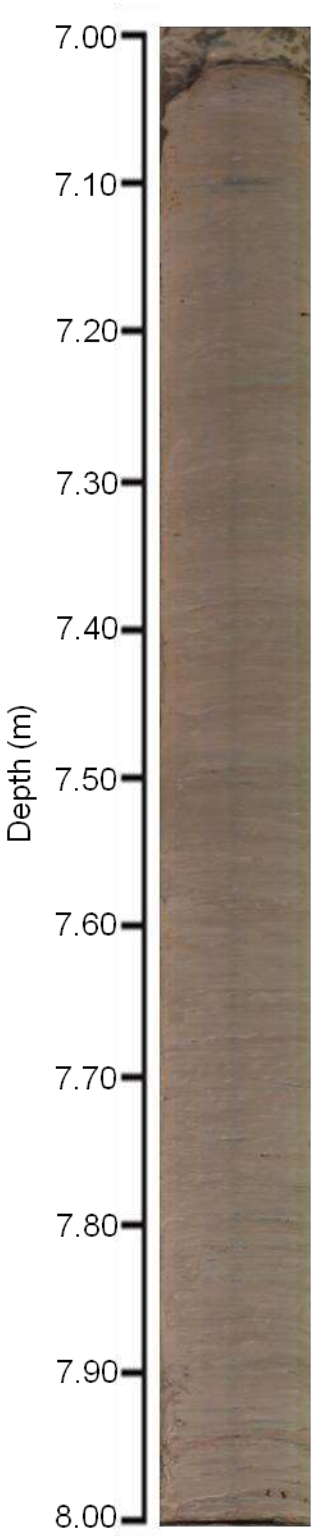

Core 1334: 7.00-8.00 m

- No sediment from 7.00 to 7.03 m
- Transition to glacial lacustrine clays
- Faint pink banding millimeters in size, difficult to classify with Munsell Color Chart
- Massive, grayish brown (10YR 5/2) throughout section
- Section is very dense
- Grain size at 7.105 m (diameter 50 %) is 8.22 μm
- Unit D? (Hutchinson et al., 1993), Unit 2c? (Pippert et al., 1996)

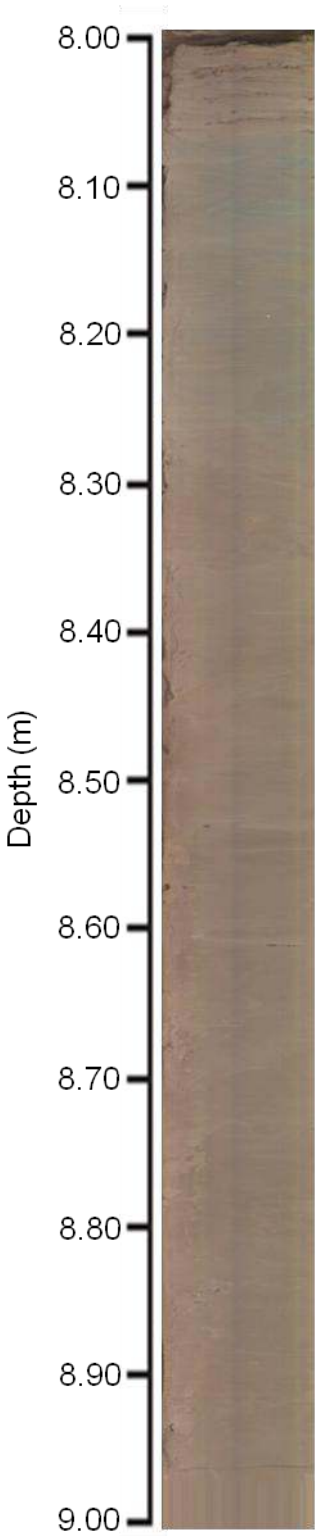

Core 1334: 8.00-9.00 m

- Faint pink banding millimeters in size, stops at 8.05 m
- Massive, grayish brown (10YR 5/2) unit between 8.06 to 8.22 m
- Weak red (2.5YR 4/2) throughout section
- Grain size at 8.105 m (diameter 50 %) is 4.77 μm
- Grain size at 8.905 m (diameter 50 %) is 9.47 μm
- Unit D? (Hutchinson et al., 1993), Unit 2b? (Pippert et al., 1996)

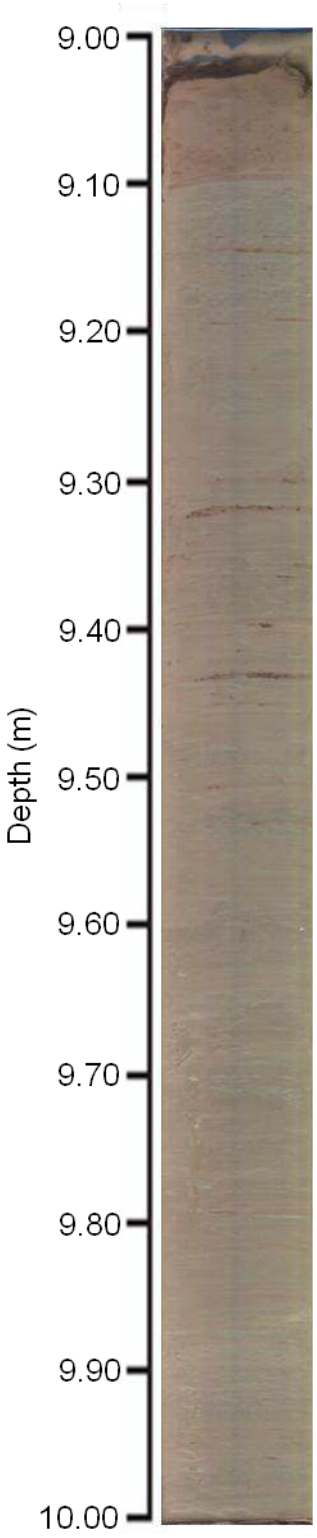

Core 1334: 9.00-10.00 m

- No sediment from 9.00 to 10.06 m
- Top of the core section, 9.06 to 9.10 m has a weak red (2.5YR 4/2) lithological unit
- Faint pink banding millimeters to centimeters in size from 9.10 to 10.00 m
- Massive, grayish brown (10YR 5/2) unit from 9.10 to 10.00 m
- Unit D? (Hutchinson et al., 1993), Unit 2b? (Pippert et al., 1996)

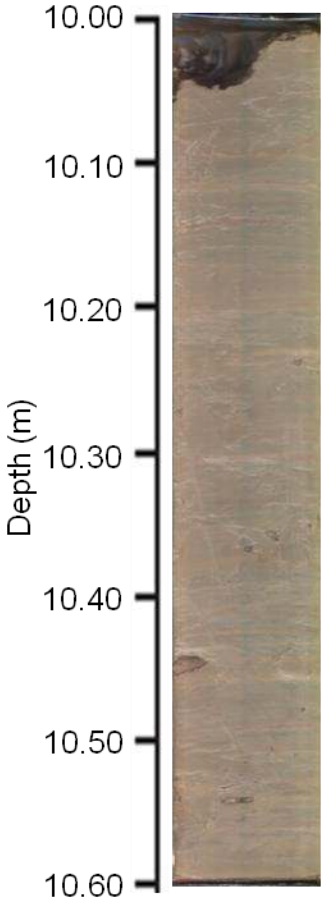

Core 1334: 10.00-10.57 m

- Faint pink banding millimeters to centimeters in size
- Massive, grayish brown (10YR 5/2) throughout section
- Grain size at 10.105 m (diameter 50 %) is 3.41 μm
- Unit D? (Hutchinson et al., 1993), Unit 2b? (Pippert et al., 1996)

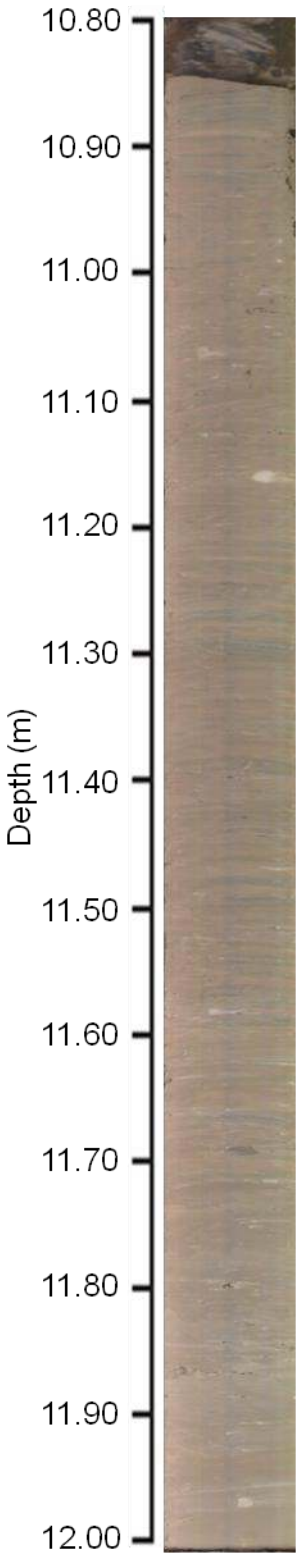

Core 1334: 10.84-12.00 m

- No sediment from 10.80 to 10.84 m
- Very pronounced centimeter size pink banding from 10.84 to 11.70 m
- Clay/silt balls throughout section, overlaps pink laminations
- Sediment is grayish brown (10YR 5/2) throughout section
- Grain size at 11.105 m (diameter 50 %) is 3.63 μm
- Transition from Unit D (Hutchinson et al., 1993), Unit 2c? (Pippert et al., 1996) to Unit C (Hutchinson et al., 1993), Unit 2a? (Pippert et al., 1996) at 10.84 m

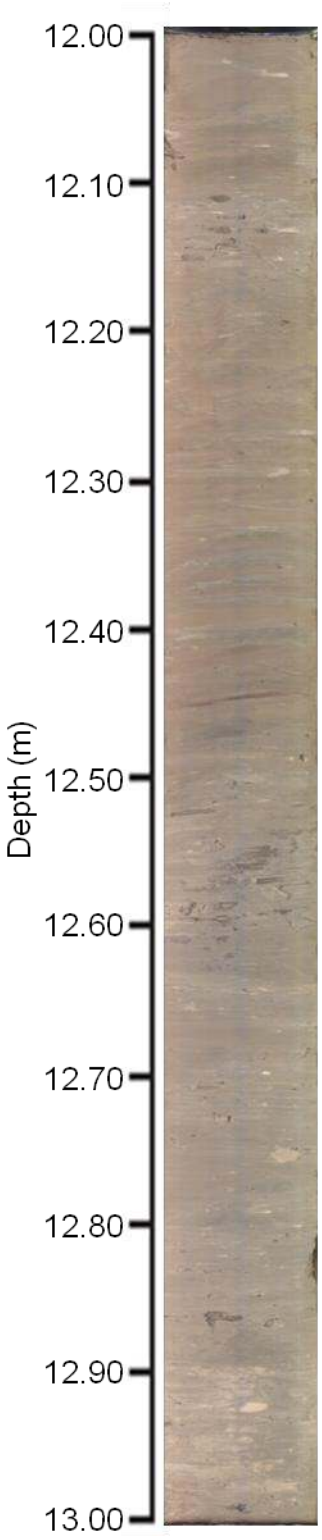

Core 1334: 12.00-13.00 m

- Gray band from 12.10 to 12.15 m
- Greater than 12.15 m sediment is grayish brown (10YR 5/2)
- Silt balls within clays
- Faint pink banding millimeters to centimeters in size from 12.15 to 12.97 m
- Coarser grained band sediment at 12.45 m
- Numerous light-gray silt balls centimeters in size
- Grain size at 12.105 m (diameter 50 %) is 3.56 μm
- Grain size at 12.395 m (diameter 50 %) is 2.95 μm
- Transition from Unit C (Hutchinson et al., 1993), Unit 2a? (Pippert et al., 1996) to Unit D (Hutchinson et al., 1993), Unit 3 (Pippert et al., 1996) at 12.97 m

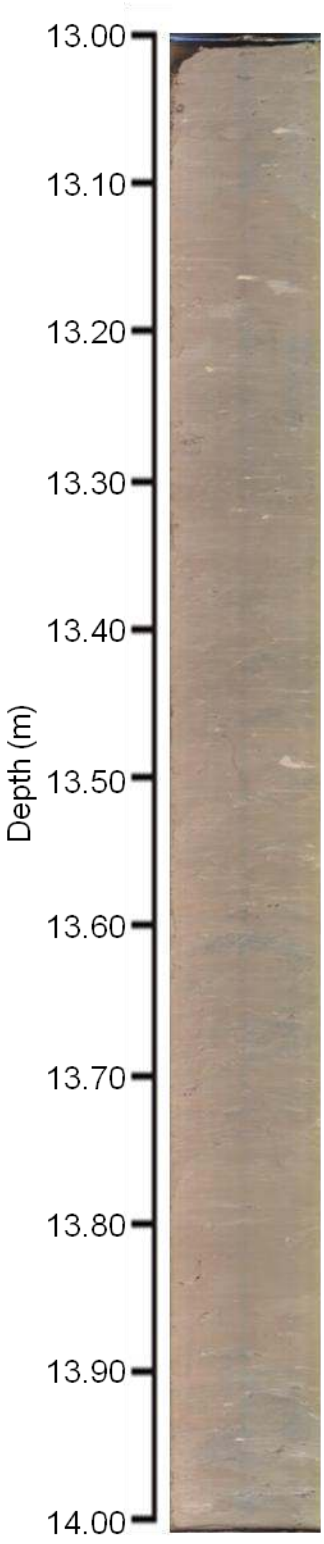

Core 1334: 13.00-14.00 m

- Mainly featureless sediment
- Massive, grayish brown (10YR 5/2) sediment throughout
- Some silt balls, light-gray in colour
- Decrease in pink banding frequency, almost none
- Grain size at 13.505 m (diameter 50 %) is 2.86 μm
- Unit D (Hutchinson et al., 1993), Unit 3 (Pippert et al., 1996)

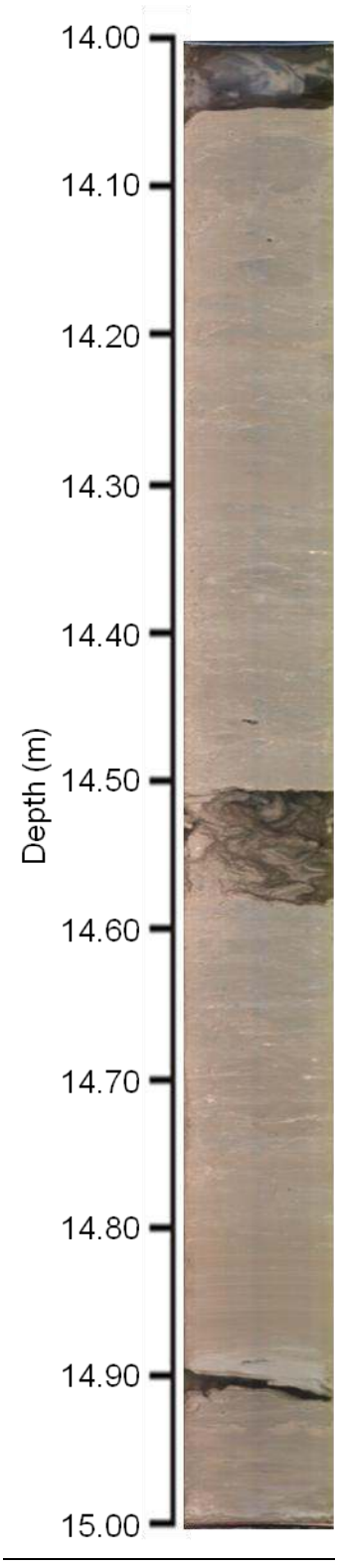

Core 1334: 14.00-15.00 m

- No sediment from 14.00 to 14.04 m and void from 14.88 to 14.90 m
- Mainly featureless sediment
- Massive, grayish brown (10YR 5/2) sediment throughout
- Some silt balls, light-gray in colour
- Grain size at 14.195 m (diameter 50 %) is 2.85 μm
- Unit D (Hutchinson et al., 1993), Unit 3 (Pippert et al., 1996)

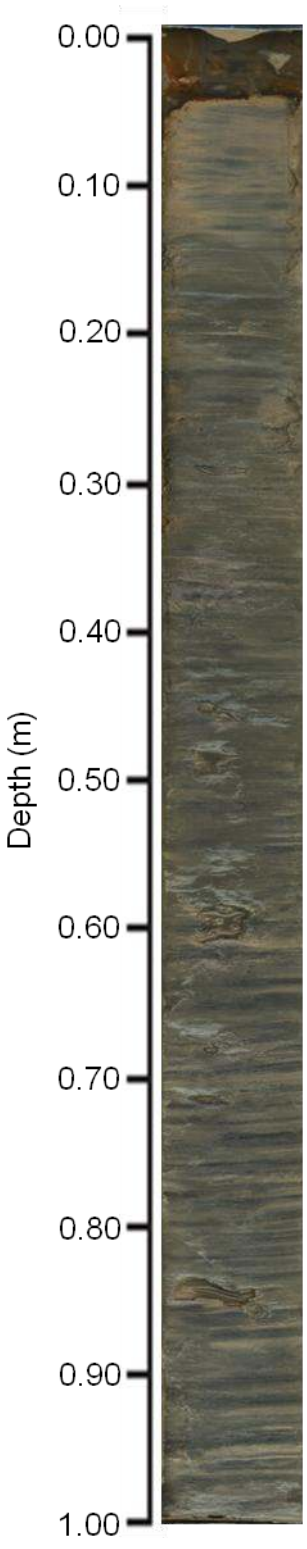

Core 1335: 0.00-1.00 m

- No sediment from 0.00 to 0.05 m
- Oxidized iron sulfide, yellowish red (5Y 5/8)
- Massive, dark grayish brown (10YR 4/2) throughout section
- Very watery
- Grain size at 0.505 m (diameter 50 %) is 9.47 μm
- Unit E (Hutchinson et al., 1993), Unit 1 (Pippert et al., 1996)

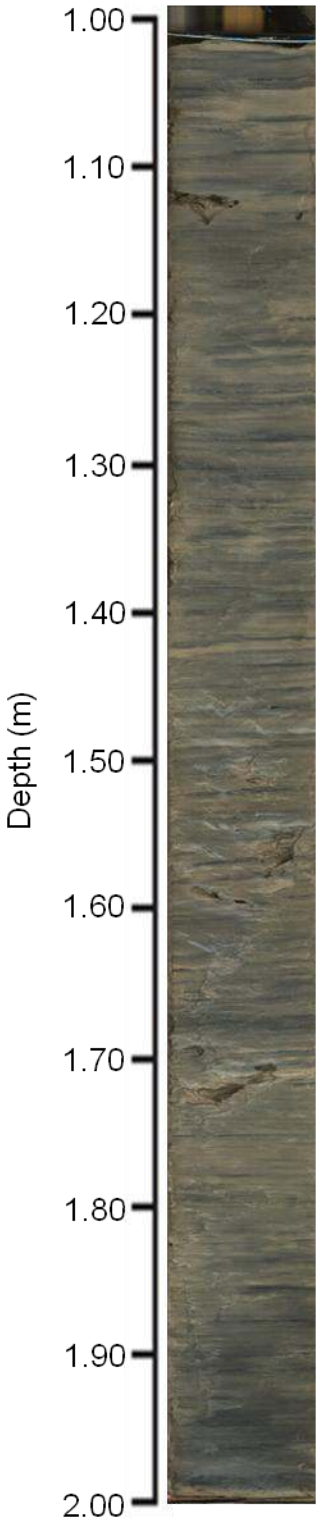

Core 1335: 1.00-2.00 m

- No sediment from 1.00 to 1.01 m
- Oxidized iron sulfide banding millimeters in size, yellowish red (5Y 5/8)
- Massive, dark grayish brown (10YR 4/2) throughout section
- Iron sulfide ball at 1.86 m
- Grain size at 1.595 m (diameter 50 %) is 5.34 μm
- Unit E (Hutchinson et al., 1993), Unit 1 (Pippert et al., 1996)

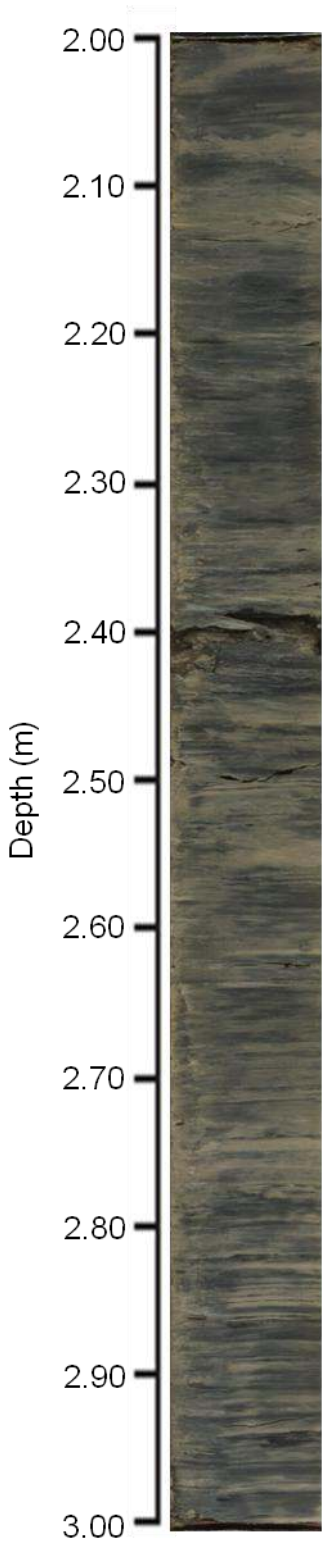

Core 1335: 2.00-3.00 m

- No sediment from 2.38 to 2.41 m
- Oxidized iron sulfide balls throughout section, yellowish red (5Y 5/8)
- Massive, dark grayish brown (10YR 4/2) throughout section
- Dry desiccation cracks throughout section
- Grain size at 2.105 m (diameter 50 %) is 8.34 μm
- Unit E (Hutchinson et al., 1993), Unit 1 (Pippert et al., 1996)

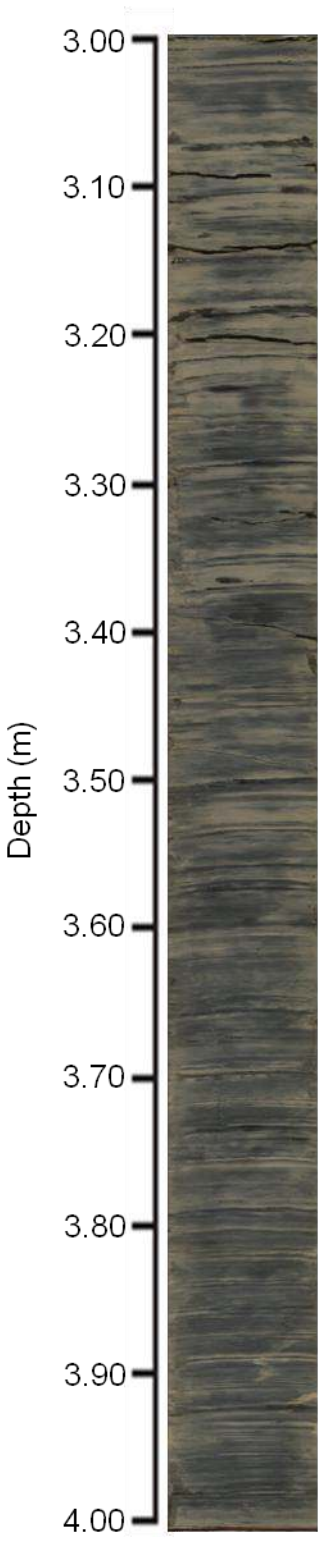

Core 1335: 3.00-4.00 m

- Dry desiccation cracks from 3.00 to 3.30 m
- Oxidized iron sulfide bands throughout section, yellowish red (5Y 5/8)
- Massive, dark grayish brown (10YR 4/2) throughout section
- Dry desiccation cracks throughout section
- Grain size at 3.105 m (diameter 50 %) is 6.81 μm
- Unit E (Hutchinson et al., 1993), Unit 1 (Pippert et al., 1996)

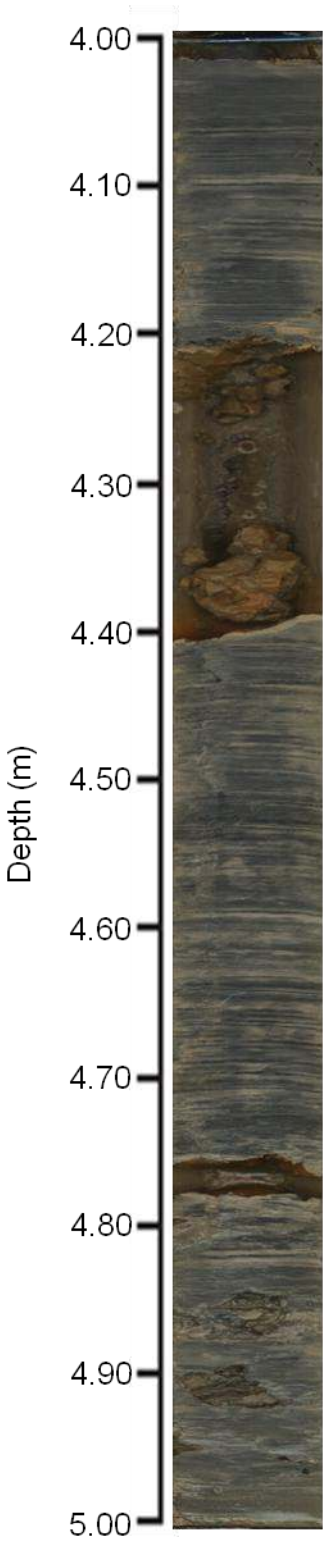

Core 1335: 4.00-5.00 m

- No sediment from 4.00 to 4.01 m, 4.20 to 4.40 m and 4.73 to 4.77 m
- Watery sediment from 4.77 to 4.97 m
- Black banding throughout section, oxidized iron sulfide bands millimeters in size, yellowish red (5Y 5/8)
- Massive, dark grayish brown (10YR 4/2) throughout section
- Grain size at 4.105 m (diameter 50 %) is 6.49 μm
- Unit E (Hutchinson et al., 1993), Unit 1 (Pippert et al., 1996)

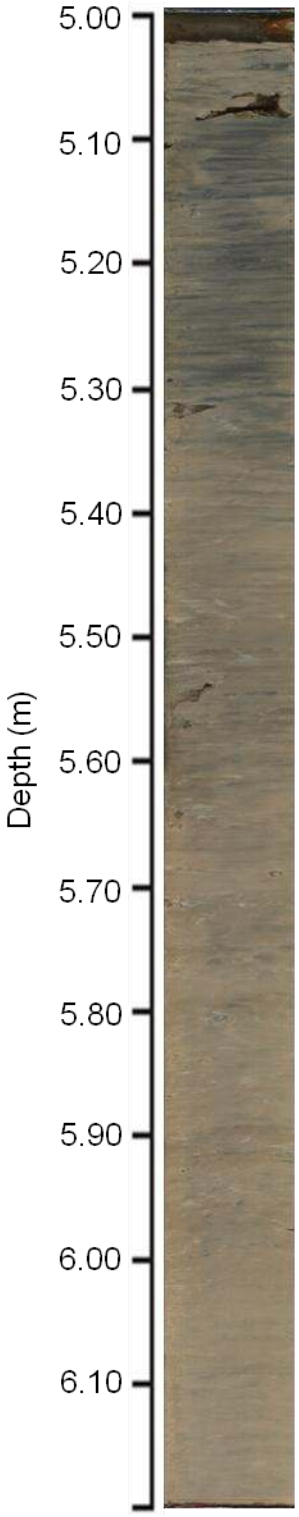

Core 1335: 5.00-6.15 m

- No sediment from 5.00 to 5.02 m
- Faint black (10YR 2/1) bands, barely visible
- Some oxidized iron sulfide balls from 5.05 to 5.25 m, yellowish red (5YR 5/8)
- Massive, dark grayish brown (10YR 4/2) throughout section
- Grain size at 5.105 m (diameter 50 %) is 5.46 μm
- Grain size at 6.105 m (diameter 50 %) is 5.25 μm
- Unit E (Hutchinson et al., 1993), Unit 1 (Pippert et al., 1996)

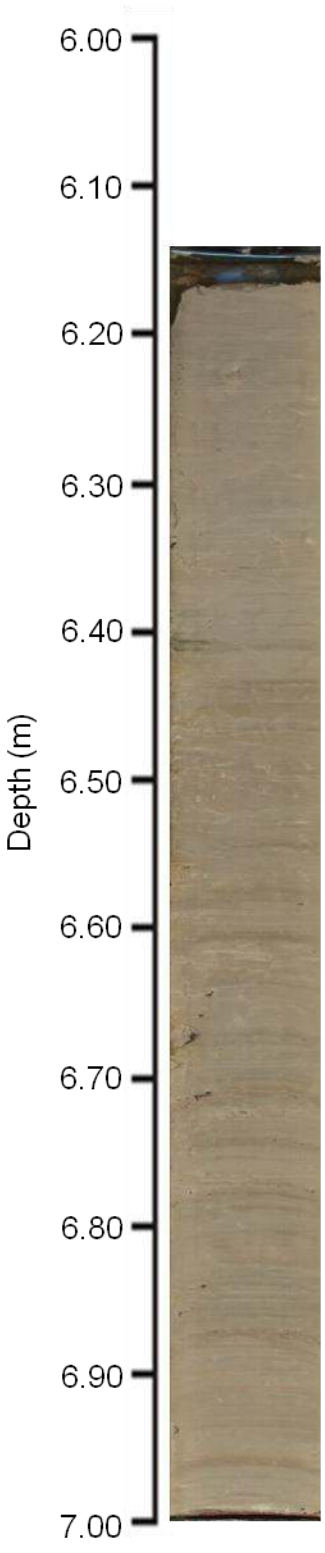

Core 1335: 6.15-7.00 m

- No sediment from 6.15 to 6.16 m
- Faint black (10YR 2/1) banding millimeters to centimeters in size
- Sediment colour changing, grayish brown (10YR 5/2)
- Some oxidized iron sulfide at the top of this section
- Transition from Unit E (Hutchinson et al., 1993), Unit 1 (Pippert et al., 1996) to Unit D (Hutchinson et al., 1993), Unit 2c? (Pippert et al., 1996) at 6.20 m

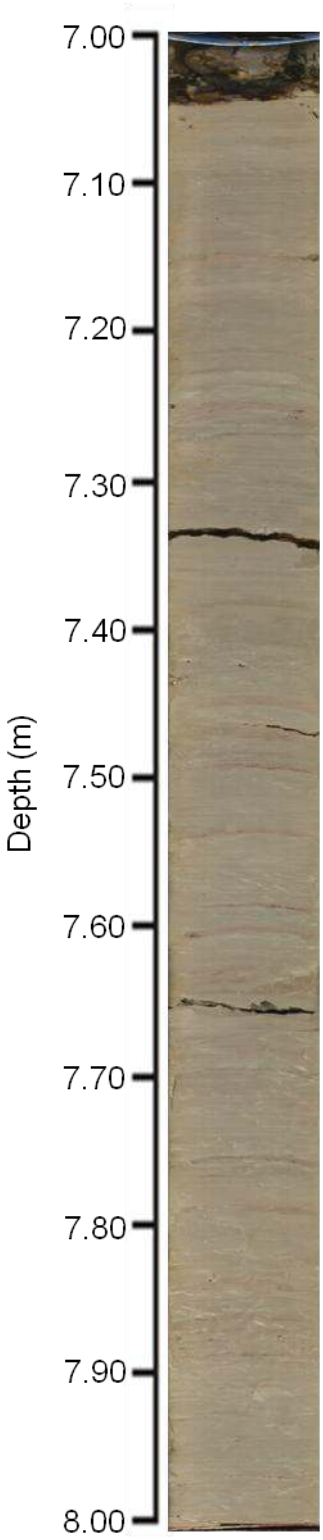

Core 1335: 7.00-8.00 m

- No sediment from 7.00 to 7.05 m
- Faint pink banding millimeters in size, weak red (2.5YR 5/2), difficult to classify with Munsell Colour Chart because of small size, banding occurs throughout core
- Grayish brown (10YR 5/2) throughout section
- Some oxidized iron sulfide at the top of this section
- Grain size at 7.105 m (diameter 50 %) is 4.02 μm
- Unit D (Hutchinson et al., 1993), Unit 2c? (Pippert et al., 1996)

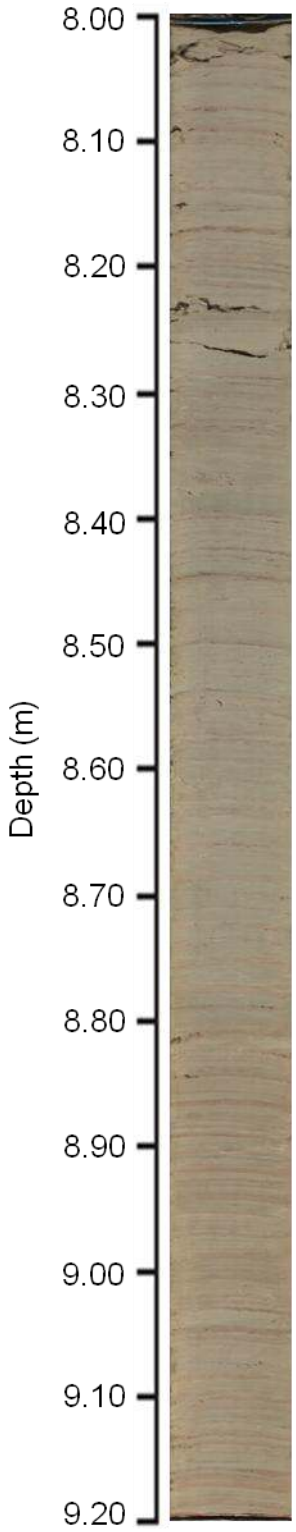

Core 1335: 8.00-9.23 m

- Very pronounced pink banding, perhaps rhythmites or annual laminations, millimeters to centimeters in size, weak red (2.5YR 5/2)
- Grayish brown (10YR 5/2) throughout section
- Grain size at 8.105 m (diameter 50 %) is 6.87 μm
- Grain size at 8.505 m (diameter 50 %) is 4.92 μm
- Grain size at 9.105 m (diameter 50 %) is 3.92 μm
- Transition from Unit D (Hutchinson et al., 1993), Unit 2c? (Pippert et al., 1996) to Unit C (Hutchinson et al., 1993), Unit 2a? (Pippert et al., 1996) at 9.00 m

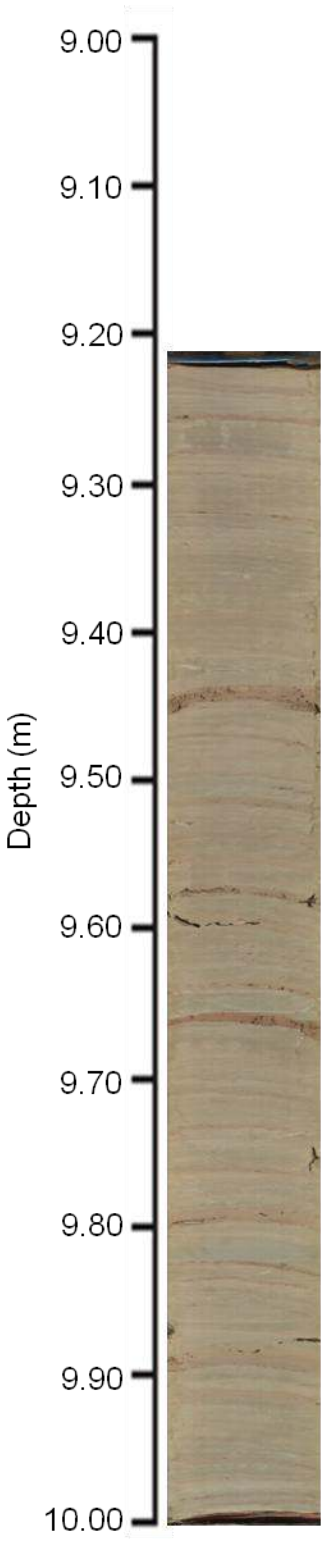

Core 1335: 9.23-10.00 m

- Very large pink band from 9.45 to 9.47 m and 9.65 to 9.67 m, weak red (2.5YR 5/2)
- Faint black (10YR 2/1) banding millimeters to centimeters in size
- Glacial lacustrine clay
- Grayish brown (10YR 5/2) throughout section
- Unit C (Hutchinson et al., 1993), Unit 2a? (Pippert et al., 1996)

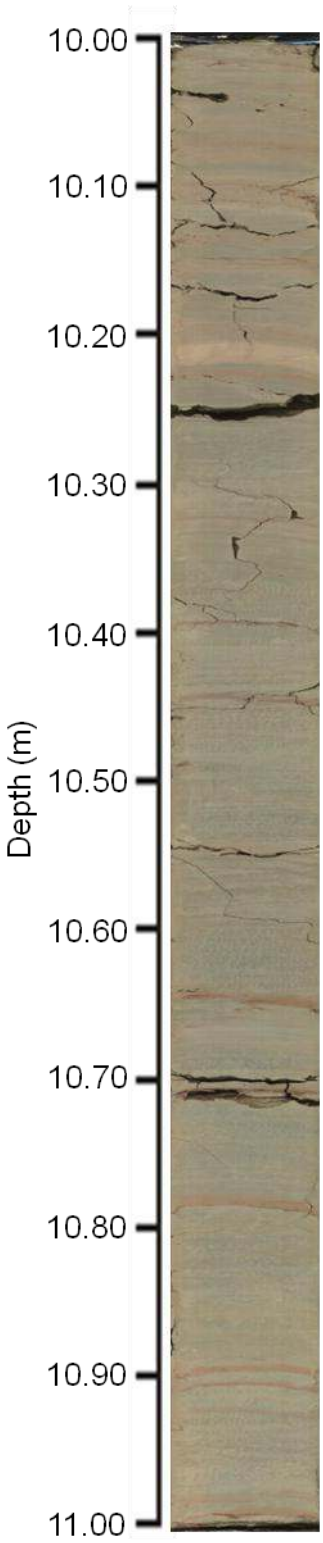

Core 1335: 10.00-11.00 m

- Very prominent pink banding, weak red (10R 5/3)
- Pink banding very frequent from 10.00 to 10.65 m, millimeters to centimeters in size
- Three very large ~1.5 cm bands at 10.64, 10.76 and 10.89 m
- Grayish brown (10YR 5/2) throughout section
- No sediment from 10.235 to 10.245 m
- Grain size at 10.105 m (diameter 50 %) is 5.61 μm
- Unit C (Hutchinson et al., 1993), Unit 2a? (Pippert et al., 1996)

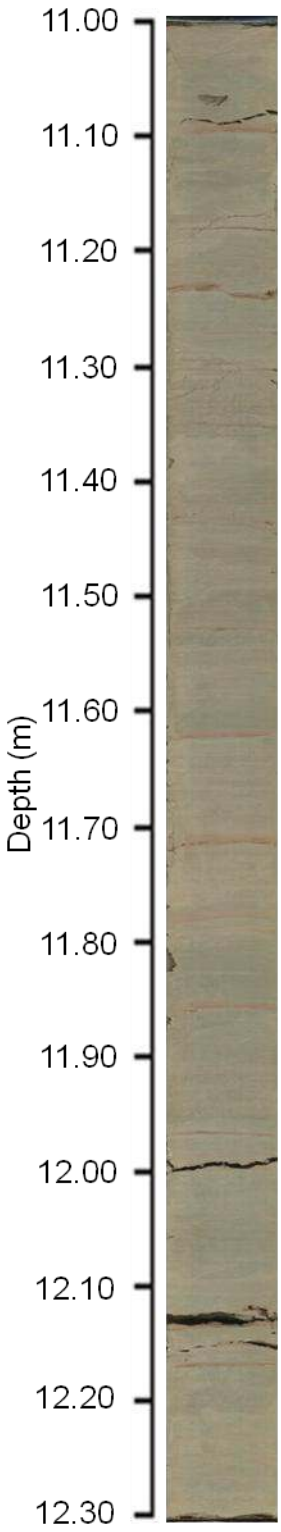

Core 1335: 11.00-12.37 m

- Less frequent pink banding, weak red (2.5YR 5/2)
- Grayish brown (10YR 5/2) throughout section
- Grain size at 11.105 m (diameter 50 %) is 1.84 μm
- Grain size at 12.105 m (diameter 50 %) is 1.98 μm
- Unit C (Hutchinson et al., 1993), Unit 2a? (Pippert et al., 1996)

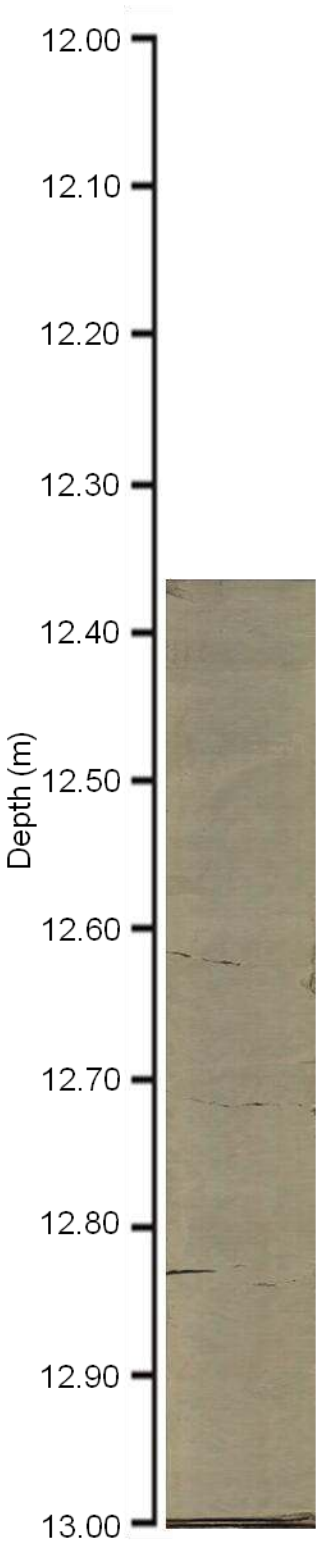

Core 1335: 12.37-13.00 m

- Massive, grayish brown (10YR 5/2) throughout section
- Horizontal pink banding absent
- Transition from Unit C (Hutchinson et al., 1993), Unit 2a? (Pippert et al., 1996) to Unit D (Hutchinson et al., 1993), Unit 3 (Pippert et al., 1996) at 12.37 m

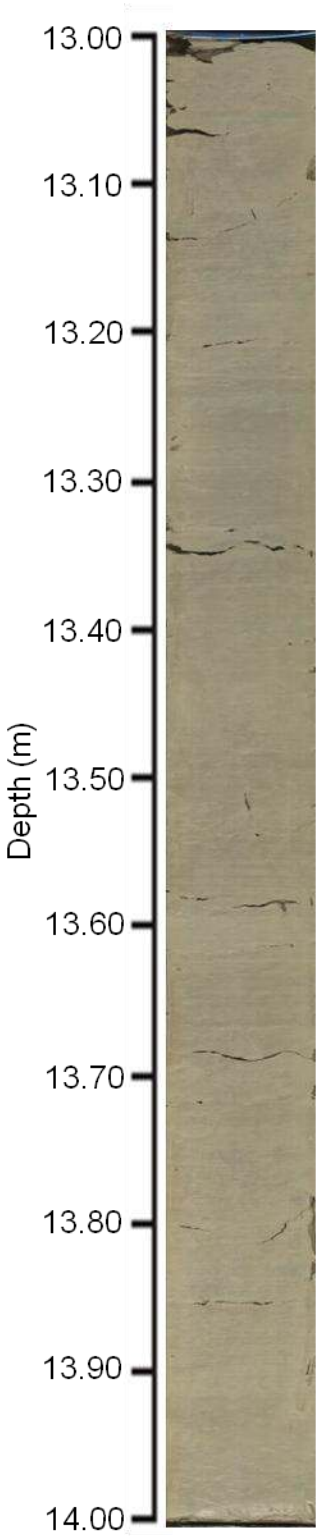

Core 1335: 13.00-14.00 m

- Massive, grayish brown (10YR 5/2) throughout section
- Grain size at 13.105 m (diameter 50 %) is 2.47 μm
- Unit D (Hutchinson et al., 1993), Unit 3 (Pippert et al., 1996)

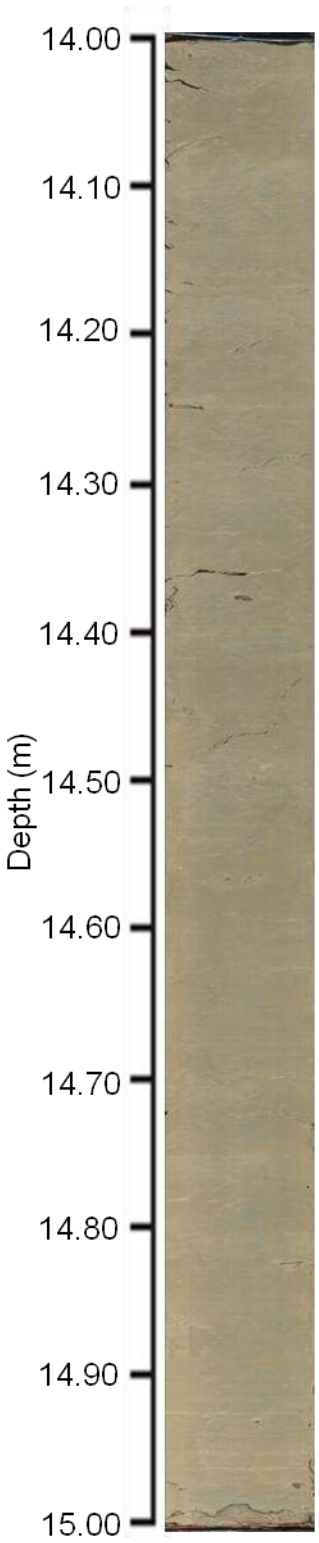

Core 1335: 14.00-15.00 m

- Massive, grayish brown (10YR 5/2) throughout section
- Two silt balls present ~1 cm in diameter at 14.37 and 14.92 m
- Grain size at 14.105 m (diameter 50 %) is 1.97 μm
- Grain size at 14.595 m (diameter 50 %) is 1.83 μm
- Unit D (Hutchinson et al., 1993), Unit 3 (Pippert et al., 1996)

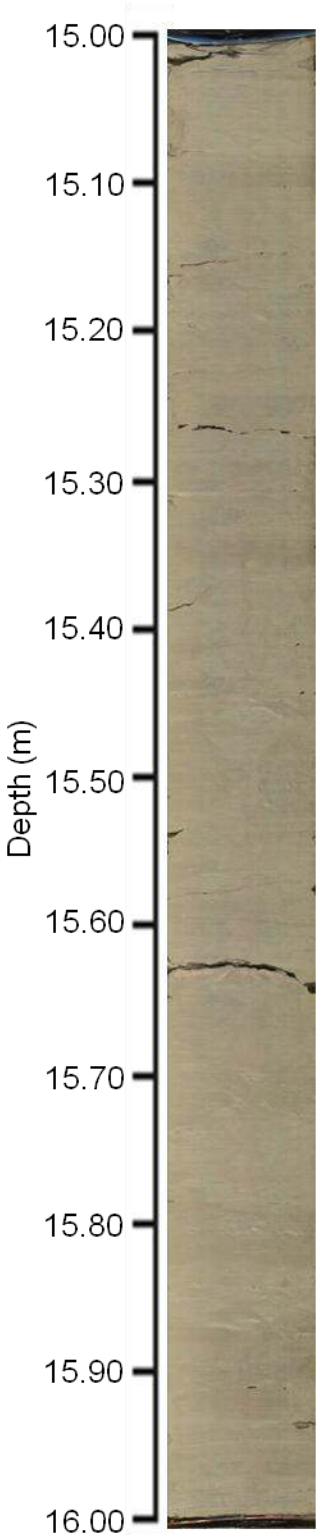

Core 1335: 15.00-16.00 m

- Massive, grayish brown (10YR 5/2) throughout section
- Minor vertical streaking (distortion) caused by drawn in sediment during coring process
- Grain size at 15.105 m (diameter 50 %) is 1.94 μm
- Unit D (Hutchinson et al., 1993), Unit 3 (Pippert et al., 1996)

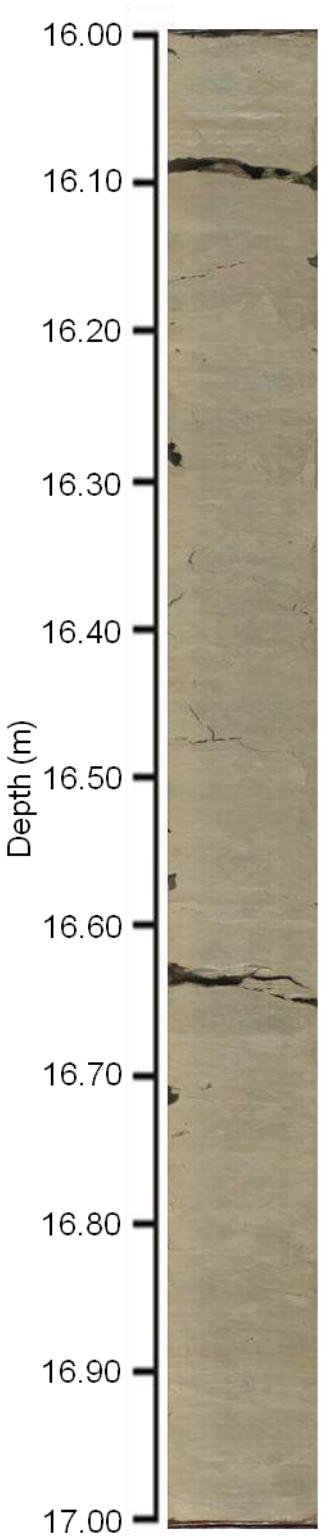

Core 1335: 16.00-17.00 m

- Silt ball 1.5 cm in diameter at 16.25 m
- Massive, grayish brown (10YR 5/2) throughout section
- Minor vertical streaking of pink bands caused by drawn up sediment during the coring process
- Dark spots, from 16.53 to 16.74 m, very dark grayish brown (10YR 3/2)
- Grain size at 16.105 m (diameter 50 %) is 2.05 μm
- Unit D (Hutchinson et al., 1993), Unit 3 (Pippert et al., 1996)

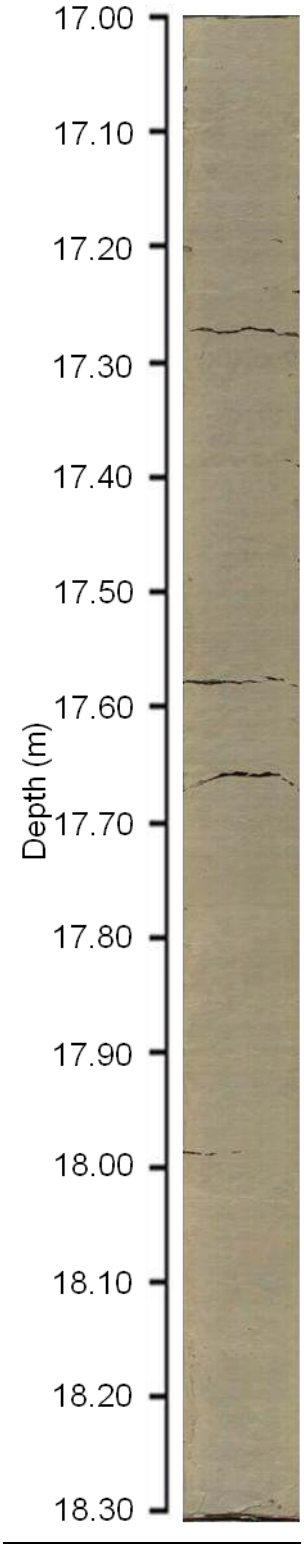

Core 1335: 17.00-18.30 m

- Massive, grayish brown (10YR 5/2) throughout section
- Minor vertical streaking of pink bands caused by drawn up sediment during the coring process
- Grain size at 17.105 m (diameter 50 %) is 2.15 μm
- Grain size at 18.105 m (diameter 50 %) is 2.00 μm
- Unit D (Hutchinson et al., 1993), Unit 3 (Pippert et al., 1996)

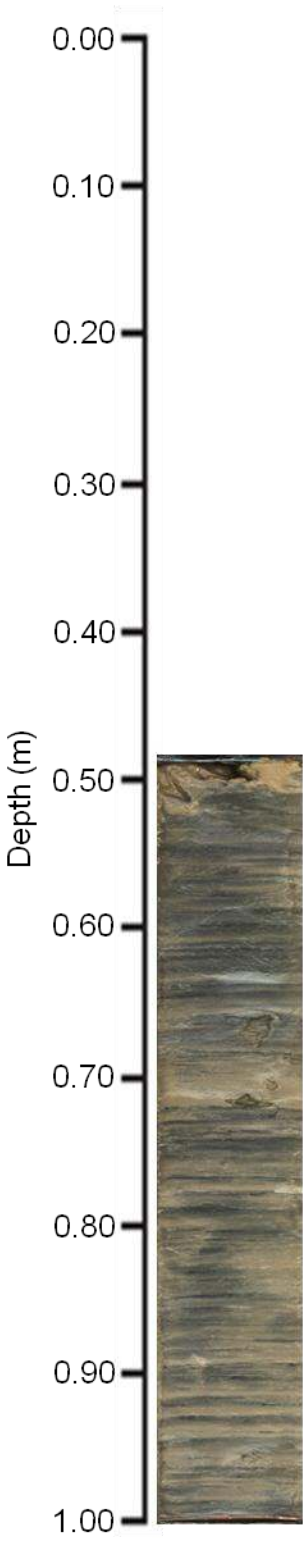

Core 1336: 0.49- 1.00 m

- No sediment from 0.00 to 0.49 m
- Very watery
- Black bands throughout core, ~0.5 cm thick
- Massive, dark grayish brown (10YR 4/2) throughout section
- Unit E (Hutchinson et al., 1993), Unit 1 (Pippert et al., 1996)

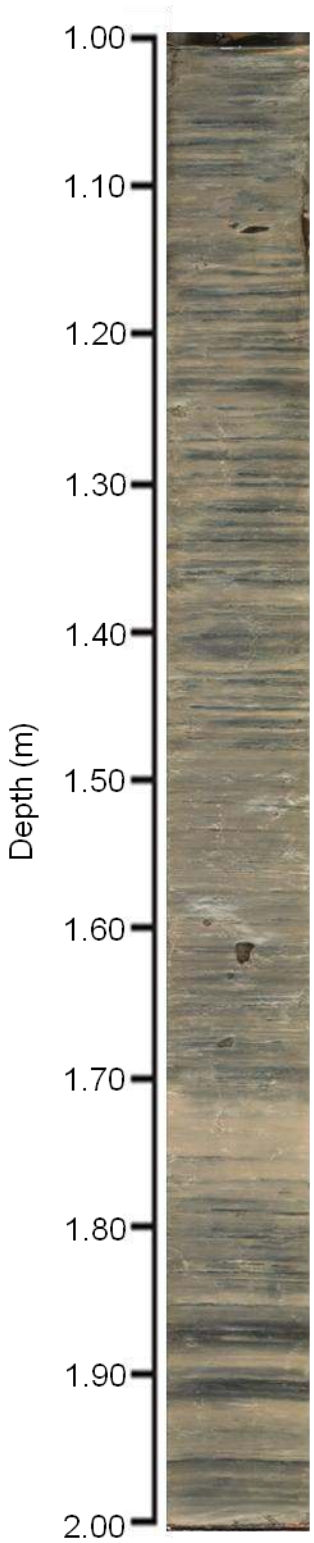

Core 1336: 1.00-2.00 m

- Less watery
- Black bands throughout core, thickening towards the base of the section to ~1.0 cm
- Massive, dark grayish brown (10YR 4/2) throughout section
- Grain size at 1.105 m (diameter 50 %) is 5.99 μm
- Unit E (Hutchinson et al., 1993), Unit 1 (Pippert et al., 1996)

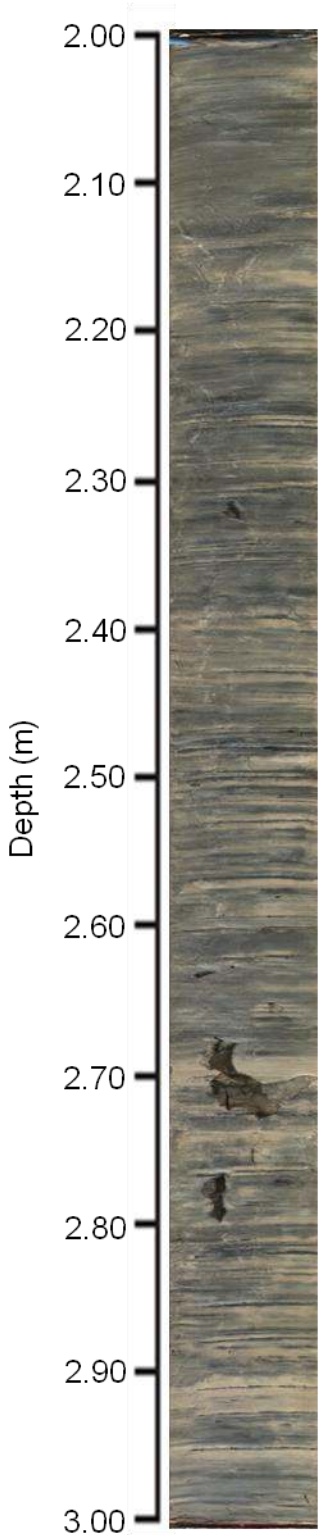

Core 1336: 2.00-3.00 m

- Negligible water
- Black bands throughout core, ~0.2 cm at the top of the core thickening to 0.5 cm near the base of the section
- Massive, dark grayish brown (10YR 4/2) throughout section
- Grain size at 2.195 m (diameter 50 %) is 6.12 μm
- Unit E (Hutchinson et al., 1993), Unit 1 (Pippert et al., 1996)

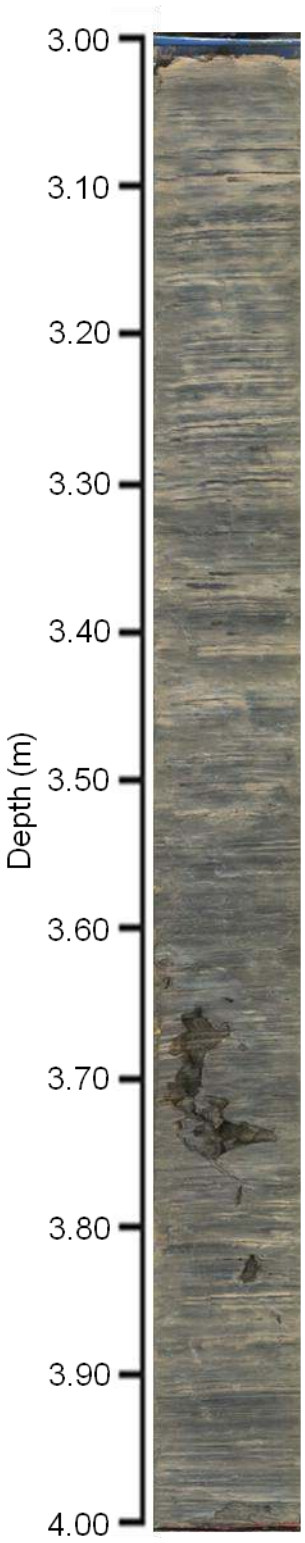

Core 1336: 3.00-4.00 m

- Negligible water
- Black bands throughout core, ~0.2 cm thick
- Massive, dark grayish brown (10YR 4/2) throughout section
- Grain size at 3.105 m (diameter 50 %) is 5.04 μm
- Unit E (Hutchinson et al., 1993), Unit 1 (Pippert et al., 1996)

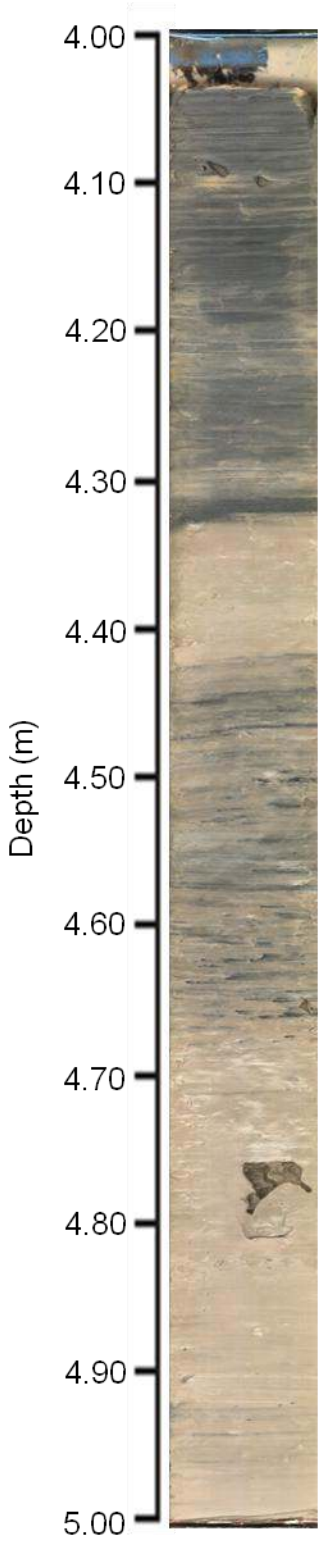

Core 1336: 4.00-5.00 m

- No water
- No sediment from 4.00 to 4.04 m
- Interclasts, ~1.0 cm in diameter at 4.13 m in core section
- Black banding from 4.04 to 4.34 m and continues from 4.49 to 4.67 m
- Massive, dark grayish brown (10YR 4/2) throughout sections of black banding
- Colour changing, grayish brown (10YR 5/2) sediment from 4.34 to 4.49 m and 4.67 m to the base of the section
- Faint black dots from 4.58 to 4.72 m
- Increased core density
- Grain size at 4.145 m (diameter 50 %) is 5.41 μm
- Transition from Unit E (Hutchinson et al., 1993), Unit 1 (Pippert et al., 1996) to Unit D? (Hutchinson et al., 1993), Unit 2b? (Pippert et al., 1996) at 4.62 m

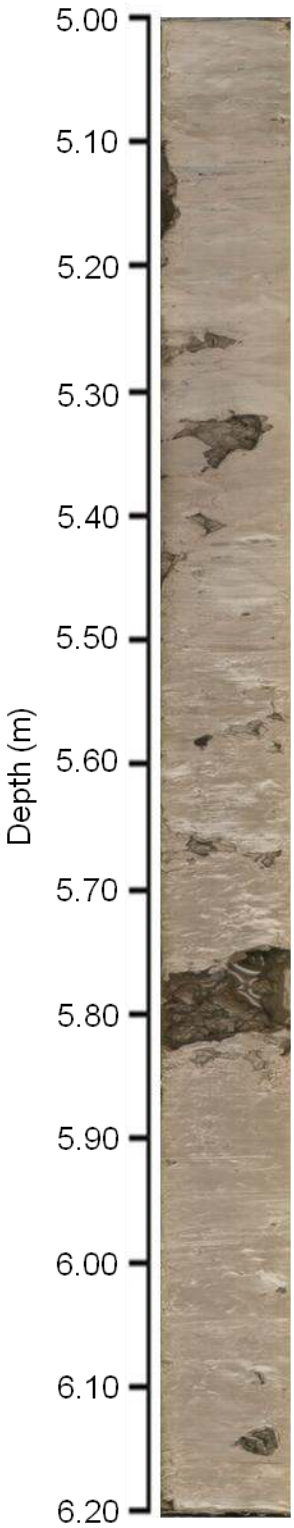

Core 1336: 5.00-6.17 m

- No sediment from 5.67 to 5.79 m
- No distinct banding
- Mainly featureless
- Massive, grayish brown (10YR 5/2) sediment throughout
- Grain size at 5.105 m (diameter 50 %) is 3.54 μm
- Grain size at 6.105 m (diameter 50 %) is 3.04 μm
- Unit D? (Hutchinson et al., 1993), Unit 2b? (Pippert et al., 1996)

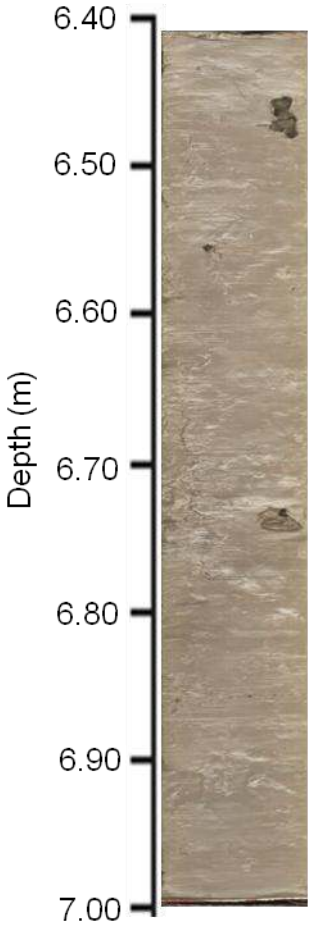

Core 1336: 6.42-7.00 m

- Massive, grayish brown (10YR 5/2) throughout section
- Grain size at 6.905 m (diameter 50 %) is 3.19 μm
- Unit D? (Hutchinson et al., 1993), Unit 2b? (Pippert et al., 1996)

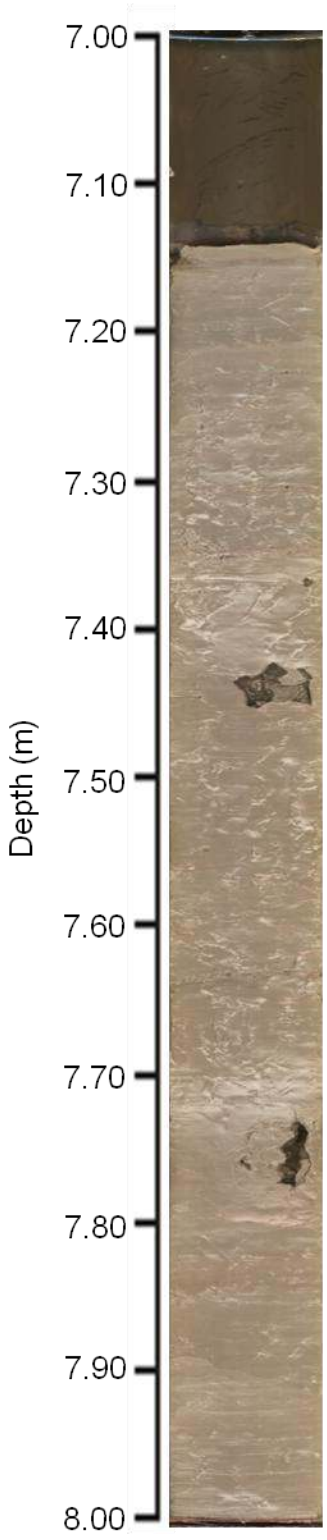

Core 1336: 7.00-8.00 m

- No sediment from 7.00 to 7.15 m
- Massive, grayish brown (10YR 5/2) sediment throughout
- Faint pink banding, difficult to classify with Munsell Color Chart
- Grain size at 7.295 m (diameter 50 %) is 7.49 μm
- Unit D? (Hutchinson et al., 1993), Unit 2b? (Pippert et al., 1996)

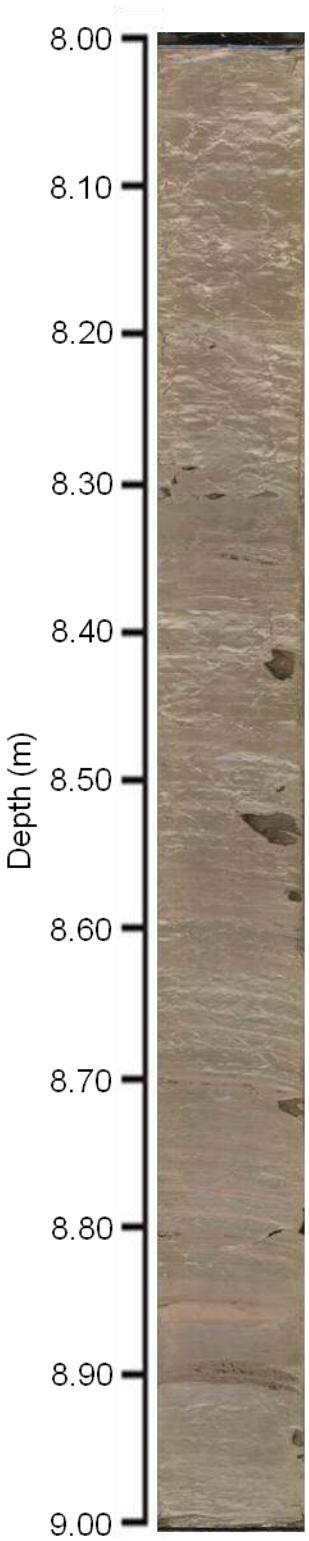

Core 1336: 8.00-9.00 m

- Massive, grayish brown (10YR 5/2) sediment throughout
- Faint pink banding throughout section, millimeters in size, weak red (2.5YR 5/2)
- Grain size at 8.105 m (diameter 50 %) is 3.13 μm
- Transition from Unit D? (Hutchinson et al., 1993), Unit 2b? (Pippert et al., 1996) to Unit C (Hutchinson et al., 1993), Unit 2a? (Pippert et al., 1996) at 9.00 m

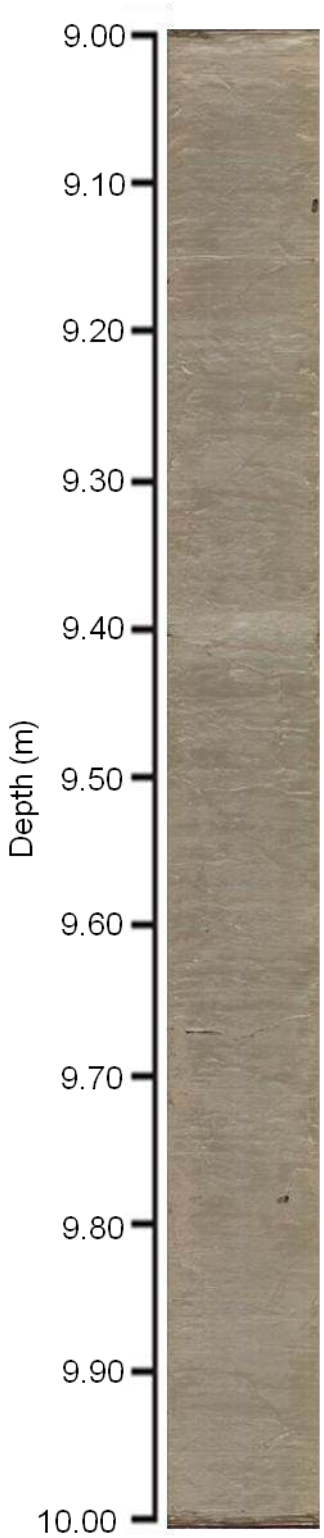

Core 1336: 9.00-10.00 m

- Massive, grayish brown (10YR 5/2) sediment throughout
- Weak red (2.5YR 5/2) banding throughout section, millimeters to centimeters in size
- Grain size at 9.105 m (diameter 50 %) is 2.32 μm
- Unit C (Hutchinson et al., 1993), Unit 2a? (Pippert et al., 1996)

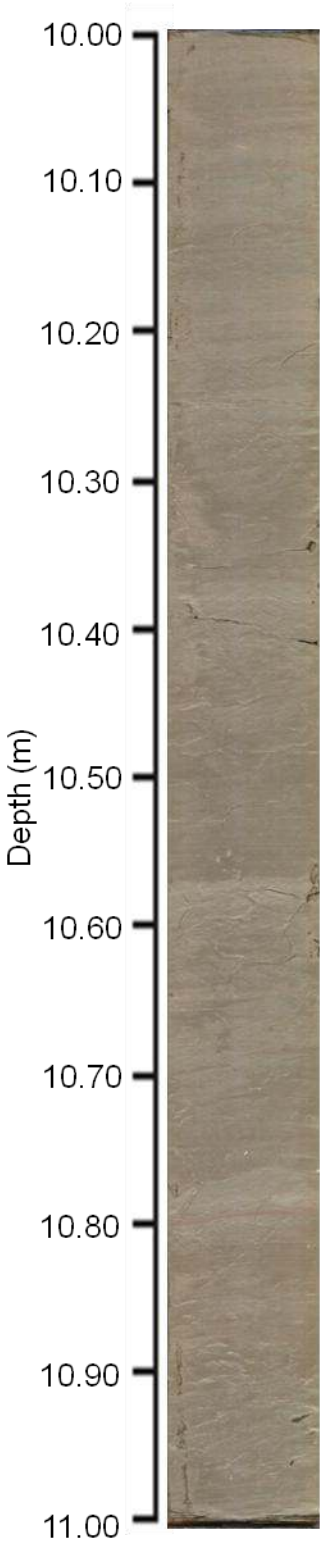

Core 1336: 10.00-11.00 m

- Massive, grayish brown (10YR 5/2) sediment throughout
- Weak red (2.5YR 5/2) banding throughout section, millimeters to centimeters in size
- Grain size at 10.105 m (diameter 50 %) is 1.79 μm
- Unit C (Hutchinson et al., 1993), Unit 2a? (Pippert et al., 1996)

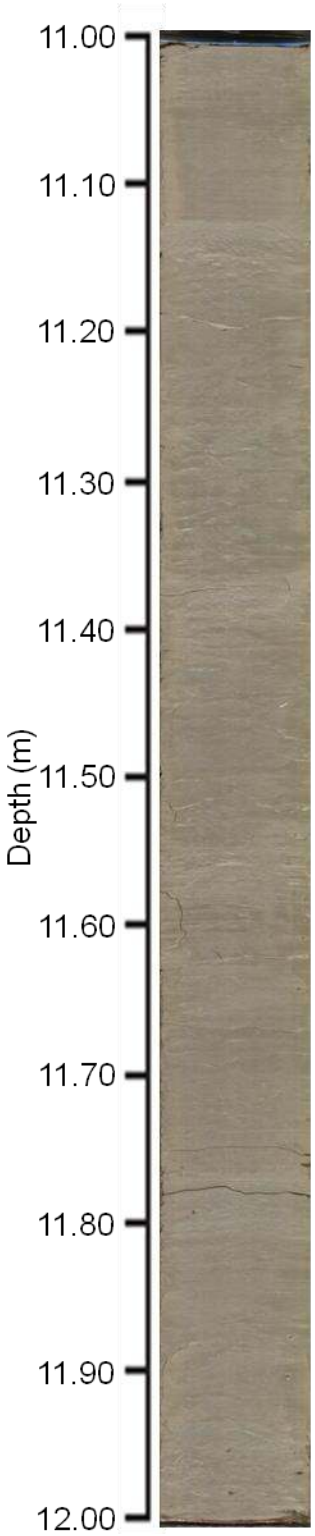

Core 1336: 11.00-12.00 m

- Massive, grayish brown (10YR 5/2) sediment throughout
- Weak red (2.5YR 5/2) banding throughout section, millimeters in size
- Grain size at 11.105 m (diameter 50 %) is 2.03 μm
- Unit C (Hutchinson et al., 1993), Unit 2a? (Pippert et al., 1996)

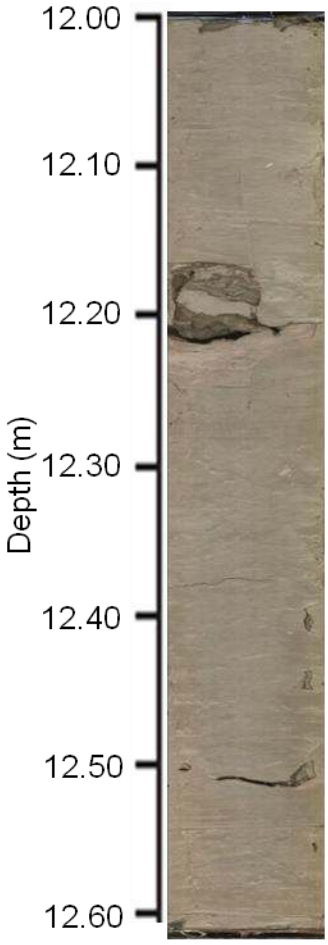

Core 1336: 12.00-12.62 m

- Massive, grayish brown (10YR 5/2) sediment throughout
- Weak red (2.5YR 5/2) banding throughout section, millimeters in size
- Grain size at 12.105 m (diameter 50 %) is 1.66 μm
- Unit C (Hutchinson et al., 1993), Unit 2a? (Pippert et al., 1996)

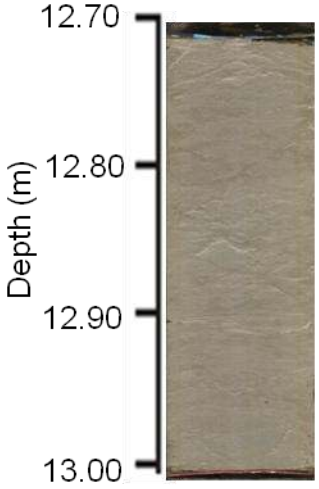

Core 1336: 12.72-13.00 m

- Massive, grayish brown (10YR 5/2) sediment throughout
- Weak red (2.5YR 5/2) banding throughout section, millimeters in size
- Unit C (Hutchinson et al., 1993), Unit 2a? (Pippert et al., 1996)

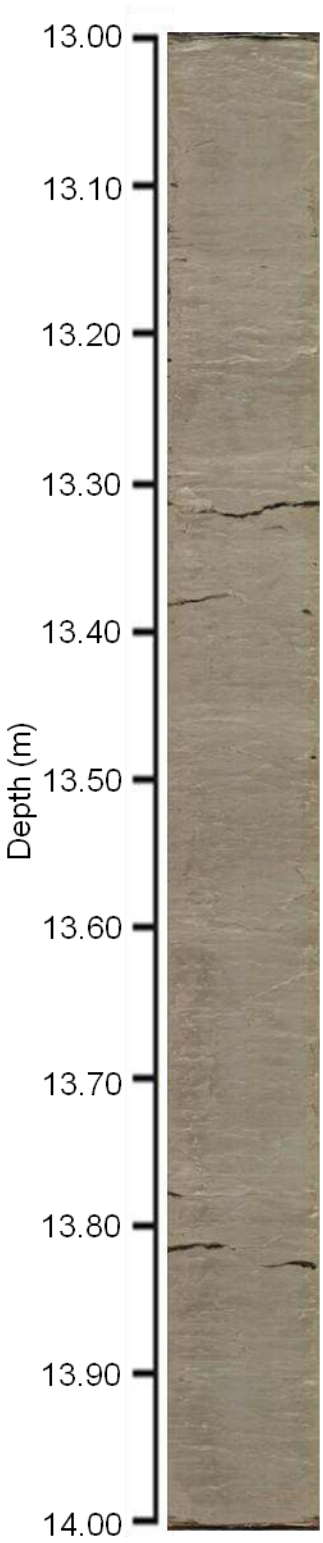

Core 1336: 13.00-14.00 m

- Massive, grayish brown (10YR 5/2) sediment throughout
- Weak red (2.5YR 5/2) banding throughout section, millimeters in size
- Grain size at 13.105 m (diameter 50 %) is 1.73 μm
- Unit C (Hutchinson et al., 1993), Unit 2a? (Pippert et al., 1996)

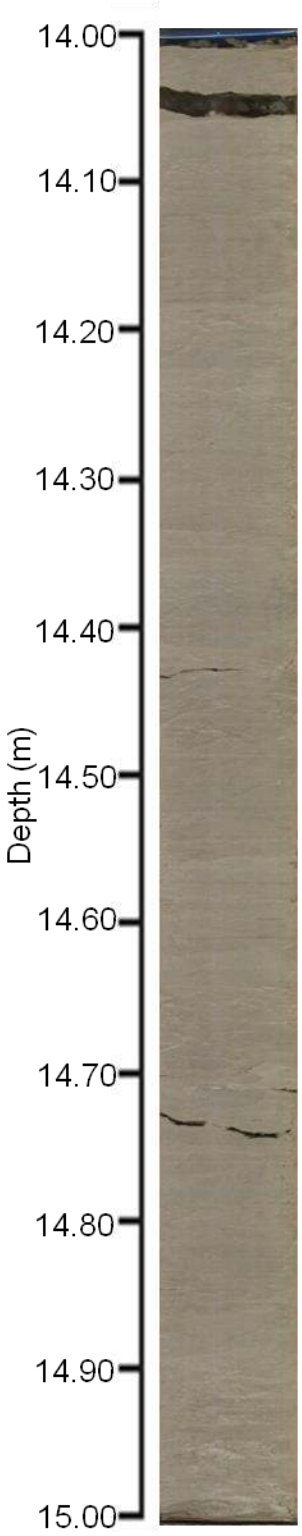

Core 1336: 14.00-15.00 m

- Massive, grayish brown (10YR 5/2) sediment throughout
- Weak red (2.5YR 5/2) banding throughout section, millimeters in size
- Prominent weak red (2.5YR 5/2) banding at 14.73 and 14.78 m
- Grain size at 14.105 m (diameter 50 %) is 2.05 μm
- Unit C (Hutchinson et al., 1993), Unit 2a? (Pippert et al., 1996)

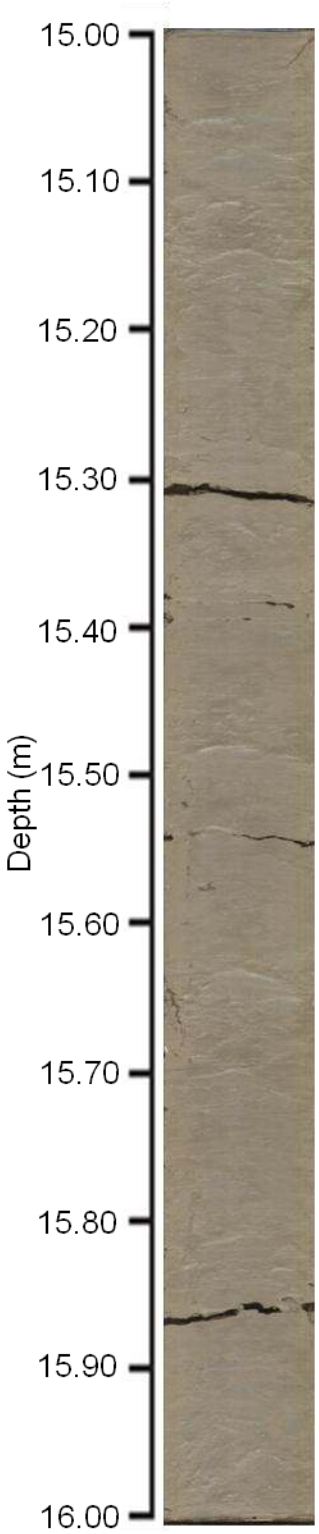

Core 1336: 15.00-16.00 m

- Massive, grayish brown (10YR 5/2) sediment throughout
- Weak red (2.5YR 5/2) banding throughout section, millimeters in size
- Grain size at 15.105 m (diameter 50 %) is 1.89 μm
- Unit C (Hutchinson et al., 1993), Unit 2a? (Pippert et al., 1996)

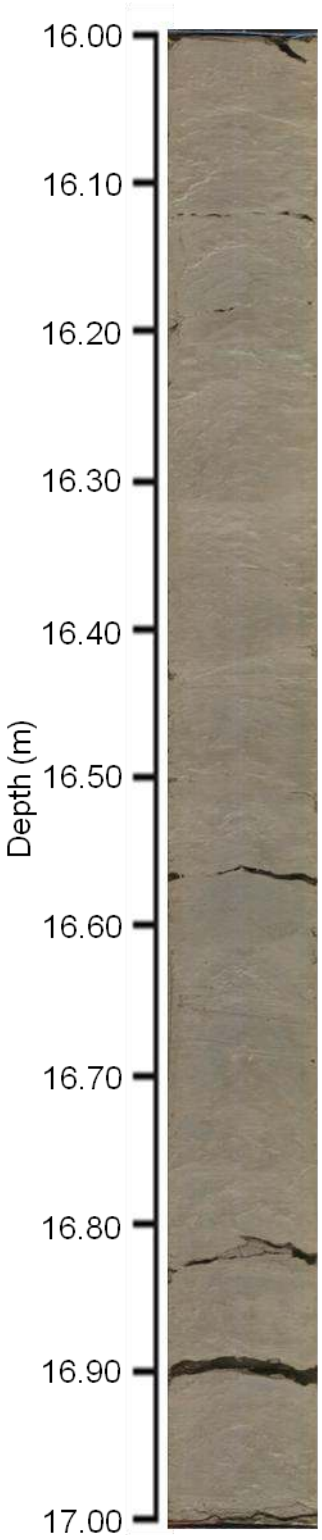

Core 1336: 16.00-17.00 m

- Massive, grayish brown (10YR 5/2) sediment throughout
- Weak red (2.5YR 5/2) banding throughout section, millimeters in size
- Minor vertical streaking of pink bands caused by drawn up sediment during the coring process
- Grain size at 16.105 m (diameter 50 %) is 2.03 μm
- Unit C (Hutchinson et al., 1993), Unit 2a? (Pippert et al., 1996)

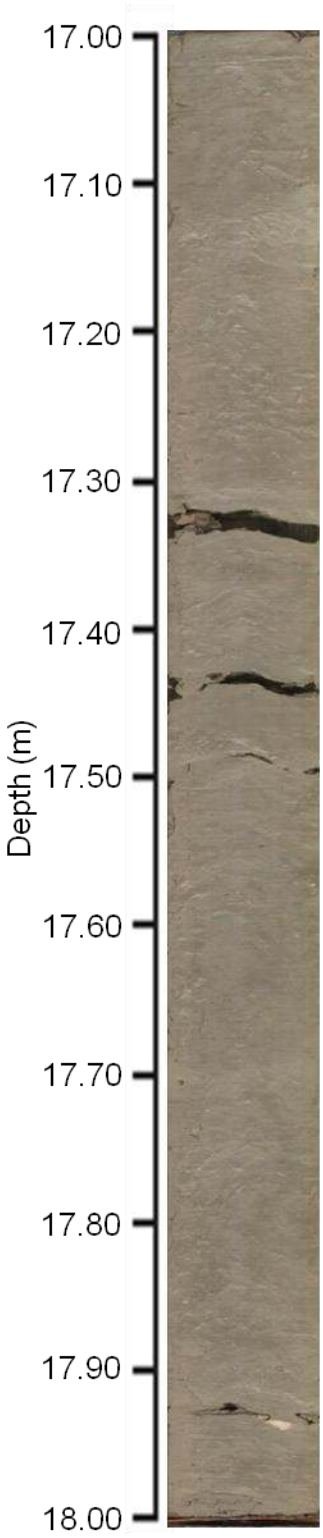

Core 1336: 17.00-18.00 m

- Massive, grayish brown (10YR 5/2) sediment throughout
- Pronounced vertical, dark black streak is present, indication of sediment drawn up during the coring process
- Silt ball at 17.95 m
- Grain size at 17.105 m (diameter 50 %) is 1.97 μm
- Unit C (Hutchinson et al., 1993), Unit 2a? (Pippert et al., 1996)

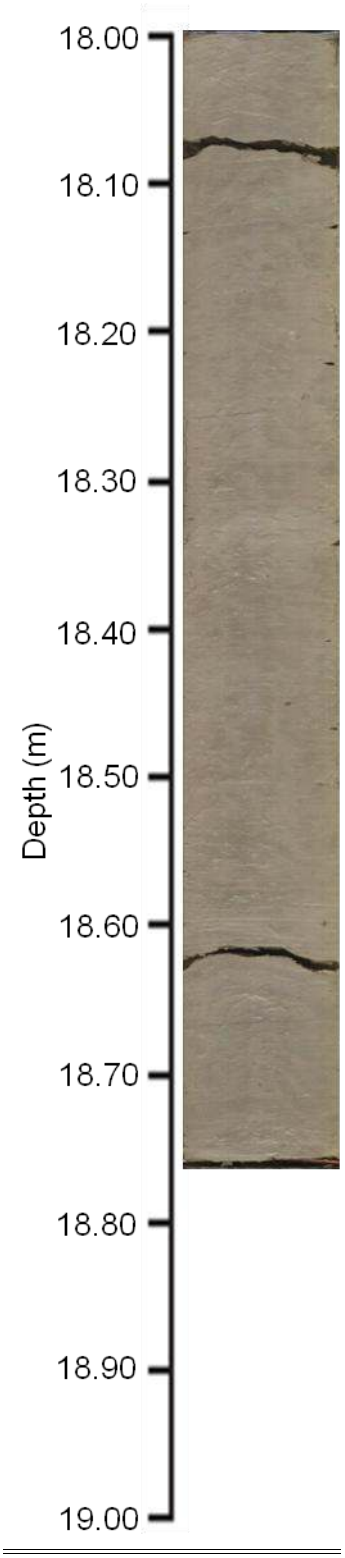

Core 1336: 18.00-18.75 m

- Massive, grayish brown (10YR 5/2) sediment throughout, intermixed with light brown sediment (indication of drawn up sediment during the coring process)
- Pronounced vertical streaking is present, indication of sediment drawn up during the coring process
- Grain size at 18.305 m (diameter 50 %) is 2.33 μm
- Unit C (Hutchinson et al., 1993), Unit 2a? (Pippert et al., 1996)

Appendix II reports the results obtained for isotopic and elemental standards.

Ostracodes

Standard	$\delta^{13}C$ (‰, VPDB)	$\delta^{18}O$ (‰, VSMOW)
Suprapur	–35.35	+13.00
Suprapur	–35.27	+13.11
Suprapur	–35.22	+13.21
Suprapur	–35.13	+13.17
Suprapur	–35.43	+13.12
Suprapur	–34.97	+13.06
Suprapur	–35.59	+13.25
Suprapur	–35.28	+13.25
Suprapur	–35.26	+13.23
Suprapur	–35.30	+13.23
Suprapur	–35.16	+13.25
Suprapur	–35.40	+13.24
Suprapur	–35.25	+13.25
Suprapur	–35.25	+13.23
Suprapur	–35.34	+13.25
Suprapur	–35.29	+13.17
Suprapur	–35.27	+13.19
Suprapur	–35.25	+13.38
Suprapur	–35.30	+13.30
Suprapur	–35.29	+13.24
Suprapur	–35.28	+13.05
Suprapur	–35.36	+13.20
Suprapur	–35.12	+13.23
Suprapur	–35.36	+13.12
Suprapur	–35.28	+13.20

*Suprapur carbon isotopic composition defined by calibration curve.

*Suprapur oxygen isotopic composition is defined independently from calibration curve.

Standard	$\delta^{18}O$ (‰, VSMOW)
NBS–18	+7.22
NBS–18	+7.27
NBS–18	+7.10
NBS–18	+7.33
NBS–18	+7.07
NBS–18	+7.13
NBS–18	+7.23
NBS–18	+7.24
NBS–18	+7.27
NBS–18	+7.18
NBS–18	+7.14
NBS–18	+7.24
NBS–18	+7.16
NBS–18	+7.24
NBS–18	+7.16
NBS–18	+7.37
NBS–18	+7.15
NBS–18	+7.08
NBS–18	+7.28
NBS–18	+7.22
NBS–18	+7.11
NBS–18	+7.34
NBS–18	+7.31
NBS–18	+6.95
NBS–18	+7.20
NBS–18	+7.31

*NBS–18 oxygen isotopic composition defined by calibration curve.

Standard	$\delta^{13}C$ (‰, VPDB)	$\delta^{18}O$ (‰, VSMOW)
NBS–19	+1.90	+28.52
NBS–19	+1.95	+28.57
NBS–19	+1.98	+28.65
NBS–19	+1.97	+28.66
NBS–19	+1.95	+28.57
NBS–19	+1.96	+28.59
NBS–19	+1.95	+28.63
NBS–19	+1.89	+28.57
NBS–19	+1.98	+28.59
NBS–19	+1.97	+28.62
NBS–19	+1.97	+28.61
NBS–19	+1.94	+28.58
NBS–19	+1.94	+28.51
NBS–19	+1.94	+28.67
NBS–19	+1.97	+28.63
NBS–19	+1.93	+28.56
NBS–19	+1.93	+28.45
NBS–19	+2.00	+28.79
NBS–19	+1.94	+28.58
NBS–19	+1.96	+28.62
NBS–19	+1.89	+28.47
NBS–19	+1.92	+28.62
NBS–19	+1.98	+28.65
NBS–19	+2.00	+28.66
NBS–19	+1.95	+28.57
NBS–19	+1.95	+28.63
NBS–19	+1.97	+28.75
NBS–19	+1.95	+28.71
NBS–19	+1.97	+28.65

*NBS–19 carbon isotopic composition defined by calibration curve.

*NBS–19 oxygen isotopic composition defined by calibration curve.

Standard	$\delta^{13}C$ (‰, VPDB)	$\delta^{18}O$ (‰, VSMOW)
NBS–19	+1.94	+28.47
NBS–19	+1.91	+28.41
NBS–19	+1.95	+28.54
NBS–19	+1.97	+28.68
NBS–19	+1.93	+28.57
NBS–19	+1.93	+28.63
NBS–19	+1.96	+28.66
NBS–19	+1.96	+28.51
WS–1	+0.57	+26.15
WS–1	+0.80	+26.25
WS–1	+0.82	+26.29
WS–1	+0.85	+26.49
WS–1	+0.86	+26.53
WS–1	+0.74	+26.18
WS–1	+0.39	+26.16
WS–1	+0.79	+26.18
WS–1	+0.67	+26.17

*WS–1 carbon and oxygen isotopic compositions are defined independently from calibration curve.

Bulk organic matter

Standard	TN (%)	TOC (%)	Standard	TN (%)	TOC (%)
LowOrg	0.13	1.75	LowOrg	0.14	1.90
LowOrg	0.13	1.53	LowOrg	0.13	1.57
LowOrg	0.13	1.50	LowOrg	0.13	1.52
LowOrg	0.13	1.52	LowOrg	0.13	1.70
LowOrg	0.14	1.85	LowOrg	0.13	1.54
LowOrg	0.13	1.53	LowOrg	0.13	1.55
LowOrg	0.13	1.51	LowOrg	0.12	1.44
LowOrg	0.13	1.52	LowOrg	0.14	1.64
LowOrg	0.13	1.63	LowOrg	0.14	1.58
LowOrg	0.13	1.53	LowOrg	0.14	1.58
LowOrg	0.13	1.51	LowOrg	0.13	1.69
LowOrg	0.13	1.55	LowOrg	0.18	1.62
LowOrg	0.13	1.50	LowOrg	0.16	1.60
LowOrg	0.13	1.67	LowOrg	0.14	1.52
LowOrg	0.13	1.50	LowOrg	0.12	1.52
LowOrg	0.13	1.50	LowOrg	0.14	1.56
LowOrg	0.14	1.59	LowOrg	0.13	1.49
LowOrg	0.15	1.72	LowOrg	0.13	1.52
LowOrg	0.13	1.47	LowOrg	0.11	1.50
LowOrg	0.13	1.78	LowOrg	0.13	1.55
LowOrg	0.12	1.52	LowOrg	0.13	1.54
LowOrg	0.12	1.49	LowOrg	0.13	1.53
LowOrg	0.12	1.47	LowOrg	0.12	1.52
LowOrg	0.12	1.49			
LowOrg	0.13	1.60			
LowOrg	0.13	1.56			
LowOrg	0.13	1.54			
LowOrg	0.12	1.49			

*LowOrg= Low Organic Content Soil, percent total nitrogen (TN) and carbon (TOC) defined by calibration curve.

Standard	TN (%)	TOC (%)	Standard	TN (%)	TOC (%)
HighOrg	0.46	6.34	HighOrg	0.46	6.08
HighOrg	0.46	6.16	HighOrg	0.46	6.24
HighOrg	0.46	6.07	HighOrg	0.46	6.14
HighOrg	0.46	6.08	HighOrg	0.46	6.05
HighOrg	0.46	6.32	HighOrg	0.46	6.20
HighOrg	0.47	6.17	HighOrg	0.46	6.20
HighOrg	0.46	6.06	HighOrg	0.46	6.07
HighOrg	0.46	6.08	HighOrg	0.46	6.26
HighOrg	0.46	6.07	HighOrg	0.46	6.10
HighOrg	0.46	6.18	HighOrg	0.46	6.14
HighOrg	0.46	6.34	HighOrg	0.46	5.98
HighOrg	0.46	6.10	HighOrg	0.54	6.16
HighOrg	0.46	6.10	HighOrg	0.48	6.29
HighOrg	0.44	5.84	HighOrg	0.46	6.14
HighOrg	0.46	6.13	HighOrg	0.44	5.98
HighOrg	0.46	6.08	HighOrg	0.49	6.09
HighOrg	0.46	6.12	HighOrg	0.47	6.21
HighOrg	0.49	6.16	HighOrg	0.47	6.16
HighOrg	0.47	6.11	HighOrg	0.45	6.00
HighOrg	0.46	6.00	HighOrg	0.47	6.05
HighOrg	0.45	6.03	HighOrg	0.46	6.05
HighOrg	0.46	6.01	HighOrg	0.46	6.08
HighOrg	0.46	6.13	HighOrg	0.46	6.15
HighOrg	0.46	6.00	HighOrg	0.44	6.07
HighOrg	0.45	6.06			
HighOrg	0.46	6.17			
HighOrg	0.46	6.12			

*HighOrg= High Organic Content Soil, percent total nitrogen (TN) and carbon (TOC) defined by calibration curve.

Standard	$\delta^{13}C$ (‰, VPDB)	Standard	$\delta^{13}C$ (‰, VPDB)
Keratin	–24.12		
Keratin	–24.05	IAEA–CH–6	–10.47
Keratin	–24.00	IAEA–CH–6	–10.50
Keratin	–24.09	IAEA–CH–6	–10.56
Keratin	–24.17	IAEA–CH–6	–10.58
Keratin	–23.97	IAEA–CH–6	–10.54
Keratin	–24.08	IAEA–CH–6	–10.53
Keratin	–24.05	IAEA–CH–6	–10.22
Keratin	–24.16	IAEA–CH–6	–10.29
Keratin	–23.97	IAEA–CH–6	–10.27
Keratin	–24.04	IAEA–CH–6	–10.30
Keratin	–24.25	IAEA–CH–6	–10.58
Keratin	–24.02	IAEA–CH–6	–10.40
Keratin	–23.99	USGS–41	+37.47
Keratin	–24.12	USGS–41	+37.37
Keratin	–24.14	USGS–41	+37.96
Keratin	–24.20	USGS–41	+37.57
USGS–40	–26.44	USGS–41	+37.67
USGS–40	–26.37	USGS–41	+37.56
USGS–40	–26.39	USGS–41	+37.27
USGS–40	–26.43	USGS–41	+38.10
USGS–40	–26.34	USGS–41	+37.43
USGS–40	–26.42	USGS–41	+37.78
USGS–40	–26.44	USGS–41	+37.54
USGS–40	–26.30		
USGS–40	–26.45		
USGS–40	–26.27		
USGS–40	–26.41		
USGS–40	–26.54		

* USGS–40, USGS–41 and IAEA–CH–6 carbon isotopic compositions are defined by the calibration curve.

* Keratin carbon isotopic composition is defined independently from calibration curve

Standard	$\delta^{15}N$ (‰, AIR)
Keratin	+6.36
Keratin	+6.43
Keratin	+6.50
Keratin	+6.44
Keratin	+6.46
USGS–41	+47.57
USGS–40	–4.57
USGS–40	–4.43
N2	+20.44
N2	+20.34

* USGS–40 and USGS–41 nitrogen isotopic compositions are defined by the calibration curve.

* Keratin nitrogen isotopic composition is defined independently from calibration curve

* N2 nitrogen isotopic composition is defined independently from calibration curve

n-Alkanes

Standard: C_{16} to C_{30} *n*-alkane mixture from Indiana University, USA, (prepared by A. Schimmelmann) values in $\delta^{13}C$ ‰ (VPDB).

C_{16}	–26.15	–26.12	–26.13	–26.14	–26.05	–25.96	–26.13	–26.05	–26.28
C_{17}	–31.88	–31.64	–31.72	–31.76	–31.56	–31.63	–31.70	–31.55	–31.36
C_{18}	–31.11	–30.83	–31.01	–30.87	–30.91	–30.92	–30.77	–30.73	–30.55
C_{19}	–31.99	–31.92	–31.95	–31.84	–31.82	–31.86	–31.90	–31.64	–31.47
C_{20}	–32.35	–32.29	–32.35	–32.50	–32.20	–32.20	–32.34	–31.91	–31.70
C_{21}	–29.10	–29.13	–29.15	–28.99	–29.01	–29.28	–29.15	–28.85	–28.78
C_{22}	–32.87	–32.86	–32.91	–32.70	–32.79	–32.91	–32.90	–32.50	–32.21
C_{23}	–31.77	–31.72	–31.68	–31.83	–31.90	–31.71	–31.74	–31.77	–31.29
C_{24}	–33.34	–33.40	–33.28	–33.53	–33.53	–33.44	–33.35	–33.25	–32.75
C_{25}	–28.48	–28.51	–28.50	–28.52	–28.71	–28.60	–28.68	–28.70	–28.81
C_{26}	–32.94	–33.03	–33.07	–32.97	–32.90	–32.94	–32.91	–33.13	–32.78
C_{27}	–30.49	–30.58	–30.48	–30.56	–30.59	–30.61	–30.36	–30.91	–30.53
C_{28}	–32.21	–32.34	–32.22	–32.03	–32.30	–32.32	–32.50	–32.52	–32.22
C_{29}	–31.08	–31.19	–31.29	–31.11	–31.28	–31.05	–31.31	–31.69	–31.27
C_{30}	–29.84	–30.04	–29.84	–30.26	–30.06	–30.18	–29.86	–30.38	–30.10

Compound	Mean $\delta^{13}C$ (‰, VPDB)	Standard deviation	Actual $\delta^{13}C$ (‰, VPDB)
C_{16}	–26.11	0.09	–26.15
C_{17}	–31.61	0.12	–31.88
C_{18}	–30.82	0.14	–31.11
C_{19}	–31.80	0.16	–31.99
C_{20}	–32.19	0.26	–32.35
C_{21}	–29.04	0.17	–29.10
C_{22}	–32.72	0.25	–32.87
C_{23}	–31.70	0.18	–31.77
C_{24}	–33.32	0.25	–33.34
C_{25}	–28.63	0.11	–28.48
C_{26}	–32.97	0.11	–32.94
C_{27}	–30.58	0.16	–30.49
C_{28}	–32.31	0.16	–32.21
C_{29}	–31.27	0.19	–31.08
C_{30}	–30.09	0.19	–29.84
5α-androstane	–31.20	0.14	–31.66

Appendix III describes the sediment depths and age of grain-size measurements obtained.

Core 1334- Niagara basin

Depth (m)	Age (cal BP)	Diameter at 50 % (μm)	Mean diameter (μm)
1.205	2752	8.23	9.50
2.105	4423	6.67	7.92
3.105	6238	5.13	6.52
4.505	8648	7.20	8.67
5.315	10042	6.92	8.43
6.185	11517	6.40	8.00
7.105	12549	8.22	10.04
8.105	12742	4.77	7.96
8.905	12896	9.47	12.62
10.105	13128	3.41	5.03
11.105	13423	3.63	5.09
12.105	14005	3.56	6.34
12.395	14174	2.23	3.71
13.195	15116	2.95	5.30
13.505	15713	2.86	4.63
14.195	16700	2.85	5.21

Core 1335- Mississauga basin

Depth (m)	Age (cal BP)	Diameter at 50 % (μm)	Mean diameter (μm)
1.595	3279	5.34	6.47
2.105	4163	8.34	9.72
3.105	5978	6.81	8.32
4.105	8535	6.49	7.84
5.105	11091	5.46	6.66
6.105	12376	5.25	7.50
7.105	12702	4.02	5.74
8.105	12945	6.87	9.06
8.505	13043	4.92	7.14
9.105	13189	3.92	5.90
10.105	13521	5.61	7.06
11.105	13896	1.84	2.67
12.105	14377	1.98	2.65

13.105	15010	2.47	3.72
14.105	15437	1.97	2.74
14.595	15646	1.83	2.47
15.105	15864	1.94	2.59
16.105	16291	2.05	2.82
17.105	16680	2.15	3.21
18.105		2.00	2.78

Core 1336- Rochester basin

Depth (m)	Age (cal BP)	Diameter at 50 % (μm)	Mean diameter (μm)
2.195	6812	6.12	7.37
3.105	8494	5.04	6.30
4.145	10416	5.41	6.76
5.105	12571	3.54	4.80
6.105	12751	3.04	4.01
6.905	12895	3.19	4.71
7.295	12965	7.49	9.17
8.105	13111	3.13	4.25
9.105	13312	2.32	3.18
10.105	13702	1.79	2.36
11.105	14092	2.03	2.88
12.105	14336	1.66	2.22
13.105	14483	1.73	2.30
14.105	14630	2.05	2.84
15.105	14777	1.89	2.68
16.105	14924	2.03	3.03
17.105		1.97	2.75
18.305		2.33	3.36

Appendix IV reports the mineralogy for each core as determined by powder X-ray diffraction.

Core 1334- Niagara basin

		Weighted peak height (%)							
Depth (m)	Age (cal BP)	Quartz	Plagioclase	Potassium-Feldspar	Kaolinte (0.7 nm)	Illite (1.0 nm)	Chlorite (1.4 nm)	Calcite	Dolomite
0.995	2362	73	5	1	6	12	2	1	1
1.205	2752	78	6	1	5	8	1	1	1
2.105	4423	82	5	1	4	3	1	1	3
2.905	5894	60	4	5	7	12	3	8	1
3.105	6238	67	4	1	4	4	1	13	6
4.505	8648	70	5	1	5	7	1	10	2
5.305	10025	66	4	3	4	6	1	13	2
5.315	10042	66	4	3	4	6	1	13	2
6.185	11517	63	8	1	5	4	1	14	4
6.195	11534	62	7	2	5	6	2	12	3
7.105	12549	64	9	1	3	2	2	15	3
8.105	12742	62	8	3	5	8	4	6	4
8.905	12896	63	8	3	2	6	1	14	4
10.105	13128	56	8	2	4	9	3	14	5
10.505	13205	57	7	2	5	6	2	18	4
11.105	13423	47	7	3	6	9	2	21	5
11.395	13592	57	5	1	6	7	3	17	4
12.105	14005	52	5	2	5	7	2	24	4
12.395	14147	35	8	2	6	12	3	26	6
12.905	14627	30	25	3	3	3	2	31	4
13.195	15116	46	7	2	6	6	1	27	5

13.505	15713	44	7	1	7	10	2	25	4
14.195	16700	37	5	3	8	9	4	30	5
14.905		71	5	2	4	5	1	9	4

Core 1335- Mississauga basin

		Weighted peak height (%)							
Depth (m)	Age (cal BP)	Quartz	Plagioclase	Potassium-Feldspar	Kaolinte (0.7 nm)	Illite (1.0 nm)	Chlorite (1.4 nm)	Calcite	Dolomite
0.995	2240	77	5	1	6	8	1	1	1
1.595	3279	70	6	1	6	9	1	5	3
2.105	4163	64	5	1	3	8	4	13	2
3.105	5978	56	3	2	5	7	1	23	2
3.395	6720	61	2	1	4	10	1	18	2
4.105	8535	45	4	2	4	9	1	32	2
5.105	11091	57	7	1	5	7	3	17	3
5.395	11623	60	5	1	5	8	1	16	5
6.105	12376	62	4	1	3	6	2	19	3
6.505	12556	58	6	3	5	8	2	15	3
7.105	12702	54	8	1	4	9	2	18	4
7.505	12799	61	5	2	4	8	1	17	3
7.995	12919	54	7	1	5	4	1	25	4
8.105	12945	59	7	2	4	4	1	20	3
8.505	13043	52	8	3	5	8	3	17	4
9.105	13189	53	10	4	4	9	4	12	5
9.505	13296	57	15	3	5	7	1	9	3
10.105	13521	62	7	2	5	4	2	15	4
10.905	13821	68	8	1	5	7	2	6	3
11.105	13896	48	13	6	6	18	4	3	3
12.105	14377	46	14	4	9	16	6	4	2
12.705	14839	59	9	3	6	12	1	6	3

13.105	15010	58	12	2	5	12	2	5	4
13.905	15352	49	12	8	7	17	3	1	4
14.105	15437	38	12	5	10	20	8	3	3
14.595	15646	41	13	6	12	19	4	2	3
15.105	15864	42	14	5	8	20	4	4	4
16.105	16291	43	13	6	14	13	2	4	5
17.105	16680	46	12	6	8	16	7	2	3
17.705		45	12	5	6	22	4	3	3
18.105		44	15	4	8	17	5	5	1

Core 1336- Rochester basin

		Weighted peak height (%)							
Depth (m)	Age (cal BP)	Quartz	Plagioclase	Potassium-Feldspar	Kaolinte (0.7 nm)	Illite (1.0 nm)	Chlorite (1.4 nm)	Calcite	Dolomite
1.595	5701	62	4	2	6	8	2	14	3
2.195	6812	53	5	1	4	7	3	26	2
3.105	8494	54	4	1	5	9	2	22	3
3.795	9769	43	2	1	4	8	1	38	3
4.145	10416	43	3	1	4	6	2	38	3
4.905	12535	63	5	1	7	10	1	11	3
5.105	12571	58	5	2	8	11	2	11	4
5.705	12679	62	5	2	6	6	3	13	3
6.105	12751	50	5	2	7	12	5	15	3
6.905	12895	50	5	3	5	8	2	20	7
7.295	12965	67	6	2	4	4	1	10	5
7.905	13075	75	6	2	5	3	1	4	4
8.105	13111	55	11	4	6	13	3	4	4
8.705	13219	55	10	3	6	6	2	8	3
9.105	13312	55	13	3	4	15	5	3	3
10.105	13702	41	15	5	6	22	4	4	3
10.905	14014	56	14	7	6	10	3	2	1
11.105	14092	45	13	5	9	17	5	2	4
12.105	14336	45	14	4	8	19	6	3	3
12.995	14467	52	16	6	6	10	7	2	1
13.105	14483	43	15	4	8	16	4	4	6

14.105	14630	45	16	5	8	16	4	4	4
14.995	14761	64	13	4	6	9	2	2	2
15.105	14777	42	14	4	7	21	4	4	3
16.105	14924	47	11	5	9	18	4	3	2
16.905	15041	53	9	9	8	13	2	5	3
17.105		45	13	4	10	17	4	3	4
18.305		57	9	3	7	12	4	3	4
18.705		66	9	4	7	7	2	1	3

Appendix V ostracode valves and clam shells carbon and oxygen-isotopic compositions. Calculated lakewater oxygen-isotope compositions are also reported.

Core 1334- Niagara basin (*Candona subtriangulata*)

Depth (m)	Age (cal BP)	Ostracode $\delta^{13}C$ (‰, VPDB)	Ostracode $\delta^{18}O$ (‰, VPDB)	Lakewater $\delta^{18}O$ (‰,VSMOW)
5.85	10959	–3.51	–4.85	–9.94
6.25	11636	–3.52	–3.98	–9.07
6.45	11974	–3.75	–4.60	–9.69
6.65	12312	–3.84	–4.76	–9.85
6.85	12500	–3.62	–6.07	–11.17
7.05	12539	–3.47	–5.41	–10.50
7.25	12578	–2.58	–8.08	–13.19
7.45	12616	–4.45	–8.32	–13.43
7.65	12655	–4.20	–5.58	–10.68
7.85	12693	–3.51	–6.61	–11.71
8.05	12732	–4.02	–7.99	–13.10
8.25	12771	–3.75	–13.00	–18.13
8.45	12809	–3.56	–7.71	–12.82
8.65	12848	–2.71	–12.50	–17.63
8.85	12887	–3.82	–11.22	–16.34
9.05	12925	–1.45	–12.71	–17.84
9.25	12964	–4.08	–11.06	–16.18
9.45	13003	–2.84	–11.97	–17.10
9.65	13041	–3.01	–12.23	–17.36
9.85	13080	–3.90	–12.73	–17.86
10.05	13119	–3.37	–12.76	–17.89
10.25	13157	–2.47	–12.65	–17.78
10.45	13196	–3.05	–12.99	–18.12
11.05	13394	–4.41	–13.07	–18.20
11.25	13510	–3.36	–12.67	–17.80
11.45	13627	–3.90	–12.69	–17.82
11.65	13743	–3.21	–12.82	–17.95
11.85	13860	–3.24	–12.51	–17.64
12.05	13976	–3.69	–12.64	–17.77
12.45	14209	–3.46	–12.65	–17.78
12.85	14580	–3.66	–11.98	–17.11
13.05	14846	–3.70	–12.44	–17.57
13.25	15231	–4.02	–12.70	–17.83
13.45	15617	–4.43	–12.58	–17.71

13.65	16002	–3.70	–12.58	–17.71
13.85	16388	–3.46	–12.63	–17.76
14.25		–4.29	–12.55	–17.68
14.45		–4.12	–12.69	–17.82
14.65		–3.82	–12.02	–17.15
14.85		–3.86	–12.52	–17.65

Core 1334– Niagara basin (*Pisidium* sp. clams)

Depth (m)	Age (cal BP)	Clam $\delta^{13}C$ (‰, VPDB)	Clam $\delta^{18}O$ (‰, VPDB)	Lakewater $\delta^{18}O$ (‰,VSMOW)
4.05	7873	+0.63	–1.80	–4.67
4.45	8562	–0.01	–1.52	–4.38
4.65	8906	+0.56	–1.32	–4.18
4.85	9250	+0.01	–2.12	–4.99
5.05	9595	–0.04	–1.73	–4.59
5.25	9939	+0.15	–2.29	–5.16
5.45	10283	–0.47	–2.38	–5.25
5.65	10621	–2.21	–4.29	–7.17
5.85	10959	–3.05	–5.91	–8.80
6.25	11636	–2.56	–6.18	–9.07
6.45	11974	–3.45	–5.86	–8.75
6.65	12312	–3.26	–7.59	–10.48
6.85	12500	–2.96	–9.48	–12.38
7.05	12539	–2.65	–9.94	–12.85
7.25	12578	–3.26	–9.51	–12.41
7.45	12616	–2.60	–10.20	–13.11
7.65	12655	–3.78	–9.77	–12.68
7.85	12693	–3.48	–9.46	–12.36
8.45	12809	+0.50	–2.48	–5.35
9.45	13003	–2.27	–9.35	–12.25

Core 1335– Mississauga basin (*Candona subtriangulata*)

Depth (m)	Age (cal BP)	Ostracode $\delta^{13}C$ (‰, VPDB)	Ostracode $\delta^{18}O$ (‰, VPDB)	Lakewater $\delta^{18}O$ (‰,VSMOW)
3.65	7384	–5.76	–2.01	–7.09
3.85	7896	–6.36	–2.00	–7.08
4.05	8407	–5.10	–1.60	–6.68
5.25	11475	–4.59	–3.08	–8.16
5.45	11687	–4.35	–4.66	–9.75
5.65	11899	–4.66	–5.76	–10.86
5.85	12111	–4.79	–5.32	–10.41
6.05	12323	–5.11	–4.79	–9.88
6.25	12495	–4.46	–7.72	–12.83
6.45	12543	–3.24	–9.10	–14.21
6.65	12592	–4.86	–8.47	–13.58
6.85	12641	–3.52	–8.93	–14.04
7.05	12690	–4.99	–9.76	–14.88
7.25	12738	–4.68	–8.75	–13.86
7.45	12787	–2.99	–8.70	–13.81
7.65	12836	–4.64	–8.11	–13.22
7.85	12885	–4.58	–8.06	–13.17
8.05	12933	–4.80	–6.87	–11.97
8.25	12982	–3.53	–7.63	–12.74
8.45	13031	–3.19	–6.72	–11.82
8.65	13080	–4.60	–7.94	–13.05
8.85	13128	–3.11	–10.71	–15.83
9.05	13177	–3.37	–11.89	–17.02
9.45	13277	–4.22	–12.65	–17.78
9.65	13352	–3.37	–12.71	–17.84
9.85	13427	–4.53	–12.54	–17.67
10.05	13502	–5.20	–13.59	–18.73
10.25	13577	–5.23	–11.85	–16.98
10.45	13652	–5.12	–11.13	–16.25
10.65	13727	–5.46	–11.31	–16.43
10.85	13802	–4.88	–12.98	–18.11
11.05	13877	–4.85	–13.87	–19.01
11.25	13952	–5.13	–13.30	–18.43
11.45	14027	–6.30	–12.20	–17.33
11.65	14102	–5.53	–12.33	–17.46
11.85	14177	–5.08	–11.87	–17.00
12.05	14317	–5.05	–13.38	–18.52

12.45	14732	–4.13	–13.36	–18.50
12.65	14818	–4.17	–12.93	–18.06
12.85	14903	–4.51	–13.27	–18.40
13.05	14989	–3.73	–13.25	–18.38
13.25	15074	–5.13	–12.93	–18.06
13.45	15160	–5.56	–12.49	–17.62
13.65	15245	–6.17	–11.52	–16.65
13.85	15330	–5.92	–11.58	–16.71
14.05	15416	–4.29	–13.22	–18.35
14.45	15587	–5.37	–13.05	–18.18
14.65	15672	–7.13	–12.02	–17.15
14.85	15758	–8.57	–10.91	–16.03
15.05	15843	–6.29	–13.20	–18.33
15.25	15928	–6.59	–12.41	–17.54
15.45	16014	–5.24	–12.76	–17.89
15.65	16099	–5.19	–13.11	–18.24
15.85	16185	–4.19	–13.27	–18.40
16.05	16270	–5.27	–12.98	–18.11
16.45	16441	–4.10	–12.65	–17.78
16.65	16526	–6.32	–12.64	–17.77
16.85	16612	–5.13	–12.82	–17.95
17.05	16680	–6.51	–12.92	–18.05
17.25		–5.72	–12.94	–18.07
17.45		–5.83	–13.28	–18.41
17.65		–5.31	–13.16	–18.29
17.85			–12.85	–17.98
18.05		–6.25	–11.91	–17.04

Core 1335– Mississauga basin (*Pisidium* sp. clams)

Depth (m)	Age (cal BP)	Clam $\delta^{13}C$ (‰, VPDB)	Clam $\delta^{18}O$ (‰, VPDB)	Lakewater $\delta^{18}O$ (‰,VSMOW)
3.05	5850	+0.66	–1.16	–4.02
3.45	6873	+0.31	–1.97	–4.84
3.65	7384	+0.83	–1.97	–4.84
4.05	8407	+0.48	–1.94	–4.81
4.45	9429	+0.57	–1.97	–4.84
4.65	9941	–0.27	–2.22	–5.09
4.85	10452	–0.41	–2.25	–5.12
5.05	10963	–0.99	–2.77	–5.64
5.25	11475	–1.54	–4.01	–6.89
5.45	11687	–2.16	–5.12	–8.00
5.65	11899	–2.27	–5.21	–8.09
5.85	12111	–3.21	–5.82	–8.71
6.05	12323	–2.94	–5.94	–8.83

Core 1335– Mississauga basin (*Fabaeformiscandona caudata*)

Depth (m)	Age (cal BP)	Clam $\delta^{13}C$ (‰, VPDB)	Clam $\delta^{18}O$ (‰, VPDB)	Lakewater $\delta^{18}O$ (‰,VSMOW)
3.05	5850	–2.94	+0.16	–4.91

Core 1336– Rochester basin (*Candona subtriangulata*)

Depth (m)	Age (cal BP)	Ostracode $\delta^{13}C$ (‰, VPDB)	Ostracode $\delta^{18}O$ (‰, VPDB)	Lakewater $\delta^{18}O$ (‰,VSMOW)
1.65	5813	–2.03	–1.31	–6.39
2.65	7662	–4.45	–0.81	–5.89
2.85	8032	–5.48	–1.18	–6.26
3.05	8401	–4.96	–1.65	–6.73
3.25	8771	–4.95	–1.18	–6.26
3.45	9141	–5.40	–1.94	–7.02
3.65	9511	–3.77	–1.81	–6.89
3.85	9880	–2.90	–1.46	–6.54
4.09	10324	–3.05	–1.71	–6.79
4.25	10620	–2.70	–1.68	–6.76
4.45	11628	–4.62	–3.26	–8.35
4.65	12490	–2.92	–4.11	–9.20
4.85	12526	–3.08	–4.51	–9.61
5.05	12562	–3.99	–5.00	–10.10
5.25	12598	–5.47	–5.33	–10.43
5.45	12634	–5.40	–7.40	–12.51
5.65	12670	–2.05	–8.58	–13.70
5.85	12706	–5.12	–8.66	–13.78
6.05	12742	–4.47	–8.86	–13.98
6.65	12850	–3.41	–8.93	–14.05
6.85	12886	–3.19	–7.40	–12.51
7.25	12958	–4.71	–9.80	–14.92
7.45	12994	–3.01	–12.40	–17.54
7.65	13030	–3.55	–12.62	–17.76
7.85	13066	–5.34	–12.91	–18.05
8.05	13102	–3.88	–12.87	–18.01
8.25	13138	–3.53	–12.85	–17.99
8.45	13174	–3.52	–13.05	–18.19
8.65	13210	–4.76	–13.73	–18.87
8.85	13246	–5.06	–13.97	–19.11
10.05	13683	–6.23	–13.59	–18.73
10.65	13917	–6.43	–11.50	–16.63
10.85	13995	–5.68	–12.70	–17.84
11.25	14151	–7.84	–12.00	–17.13
11.45	14229	–7.50	–11.31	–16.44
11.65	14270	–6.50	–10.49	–15.62
12.05	14329	–7.16	–11.62	–16.75

12.25	14358	–5.74	–12.71	–17.85
12.45	14388	–7.05	–11.73	–16.86
12.85	14447	–4.91	–9.27	–14.39
13.05	14476	–5.66	–12.09	–17.22
13.25	14505	–5.66	–11.58	–16.71
13.45	14535	–6.58	–11.64	–16.77
13.65	14564	–5.76	–11.48	–16.61
13.85	14593	–8.69	–11.12	–16.25
14.05	14623	–6.01	–11.83	–16.96
14.25	14652	–5.12	–12.29	–17.42
14.45	14681	–5.52	–12.05	–17.18
14.65	14711	–6.94	–12.53	–17.67
14.85	14740	–7.61	–11.51	–16.64
15.05	14770	–4.57	–11.28	–16.41
15.25	14799	–4.72	–12.79	–17.93
15.45	14828	–4.49	–13.22	–18.36
15.65	14858	–5.30	–11.99	–17.12
15.85	14887	–6.30	–12.36	–17.50
16.05	14916	–4.39	–13.18	–18.32
16.25	14946	–7.09	–11.76	–16.89
16.45	14975	–3.60	–12.94	–18.08
16.65	15004	–4.69	–12.62	–17.76
16.85	15034	–4.44	–13.44	–18.58
17.05	15060	–3.08	–12.83	–17.97
17.25		–4.83	–12.61	–17.75
17.45		–6.45	–12.10	–17.23
17.65		–4.47	–13.43	–18.57
17.85		–3.50	–13.02	–18.16
18.05		–4.25	–12.97	–18.11
18.25		–4.42	–12.83	–17.97
18.45		–4.07	–12.95	–18.09
18.65		–4.71	–12.78	–17.92

Core 1336– Rochester basin (*Pisidium* sp. clams)

Depth (m)	Age (cal BP)	Clam $\delta^{13}C$ (‰, VPDB)	Clam $\delta^{18}O$ (‰, VPDB)	Lakewater $\delta^{18}O$ (‰,VSMOW)
3.05	8401	+0.43	–2.00	–4.90
3.25	9141	+0.97	–1.57	–4.47
4.25	10620	–0.30	–2.71	–5.62
4.45	11628	–2.23	–4.78	–7.70

Core 1336– Rochester basin (*Fabaeformiscandona caudata*)

Depth (m)	Age (cal BP)	Ostracode $\delta^{13}C$ (‰, VPDB)	Ostracode $\delta^{18}O$ (‰, VPDB)	Lakewater $\delta^{18}O$ (‰,VSMOW)
1.85	6183	–2.89	–1.23	–6.31
2.45	7292	–1.58	–0.78	–5.86
2.65	7662	–2.84	–1.00	–6.08
2.85	8032	–2.83	–0.49	–5.57
3.05	8401	–5.34	–1.70	–6.78
3.25	8771	–2.59	–0.99	–6.07
3.85	9880	–4.62	–1.71	–6.79
4.09	10324	–4.16	–1.46	–6.54

Appendix VI bulk organic matter carbon and nitrogen elemental and isotopic compositions. Calculated molar carbon to nitrogen ratios are also reported.

Core 1334- Niagara basin

Depth (m)	Age (cal BP)	TN (%)	OC (%)	C/N	δ^{15}N (‰, AIR)	δ^{13}C (‰, VPDB)
0.995	2362	0.20	1.47	8.7	+3.92	–27.21
1.205	2752	0.18	1.37	8.7	+3.87	–27.48
2.105	4423	0.15	1.15	8.7	+3.77	–27.50
2.905	5894	0.14	1.02	8.6	+3.57	–27.41
3.105	6238	0.11	0.68	7.4	+3.82	–27.48
4.505	8648	0.17	1.46	10.1	+4.59	–27.67
5.305	10025	0.16	1.34	9.8	+4.22	–27.76
5.315	10042	0.15	1.25	9.6	+4.18	–27.72
6.185	11517	0.06	0.43	8.8		–27.85
6.195	11534	0.06	0.45	8.8		–29.25
7.105	12549					–27.97
8.105	12742	0.04	0.23	7.0		–27.15
8.905	12896	0.02	0.15	7.3		–27.36
10.105	13128	0.03	0.26	8.9		
10.505	13205	0.04	0.27	8.2		–27.87
11.105	13423	0.05	0.29	7.5		
11.395	13592	0.05	0.34	7.4		–28.53
12.105	14005	0.05	0.33	7.9		–28.25
12.905	14627	0.03	0.26	8.8		
13.195	15116	0.04	0.29	7.5		–28.85
13.505	15713	0.05	0.37	8.4		
14.195		0.04	0.28	7.6		–28.5
14.905		0.03	0.26	9.3		

Core 1335– Mississauga basin

Depth (m)	Age (cal BP)	TN (%)	OC (%)	C/N	δ^{15}N (‰, AIR)	δ^{13}C (‰, VPDB)
0.505	1391	0.25	1.77	8.4	+4.30	–27.42
0.995	2240	0.20	1.56	8.9	+4.13	–27.82
1.595	3279	0.17	1.19	8.2	+4.08	–27.71
2.105	4163	0.28	2.23	9.2	+4.58	–27.64
3.105	5978	0.20	1.77	10.2	+4.63	–27.90
3.395	6720	0.21	1.78	9.8	+4.57	–28.10
4.105	8535	0.19	1.55	9.5	+4.22	–28.04
5.105	11091	0.13	1.07	9.5	+4.57	–28.30
5.395	11623	0.08	0.63	9.2		–28.84
6.105	12376	0.06	0.44	8.4		–29.13
6.505	12556	0.05	0.39	8.7		–28.01
7.105	12702	0.05	0.31	7.9		–27.86
7.505	12799	0.05	0.32	7.0		–27.73
7.995	12919	0.04	0.29	8.3		–28.25
8.105	12945	0.03	0.23	7.9		
8.505	13043	0.04	0.22	7.0		–28.23
9.105	13189	0.04	0.24	6.7		
9.505	13296	0.04	0.27	7.6		–27.28
10.105	13521	0.04	0.22	7.3		
10.905	13821	0.04	0.27	7.8		–27.41
11.105	13896	0.04	0.26	6.9		
12.105	14377	0.04	0.24	6.6		–27.16
12.705	14839	0.04	0.27	8.0		
13.105	15010	0.04	0.24	6.8		–27.29
13.905	15352	0.04	0.28	8.3		
14.105	15437	0.04	0.24	6.7		–27.59
14.595	15646	0.04	0.25	7.0		
15.105	15864	0.04	0.25	7.0		–27.07
16.105	16291	0.04	0.25	7.0		–27.27
17.105		0.04	0.25	7.1		–27.13
17.705		0.04	0.26	7.7		
18.105		0.04	0.24	7.1		–27.19

Core 1336– Rochester basin

Depth (m)	Age (cal BP)	TN (%)	OC (%)	C/N	δ^{15}N (‰, AIR)	δ^{13}C (‰, VPDB)
1.015	4563	0.20	1.53	8.8	+3.96	–27.49
1.595	5701	0.15	0.94	7.4	+3.84	–27.39
2.195	6812	0.23	1.89	9.5	+4.44	
3.105	8494	0.15	1.27	10.0	+4.30	–27.93
3.795	9769	0.16	1.30	9.5	+4.04	–28.76
4.145	10416	0.15	1.26	9.6	+4.10	–28.95
4.595	12334	0.10	0.71	8.4	+4.40	–28.61
4.905	12535	0.09	0.59	7.8		–29.16
5.105	12571	0.09	0.61	7.9		–29.28
5.705	12679	0.07	0.41	7.0		–28.15
6.105	12751	0.06	0.36	6.7		–27.98
6.905	12895	0.05	0.32	7.3		–28.52
7.295	12965	0.03	0.22	7.6		–28.18
7.105	13075	0.05	0.32	7.0		–27.73
7.905	13111	0.05	0.31	7.3		–27.45
8.105	13219	0.04	0.30	7.8		–27.51
8.705	13312	0.05	0.26	6.6		
9.105	13702	0.05	0.29	7.4		–27.45
10.105	14014	0.04	0.28	7.7		–27.54
10.905	14092	0.05	0.28	6.9		
11.105	14336	0.04	0.29	7.5		–27.55
12.105	14467	0.04	0.29	7.8		–27.84
12.995	14483	0.04	0.27	7.2		
13.105	14630	0.04	0.26	7.2		
14.105	14777	0.05	0.29	7.4		–27.76
15.105	14924	0.05	0.32	8.0		–27.83
16.105		0.05	0.30	7.4		
17.105		0.05	0.37	8.4		–28.20
18.305		0.05	0.38	8.5		

Appendix VII reports the *n*-alkane abundances and carbon isotopic compositions.

Core 1336- Rochester basin

Depth (m)	Age (cal BP)	Abundance (μg/g)									
		C_{17}	C_{19}	C_{21}	C_{23}	C_{25}	C_{27}	C_{29}	C_{31}	C_{33}	C_{35}
0.515	3583	0.52	0.33	0.38	0.34	0.31	0.35	0.47	0.36	0.13	0.08
1.38	5289	0.23	0.32	0.36	0.31	0.29	0.35	0.42	0.34	0.14	0.07
1.91	6294	0.25	0.51	0.34	0.34	0.28	0.36	0.47	0.38	0.23	0.05
2.315	7033	0.13	0.18	0.30	0.41	0.39	1.02	0.52	0.38	0.14	0.05
2.715	7773	0.18	0.22	0.35	0.44	0.34	0.42	0.63	0.45	0.19	0.06
3.105	8512	0.26	0.25	0.30	0.37	0.26	0.30	0.38	0.29	0.11	0.04
4.31	10922	0.30	0.45	0.27	0.32	0.25	0.37	0.33	0.23	0.13	0.03
5.13	12577	0.31	0.45	0.46	0.44	0.32	0.34	0.30	0.23	0.20	0.14
5.51	12645	0.35	0.47	0.44	0.38	0.30	0.31	0.29	0.23	0.19	0.06
5.99	12731	0.48	0.46	0.44	0.35	0.29	0.29	0.26	0.21	0.17	0.04
6.97	12908	0.27	0.32	0.27	0.26	0.22	0.26	0.26	0.23	0.25	0.08
7.51	13005	0.27	0.30	0.30	0.31	0.27	0.27	0.26	0.20	0.16	0.04
7.96	13086	0.19	0.22	0.24	0.28	0.25	0.27	0.25	0.20	0.19	0.03
8.99	13271	0.08	0.17	0.21	0.33	0.32	0.38	0.32	0.25	0.10	0.04
9.99	13659	0.15	0.18	0.18	0.23	0.18	0.18	0.14	0.09	0.04	0.01
10.99	14049	0.15	0.21	0.25	0.39	0.35	0.35	0.27	0.19	0.08	0.03
11.99	14320	0.16	0.19	0.22	0.30	0.26	0.26	0.21	0.15	0.06	0.02
14.93	14752	0.18	0.24	0.25	0.30	0.25	0.27	0.22	0.17	0.12	0.04
16.51	14984	0.37	0.39	0.39	0.43	0.37	0.40	0.34	0.26	0.13	0.05

Depth (m)	Age (cal BP)	$\delta^{13}C$ (‰,VPDB)								
		C_{17}	C_{19}	C_{21}	C_{23}	C_{25}	C_{27}	C_{29}	C_{31}	C_{33}
0.515	3583	–34.0	–31.4	–32.3	–33.4	–30.5	–30.7	–31.1	–31.1	–30.4
1.38	5289	–31.6	–31.2	–32.0	–31.7	–30.1	–30.1	–30.9	–30.9	–30.8
1.91	6294	–31.8	–32.5	–32.5	–31.4	–29.7	–30.4	–31.0	–31.4	–30.9
2.315	7033	–30.3	–30.8	–31.8	–32.4	–28.3	–33.0	–29.9	–30.3	–29.4
2.715	7773	–29.6	–31.3	–29.9	–30.9	–25.1	–26.8	–28.9	–30.3	–30.1
3.105	8512	–29.6	–30.3	–30.0	–33.6	–28.2	–29.3	–30.8	–30.9	–30.0
4.31	10922	–29.7	–30.0	–30.8	–32.8	–28.6	–31.1	–30.5	–31.5	–31.2
5.13	12577	–29.8	–30.4	–31.8	–32.4	–31.2	–31.8	–31.2	–31.2	–31.1
5.51	12645	–30.7	–30.7	–31.4	–31.8	–31.7	–31.5	–31.9	–32.8	–32.3
5.99	12731	–29.9	–29.2	–31.2	–31.2	–32.9	–31.2	–31.8	–32.4	–31.4
6.97	12908	–29.3	–29.8	–31.3	–31.5	–31.5	–32.0	–32.2	–32.4	–32.0
7.51	13005	–30.3	–30.5	–31.5	–32.3	–31.7	–31.6	–32.4	–33.2	–33.3
7.96	13086	–29.5	–30.0	–31.5	–31.5	–31.6	–31.5	–32.0	–32.8	–32.2
8.99	13271	–29.7	–30.0	–30.5	–31.6	–31.7	–31.5	–31.9	–32.0	–32.0
9.99	13659	–29.1	–30.3	–30.4	–31.2	–31.9	–31.4	–31.8	–32.3	–31.7
10.99	14049	–29.9	–29.5	–30.0	–31.4	–31.2	–31.4	–32.2	–31.7	–31.5
11.99	14320	–29.1	–29.4	–30.3	–32.0	–32.2	–31.9	–32.3	–32.7	–31.3
14.93	14752	–29.8	–30.2	–31.6	–31.7	–31.9	–32.0	–32.6	–33.2	–32.5
16.51	14984	–30.2	–29.8	–32.8	–32.9	–33.3	–32.6	–33.2	–33.4	–33.6

Appendix VIII provides the gas-chromatograph spectrums used to calculate *n*-alkane abundances.

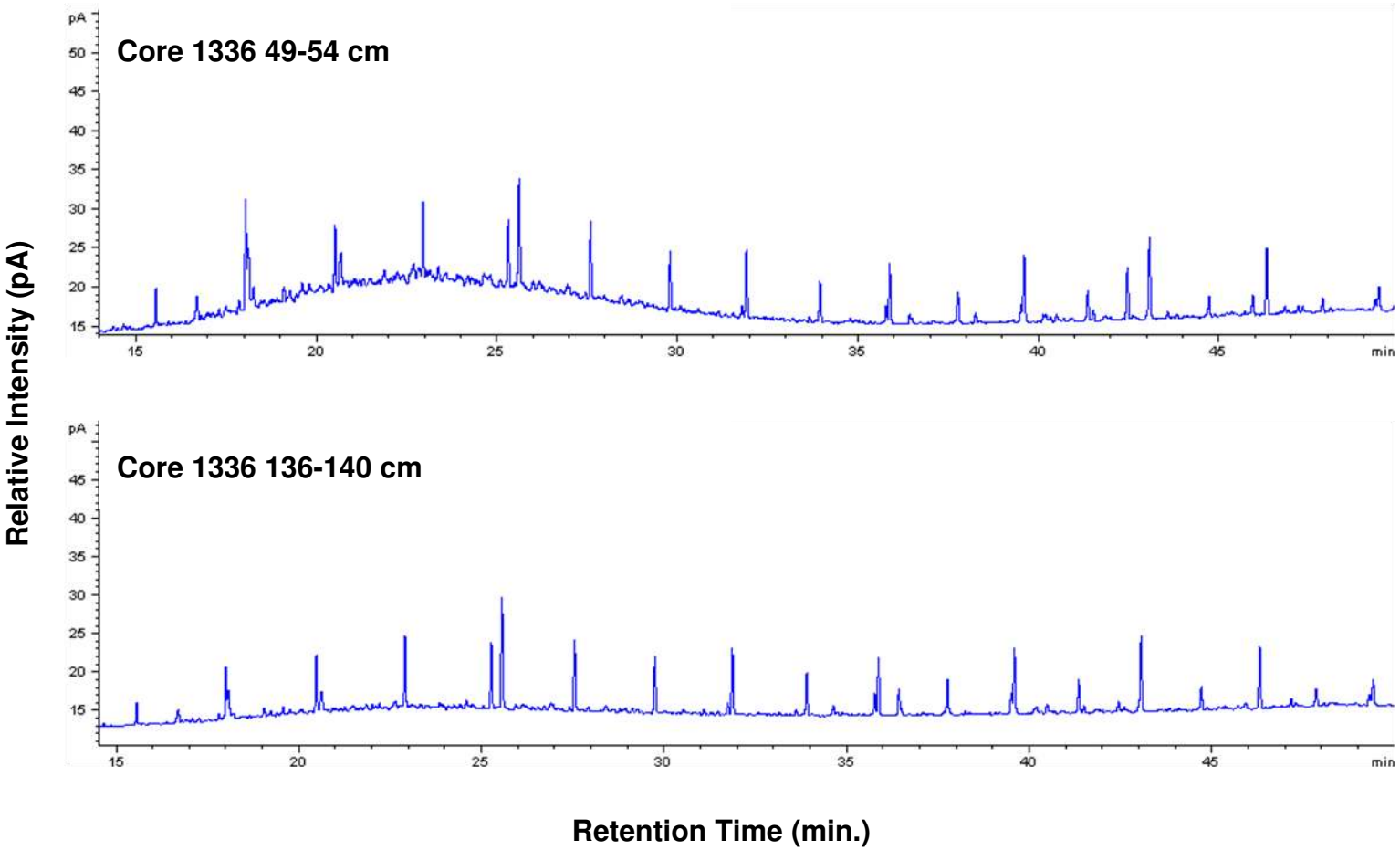

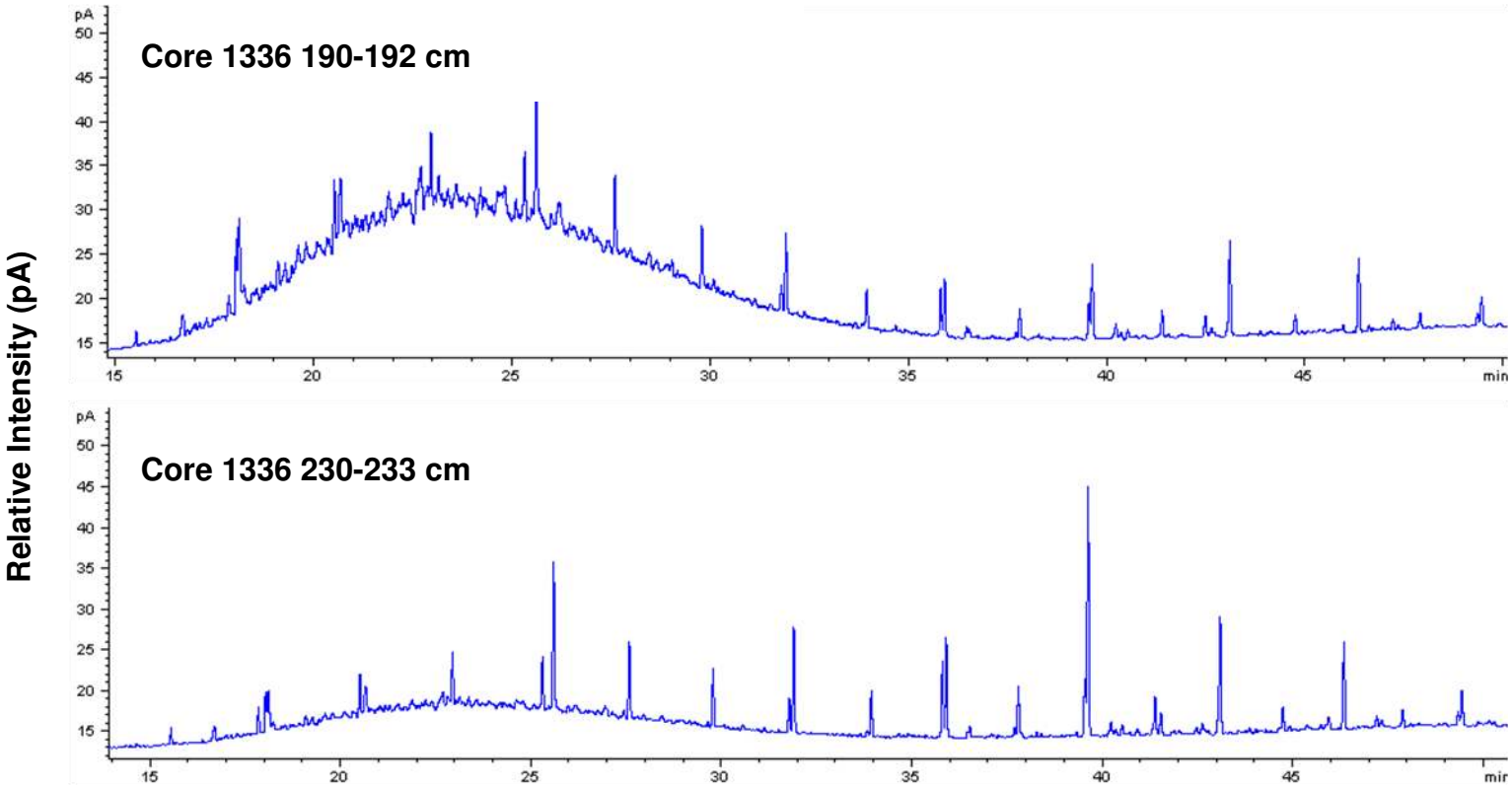
Core 1336 190-192 cm
Core 1336 230-233 cm
pA
50
45
40
35
30
25
20
15
15
20
25
30
35
40
45
min
mir
Relative Intensity (pA)
Retention Time (min.)

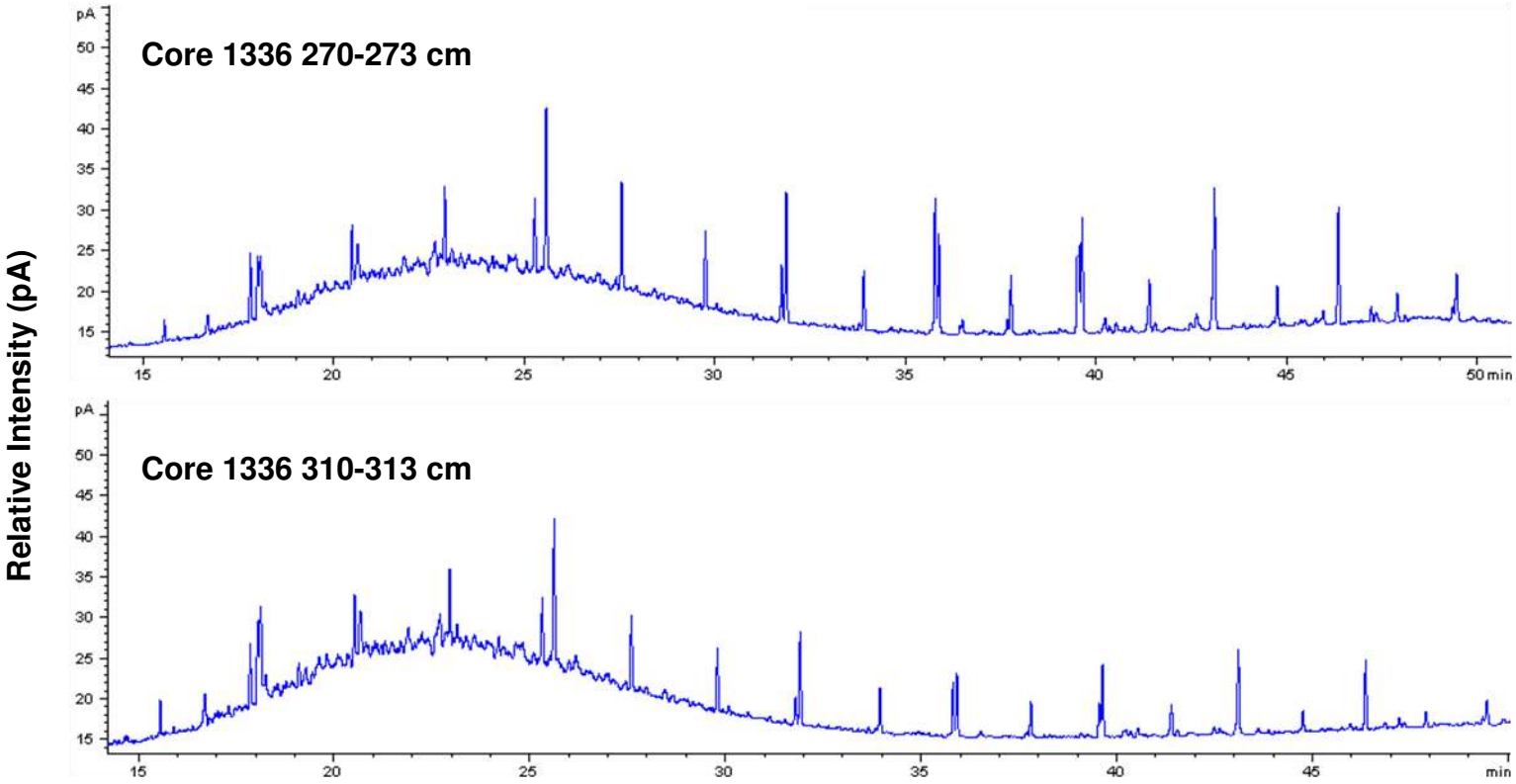
Core 1336 270-273 cm
Core 1336 310-313 cm
pA
50
45
40
35
30
25
20
15
15
20
25
30
35
40
45
50 min
min
Relative Intensity (pA)
Retention Time (min.)

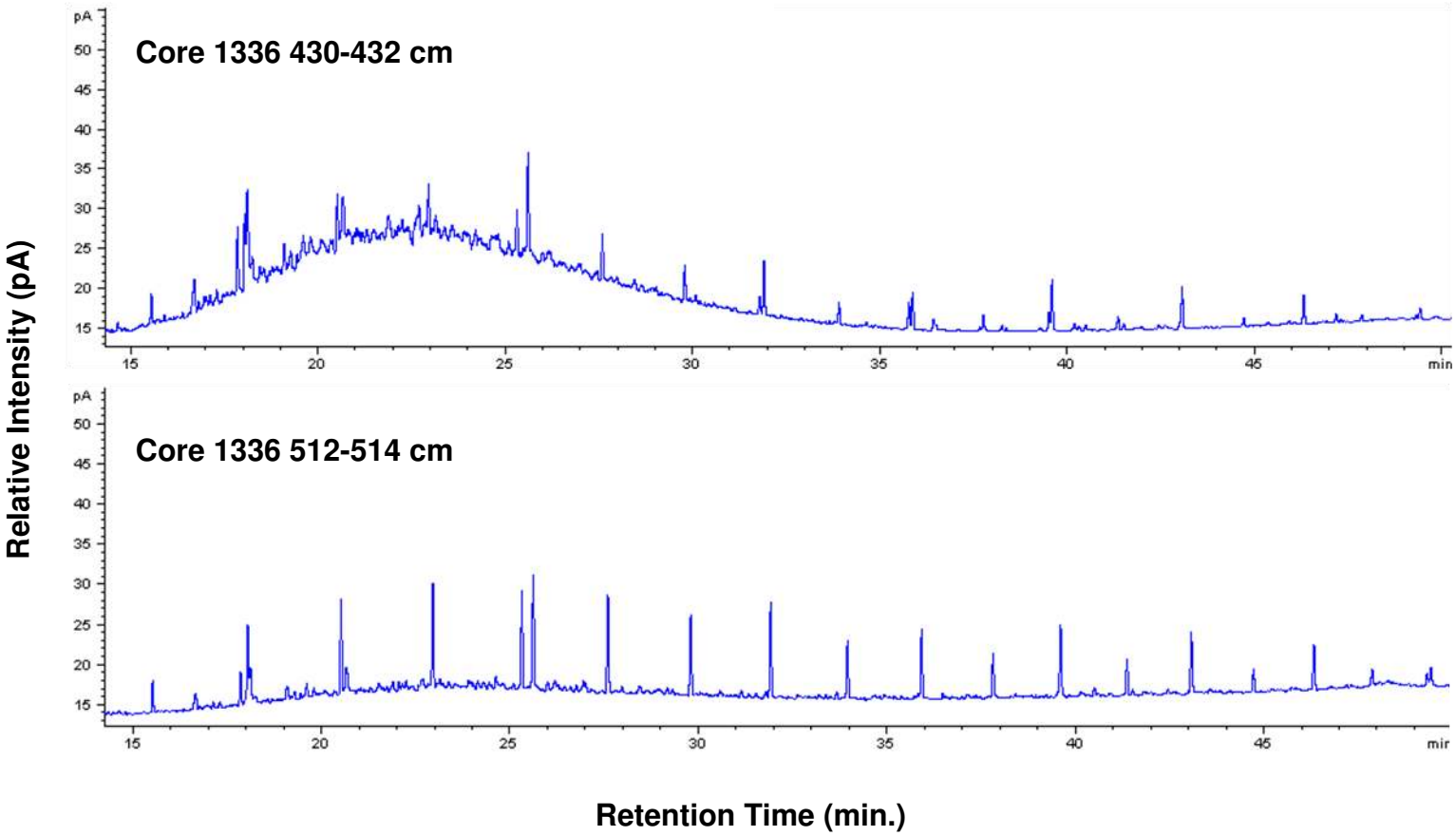
Core 1336 430-432 cm
Core 1336 512-514 cm
pA
50
45
40
35
30
25
20
15
15
20
25
30
35
40
45
min
mir
Relative Intensity (pA)
Retention Time (min.)

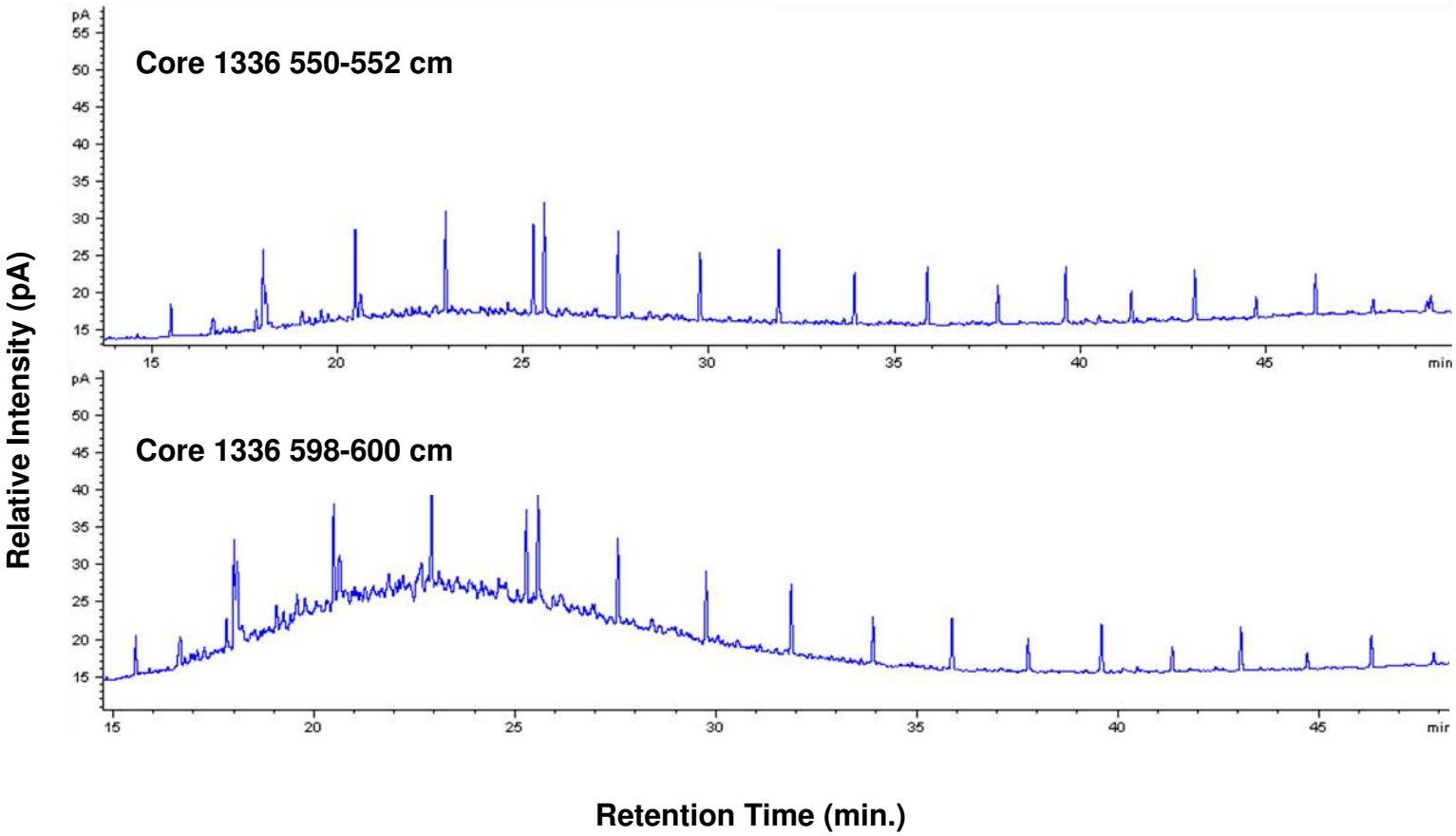
Core 1336 550-552 cm
Core 1336 598-600 cm
pA
55
50
45
40
35
30
25
20
15
15
20
25
30
35
40
45
min
mir
Relative Intensity (pA)
Retention Time (min.)

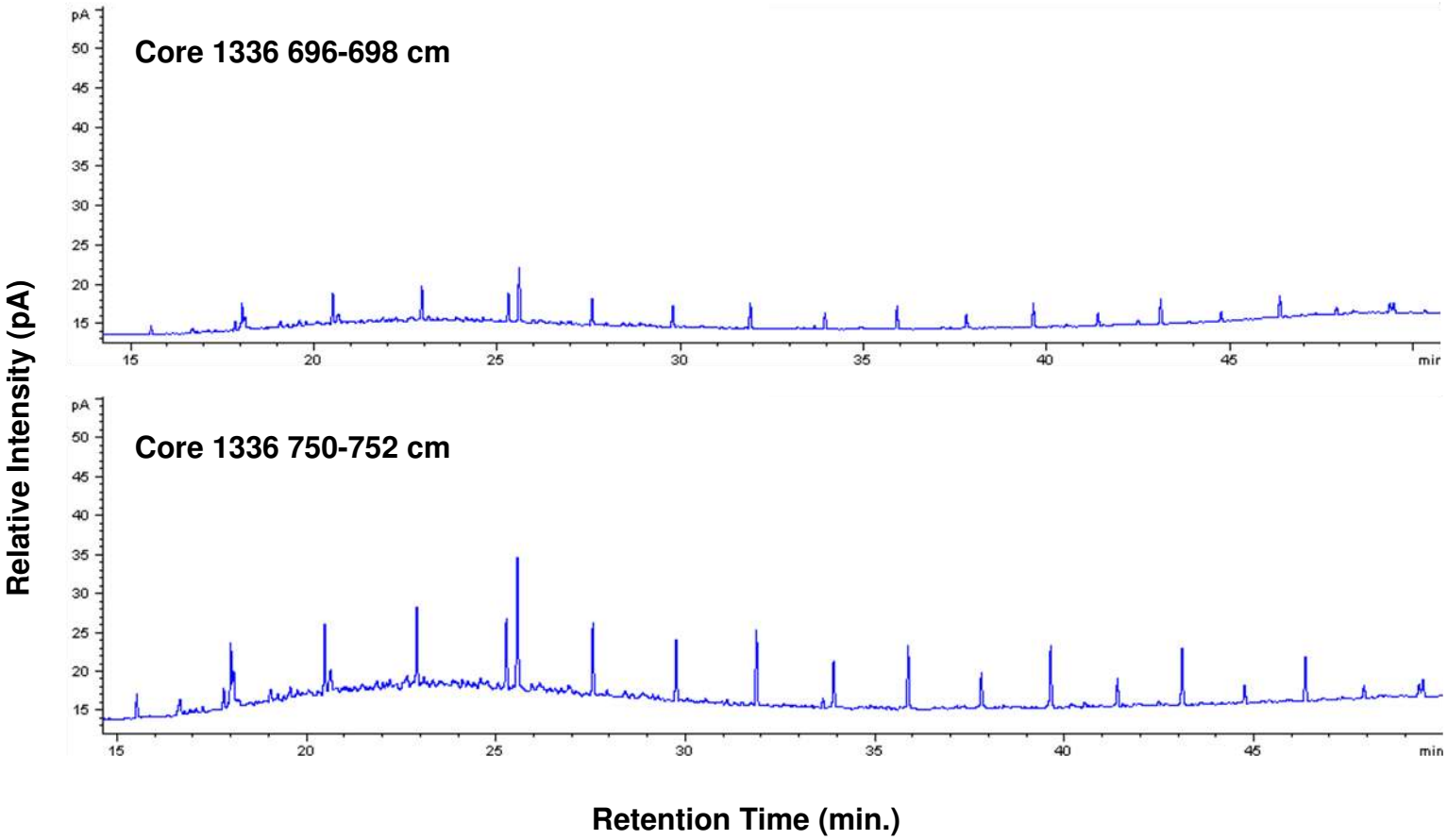
Core 1336 696-698 cm
Core 1336 750-752 cm
pA
50
45
40
35
30
25
20
15
15
20
25
30
35
40
45
min
Relative Intensity (pA)
Retention Time (min.)

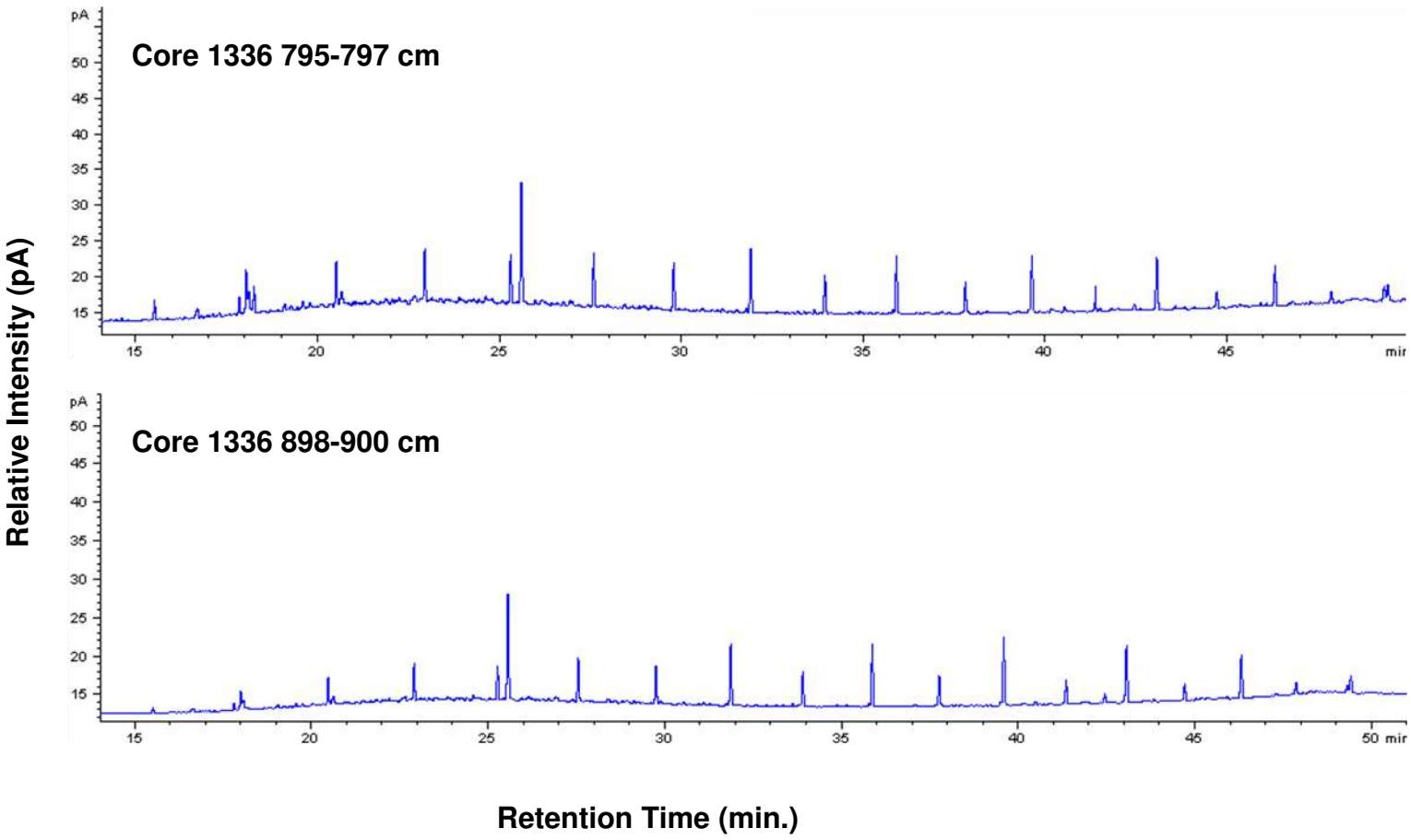
Core 1336 795-797 cm
Core 1336 898-900 cm
pA
50
45
40
35
30
25
20
15
15
20
25
30
35
40
45
50 min
Relative Intensity (pA)
Retention Time (min.)

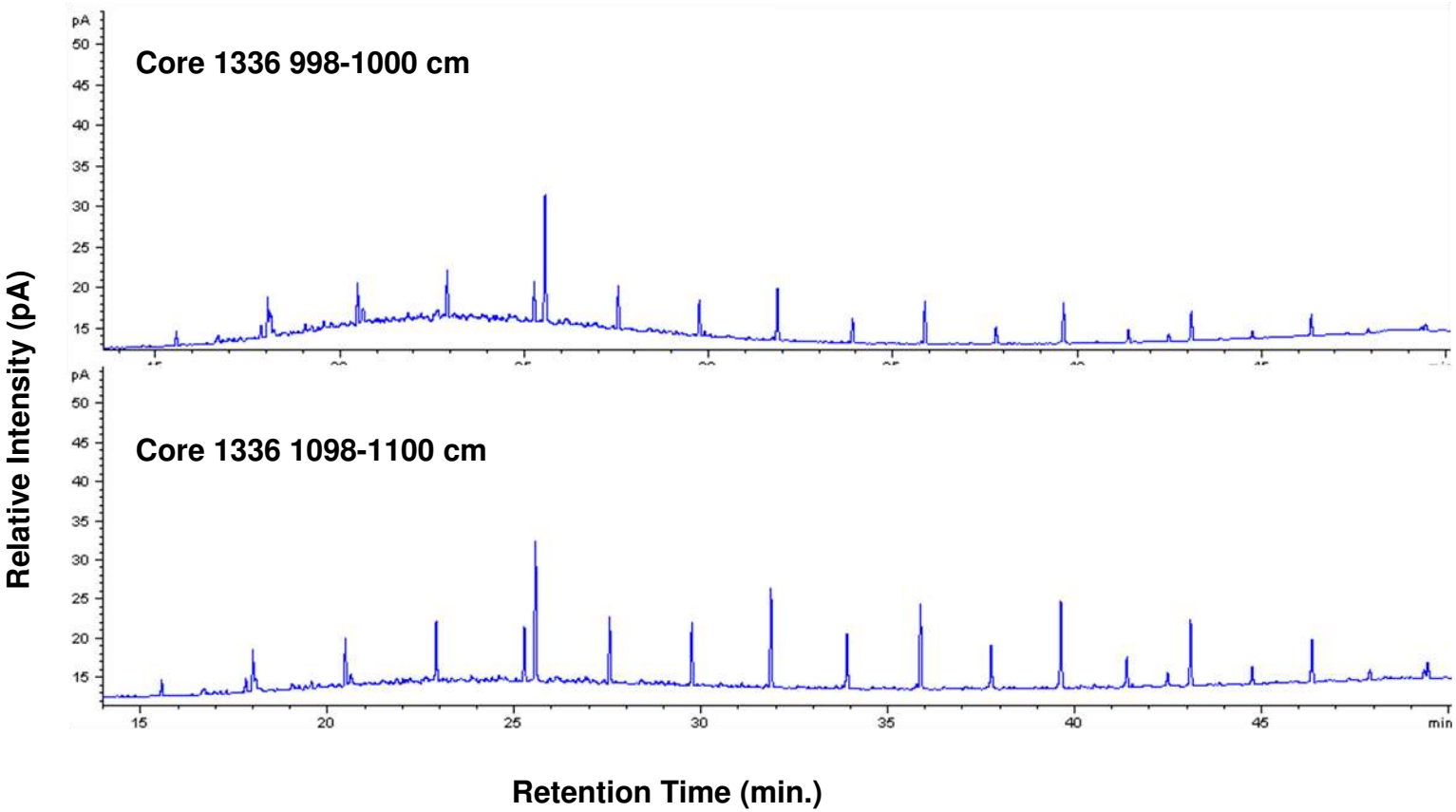
Core 1336 998-1000 cm
Core 1336 1098-1100 cm
pA
50
45
40
35
30
25
20
15
15
20
25
30
35
40
45
min
Relative Intensity (pA)
Retention Time (min.)

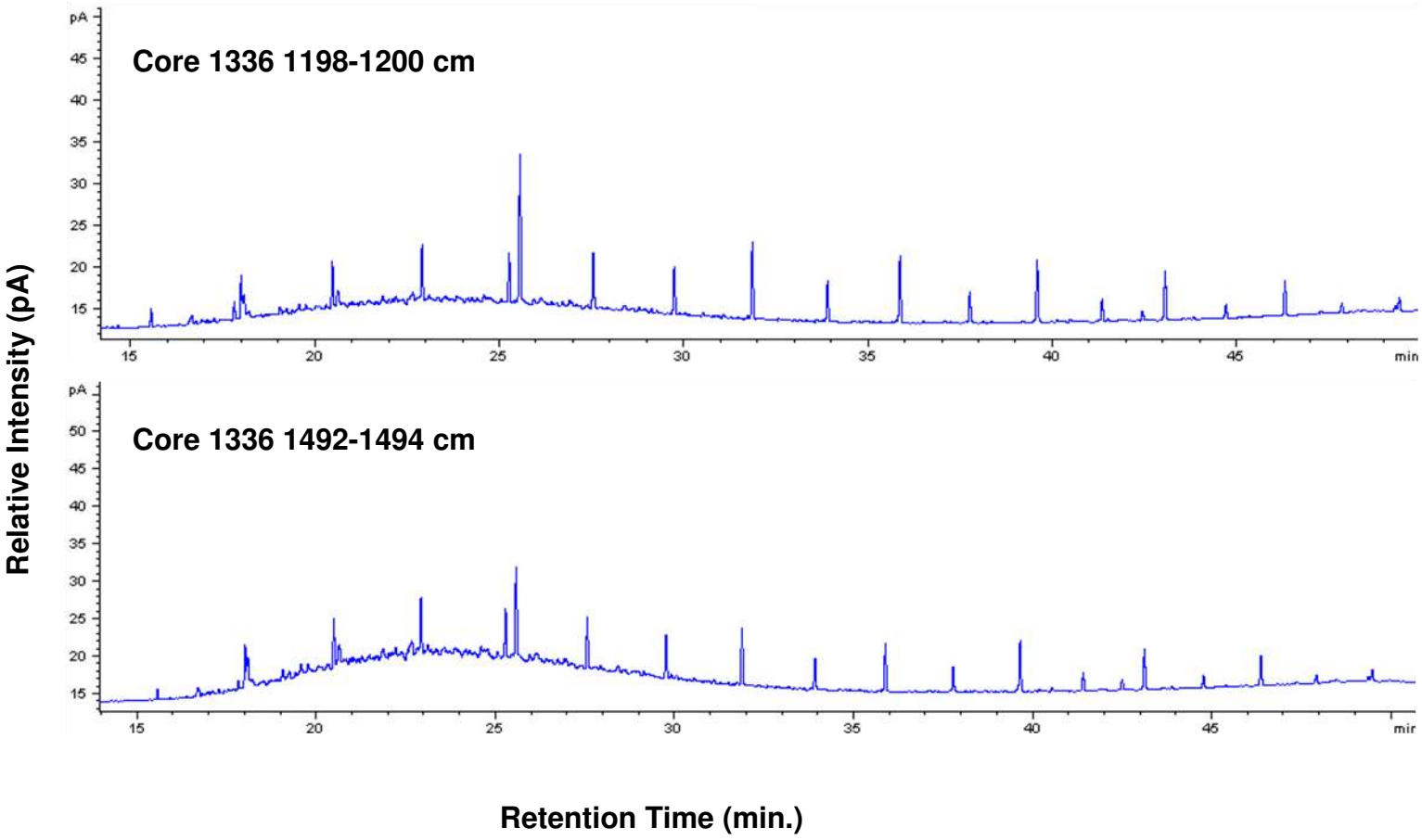
Core 1336 1198-1200 cm
Core 1336 1492-1494 cm
Relative Intensity (pA)
Retention Time (min.)
pA
min

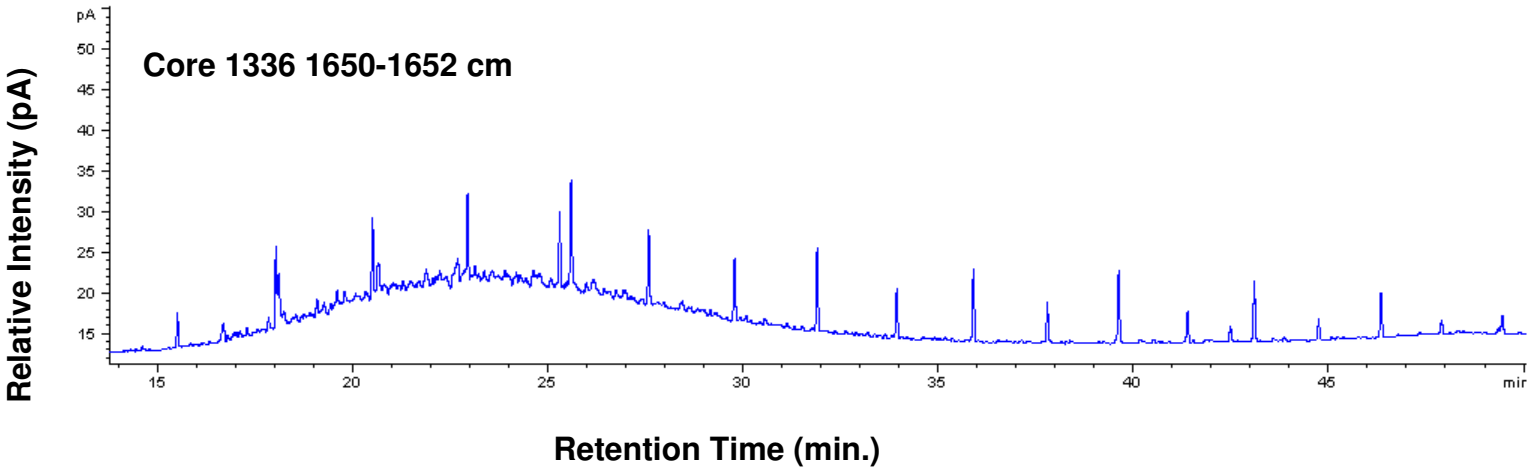
Core 1336 1650-1652 cm
Relative Intensity (pA)
pA
50
45
40
35
30
25
20
15
15
20
25
30
35
40
45
mir
Retention Time (min.)

Curriculum Vitae

Name: Ryan Hladyniuk

Post-secondary Education and Degrees:
The University of Western Ontario
London, Ontario, Canada
2008-present; Ph.D. Geology candidate

The University of Western Ontario
London, Ontario, Canada
2003-2008; B.Sc. (Honours) Medical Science Major, Earth and Planetary Science Major

Honours and Awards:
Faculty of Science Teaching Assistant Award
2013
Robert and Ruth Lumsden Award
2010, 2011, 2013
Ontario Graduate Scholarship
2011-2012
Graduate Thesis Research Award
2011, 2012

Related Work Experience
Teaching Assistant
The University of Western Ontario
2008-2013

Peer Reviewed Publications:

Hundey E.J., Moser, K.A., Longstaffe, F.J., Michelutti, N., Hladyniuk, R. (accepted). Recent changes in production in oligotrophic Uinta Mountain lakes, Utah, identified using paleolimnology. Limnology and Oceanography.

Invited abstracts (*denotes presenter):

Longstaffe, F.J.*, Dildar, N., Hladyniuk, R. (2013). Isotopic and *n*-alkane evidence for the origin of organic matter in the ancestral Great Lakes. *Canadian Quaternary Association and Canadian Geomorphology Research Group joint meeting.* Edmonton, Alberta (*Aug. 18-22).*

Selected abstracts (14 total) (*denotes presenter):

Hladyniuk, R.*, Dildar, N., Longstaffe, F.J. (2014). The stable-isotope paleolimnology of Lake Ontario. *V.M. Goldschmidt Conference.* Sacramento, California (*June 8-13).*

Hladyniuk, R.*, Dildar, N., Longstaffe, F.J. (2013). The *n*-alkane and carbon-isotope signatures of organic matter in Lake Ontario since 14,000 cal yr BP. *Geological Society of America- Northcentral meeting.* Kalamazoo, Michigan (*May 2-3).*

Hladyniuk, R.*, Longstaffe, F.J. (2009). Paleolimnology of Lake Ontario: an assessment of meltwater influx using the oxygen isotope composition of ostracodes. *International Paleolimnology Symposium.* Guadalajara, Mexico (*Dec.15-18).*